eman ta zabal zazu

Universidad del País Vasco
Euskal Herriko Unibertsitatea

FUNCTIONAL DNA IN NON-CONVENTIONAL SOLVENTS

Beñat Olave

Doctoral Thesis

Supervised by Prof. Dr.-Ing. Thomas Schäfer

2021

Agradecimientos

Antes de nada, me gustaría agradecer a Thomas Schäfer, mi director de tesis, su apoyo y confianza durante estos años. La colaboración de los profesores Carmelo Di Primo, Fernando P. Cossio y Günter Mayer ha sido también esencial para llevar a cabo la investigación. Gracias a Isabel Machado, ya que esta tesis se cimenta en su trabajo previo. Y gracias a mis compañeros de grupo más cercanos: Diego Ramírez e Iliane Rafaniello, por compartir los momentos buenos y también los difíciles.

Gracias a las personas que me han enseñado a utilizar numerosas técnicas y me han transmitido su pasión por la ciencia: Iván Rivilla, Laura Lledó, Moujab Choukeife, One-Sun Lee, Ronen Zangi, Sebastian Pilsl, Tjaša Legen y Zoraida Freixa. Tampoco me quiero olvidar del resto de estudiantes e investigadores que me han acompañado: Alba, Ali, Andoni, Anna, Borja, Eider, Ignazio, Irene, Itxaso, Jinxiu, Jon, Jörg, Julia, Lidya, Lourdes, Mikel, Nerea y Pablo.

Gracias también al personal técnico, que me ha dado la oportunidad de utilizar técnicas de manera rápida y eficaz: Aitziber Eleta, Amaia Agirre, Armando Izquierdo, José Ignacio Miranda, José Ignacio Santos, Ricardo Andrade, Stefan Breuers y Txema Mercero. Por otro lado, gracias a la gran labor administrativa de las siguientes personas he podido centrarme en las tareas de investigación: Eider Garcia, Idoia Azaldegui, Iosune Arrastia, Izaskun Balza, Monica Moreno y Onintza Pescador.

Gracias a todas esas personas que de una manera menos visible ayudan a la investigación. Especialmente a Silvia, que no sólo me ha ayudado a mantener todo limpio y ordenado, también me ha llenado de alegría y optimismo. Y por supuesto, gracias a Amparo, Helena y Josune por sus exquisitos platos diarios. Por otro lado, quiero agradecer a mi familia de Loiola el haberme acompañado en este viaje, gracias Bakartxo, Blas, Eukene, Kintxo, Marisol, Mikel y en especial Irati, mi compañera de vida. Contigo todo parece posible. Por último, quiero dedicar esta tesis a mis abuelas, Eusebia y Nati y a mis padres, Iñaki y Puerto. Gracias por cuidarme y educarme durante toda mi vida.

Acknowledgements

First of all, I would like to thank Thomas Schäfer, my thesis supervisor, for his support and trust during these years. The collaboration of professors Carmelo Di Primo, Fernando P. Cossio and Günter Mayer has also been essential to carry out the research. Thanks to Isabel Machado, as this thesis is based on her previous work. Thanks to my closest colleagues: Diego Ramírez and Iliane Rafaniello, for sharing the good times and also the difficult ones.

Thanks to the people who have taught me how to use many techniques and have passed on their passion for science: Iván Rivilla, Laura Lledó, Moujab Choukeife, One-Sun Lee, Ronen Zangi, Sebastian Pilsl, Tjaša Legen and Zoraida Freixa. Nor do I want to forget the other students and researchers who have accompanied me: Alba, Ali, Andoni, Anna, Borja, Eider, Ignazio, Irene, Itxaso, Jinxiu, Jon, Jörg, Julia, Lidya, Lourdes, Mikel, Nerea and Pablo.

Thanks also to the technical staff, who have given me the opportunity to use techniques quickly and efficiently: Aitziber Eleta, Amaia Agirre, Armando Izquierdo, José Ignacio Miranda, José Ignacio Santos, Ricardo Andrade, Stefan Breuers and Txema Mercero. On the other hand, thanks to the great administrative work of the following people I have been able to focus on research tasks: Eider Garcia, Idoia Azaldegui, Iosune Arrastia, Izaskun Balza, Monica Moreno and Onintza Pescador.

Thanks to all those people who in a less visible way help research. Especially to Silvia, who has not only helped me to keep everything clean and tidy, but has also filled me with joy and optimism. Of course, thanks also to Amparo, Helena and Josune for their delicious daily meals. On the other hand, I would like to thank my family from Loiola for accompanying me on this journey, thank you Bakartxo, Blas, Eukene, Kintxo, Marisol, Mikel and especially Irati, my partner in life. Everything seems possible with you. Finally, I would like to dedicate this thesis to my grandmothers, Eusebia and Nati, and to my parents, Iñaki and Puerto. Thank you for taking care of me and educating me throughout my life.

Table of Contents

List of Abbreviations

A	Adenosine or adenine
AAO	Anodized aluminum oxide
AF	Alexa Fluor
AMP	Adenosine monophosphate
AP	Aptamer probe
APTES	3-Aminopropyltriethoxysilane
ATP	Adenosine triphosphate
BHQ	Black Hole Quencher
Bp	Base pair
C	Cytosine
CC	Choline chloride
CD	Circular dichroism
CDHP	Choline dihydrogenphosphate
CF	Choline formate
CL	Choline lactate
CM	Confocal microscopy
CN	Choline nitrate
COVID	Coronavirus disease
CP	Capture probe
CPM	Counts per minute
DCM	Dichloromethane
DES	Deep eutectic solvent
DFT	Density functional theory
DNA	Deoxyribonucleic acid
dsDNA	double-stranded DNA
EG	Ethylene glycol
EGDS	Erioglaucine Disodium Salt
FNA	Functional nucleic acid
FRET	Förster Resonance Energy Transfer
G	Guanosine or guanine
GE	Gel electrophoresis
Gly	Glycerol
GMP	Guanosine monophosphate
GPC	Gel permeation chromatography
GTP	Guanosine triphosphate
HBA	Hydrogen bond acceptor
HBD	Hydrogen bond donor
HEPES	4-(2-hydroxyethyl)-1-piperazineethanesulfonic acid
HG	Hoogsteen
HPLC	High performance liquid chromatography
IL	Ionic liquid
KF	Karl Fischer
L-b-L	Layer-by-layer
LSC	Liquid scintillation counting
MB	Molecular beacon
MD	Molecular dynamics

MOPS 3-(N-morpholino)propanesulfonic acid

MW Molecular weight

NMR Nuclear magnetic resonance

NTP Nucleoside triphosphate

PAGE Polyacrylamide gel electrophoresis

PB Phosphate backbone

PBS Phosphate-buffered saline

PCR Polymerase chain reaction

PDB Protein Data Bank

PDI Polydispersity index

PEEK Polyether ether ketone

PEG Polyethyelene glycol

PTFE Polytetrafluoroethylene

QCM-D Quartz crystal microbalance with dissipation monitoring

RDF Radial distribution function

RI Refractive index

RMSD Root-mean-square deviation

RNA Ribonucleic acid

RT Room temperature

RTIL Room temperature ionic liquid

RU Response units or resonance units

SDR Strand displacement reaction

SDS Sodium dodecyl sulfate

SEC Size exclusion chromatography

SELEX Systematic evolution of ligands by exponential enrichment

SEM Scanning electron microscopy

SPR Surface plasmon resonance

ssDNA Single-stranded DNA

s-sDNA Salmon-sperm DNA

T Thymine

TBA Thrombin binding aptamer

TBS Tris-buffered saline

TEG Triethylene glycol

TSIL Task specific ionic liquid

WC Watson–Crick

List of Figures, Schemes and Tables

Figure S4.2. Geometries obtained optimizing solvent compounds and phosphate backbone.

Table S4.2. The number of ethylene glycol or glycerol molecules within 3.5 Å of DNA and the number of H-Bonds donned by these molecules to different DNA sites. In hydrogen bonding analysis, the ending nucleotides were not considered.

Table S4.3. The number of water molecules within 3.5 Å of DNA and the number of H-Bonds donned and accepted between water, the selected molecules of the major groove of DNA and the relationship between these two values.

Figure S4.3. RDF curves of choline, sodium and chloride from (A) Oligo1, (B) Oligo2 and (C) the dsDNA formed between Oligo1 and Oligo2. The RDF analysis were done for different mixtures containing choline chloride at 0, 0.44, 0.87, 1.31, 1.74, 2.18, 2.61 and 3.4 M (from light to darker colors).

Figure S4.4. Number of hydrogen bonds detected per water molecule at different molar fractions. H-bonds formed between (A) water molecules (B) non-water molecules with water as donor and (C) non-water molecules with water as acceptor.

Figure S4.5. Mean values and standard deviation obtained for different structural parameters of DNA. The concentration of each mixed solvent increases from left to right.

Figure S4.6. Mean values and standard deviation obtained for different structural parameters of DNA. The concentration of each mixed solvent increases from left to right.

Chapter five: Long-term use and function of DNA in deep eutectic solvents

Figure 5.1. Circular dichroism measurements of DNA in presence of different concentrations of choline chloride. All the oligonucleotides were at 5 µM and the temperature was 25 ^{o}C.

Figure 5.2. Circular dichroism measurements of DNA in presence of different concentrations of (A) ethylene glycol. (B) Glycerol. (C) Urea. All the oligonucleotides were at 5 µM and the temperature was 25 ^{o}C.

Figure 5.3. Circular Dichroism measurements of ATP DNA-aptamer in presence of different concentrations of (A) ethaline, (B) CC/EG (1:3), (C) glyceline and (D) urea. All the oligonucleotides were at 5 µM and the temperature was 25 ^{o}C.

Figure S5.1. Circular dichroism spectra of the ATP DNA-aptamer stored at RT for different periods.

Figure S5.2. Circular dichroism spectra of the ATP DNA-aptamer stored at RT for different periods.

Figure S5.3. Circular dichroism spectra of solutions containing Oligo1 and Oligo2 during a period stored at RT or at -20 ^{o}C.

Figure S5.4. Circular dichroism spectra of solutions containing Oligo1 and Oligo2 during a period stored at RT.

Figure S5.5. Mean response or intensity (zeroed) values obtained upon target addition at different conc. in presence of (A) ATP DNA-aptamer (4 bp), (B) ATP DNA-aptamer (8 bp) or (C) molecular beacon, while using choline chloride-containing media.

Figure S5.6. Mean response or intensity (zeroed) values obtained upon target addition at different concentrations in presence of (A) ATP DNA-aptamer (4 bp), (B) ATP DNA-aptamer (8 bp) or (C) molecular beacon, while using ethylene glycol-containing media.

Figure S5.7. Mean response or intensity (zeroed) values obtained upon target addition at different concentrations in presence of (A) ATP DNA-aptamer (4 bp), (B) ATP DNA-aptamer (8 bp) or (C) molecular beacon, while using glycerol-containing media.

Figure S5.8. Mean response or intensity (zeroed) values obtained upon target addition at different concentrations in presence of (A) ATP DNA-aptamer (4 bp), (B) ATP DNA-aptamer (8 bp) or (C) molecular beacon, while using urea-containing media.

Figure S5.9. Mean response or intensity (zeroed) values obtained upon target addition at different concentrations in presence of (A) ATP DNA-aptamer (4 bp), (B) ATP DNA-aptamer (8 bp) or (C) molecular beacon, while using ethaline-containing media.

Figure S5.10. Mean response or intensity (zeroed) values obtained upon target addition at different conc. in presence of (A) ATP DNA-aptamer (4 bp), (B) ATP DNA-aptamer (8 bp) or (C) molecular beacon, while using CC/EG (1:3)-containing media.

Figure S5.11. Mean response or intensity (zeroed) values obtained upon target addition at different conc. in presence of (A) ATP DNA-aptamer (4 bp), (B) ATP DNA-aptamer (8 bp) or (C) molecular beacon, while using glyceline-containing media.

Figure 7.14. Response curves obtained upon addition of AMP at 1 mM to (A) CP 1 or (B) CP ADA in presence of bridge probes. The flow rate was 25 µL/min.

Figure 7.15. Circular dichroism measurements of (A) BP, AP 1 and [BP + AP 1] in choline chloride 0.5 M or (B) [BP + AP 1] at different concentrations of choline chloride. All the oligonucleotides were at 5 µM and the temperature was 25 ^{o}C.

Figure 7.16. CD measurements of solutions containing [BP + AP 1] in (A) molecular solvents (B) deep eutectic solvents and (C) ionic liquids at different concentration in water. [BP + AP 1] in physiological media (NaCl 0.5 M) is always shown as reference (fine solid line). All the oligonucleotides were at 5 µM and the temperature was 25 ^{o}C.

Figure S7.1. The injection of different concentrations of bridge probe (2, 5 and 10 µM) to channels containing (A) CP 1, (B) CP 2 or (C) CP ADA. The flow rate was 25 µL/min in all cases.

Figure S7.2. The injection of different concentrations of molecular targets to channels containing (A) CP 1, (B) CP 2 or (C) CP ADA.

Figure S7.3. Two consecutive injection of molecular target and bridge probe to channels containing (A) CP 1, (B) CP 2 or (C) CP ADA.

Figure S7.4. The injection of BP at 2 µM and consecutive injection of different concentrations of (A) AMP, (B) Adenosine or (C) GMP to channel containing CP 1.

Figure S7.5. 3 wt. % agarose gel electrophoresis of solutions containing [BP + AP 1]. 90V 60 min. (A) Line 1 and 1': 3000 bp ladder. Line 3: Solution A. Line 4: Solution B. Line 5: Solution C. Line 6: Solution D. Line 8 and 8': 300 bp ladder. Line 3': Solution A with GMP instead of AMP. Line 4': Solution B with GMP instead of AMP. Line 5': Solution C with GMP instead of AMP. Line 6': Solution D with GMP instead of AMP. (B) Line 1 and 5: 0 mM NaOH. Line 2 and 6: 5 mM NaOH. Line 3 and 7: 20 mM NaOH. Line 4 and 8: 50 mM NaOH.

Figure S7.6. GPC/SEC results of solutions formed by [BP + AP 1], [BP + AP 1 + AMP] or [BP + AP 1 + GMP] measured after 25 hours.

Figure S7.7. Response curves obtained upon injection of different bridge probes to (A) CP 1, (B) CP 2 or (C) CP ADA. The flow rate was 25 µL/min.

Figure S7.8. Raw images of agarose gels containing the mixture of BP and AP 1 in molecular solvents. (A) One hour (B) one day and (C) one week after preparation.

Chapter eight: DNA-based gating membranes and asymmetric catalysis

after one day or two weeks at RT. (B) After one day in physiological media, ethylene glycol (6.9 M) or ethaline (3.4 M).

Table S8.1. Used DNA sequences.

Figure S8.1. (A and C) Frequency and dissipation curves obtained in QCM-D upon immobilization of CP 2 and consecutive injections of BP and CP 2. (B and D) Representation of the dissipation versus frequency values obtained in each layer of the supersandwich. The A and B data correspond to gold sensorchip and C and D data to aluminum oxide sensorchip.

Figure S8.2. Circular dichroism spectra of different samples containing the metal (0.3 mM). In some cases the "long" salmon-sperm DNA (1.33 mg/mL) and/or the ligand (0.39 mM). In (A) there is no ligand, in (B) the ligand is 1b, in (C) the ligand is 1c and in (D) the ligand is 1d.

Figure S8.3. (A) DNA concentration in the donor chamber when performing a permeation experiment of both salmon-sperm DNA (s-sDNA) samples in the Side-Bi-Side cell with pure water in both chambers and using the alumina membrane with mean pore diameter of 35 nm. (B) Agarose gels after gel-electrophoresis of both s-sDNA before starting the permeation experiments.

Figure S8.4. Absorbance measurements done during the preliminary solubility test. 2 mM of dienophile (3) were added to 2 mL of each media and stirred at 60 ^{o}C overnight. Then, the solutions were cooled and filtered. The obtained liquid was measured by UV-Vis.

Chapter nine: General conclusions

Resumen: ADN funcional en disolventes alternativos

Desde hace millones de años los ácidos nucleicos son esenciales en todas las formas de vida conocidas, y desde hace unas décadas, su utilidad se amplía también a contextos no biológicos. La capacidad del ADN y del ARN para formar interacciones específicas entre sus bases o incluso otras moléculas ha posibilitado su integración en diversas aplicaciones y la creación de un área de investigación propia: la nanotecnología de ADN y ARN.

Mediante diversos estudios fundamentales, en esta tesis se lleva el ADN sintético o de esperma de salmón a contextos no convencionales. De esta forma, se pretenden identificar mejor los factores que determinan su estructura, estabilidad y capacidad de reconocimiento. Además de crear nuevos entornos, se estudian también estructuras no convencionales de ADN, como pueden ser las nanoestructuras programables o los complejos entre ADN y ligando que se utilizan en reacciones catalíticas.

El primer capítulo de la tesis consta de una revisión bibliográfica centrada en el comportamiento del ADN en disolventes orgánico, eutécticos profundos y líquidos iónicos. Por otro lado, se presentan distintas aplicaciones nanotecnológicas basadas en el uso del ADN en estos medios. Después, en el segundo capítulo se detallan los materiales y métodos de todo el trabajo experimental realizado.

El trabajo experimental se ha dividido en seis partes, del capítulo tres al ocho. En los primeros dos capítulos se estudia la estabilidad conformacional y térmica de la doble hélice del ADN cuando esta disuelta en medios no fisiológicos. Estos estudios se han realizado cambiando sistemáticamente el medio y la secuencia del ADN, permitiendo así obtener información muy amplia que no se encuentra en la literatura. Los estudios se han realizado de manera experimental y computacional, utilizando los mismos sistemas en ambos casos para poder comparar entre los resultados.

Después, en el capítulo cinco se estudia un aptámero de ADN en los disolventes previos. De esta forma se quiere entender mejor cómo afecta el entorno no sólo a la estabilidad del ADN, también a su capacidad para reconocer otras moléculas. Por otro lado, la estructura del ADN se ha monitorizado durante varios años en diversos medios, observando que el medio no acuoso

reduce o incluso evita, la degradación del ADN. En el siguiente capítulo, el sexto, se sigue estudiando la capacidad de reconocimiento de los aptámeros de ADN, pero en esta ocasión no se utiliza un aptámero ya conocido, se realiza una nueva selección. De esta forma se han obtenido nuevas secuencias de aptámero especialmente adaptadas al medio no fisiológico, que además tienen nuevos mecanismos de reconocimiento.

En el séptimo capítulo de la tesis se estudia la construcción y capacidad de reconocimiento de una nanoestructura de ADN conocida como supersandwich. Hay varios artículos que plantean el uso de este diseño en sistemas estímulo-respuesta, pero hasta ahora no se había hecho un estudio a tiempo real de las cinéticas de la nanoestructura. Por otro lado, se propone la utilización de nanoestructuras de ADN en medios no fisiológicos, mostrando que los estudios fundamentales realizados en los primeros tres capítulos pueden servir para predecir la estructura y capacidad de reconocimiento del supersandwich.

En el octavo capítulo, primero, se estudia la inmovilización del ADN en superficies de alúmina. Después, con el protocolo desarrollado, se inmoviliza el supersandwich de ADN en una superficie de alúmina isoporosa para crear una membrana con capacidades estímulo-respuesta. Esta membrana inteligente se lleva después a un sistema microfluídico diseñado en la tesis. Mediante estudios de permeación se observan varias ventajas de utilizar un sistema microfluídico y distintos retos que supone el uso de nanoestructuras de ADN en estos diseños.

En la última sección del octavo capítulo, lo aprendido en todo el trabajo previo, se traslada a un proyecto de colaboración en curso. En este proyecto se pretende crear el primer reactor de ADN para llevar reacciones de catálisis asimétrica mediadas por ADN a una mayor escala. En esta tesis se hace un primer balance sobre los retos que se deben afrontar y se presentan varias propuestas. Para terminar, el noveno capítulo contiene las conclusiones generales de la tesis.

Abstract: Functional DNA in non-conventional solvents

Nucleic acids have been essential to all known life forms for millions of years, and in recent decades, their usefulness has been extended to non-biological contexts as well. The ability of DNA and RNA to form specific interactions between their bases or even other molecules has enabled their integration into various applications and the creation of two research areas: DNA and RNA nanotechnology.

By means of several fundamental studies, this thesis takes synthetic DNA or salmon-sperm DNA to unconventional contexts. In this way, the aim is to better identify the factors that determine its structure, stability and recognisability. In addition to creating new environments, unconventional DNA structures are also studied: programmable nanostructures or DNA-ligand complexes used in catalytic reactions.

The first chapter of the thesis consists of a literature review focusing on the behaviour of DNA in molecular solvents, deep eutectic solvents and ionic liquids. On the other hand, different nanotechnological applications based on the use of DNA in these media are presented. Then, in the second chapter, the materials and methods of all the experimental work carried out are detailed.

The experimental work has been divided into six parts, from chapter three to eight. In the first two chapters, the conformational and thermal stability of the DNA double helix when dissolved in non-physiological media is studied. These studies have been carried out by systematically changing the medium and the DNA sequence, allowing us to obtain extensive information not found in the literature. The studies have been carried out experimentally and computationally, using the same systems in both cases in order to be able to compare the results.

Then, in chapter five, a DNA aptamer is studied in the previous solvents. The aim is to better understand how the environment affects not only the stability of the DNA, but also its ability to recognize other molecules. On the other hand, DNA has been monitored for several years in various media, and it has been observed that the non-aqueous medium reduces, or even prevents, DNA degradation. In the following chapter, the sixth, the recognition capacity of DNA

aptamers continues to be studied, but this time a new selection is made rather than using an already known aptamer. In this way, new aptamer sequences specially adapted to the non-physiological environment have been obtained, which also have new recognition mechanisms.

In the seventh chapter of the thesis, the construction and recognition capacity of a DNA nanostructure known as supersandwich is studied. There are several articles that propose the use of this design in stimulus-response systems, but until now there has not been a real-time study of the kinetics of the nanostructure. On the other hand, the use of DNA nanostructures in non-physiological environments is proposed, showing that the fundamental studies carried out in the first three chapters can be used to predict the structure and recognition capacity of the supersandwich.

In the eighth chapter, first, the immobilisation of DNA on alumina surfaces is studied. Then, using the developed protocol, the DNA supersandwich is immobilised on an isoporous alumina surface to create a membrane with stimulus-responsive capabilities. This smart membrane is then taken to a microfluidic system designed in the thesis and manufactured in a local company. Permeation studies showed several advantages of using a microfluidic system and various challenges of using DNA nanostructures in these designs.

In the last section of the eighth chapter, the lessons learned in all the previous work are transferred to an ongoing collaborative project. This project aims to create the first DNA reactor to bring DNA-mediated asymmetric catalysis reactions to a larger scale. This thesis takes a first stock of the challenges to be faced and presents some proposals. Finally, the ninth chapter contains the general conclusions of the thesis.

CHAPTER 1

Functional DNA in non-conventional solvents

1.1 Introduction

Nucleic acids are essential in all forms of life that are known. It is estimated that life was formed on the earth 3,800,000,000 years ago[1,2] and our species origin was around 200,000 years ago[3,4]. However, it was possible to isolate them until the middle of the 19th century[5] and one hundred years later, the shape of the double helix of deoxyribonucleic acid (DNA) was elucidated[6–8]. The understanding of the most common structure of DNA triggered a revolution in life sciences with discoveries describing mechanisms of life in eukaryotes, prokaryotes or viruses[9]. Not only that, after millions of years, nucleic acids found new functions when curiousness and creativeness encouraged the scientist to study possible uses beyond their biological roll in the cell.

RNA and DNA started to be studied outside of their purely biological context in 1980s[10] and both allow the formation of a great variety of nanostructures and technological applications. Their principal advantage as a building block in nanotechnological applications is based on the fact that despite the variety of functions they may fulfil, the chemical structure always relies on four types of nucleotides and their overall physico-chemical nature basically remains unaltered whatever its sequence. In order to understand the connection between their sequence, solvation and function, it is useful to separate the events in different structures.

The primary structure corresponds to the composition of nucleic acids containing nitrogenous bases, sugars and phosphate groups. In example in Figure 1.1 is shown the composition of the phosphate backbone and the adenosine (A) and thymine (T) nucleosides. Guanosine (G) and cytosine (C) repeating units are also part of natural DNA. The secondary

structure is defined by the interactions between nucleotides and with the environment; in the example the two DNA strands are forming the classic Watson-Crick double helical secondary structure. On the other hand, the tertiary structure can be described as the three-dimensional folding of a single or multiple strands and gives information about the steric or mechanical properties. In this case, the steric properties of the double helix correspond to the B-form dsDNA[11]. The double helical DNA is usually classified in A-, B- or Z-forms depending on its geometries, which are highly dependent of the surrounding media.

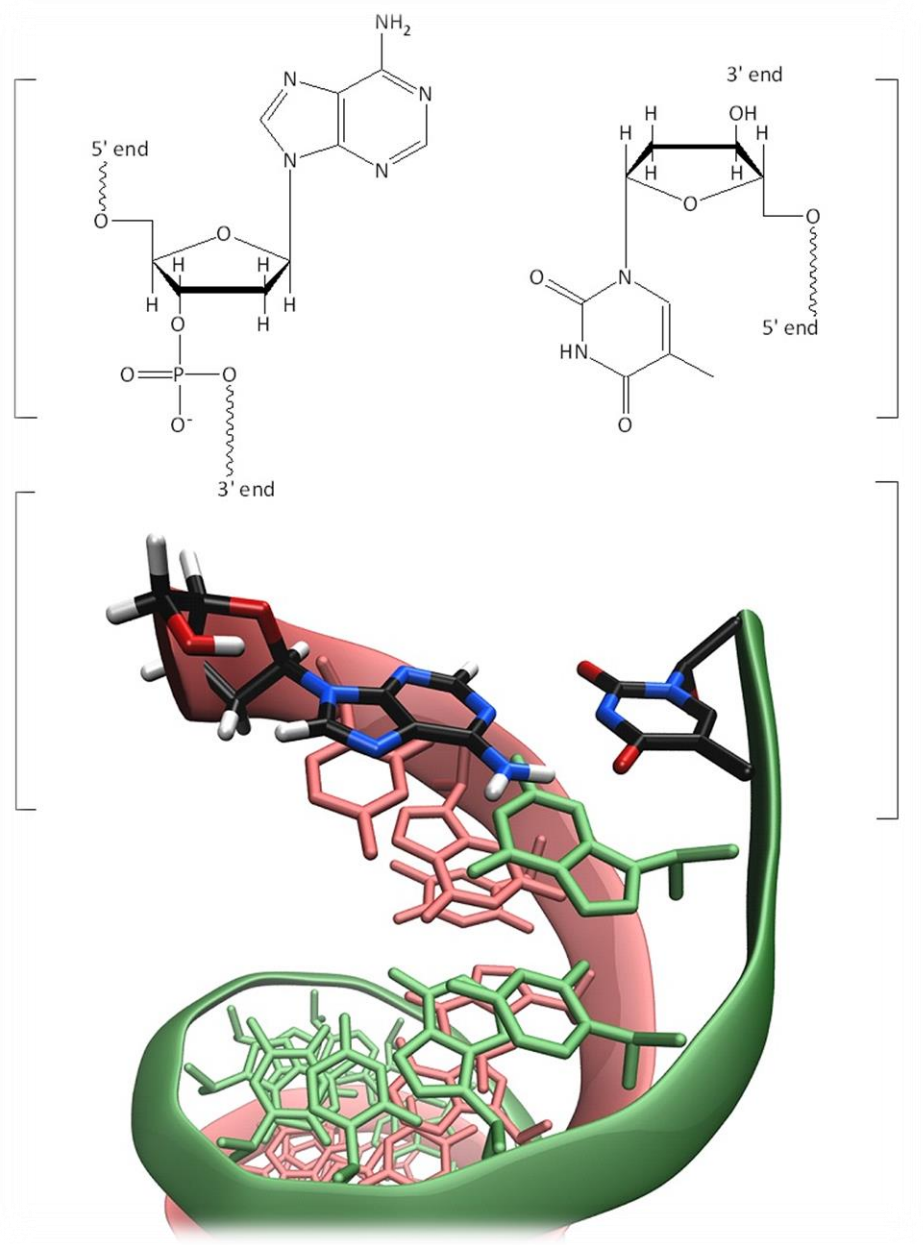

Figure 1.1. An example of the double helical DNA.

It is common to use and study DNA and RNA separately. Regarding their chemical composition, the extra hydroxyl group allows RNA to interact more strongly with surrounding molecules increasing the recognition and catalytic capacities[12]. It also has a single-stranded nature, resists better acidic pH than DNA and designed sequences can even be expressed inside the cell using a DNA template[13,14]. However, its composition makes more prone to hydrolysis or can autocleavage[15] and furthermore have increased purification and synthesis costs[15]. With regard to their conformation, both nucleic acids have an unique specific base-pairing, but their structures have huge differences in the same media[16].

In example, at physiological conditions double-stranded (ds) RNA is in A-form and dsDNA in B-form. How significant are these differences? Huge, in example the conditions needed to achieve similar conformations vary a lot: in case of the A-form in DNA, the double helix would need to be dehydrated to a 75 wt. % of water content using co-solvents or macromolecules[17]. In case of G-quadruplexes, it was seen that using the same sequences, certain metallic cations are able to stabilize only the RNA ones or vice versa[18]. Fortunately, new findings can be adapted for both nucleic acids, in example, aptamers and ribozymes were originally selected using RNA and then they extended to DNA[19,20] and higher ordered structures that were thought for DNA such as those of the origami technic, are being used also with RNA[21,22].

1.2 Bottlenecks of DNA nanotechnology in physiological media

RNA and DNA can relate and mutually benefit or even form hybrid designs[23], and bottlenecks to be fronted in nanotechnological applications are also common for both nucleic acids. One of these challenges is that static and dynamic designs need to be structurally stable

for long periods. Unfortunately, due to its primary structure, nucleic acids can be rapidly hydrolyzed due to the presence of enzymes or even in their absence[24]. In example, the depurination of DNA in water happens because the glycosidic bonds linking deoxyribose with DNA bases are labile (Figure 1.2A). These issues could be prevented modifying chemically DNA and RNA bases[25], but with an high synthesis cost[26,27].

Another bottleneck in nanotechnology are destabilizing factors such as electrostatic interactions between different double strands that prevent the formation of nanostructures. This can be faced increasing the ionic strength of the solution, shielding the high density of negative charges of both strands and allowing the formation of the double-helix at high temperatures (Figure 1.2B). However, a trade-off appears between the stability of the double-helix and the dynamic behaviour of the design[28]: stabilizing the structure also prevents new strands or molecules to form interactions with the already formed double-helix that needs to be dehybridized partially or completely[29,30].

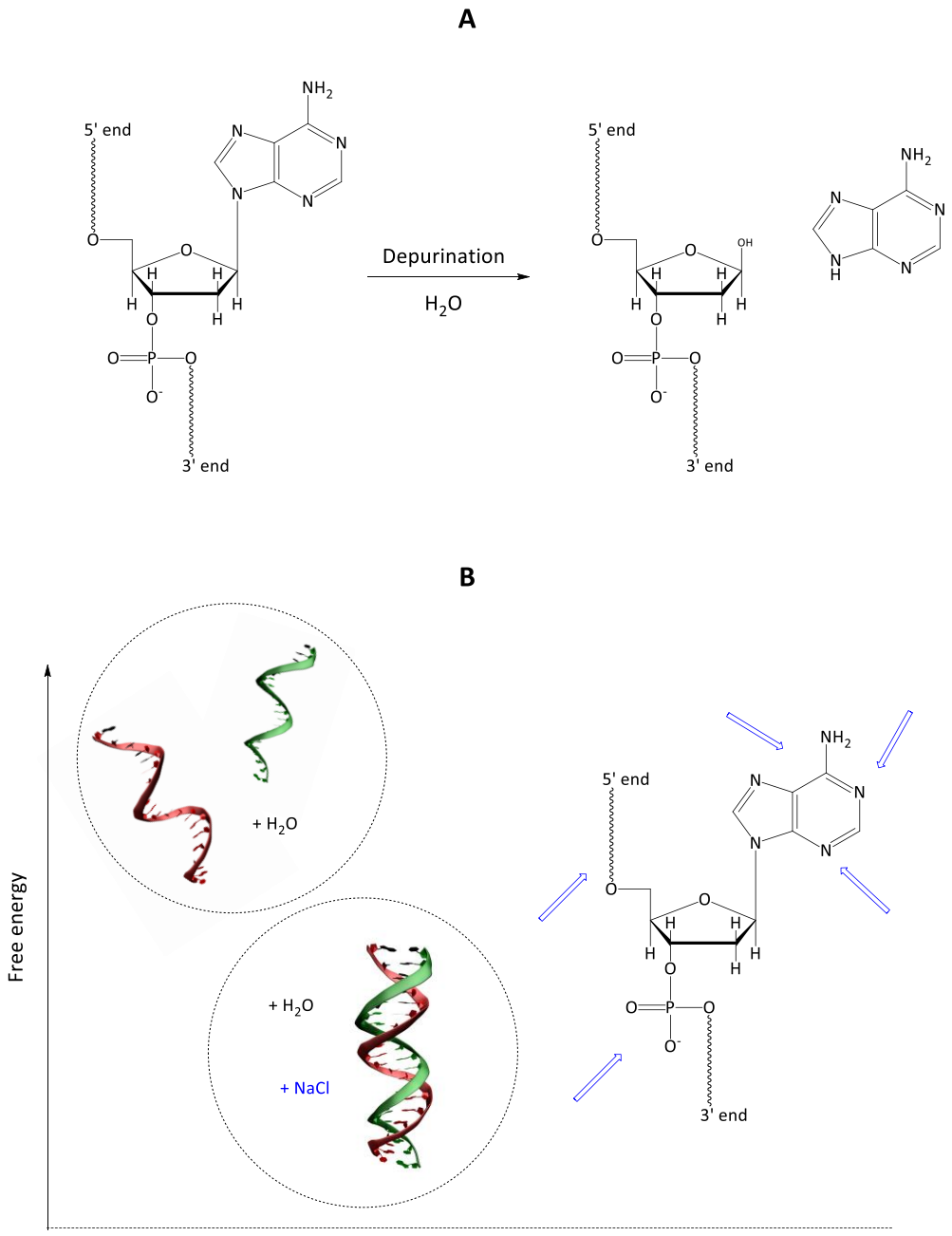

Figure 1.2. (A) DNA hydrolysis by depurination. (B) A simplistic representation of the stabilization of the double helix by salts and the interactions of these with DNA.

Usually these events consist in a strand displacement reaction (SDR)[31], where one strand of a DNA duplex or one end of a DNA-hairpin is replaced with another DNA strand that usually can form a larger number of matched nucleotides (called a fuel strand). Unfortunately, due to the trade-off between structural stability and dynamic behaviour, some nanostructure need long periods to open due to a slow kinetics and energetic traps in the dehybridization/hybridization events that can have multiple intermediate states[32,33]. This can be observed in DNA-origami boxes used as carrier which can maintain their structural stability for long periods and have a specific response but need hours to open[34,35].

The hairpin-form also appears usually while using DNA oligonucleotides with molecular recognition capacity, known as functional nucleic acids (FNAs)[36,37]. The FNAs of DNA comprise DNA-aptamers and DNAzymes, which are obtained through *in vitro* selection protocols called "systematic evolution of ligands by exponential enrichment" (SELEX)[38] and are used in a plethora of different applications[39]. The size of selected sequences commonly varies between 10 and 80 bases, which can arrange into different functional single stranded structures such as hairpins, G-quadruplexes or bulges. These sequences can be used to recognize a huge variety of different targets that comprises inorganic or organic low molecular weight compounds, nucleotides, amino acids, peptides, proteins, and even whole cells.

In nanostructures such as DNA-origami boxes, the trade-off between the structural stability and dynamic behaviour could be improved using hybrid designs formed by functionalized hydrogels[40,41] or nanoparticles[42,43] that forms less charged structures and therefore recognition events can be accelerated. However, these might not be competitive in

comparison with other stimuli-responsive materials[44]. Other alternatives could involve the modification of nucleotides using click chemistry[45] or using synthetic nucleic acids[46–48] but increasing costs and complexity of synthesis and SELEX technic.

Moreover, in other cases, the main bottleneck for the technology development might be in the physiological media, as it can easily evaporate or hydrolyse nucleic acids. Furthermore, the recognition or catalytic efficiency of reactions involving hydrophobic, negatively charged and planar molecules is limited also by this aqueous media[49]. These and previous bottlenecks encouraged researchers to study alternative media that can better regulate the structure and function of nucleic acids without modifying the natural nucleic acids[50].

1.3 Behaviour of DNA in non-physiological media

In order to develop nanotechnological applications in new media, it is important to deepen in the understanding of the thermal stability, kinetics and conformational or mechanical properties of DNA. However, the knowledge is very limited comparing with that already acquired for physiological media (composed merely by water and metallic ions). Fortunately, in the last decade different studies, mainly experimental, have started to go deeper into the subject of DNA solvation in non-conventional environments.

One of these is the crowded media, which aims to replace aqueous buffer solutions by a cellular-like environment with solutes that cause volume exclusion[51] and serve to prevent hydrolysis and digestion[52,53] or regulate processes such as aging[54]. Polyethylene glycol (PEG) is one of the most commonly used polymers in aqueous solutions to mimic cellular environment acting as a crowding agent[55], as it is assumed that PEG does not interact chemically with nucleotides but merely serves as physically reducing the space. Instead of using PEG, another strategy that increases the excluded volume of nucleic acids is the molecular confinement, in example with DNA nanocages[56], but technics are yet being developed and are somehow limited by their complexity.

There is a different approach, simpler than previous ones that prevents nucleic acid from degradation, apart from offering novel interactions and conformations with both, enthalpic and entropic contributions[57,58], the use of solvents other than water. This possibility started to be studied with molecular solvents, after the development that proteins underwent in them[59], while increasing compound solubility[60] and the degree of solvent freedom in biotransformation

for processes involving enzyme-based catalysis[61–64]. Apart from these molecular solvents, there is a more recent class of media, which could be another convenient alternative to replace water molecules and even counterions: ionic liquids (ILs) and deep eutectic solvents (DESs). ILs and DESs are also formed by organic molecules and can be liquid at room temperature but opposite from molecular solvents, they are charged, possess a reduced volatility and flammability as well as many novel properties[65].

Differently from ILs which are composed solely by a cation and an anion[66], DESs need a co-solvent to reduce their melting temperature but as an advantage, are cheaper, less-toxic[67,68] and formed by bio-based molecules[69]. Both of them, ILs and DESs, could be used to face solvent evaporation or long-term application controlling water and nuclease activity[70,71] and with them, the tuneability of DNA environment increases exponentially comparing with physiological media[72,73]. However, it is of upmost importance to understand the behaviour of DNA and develop prediction capabilities that allow choosing the best ILs or DESs in each nanotechnological application.

To make this text clearer, findings will be separated depending on the secondary structures of DNA studied. In this manner, these can be grouped in DNA structures that forms Watson-Crick (WC) interactions, the most common in DNA double helix, or Hoogsteen (HG) interactions that are characteristic of certain duplexes, or non-canonical structures such as G-quadruplexes and i-motifs. On the other hand, the interactions with specific target molecules create rare local secondary structures as happens with FNAs. Combining previously knowledge makes possible to understand the behaviour of each secondary structure in non-physiological

media but also that of complex DNA nanostructures that have multiple structures and can acquire a dynamic function.

An example of the latter is the ATP DNA-aptamer that forms the three key-interactions mentioned before with only 27 nucleotides. The Watson-Crick base pairing can be found in two base pairs close to the loop and four base pairs at the end of the hairpin (Figure 1.3A). On the other hand, the binding pocket is flanked by reversed Hoogsteen G·G mismatch pairs and recognizes the molecular target using G·A mismatches[74] (Figure 1.3B).

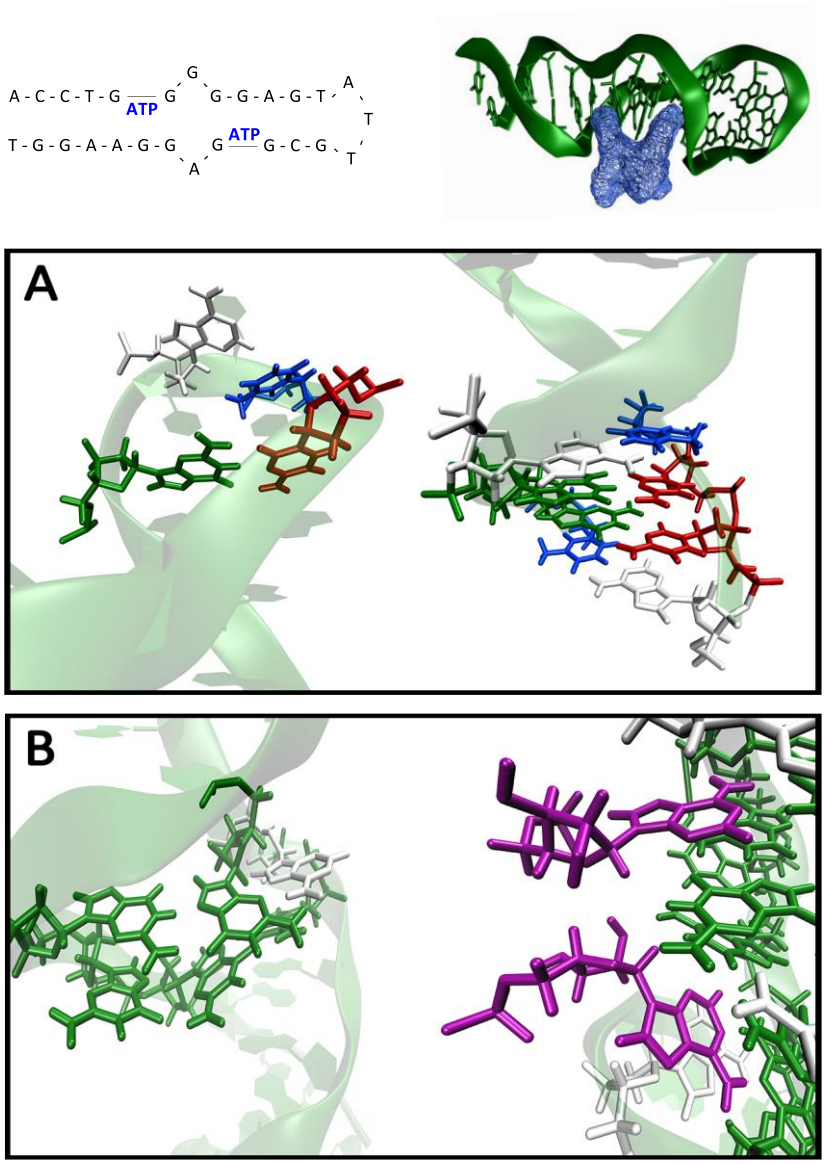

Figure 1.3. The ATP DNA-aptamer when it recognizes the AMP molecular target (PDB: **1aw4**). (A) Focus on the Watson-Crick base pairs. (B) Focus on the Hoogsteen G·G mismatch pairs and the interaction with the target.

1.3.1 While forming Watson-Crick interactions

The WC base pairing is characteristic of the most common form of DNA, the DNA double helix. Apart from this base pairing, there are other inter- and intramolecular interactions in the helical DNA that have implications in the thermal and structural stabilities of this secondary structure. In example, the electrostatic repulsion between the two double-stranded segments and the stacking between adjacent bases. Regarding the implication of the surrounding media, in physiological media, metallic salts usually increase the melting temperature of the duplex because they reduce the repulsion between strands without interfering in the interactions between DNA strands or bases and water. However, after a critical point, they can reduce the melting temperature due to an excessively charged environment and replacement of water molecules. It is already possible to predict the conformation, thermal stability and kinetics of DNA in these systems[75–80].

One of the major challenges to predict DNA behaviour appears when water molecules, ubiquitous in the cellular environment[81], are displaced from the double-helix solvation shell. Even if it is possible to predict qualitatively implications of water displacement[82], it is still a challenge to quantify changes in the thermal and structural stability of the DNA double helix. In fact, water forms complex nanostructures close to DNA such as the chiral spine of hydration[83] and stabilize biomolecules such as DNA beyond simple hydrogen-bonding[84–86]. In example, molecular crowding and confinement strategies (Figure 1.4) need to be applied carefully because they reduce the amount of water molecules in close contact with DNA[87]. In consequence, the latter can dehybridize, condensate or adapt its double-helix from the B- to A-

or Z-forms[88] or form non-canonical structures in specific helix sites that no longer form Watson-Crick interactions[89]. It is known that the impact on thermal stability can be reduced increasing the length of duplexes[90], due to the cooperative nature of the dehybridization process of DNA because even if water molecules per base-pair are reduced equally in both DNA sequences the probability of re-hybridization is higher in the longer DNA sequence[91].

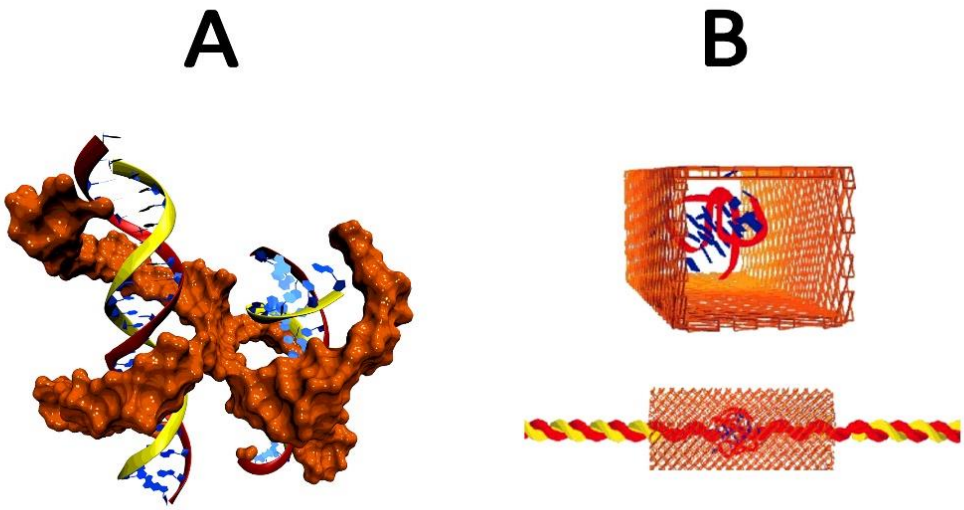

Figure 1.4. A representation of (A) macromolecular crowding and (B) confinement of DNA double helixes.

On the other hand, non-charged and highly apolar macromolecules used in crowded and confined media usually do not interact strongly with DNA[92], but they can stabilize the duplexes by volume exclusion[93] because they limits the movement of the entropically favored ssDNA[94]. It is suggested that nature uses the volume exclusion to control compacted dsDNA in the cell[95,96] and it was possible to achieve new DNA-origami designs[97] or stabilize three way junctions for

nanotechnological purposes[98]. However, this stabilization is hardly noticed in short oligonucleotides, which have higher movement freedom.

Regarding the use of solvents other than water, as it is the case of molecular solvents, the stability of DNA duplexes can change drastically even at low concentrations. In different studies it is pointed that even if the molecular solvents have low dielectric constant what increases the Columbic interactions between phosphate groups of DNA and cations[99] the dsDNA thermal stability is reduced mainly due to the disruption of the hydrogen bonds between Watson-Crick base-pairs[100]. The B-form double helix can adapt in these cases a condensated shape, especially when it is formed by thousands or hundreds of thousands of base pairs[101,102]. In the worst scenario, the apolar environment of certain solvents produces the aggregation and precipitation of DNA[103]. The possibility of using high concentrations of apolar solvents in presence of peptide nucleic acids (PNAs) is under study, but this strategy increases the costs of the design[104]. Nevertheless, even if the stability of the DNA double helix is affected, these solvents can be used as co-solvents due to their ability to accelerate hybridization kinetics decreasing the activation energy barrier.

An example of the latter can be found in studies where the kinetics of the DNA strand displacement reaction (SDR) were improved between 10 to 100 fold maintaining the specificity of the hybridization using polar molecular solvents such as ethanol or isopropanol (from 20 to 55 wt %)[105,106] (Figure 1.5A). Furthermore, it can be interesting to use DNA-aptamers and DNAzymes in media with some quantity of molecular solvents because a static stable system (high thermal stability of the duplex) is not always the best scenario to perform dynamic actions.

It was found that the hybridization or recognition kinetics of aptamers[107] and DNAzymes[108,109] also can have faster kinetics. This accelerated unwind of the duplexes in apolar environments could be used by helicases in the cell as catalyst[110].

Polyol solvents are usually used to increase thermal stability of proteins[111]. As can be observed in Figure 1.5B, they do not stabilize the Watson-Crick base pairing but these media reduce less the thermal stability of the DNA duplex than other molecular solvents[112]. Unfortunately it is still not possible to predict the solvation of DNA in these media but systematic studies have shown that between the different molecular solvents[113], the chemo-physical properties of ethylene glycol (i.e. relative low viscosity and wide liquid range[114]) make it an interesting polyol media to substitute water[115,116].

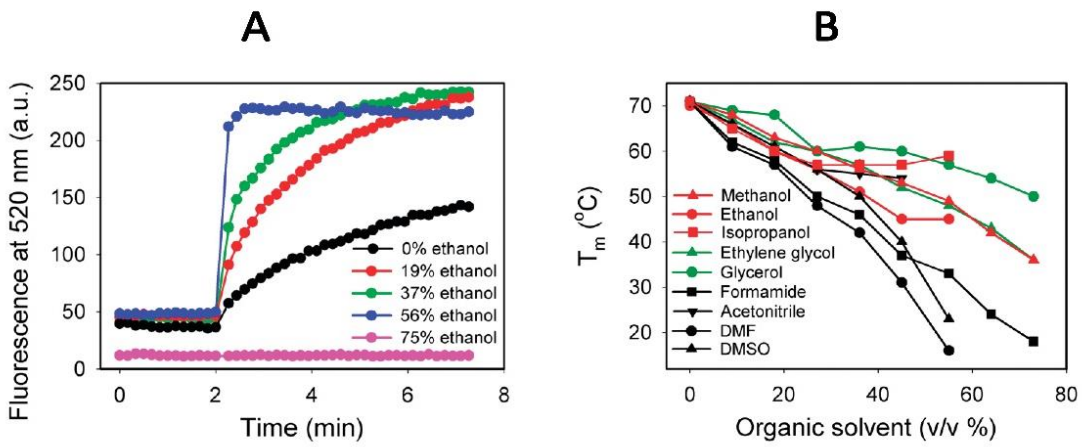

Figure 1.5. (A) Kinetics of molecular beacon hybridization in 300 mM NaCl 10 mM HEPES, pH 7.6 with different ethanol percentages and with 50 nM molecular beacon and 200 nM target DNA. (B) Melting temperatures of the molecular beacon hybridized to the target DNA in 300 mM NaCl, 10 mM HEPES, pH 7.6 with various percentages of molecular solvents. Reproduced with permission from ref. 106.

However, it is interesting to broaden the plethora of alternative media and ionic liquids were proposed as an alternative a decade ago. Ionic liquids offer a much greater diversity of environment compared to crowded and confined media or polyol solvents, as they can have multiple combinations of cation and anions. The possibility of solvating DNA in almost anhydrous media cannot be achieved with any salt or crowding agent, i.e. PEG saturates in water at a maximum concentration of 60 wt %[117]. Moreover, with most molecular solvents or even polyols, short duplexes would not be stable at RT in anhydrous media. ILs offer the possibility of improving the trade-off between water reduction and thermal stability of the duplex apart from having unique properties as solvents.

Firstly, DNA was started to be studied in imidazolium-based ILs, as they were the best known class of these solvents, had low viscosity, had high nucleobases-solubilizing ability[118] and had been previously used to increase conductivity of DNA films[119,120]. At low concentrations, these ionic liquids behaved as salts stabilizing duplex structures effectively, differently from molecular solvents and caused by the charged nature of ILs, but while using them at more than 15-30 wt % they destabilized DNA[121,122]. It was found that anions used, usually composed by functional groups, competed with Watson-Crick base-pairing *via* hydrogen bonding interactions[123], but their hydrogen bonding ability could be tuned and reduced[124,125].

On the other hand, even if they can act as counterions[126], imidazolium cations had also a destabilizing effect because apart of forming hydrophobic[127] and H-bonds[128] interactions, its planar charged ring has been proposed as intercalating and destabilizing agent at high concentrations *via* NH-π interactions[129–132]. As seen at highly crowded conditions and molecular

solvents, long dsDNA such as that of calf-thymus or salmon-sperm was able to maintain the duplex structure at RT and high concentrations of these ILs (up to 75 wt %)[133,134], but DNA nanotechnological applications usually use shorter duplexes.

ILs based on alkylammonium cations[135] were soon presented as an alternative to imidazolium- or morpholinium-based[136] ILs. Firstly, because salts containing these cations had previously probed to maintain short duplexes stable at high concentrations[137–139] and secondly, because there were already studies about the protein solvation capacity of these ILs[140], which allowed the use of enzymes at very high temperatures[141,142]. It was seen that salmon-sperm and calf-thymus DNA were stable in choline-based ILs with different anions[143] and lower hydration levels of the duplex could be achieved to obtain the same thermal stability than that of imidazolium-based ones[144,145].

The enhanced thermal stability of DNA in this ILs is explained principally by the chemo-physical differences between imidazolium- and alkylammonium-based cations, as anions are in general the same[146]. Between the huge variety of possible anions, small ones offer relative low viscosity and wide liquid range to the IL, i.e. choline lactate[147] (CL) or choline formate[148,149]. (CF) that are liquid in a range from -70 to more than 200 °C in anhydrous conditions. Other choline-based ILs just need small amounts of co-solvents (20 wt % water) to be in a liquid state at RT, as it is the case of choline dihydrogenphosphate (CDHP) or choline nitrate (CN)[150,151] and in the last years, alkylammonium ILs based on biocompatible anions are being developed[152]. However, the nanostructure of neat[153,154] and aqueous[155–157] ionic liquid media is still matter of study what is necessary to further predict DNA solvation.

There are different *in vitro* and *in silico* studies that aim to understand the main solvation mechanisms of DNA in presence of these ILs. In case of the cation, it seems to be more appropriate than larger ones such as imidazolium, because the latter are less effective at shielding the charged phosphate residues in B-form as they cannot approach to the DNA backbone as closely as choline[138]. Moreover, the hydrogen-bonding ability with water and DNA allows choline to stay more time close to DNA backbone than sodium or imidazolium what improves the stabilization capacity at low concentrations[158,159].

There are very few systematic studies about DNA solvation, but recently it was published one where multiple tetraalkylammonium-based ILs were used as co-solvents to solvate salmon-sperm DNA[152]. It was possible to detect the main interactions in the backbone that affect dsDNA stability in IL aqueous solutions using NMR technic. It was seen that at low concentrations (5 wt. %), less electrostatic interactions are established between the IL cation and the DNA phosphate groups compared with slightly higher IL concentrations (30 wt. %). On the other hand, at these higher concentrations, ILs could compete more effectively with water molecules for the dsDNA phosphate backbone, as seen in the decrease of the ^{31}P NMR intensity peak values. Moreover, the hydrophobicity of the IL cation played a main role since an increase in the DNA ellipticity and a decrease in π–π base stacking was observed with more hydrophobic ILs cations, leading to the perturbation of the dsDNA native B-form conformation.

Regarding the interactions with the base-pairs, studies conducted by the group of Naoki Sugimoto found that tetraalkylammonium-based salts and ILs interact with the base pairs of B-form duplexes mainly throw H-bonding[160] and in a very specific manner, destabilizing more GC-

rich duplex sequences than AT-rich ones, to the point that they can even have similar melting temperatures[161]. The latter was not surprising as it was previously observed in alkylammonium osmolytes such as glycine betaine[162–165]. Presumably these cations bind strongly to guanine and cytosine bases when they are not paired[166] and preferentially interact with the AT minor groove due to its narrower width and more electrostatically polar environment relative to the major groove (Figure 1.6). This specific behaviour has been proposed as the reason for the enhanced destabilization of GC- over AT-rich sequences which is not observed with other cations[167].

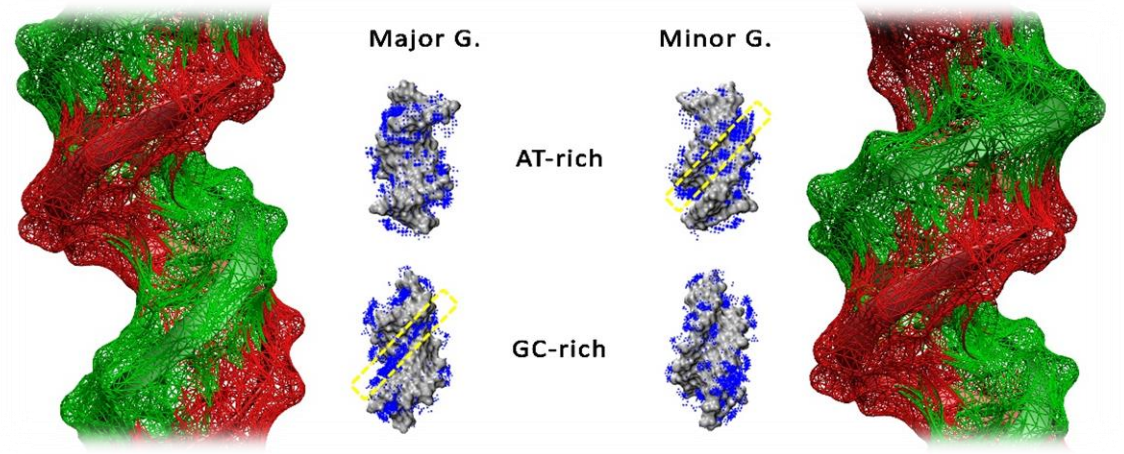

Figure 1.6. Base-specific interactions between choline cations (blue dots) and DNA major and minor grooves. Adapted with permission from ref. 166.

The library of possible choline-based media has been recently expanded with deep eutectic solvents[168,169], which are usually formed by choline chloride salt as hydrogen bond acceptor (HBA) group and polyols or urea as hydrogen bond donor (HBD) groups[170–176]. These can be obtained with a lower cost and greener synthesis compared with ILs. At this moment, there are fewer studies about the solvation of DNA duplexes in DES media than in ILs. Probably

because at high concentrations the thermal stability of DNA duplexes is equally or even more reduced than using ionic liquids with the same cation, principally due to the HBD group[177]. Therefore, the challenge of maintaining the thermal stability of short duplexes in absence of water cannot be faced at least with DESs studied so far. DES has been applied in neat conditions to longer duplexed structures that remain stable at room temperature.

It has been reported that it is possible to form self-assembled nanostructures with duplexes of 32 base pairs at RT[178]. In that study, the solvent consisted in a mixture of choline chloride with glycerol (1:4 molar ratio) and different DNA nanostructures where built in anhydrous or residual water conditions. Apart from maintaining its B-form double helical structure at room temperature, it was found that the design reached to a new thermodynamic minimum compared with aqueous media, maximizing the base pairings. This could not be achieved in physiological media because the intermediate shapes had an enhanced stability in aqueous media.

Leaving aside the thermal stability, ILs and DESs offer new opportunities for DNA nanostructures, i. e. achieving the energetically lowest landscapes as in the previous study it was possible to prevent the mechanical strain induced by the crossovers[179], increasing the usage time of DNA nanostructures[180]. Therefore, in sensing, nanofabrication or nanoelectronics technologies, these solvents might present opportunities other than negligible solvent volatility and prevention of DNA degradation but there is still a lot of research to be done. On the other hand, during the self-assembly in that DES, it was possible to control the folding kinetics changing the viscosity of the solvent, varying from less than 3 hours to more than 6 days.

The structure of the different forms of the DNA double helixes in ILs and DESs can be of interest not only from the nanotechnological but also from the fundamental point of view, because they could help understanding how DNA structure is regulated into the cell. It is known that the B-form DNA can be locally transformed into A- and Z-forms that usually keep the Watson-Crick base pairing but helix structure is altered or even left-handed as it is the case of the Z-form (Table 1.1). Regarding its biological role, i.e. the Z-form is recognized with high affinity and great specificity by certain classes of proteins[181].

Table 1.1. General properties of B-, A- and Z-forms of DNA.

	B	**A**	**Z**
Helix sense	Right handed	Right handed	Left handed
Bp per turn	10	11	12
Vertical rise per bp	3.4 Å	2.56 Å	19 Å
Rotation per bp	+36 degrees	+33 degrees	-30 degrees
Helical diameter	19 Å	19 Å	19 Å

From a nanotechnological point of view, this could be useful i.e. to expand the utility of DNA-hybrid catalysis or create new nanostructure designs for sensing and actuation at the nanoscale[182,183]. In a systematic study of several short double helixes, it was found that in neat reline DES the duplexes can adapt partially the A- and Z-forms depending on their sequence[144]. It is also interesting that ILs and DESs have the ability of displacing sodium cations from DNA what can be used as co-solvents to accelerate the recovery of B-form duplexes after being stored in ethanol solution in condensated A-form[184]. However, more studies are needed to understand the interconversion mechanism in both directions.

Moreover, even if the general structure of double helixes is not altered at low concentrations, their mechanical properties can be changed upon addition of ILs and DESs. The persistence length of DNA is higher in presence of ILs[185–187], something contrary to what was found with common salts and this can prevent the entanglement of the double-helix that is an issue in sensing applications[188]. It is suggested that the greater number of interactions formed between ILs and DNA grooves compared with common salts and the release of water molecules close to DNA are the major reasons for the increase in DNA rigidity[189,190].

1.3.2 While forming Hoogsteen and other non-canonical interactions

There is evidence about the presence of Hoogsteen base pairs in double helixes, especially for A- and Z-forms[191]. Nevertheless, HG interactions are well known for being of three non-canonical structures of DNA: G-quadruplexes, i-motifs and triplexes[192] (Figure 1.7). These structures are of upmost importance in cells to perform specific DNA and RNA functions[193–195] and are also part of different nanotechnological applications[196,197] such as sensors[198,199], gating systems[200201] or nanomachines[202]. *In vitro* and using physiological media, acidic conditions or specific metallic cations are needed for their formation[203–205]. But contrary to what happened with Watson-Crick based structures, non-physiological conditions can enhance the thermal stability of these structures, because they are naturally designed to work at lower hydration levels[206,207].

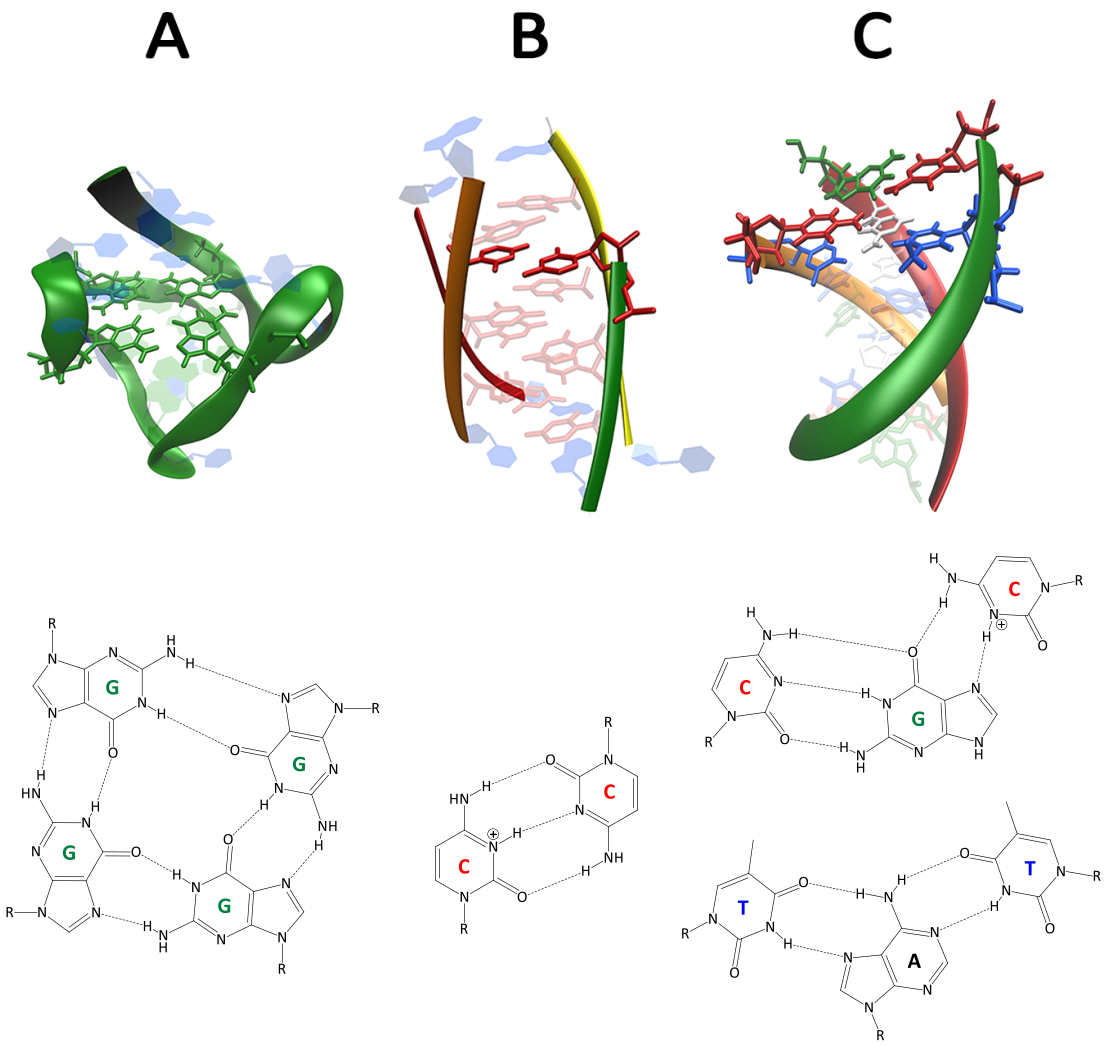

Figure 1.7. Different secondary structures of DNA that are formed throw Hoogsteen base pairing. (A) Intramolecular G-quadruplex (PDB: **2hy9**). (B) Intermolecular i-motif (**1cn0**). (C) Intermolecular triplex (**149d**).

In nature, these structures are formed usually with the partial denaturation of the duplex, in example to create parallel or anti-parallel G-quadruplexes, as has been seen *in vivo*[208]. Usually the environment of cell nucleus is mimicked with crowding agents, i.e. parallel[209,210] and antiparallel[211] G-quadruplexes formed in crowded and confined media have been applied in

biosensing[212]. The dehydration capacity of PEG also served to stabilize i-motifs[213] and triplexes[89,214,215]. The studies about non-canonical structures in cellular-like environments have been revisited very recently in an extensive review[216]. These can enable the development of therapeutic strategies for cancer, neurodegenerative, and age-related diseases by targeting specific non-canonical structures of nucleic acids or the design of DNA designs that can function in intracellular environments[195,217].

However, for nanotechnological purposes, the use of crowding or confinement strategies might not be appropriate, as they need macromolecular solutes that narrow the working conditions or need complex designs[218,219]. Solvents other than water could be more versatile as they can be finely tuned. In case of molecular solvents, only few of them are able to enhance thermal stability of non-canonical structures, probably due to their apolar behaviour[220,221]. The melting temperature only increased, compared to physiological media, while conjugating DNA with lipids, other surfactants[222] or adding polyethylene glycol (PEG) to the oligonucleotide chain (DNA PEGylation[223]), as it is the case of these DNAzymes that remained active in methanol[224,225]. Fortunately, ILs and DESs offer a more favorable media to solvate G-quadruplexes, i-motifs and triplex structures without the need of modifying DNA.

There are few studies about their use, but it was seen that choline dihydrogenphosphate (CDHP) ionic liquid increases the melting temperature of the three types of structures, comparing with physiological media[226–230]. Very recently, it was verified for the first time and using ionic liquids, the presence of G-quadruplexes in extracellular DNA structures that are used by *P. aeruginosa* in the formation of biofilms[231] that are used as protection[232]. These G-

quadruplex structures could not be detected using apolar solvents in extractions procedures because they lyse biofilms, but the use the ionic liquid maintained the networked structure and it was found using NMR that G-quadruplexes were essential for its formation.

Unaware that nature was already doing so, the tetrameric conformation of guanines has been already used to produce viscoelastic hydrogels[233–235] and conductive nanowires[236]. Recently, the G-based higher order structure has been formed for the first time in a deep eutectic solvent and was named as "G4 eutectogel"[237], showing viscoelastic properties, injectable nature, high thermal stability and ionic conductivity that make these eutectogels well suited for use in flexible optoelectronic devices. The latter example is based in individual guanine molecules, but it is known that G-quadruplexes formed by DNA has also an enhanced thermal stability in DES compared with physiological or crowded media[238] (so far, only probed with parallel G-quadruplexes). H-bonds are pointed as the main forces that enhance the thermal stability of these G-quadruplexes in reline and can be formed even in absence of metallic cations[238].

As observed in DNA double helix, the effect of urea on DNA is different when it is part of a DES (reline) or it is solvated in pure water. The same concentration of urea that would denature DNA in aqueous media[239–241] can stabilize G-quadruplexes in presence of choline chloride[242]. Moreover, tuning the solvent it is possible to achieve new secondary structures as those obtained with the human telomere sequence $((TTAGGG)_n)$[243] and the previously mentioned thermal stability of G-quadruplexes in reline has been further applied in nanotechnological designs[244]. Moreover, the thrombin binding aptamer (TBA) which recognition

site is based-on a G-quadruplex can be used also in this media[245]. Unfortunately, the recognition capacity of the TBA was not matter of study, just the structural and thermal stabilities.

1.3.3 While forming interactions with target molecules

It is of upmost importance to not only study the static structures that DNA can adopt in ILs and DESs, but also the dynamic movements of these conformations when they are part of functional nucleic acids (FNAs). In this work, aptamers are considered as the main FNA to create dynamic DNA nanotechnology. However, DNAzymes or their RNA equivalents (ribozymes) are also capable of giving dynamic action, although they are especially used in catalysis and their recognition capacity is focused on metal ions. In addition, a recently published review has already dealt with the ability of the latter to function in non-physiological environments[246].

The use DNA-aptamer in non-physiological media would allow the detection of new targets (hydrophobic, negatively charged and planar molecules) or the use of DNA-based sensing devices for long-periods among other benefits. Another advantage is that kinetics might be accelerated in these media due to a reduction in the thermal stability of certain structures that are formed in absence of the target as in case of FNAs based on stem-loops[247] or molecular beacons[248]. However, these solvents might have an effect on the molecular recognition site of DNA-aptamers, which may loose sensitivity and selectivity, because they ensure fitting and high specificity toward their targets through multiple molecular interactions as well as steric arrangements based in a non-covalent and an energetically favourable interaction. All of these are optimized for the incubation media used in SELEX technic[249] (Figure 1.8).

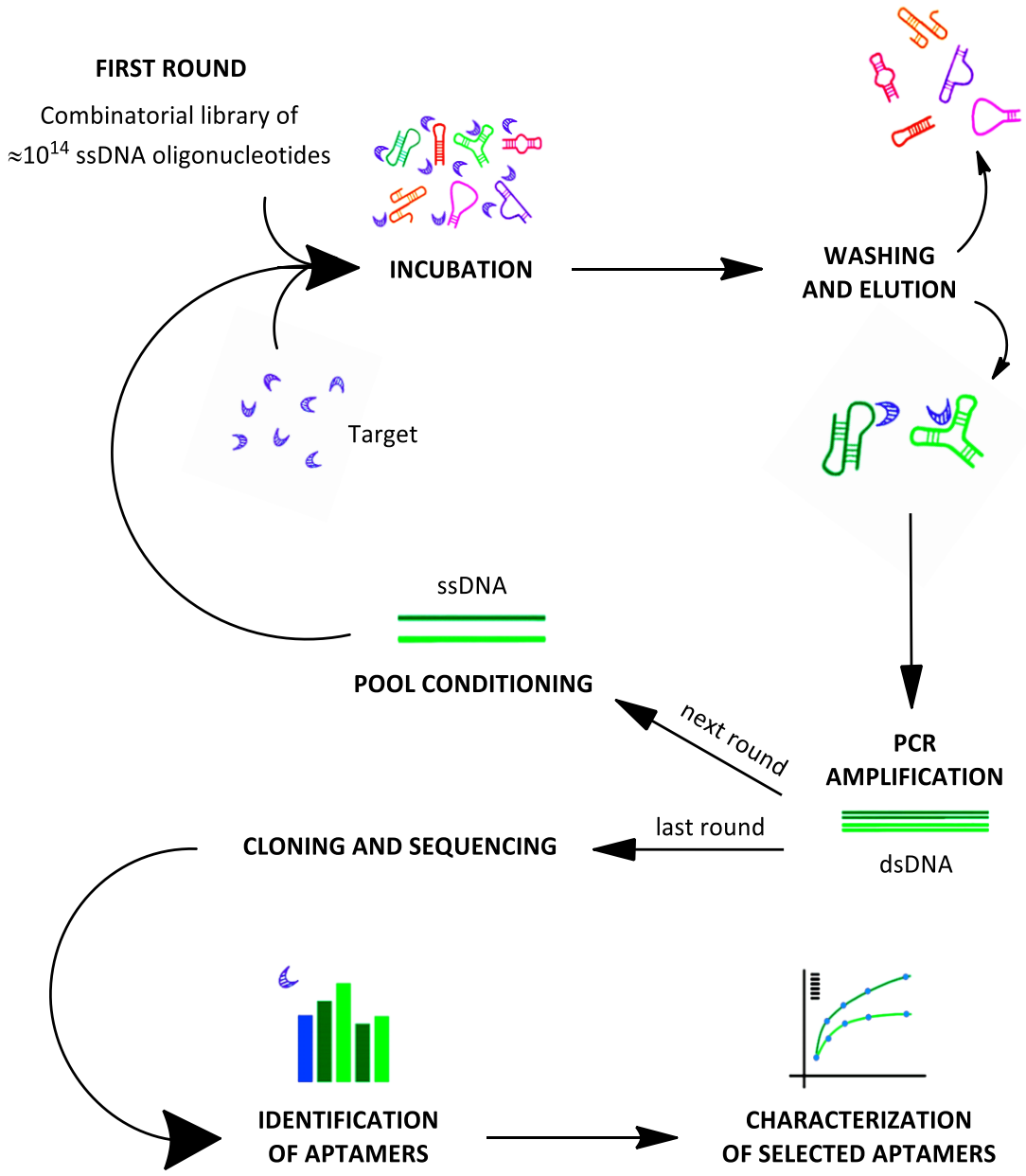

Figure 1.8. A schematic representation of the conventional SELEX procedure.

It is not surprising that the ATP DNA-aptamer originally reported by Huizenga et al. in aqueous buffer[74,250], was able to maintain its function in a hydrated alkylammonium ionic liquid at least until 20% (v/v), but with a significantly reduced extent[251]. This shows that changing media conditions will in many cases need a repetition of SELEX, what is time and cost consuming. However, the repetition or the realization of new selections in ILs and DESs might bring new opportunities because these media conceive a toolbox comprising the versatility of functional nucleic acids and the tuneability of the solvent, which would enable a selection of unprecedented sequences for previous and new targets.

To this day, two studies have repeated a SELEX using high contents of non-aqueous solvents. In the first case, methanol in 25% (v/v) was used[252], and DNA was modified to increase its potential interactions and solubility in the organic media[253,254] but at the same time complicating the procedure and raising its costs. They obtained an adenine aptamer with higher binding affinity in methanol than the original aptamer selected in aqueous media, but in expense of the modified nucleotide to achieve this enhanced affinity and target specificity.

In the second case, not-modified DNA-aptamers were selected using deep eutectic solvents[255], specifically ethaline solvent[256,257].These selection was done towards a 33-mer peptide of gluten, which is usually recognized by antibodies but these have low efficiency in extraction media. Those sequences with a recognition motif similar to the aptamers selected in aqueous media but new secondary structure were studied, and these could recognize the peptide in ethaline media with similar sensitivity. Unfortunately, a vast number of sequences

appeared while sequencing (830000) and due to this, it was not possible to study if those with new motifs had an enhanced recognition capacity.

Then, the challenge has remained to prove that sequences of FNAs can exist which are different from those encountered in mainly aqueous solutions and which are particularly better adapted to work in non-physiological environments.

1.4 DNA nanotechnology in non-physiological media

DNA nanotechnology started in the 80s[258,259], with the aim of creating 2D and 3D immobile networks using a Holliday Junction[260]. This approach has enabled the construction of nanostructures with high accuracy for further use in crystal engineering, due to the formation of regular lattices able to act as host scaffold for guest molecules[261] and it continued gaining complexity and nanoscale accuracy with the introduction of DNA-origami[262,263]. The aim was to create higher ordered DNA nanostructures as template, for synthesis, characterization or sensing for applications such as X-ray[264,265], single-molecule studies[266], or drug/gene delivery[267].

However, nowadays these designs have evolved[268] to include also a dynamic behaviour and a wider variety of uses that need an optimal trade-off between static structural stability and dynamic behaviour. A widely used mechanism in these designs is the strand displacement reaction (SDR)[269–271]. This plays a key-role to create nanomachines that include nanotweezers[272] and DNA walkers[273] or platforms as DNA circuits or logic gates[274,275], nanochannels[276], dynamic origami objects[277] or the creation of diagnostic tools and sensors[278,279] to be used *ex vivo*[280,281] and *in vivo*[282,283].

On the other hand, the molecular recognition capacity of DNA using DNA-aptamers[284,285] or DNAzymes[286,287], are also of upmost importance, improving the variety of dynamic functions that previous designs can achieve. DNA-aptamers are used in a wide variety of fields[288], as biosensors in order to detect allergens, pathogens and toxins[289] or as an alternative to antibodies[290]. Moreover, their conformational change upon target recognition make them suitable to be used in nanopores as drug-delivery systems, as sensors or as gatekeepers in a

single-molecule manner[291]. In case of DNAzymes, they are usually specific to metallic cofactors and are able to cleave specific bonds; they are used as gene-silencing agents[292] or in sensors[293] and can be integrated in bigger structures as happens with DNA-aptamers[294]. Moreover, thanks to its programmability, biocompability and modular nature[295,296], DNA can also form hybrid nanostructures with other materials, such as peptides[297], hydrogels[298–300], dendrimers[301], nanotubes[302] or nanoparticles[303,304].

Some of these nanotechnological designs are patented and few are being commercialized[305], the latter cases are based on DNA-origami for super-resolution microscopy[306], DNA microarrays[307] and drug-delivery[308]. As explained in previous section, new opportunities could emerge solvating nucleic acids in non-physiological media, especially in ionic liquids and deep eutectic solvents. In this manner, it can be possible to face solvent evaporation, DNA degradation or bottlenecks in the dynamic function without being necessary the chemical modification of nucleic acids[309].

At first, the use of these solvents was intended only to replace molecular solvents in different procedures, such as extraction[310–315] and purification[316,317] applications because ILs and DESs not evaporate and their chemo-physical properties can be finely tuned to optimize product recovery, moreover they can be magnetic to facilitate DNA extraction[318–320]. They have been also proposed as co-solvents in polymerase chain reaction (PCR) to enhance the traditional and isothermal amplifications or extraction procedures[320–322] because ILs can reduce the melting temperature of DNA duplexes without affecting the efficiency of the enzyme, in contrast to organic solvents. But after foretelling their potential while observing that DNA could maintain

its structural stability in ILs and DESs[323,324], they started to be used as main media for DNA nanotechnological applications[325–328].

1.4.1 DNA-linked gold nanoparticles

One of the first studies where ILs were used as main media for a technological application showed that DNA-linked gold nanoparticles, which are usually used in aqueous colorimetric biosensing, could be used also in a great variety of hydrated ILs up to 60 wt % in water preventing DNA degradation. In similar conditions using molecular solvents, the DNA lost its hybridization capacity and the nanoparticles aggregated[329]. In this article, ethylammonium and propylammonium nitrate ILs were presented as better solvent candidates than the better-known imidazolium-based ILs, as it was found that DNA and gold nanoparticles solvated better in the former two. This marked a precedent for future studies.

A drawback found in this work related with nitrate anion-based ILs was that even if they can effectively solvate DNA, they adsorb strongly in UV region overlapping with DNA spectra what limits several sensing applications. Fortunately, the multiple possible combinations of cations and anions have solved this issue in future studies, maintaining the cations but using lactate or phosphate anions instead (Figure 1.9).

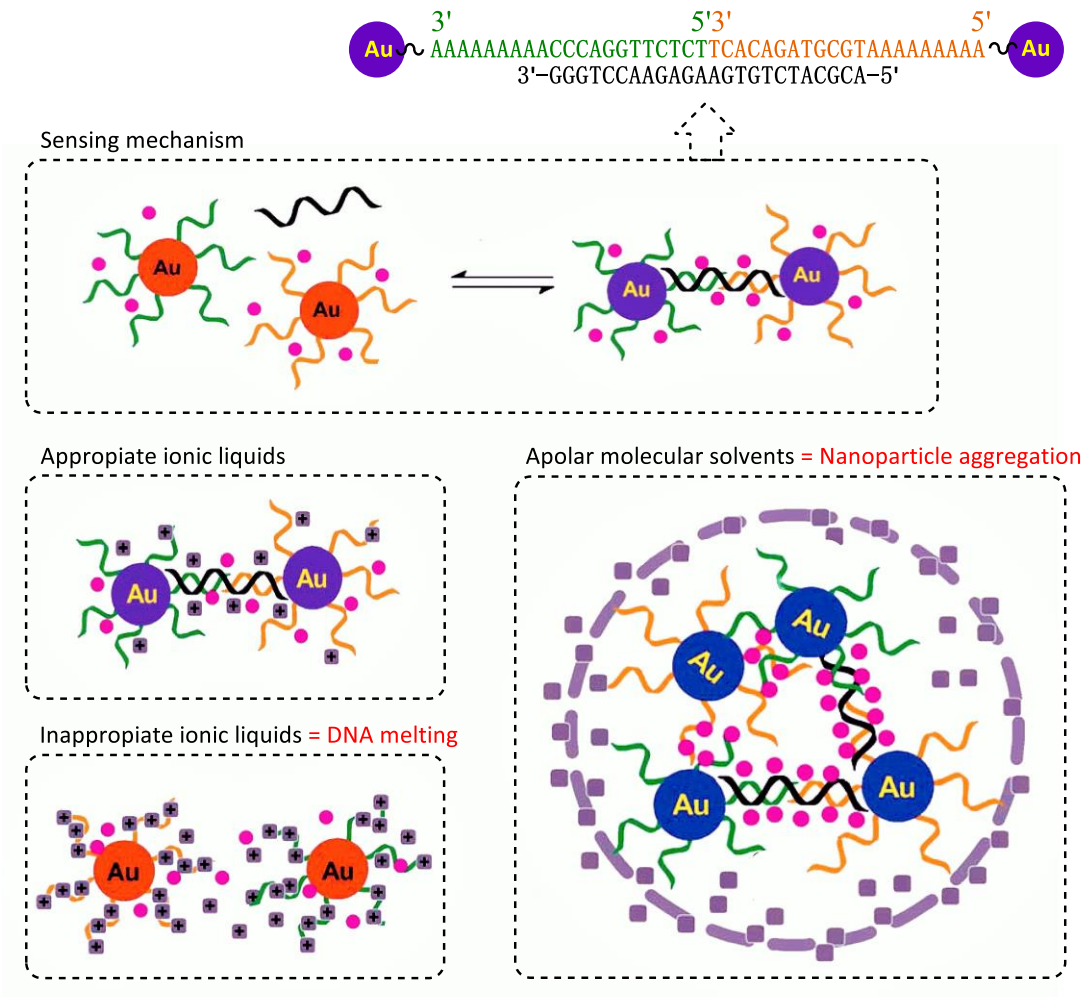

Figure 1.9. The sensing mechanism of gold nanoparticles and situations found in different non-physiological media. Adapted with permission from ref. 329.

1.4.2 Triplex-based devices

More sophisticated nanotechnological applications based on ILs emerged while understanding better the behaviour of DNA in them[324], as it is the case of triplex-based sensors. Microarrays, a common method used for DNA sequence sensing in aqueous media require to

have the analyte sequence as a single-stranded DNA (ssDNA) because they are based on Watson-Crick base-pairing[330,331]. Therefore, there is interest in being able to detect specific sequences directly in a double-stranded DNA (dsDNA) form to simplify the procedure[331]. For that purpose, the ssDNA of the sensor forms a triplex structure with the dsDNA of the analyte. Unfortunately, mismatch discrimination of triplex structures in aqueous media is low, giving rise to false positives.

The thermal stability of the triplex was enhanced using a hydrated alkylammonium IL (70 wt % of CDHP in water) and in this manner it was possible to improve the mismatch discrimination capacity. It was also possible to prevent the degradation of DNA in the sensor inhibiting the nucleases and controlling water activity even at pH7[332]. Computationally, it was observed that the increase in thermal stability was mainly due to the stabilization of the Hoogsteen base pairs by choline cations that bind specifically to the third strand[228], because HG interactions are more stable in dehydrated conditions.

1.4.3 Hemin/G-Quadruplex designs

The use of a task specific ionic liquid (TSIL) with a DNAzyme improved its matrix interference resistance[333]. Firstly, the TSIL was used to extract selectively the metallic ions from the sample and then, the TSIL solution was diluted in an aqueous solution containing the DNAzyme that was structurally stable in presence of this ionic liquid. The DNAzyme can only form a G-quadruplex if there is Hg^{2+} in the media. Then, this secondary structure coordinates with Hemin and give a colorimetric response[334]. Using the ionic liquid that specifically extracted mercury, in

this procedure it was possible to reduce interferences of other metallic ions that could also provoke the formation of the G-quadruplex.

1.4.4 Sandwich-assays for hydrophobic compounds

Very recently it has been published the first aptasensor that works in an almost anhydrous deep eutectic solvent[335]. The aptasensor sequence was obtained in the previously mentioned SELEX done in ethaline[255] (choline chloride/ethylene glycol (1:2)). The ethaline DES was able to extract efficiently gluten from food it can also solvate greater concentrations of DNA than physiological media apart from keeping it stable and be liquid between -60 and 200 °C[336]. The design of the sensor is based on a truncated aptamer that allows the creation of a sandwich-type assay. Furthermore, the sensitivity of the assay was improved compared to aqueous media due to an increased peroxidase activity in this type of DESs[337].

1.4.5 The combination of DNA and metals for catalysis

An application of DNA related with catalysis is its use as template to perform different reactions. One strategy is to synthesis nucleic acid analogues with different functional groups[338–341]. But, it is also possible to use natural DNA, the cornerstone of this text, in example DNA double-helixes or more complex DNA nanostructures can be metallized reducing the ions when they are in contact with DNA backbone[342,343]. New opportunities can appear while combining non-aqueous media with the inherent chirality and nanostructure of DNA because this media could expand the scope of reactions, improve their enantioselectivity and fasten the kinetics apart from keeping DNA stable for long periods. Different modifications of DNA nucleotides have

been already done in ILs[344] and DESs[345,346], but there is one study where ethaline DES was used not only to prepare metallized DNA (Pd−DNA−Fe_3O_4 dual functionalized) but also perform the successive C−C coupling and reduction reactions[347]. Using this strategy, the long duration of synthesis process and loss of DNA helicity that encountered in aqueous media were reduced, moreover, the recyclability of the solvent made it greener and scalable (Figure 1.10A).

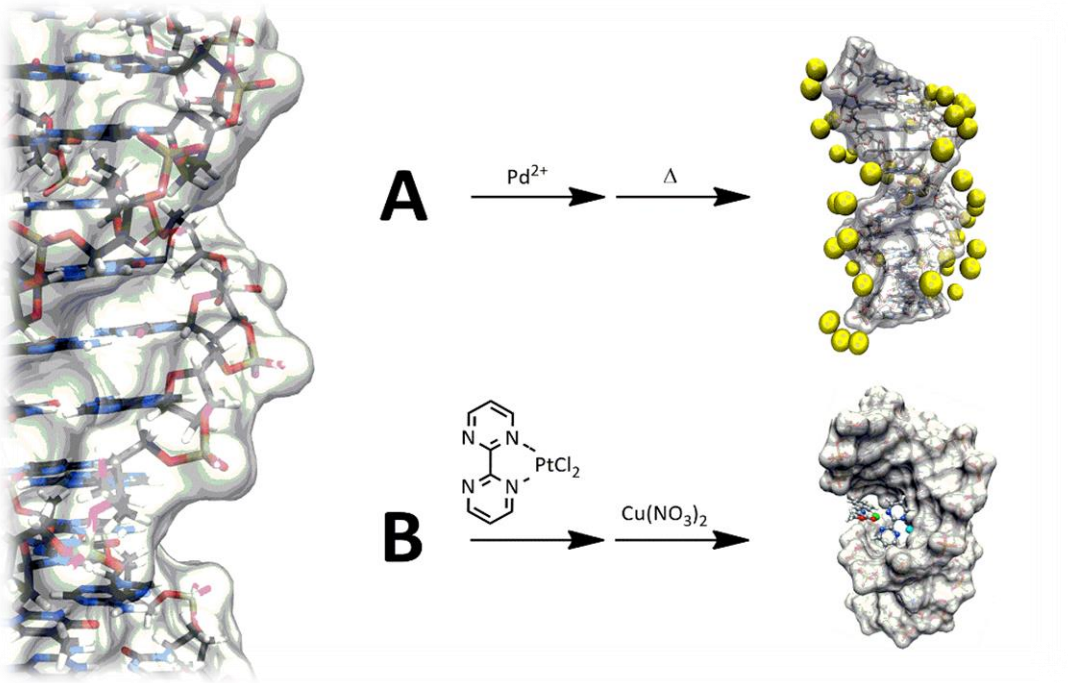

Figure 1.10. A schematic representation of (A) DNA metallization in presence of DES and (B) a metal complex anchored to DNA. Adapted with permission from ref. [348].

On the other hand, DNA has been proposed as support for asymmetric catalysis using metal complexes[349–351]. The inherent chirality of dsDNA can be transferred to metal complexes anchored with aromatic groups that are intercalated in a noncovalent manner between guanines[348,352–354] (Figure 1.10B), the procedure is simpler and have lower cost than modifying

DNA with previous methods. However, so far, ILs and DESs have only been used in a Michael reaction as co-solvents at low concentrations[355,356], but considering the plethora of enzymatic reactions that can be found in neat media[357–362] and the possibility of using G-quadruplexes[363], which are highly stable in ILs and DESs, probably similar works that use DNA will emerge.

1.4.6 DNA functionalized carbon nanostructures

Graphene and carbon quantum dots are nanostructures with sizes below 100 nm and potential applications in many technological fields such as sensors, bioimaging[364], photochemical catalysis or photovoltaic devices[365]. At first the use of DNA with these nanomaterials was intended to prepare solid films with higher mechanical properties[366,367], but nowadays its uses include also sensing using DNA base-pairing or DNA-aptamers. ILs and DESs are included in the design as media able to solubilize DNA and prevent the aggregation of graphene[368–370].

Actually, DNA is not solvated in the ILs or DESs in the sensing step, therefore these designs are somewhat removed from the context discussed in this text. But, among other advances[371], it is remarkable that these studies have aided to create a graphene field-effect transistor which in the wake of the global pandemic of COVID-19 is able to detect the SARS-CoV-2, using DNA as a complementary sequence and an ionic liquid to modulate the charge transport in the semiconductor device[372] (Figure 11).

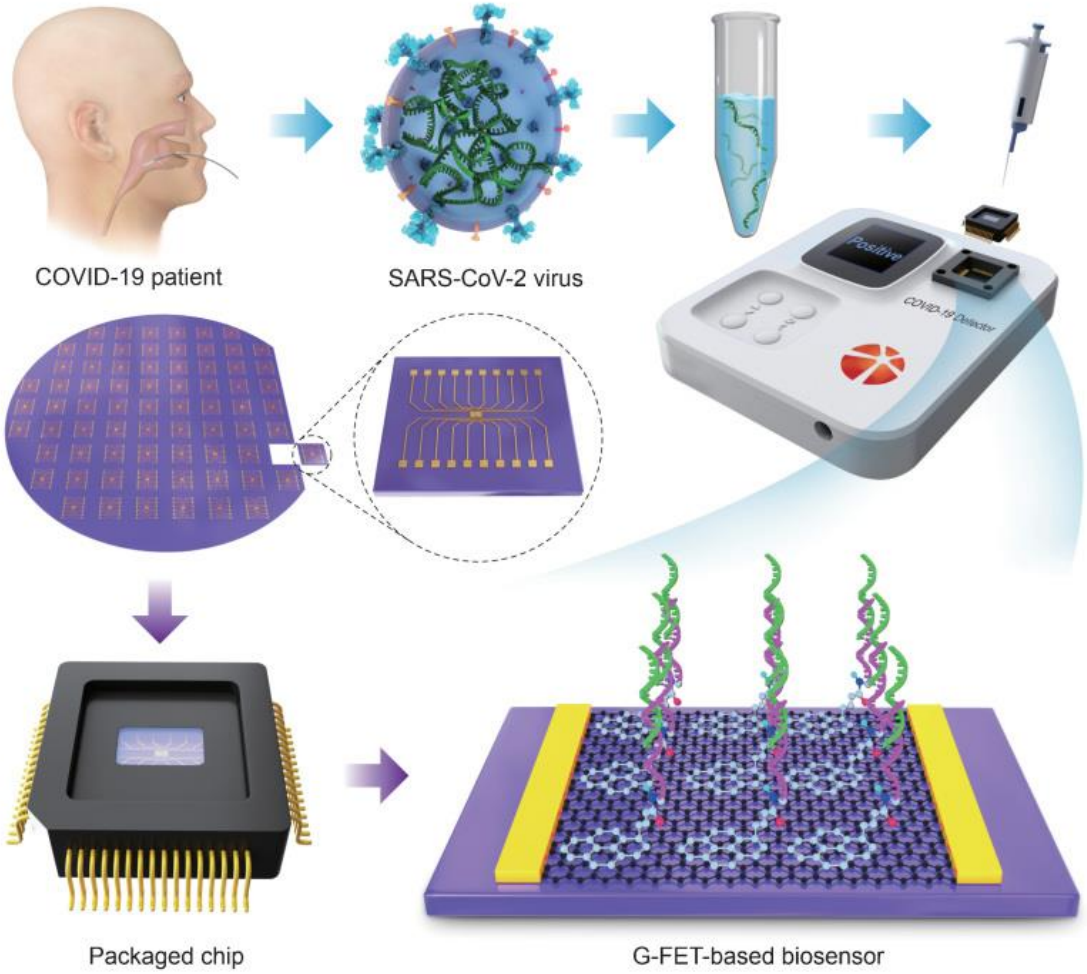

Figure 1.11. The graphene field-effect transistor containing DNA and ionic liquids. Reproduced with permission from ref. 372.

1.4.7 Long-term use and storage of nucleic acids

IL and DES media have the potential of making DNA designs usable for long-periods or store at low-cost in a wide range of temperatures. The prevention of degradation seem to be always based on the reduction of water and nuclease activity and their interactions with DNA, what prevent the hydrolysis of the phosphodiester bond, depurination and deamination[24].

However, none of the studies done so far study these events at the molecular scale or consider if there could be another non-desired changes in the structure of DNA caused by ILs and DESs. Their degradation prevention capacity has not been quantified neither and it is not possible to predict the minimum amount necessary to maintain DNA stable for a concrete period.

Nevertheless, it is a great advantage to use these non-conventional media as has been seen in numerous studies that DNA remains stable after months or years at room temperature. In example, it was possible to store plasmid DNA or salmon-sperm and calf-thymus DNA up to six months[143] or one year[373,374] at RT, even in nuclease-rich samples[375,376]. Unfortunately, so far, there are no studies about the capacity of IL and DES to preserve DNA-origami nanostructures[377] or short DNA duplexes and other non-canonical structures for long-periods.

Apart from the long-term stability, another advantage of ILs and DESs is their nucleic acid solubilization capacity, which is higher than physiological media[378]. Up to now the solubility of DNA can already be of 25 wt % in an ionic liquid[379] and 5.5 wt % in a deep eutectic solvent[380]. On the other hand, as could be expected, the preservation strategy can be used also with RNA, but differently from DNA[381], acidic ILs or DESs (pH between 3.5 and 4.2) were not able to maintain the RNA primary structure in aqueous media being lost in few hours. However, they prevented RNA degradation in neutral and alkaline media (pH between 8.6 and 12.4) for at least one month[382], what denotes the importance of buffering these media[383]. Moreover, it is possible to extract the RNA directly from cells in the preservation media even in presence of nucleases, what eliminates the necessity of purifying the samples[384].

Recently, a patent was published were it is described a method to preserve DNA and RNA integrity at room temperature for at least two years using molten salts, similar to ILs but with a higher melting temperature. Instead of using choline-based ILs, they use aprotic-protic salts (APS) and add a minimum water amount to have then in a glassy state at RT[385]. Even if the storage conditions are not suitable for most nanotechnological uses at RT, this strategy allows the direct PCR amplification of nucleic acids and their better preservation due to a greater reduction of water activity and molecular motions. On the other hand, the long-term storage has been also studied with proteins and there are some ILs and DESs that could be successfully applied to nucleic acids in the future[386].

Furthermore, most of the studied ILs and DESs seem to be biocompatible[387], even if their toxicity is yet under study[388–390] there are some studies about the use of ILs and DESs with DNA *in vivo*. In example, ILs might be able to protect DNA of plants from fungicides by interacting with DNA groove and hindering it from dodine[391]. Related with therapeutics, different media have been already proposed to be used in topical skin delivery of nucleic acids, i.e. it was observed that a DNA nanostructure remain stable during the transdermal delivery[392], what can be used in example for treatment of psoriasis[393]. A very recent patent describe a method where deep eutectic solvents are used to deliver encapsulated viruses, what can be used for vaccines with enhanced long-term stability between 2-8 °C[394].

1.5 Conclusions

New opportunities for DNA nanotechnology emerge with the use of non-physiological environments, in this work the focus is put on ionic liquids and deep eutectic solvents with negligible volatility, wide liquid range and tunable chemo-physical properties[395–397]. However, the huge scope of possible media presents an intrinsic bottleneck due to the necessary costs and time to elucidate DNA behaviour in them in absence, so far, of theoretical or computational reliable methods able to predict DNA thermal and structural stabilities beyond physiological conditions[398].

As can be seen in the fundamental studies presented, the variety of media used so far is relatively narrow and in most cases the sequence and structure of DNA is not systematically studied. Even so, with the scientific evidence so far it is already possible to observe that these solvents have the potential to achieve new DNA conformations and stabilities that were limited by the use of water or media based-on molecular solvents or crowding agents that had a limited tuneability.

On the other hand, nanotechnological applications combining the use of these solvents and nucleic acids started to emerge in the last years demonstrating that there is growing interest in the field of nanotechnology for the use of non-conventional environments. So far, these have focused in sensing or long-term use and storage of nucleic acids, but there is a huge potential in other areas such as catalysis.

1.6 References

1. Kitadai, N. & Maruyama, S. Origins of building blocks of life: A review. *Geosci. Front.* **9**, 1117–1153 (2018).

2. Powner, M. W., Gerland, B. & Sutherland, J. D. Synthesis of activated pyrimidine ribonucleotides in prebiotically plausible conditions. *Nature* **459**, 239–242 (2009).

3. McDougall, I., Brown, F. H. & Fleagle, J. G. Stratigraphic placement and age of modern humans from Kibish, Ethiopia. *Nature* **433**, 733 (2005).

4. Stringer, C. Modern human origins: Progress and prospects. *Philos. Trans. R. Soc. B Biol. Sci.* **357**, 563–579 (2002).

5. Dahm, R. Friedrich Miescher and the discovery of DNA. *Dev. Biol.* **278**, 274–288 (2005).

6. KLUG, A. Rosalind Franklin and the Discovery of the Structure of DNA. *Nature* **219**, 808 (1968).

7. Kresge, N., Simoni, R. D. & Hill, R. L. Chargaff ' s Rules : the Work of Erwin Chargaff. *Biochemistry* **280**, 172–174 (2005).

8. WATSON, J. D. & CRICK, F. H. C. Molecular Structure of Nucleic Acids: A Structure for Deoxyribose Nucleic Acid. *Nature* **171**, 737 (1953).

9. Morange, M. History of Molecular Biology. *Encycl. Life Sci.* (2009). doi:10.1002/9780470015902.a0003079.pub2

10. Seeman, N. C. Nucleic acid junctions and lattices. *J. Theor. Biol.* **99**, 237–247 (1982).

11. Ghosh, A. & Bansal, M. A glossary of DNA structures from A to Z. *Acta Crystallogr. - Sect. D Biol. Crystallogr.* **59**, 620–626 (2003).

12. Hernandez, L., Machado, I., Schafer, T. & Hernandez, F. Aptamers Overview: Selection, Features and Applications. *Curr. Top. Med. Chem.* **15**, 1066–1081 (2015).

13. Guo, P. The emerging field of RNA nanotechnology. *Nat. Nanotechnol.* **5**, 833–842 (2010).

14. Bunney, P. E., Zink, A. N., Holm, A. A., Billington, C. J. & Kotz, C. M. The RNA 3D Motif Atlas: Computational Methods for Extraction, Organization and Evaluation of RNA Motifs. *Physiol. Behav.* **176**, 139–148 (2017).

15. Dunckley, T. & Parker, R. RNA Turnover. in (eds. Brenner, S. & Miller, J. H. B. T.-E. of G.) 1748–1751 (Academic Press, 2001). doi:https://doi.org/10.1006/rwgn.2001.1138

16. Neubacher, S. & Hennig, S. RNA Structure and Cellular Applications of Fluorescent Light-Up Aptamers. *Angew. Chemie - Int. Ed.* 1266–1279 (2018). doi:10.1002/anie.201806482

17. Ussery, D. W. DNA Structure: A-, B- and Z-DNA Helix Families. in *Encyclopedia of Life Sciences* (John Wiley & Sons, Ltd, 2002). doi:10.1038/npg.els.0003122

18. Fay, M. M., Lyons, S. M. & Ivanov, P. RNA G-quadruplexes in biology: principles and molecular mechanisms. **429**, 2127–2147 (2018).

19. Ellington, a D. & Szostak, J. W. In vitro selection of RNA molecules that bind specific ligands. *Nature* **346**, 818–22 (1990).

20. Tuerk, C. & Gold, L. Systematic evolution of ligands by exponential enrichment: RNA ligands to bacteriophage T4 DNA polymerase. *Science (80-.).* **249**, 505–510 (1990).

21. Geary, C., Rothemund, P. W. K. & Andersen, E. S. A single-stranded architecture for cotranscriptional folding of RNA nanostructures. *Science (80-.).* **345**, 799–804 (2014).

22. Jasinski, D., Haque, F., Binzel, D. W. & Guo, P. Advancement of the Emerging Field of RNA Nanotechnology. *ACS Nano* **11**, 1142–1164 (2017).

23. Chen, S. & Hermann, T. RNA-DNA hybrid nanoshapes that self-assemble dependent on ligand binding. *Nanoscale* **12**, 3302–3307 (2020).

24. Lindahl, T., Jones, I. L. . & Fiona, M. H. Instability and decay of the primary structure of DNA. *Nature* **362**, 709–715 (1993).

25. Ni, X., Castanares, M., Mukherjee, A. & Lupold, S. E. Nucleic Acid Aptamers: Clinical Applications and Promising New Horizons. *Curr. Med. Chem.* **18**, 4206–4214 (2011).

26. Caruthers, M. H. The chemical synthesis of DNA/RNA: Our gift to science. *J. Biol. Chem.* **288**, 1420–1427 (2013).

27. Ngo, T. T. M. *et al.* Effects of cytosine modifications on DNA flexibility and nucleosome mechanical stability. *Nat. Commun.* **7**, 1–9 (2016).

28. Singh, A. & Singh, N. Effect of salt concentration on the stability of heterogeneous DNA. *Phys. A Stat. Mech. its Appl.* **419**, 328–334 (2015).

29. Hong, F. & Šulc, P. An emergent understanding of strand displacement in RNA biology. *J. Struct. Biol.* **207**, 241–249 (2019).

30. Chalovich, J. M. & Eisenberg, E. Effect of Molecular Crowding and Ionic Strength on the Isothermal Hybridization of Oligonucleotide. *Biophys. Chem.* **257**, 2432–2437 (2005).

31. Simmel, F. C., Yurke, B. & Singh, H. R. Principles and Applications of Nucleic Acid Strand Displacement Reactions. *Chem. Rev.* (2019). doi:10.1021/acs.chemrev.8b00580

32. Yin, Y. & Zhao, X. I. N. S. Kinetics and Dynamics of DNA Hybridization. *Acc. Chem. Res.* **44**, 1172–1181 (2011).

33. Ouldridge, T. E., Šulc, P., Romano, F., Doye, J. P. K. & Louis, A. A. DNA hybridization kinetics: Zippering, internal displacement and sequence dependence. *Nucleic Acids Res.* **41**, 8886–8895 (2013).

34. Weaver, K. D. *et al.* Structure and function of proteins in hydrated choline dihydrogen phosphate ionic liquid. *Phys. Chem. Chem. Phys.* **14**, 790–801 (2012).

35. Tang, M. S. L. *et al.* An aptamer-enabled DNA nanobox for protein sensing. *Nanomedicine Nanotechnology, Biol. Med.* **14**, 1161–1168 (2018).

36. Armstrong, R. E. & Strouse, G. F. Rationally manipulating aptamer binding affinities in a stem-loop molecular beacon. *Bioconjug. Chem.* **25**, 1769–1776 (2014).

37. Stiehl, O., Weidner-Hertrampf, K. & Weiss, M. Kinetics of conformational fluctuations in DNA hairpin-loops. *New J. Phys.* **15**, 8602–8606 (2013).

38. Wang, T., Chen, C., Larcher, L., Barrero, R. A. & Veedu, R. N. Three decades of nucleic acid aptamer technologies: Lessons learned, progress and opportunities on aptamer development. *Biotechnol. Adv.* **37**, 28–50 (2019).

39. Lu, Y. & Liu, J. Functional DNA nanotechnology: emerging applications of DNAzymes and aptamers. *Curr. Opin. Biotechnol.* **17**, 580–588 (2006).

40. Xing, Y. *et al.* Self-assembled DNA hydrogels with designable thermal and enzymatic responsiveness. *Adv. Mater.* **23**, 1117–1121 (2011).

41. Soontornworajit, B., Zhou, J., Shaw, M. T., Fan, T. H. & Wang, Y. Hydrogel functionalization with DNA aptamers for sustained PDGF-BB release. *Chem. Commun.* **46**, 1857–1859 (2010).

42. Özalp, V. C., Schäfer, T., Gmbh, C. W. V. & Kgaa, C. Aptamer-based Switchable Nanovalves for Stimuli-Responsive drug delivery. *Chem. - A Eur. J.* **17**, 9893–9896 (2011).

43. Özalp, V. C., Pinto, A., Nikulina, E., Chuvilin, A. & Schäfer, T. In situ monitoring of DNA-aptavalve gating function on mesoporous silica nanoparticles. *Part. Part. Syst. Charact.* (2014). doi:10.1002/ppsc.201300299

44. Roy, D., Cambre, J. N. & Sumerlin, B. S. Future perspectives and recent advances in stimuli-responsive materials. *Prog. Polym. Sci.* **35**, 278–301 (2010).

45. Ruiz-Hernández, E., Baeza, A. & Vallet-Regí, M. Smart drug delivery through DNA/magnetic nanoparticle gates. *ACS Nano* **5**, 1259–1266 (2011).

46. Pinheiro, V. B. & Holliger, P. The XNA world: Progress towards replication and evolution of synthetic genetic polymers. *Curr. Opin. Chem. Biol.* **16**, 245–252 (2012).

47. Dunn, M. R., McCloskey, C. M., Buckley, P., Rhea, K. & Chaput, J. C. Generating Biologically

Stable TNA Aptamers that Function with High Affinity and Thermal Stability. *J. Am. Chem. Soc.* 0–3 (2020). doi:10.1021/jacs.0c00641

48. Arangundy-Franklin, S. *et al.* A synthetic genetic polymer with an uncharged backbone chemistry based on alkyl phosphonate nucleic acids. *Nat. Chem.* (2019). doi:10.1038/s41557-019-0255-4

49. Zhang, Q. & Landgraf, R. Selecting molecular recognition. what can existing aptamers tell us about their inherent recognition capabilities and modes of interaction? *Pharmaceuticals* **5**, 493–513 (2012).

50. Nakano, S. I., Yamaguchi, D., Tateishi-Karimata, H., Miyoshi, D. & Sugimoto, N. Hydration changes upon DNA folding studied by osmotic stress experiments. *Biophys. J.* **102**, 2808–2817 (2012).

51. Ellis, R. J. Macromolecular crowding: Obvious but underappreciated. *Trends Biochem. Sci.* **26**, 597–604 (2001).

52. Sasaki, Y., Miyoshi, D. & Sugimoto, N. Regulation of DNA nucleases by molecular crowding. *Nucleic Acids Res.* **35**, 4086–4093 (2007).

53. Gates, K. S. An overview of chemical processes that damage cellular DNA: Spontaneous hydrolysis, alkylation, and reactions with radicals. *Chem. Res. Toxicol.* **22**, 1747–1760 (2009).

54. Han, H. & Hurley, L. H. G-quadruplex DNA: A potential target for anti-cancer drug design. *Trends Pharmacol. Sci.* **21**, 136–142 (2000).

55. Cheng, C., Jia, J.-L. & Ran, S.-Y. Polyethylene glycol and divalent salt-induced DNA reentrant condensation revealed by single molecule measurements. *Soft Matter* **11**, 3927–3935 (2015).

56. Shrestha, P. *et al.* Confined space facilitates G-quadruplex formation. *Nat. Nanotechnol.* 1–8 (2017). doi:10.1038/nnano.2017.29

57. Seeman, N. C. & Sleiman, H. F. DNA nanotechnology. *Nat. Rev. Mater.* **3**, (2017).

58. Keller, A. & Linko, V. Challenges and Perspectives of DNA Nanostructures in Biomedicine. *Angew. Chemie - Int. Ed.* 15818–15833 (2020). doi:10.1002/anie.201916390

59. Zaks, A. & Klibanov, A. M. Enzyme-catalyzed processes in organic solvents. *Proc. Nat. Acad. Sci. USA* **82**, 3192 (1985).

60. *Water-Insoluble Drug Formulation, Third Edition*. (CRC Press, 2018). doi:10.1201/9781315120492

61. Dordick, J. S. Enzymatic catalysis in monophasic organic solvents. *Enzyme Microb.*

Technol. **11**, 194–211 (1989).

62. Carrea, G. & Riva, S. Medium Engineering of Enzyme Reaction. *Angew Chem. Int. Ed.* **39**, 2226–2254 (2000).

63. Julio Polaina and Andrew P. MacCabe. *Industrial Enzymes: Structure , Function and Applications*. (Springer, 2007). doi:10.1007/1-4020-5377-0

64. Herbst, D., Peper, S. & Niemeyer, B. Enzyme catalysis in organic solvents: Influence of water content, solvent composition and temperature on Candida rugosa lipase catalyzed transesterification. *J. Biotechnol.* **162**, 398–403 (2012).

65. Plechkova, N. V & Seddon, K. R. Applications of ionic liquids in the chemical industry. *Chem Soc Rev* **37**, 123–150 (2008).

66. Hayes, R., Warr, G. G. & Atkin, R. Structure and Nanostructure in Ionic Liquids. *Chem. Rev.* **115**, 6357–6426 (2015).

67. Zhang, Q., De Oliveira Vigier, K., Royer, S. & Jèrôme, F. Deep eutectic solvents: syntheses, properties and applications. *Chem. Soc. Rev.* **41**, 7108–7146 (2012).

68. Zhekenov, T., Toksanbayev, N., Kazakbayeva, Z., Shah, D. & Mjalli, F. S. Formation of type III Deep Eutectic Solvents and effect of water on their intermolecular interactions. *Fluid Phase Equilib.* **441**, 43–48 (2017).

69. Paiva, A. *et al.* Natural deep eutectic solvents - Solvents for the 21st century. *ACS Sustain. Chem. Eng.* **2**, 1063–1071 (2014).

70. Khan, I. *et al.* Assessing the activity coefficients of water in cholinium-based ionic liquids: Experimental measurements and COSMO-RS modeling. *Fluid Phase Equilib.* **361**, 16–22 (2014).

71. Lindahl, T. & Nyberg, B. Rate of depurination of native deoxyribonucleic acid. *Biochemistry* **11**, 3610–3618 (1972).

72. Deetlefs, M., Seddon, K. R. & Shara, M. Predicting physical properties of ionic liquids. *Phys. Chem. Chem. Phys.* **8**, 642–649 (2006).

73. Bedrov, D. *et al.* Molecular Dynamics Simulations of Ionic Liquids and Electrolytes Using Polarizable Force Fields. *Chem. Rev.* **119**, 7940–7995 (2019).

74. Lin, C. H. & Patel, D. J. Structural basis of DNA folding and recognition in an AMP-DNA aptamer complex: Distinct architectures but common recognition motifs for DNA and RNA aptamers complexed to AMP. *Chem. Biol.* **4**, 817–832 (1997).

75. Searle, M. S. & Williams, D. H. On the stability of nucleic acid structures in solution: Enthalpy - entropy compensations, internal rotations and reversibility. *Nucleic Acids Res.*

21, 2051–2056 (1993).

76. Sugimoto, N., Honda, K. I. & Sasaki, M. Application of the thermodynamic parameters of dna stability prediction to double-helix formation of deoxyribooligonucleogtides. *Nucleosides and Nucleotides* **13**, 1311–1317 (1994).

77. Tan, Z.-J. J. & Chen, S.-J. J. Nucleic acid helix stability: Effects of salt concentration, cation valence and size, and chain length. *Biophys. J.* **90**, 1175–1190 (2006).

78. Owczarzy, R., Moreira, B. G., You, Y., Behlke, M. A. & Wälder, J. A. Predicting stability of DNA duplexes in solutions containing magnesium and monovalent cations. *Biochemistry* **47**, 5336–5353 (2008).

79. Khandelwal, G. & Bhyravabhotla, J. A phenomenological model for predicting melting temperatures of dna sequences. *PLoS One* **5**, 1–9 (2010).

80. Yakovchuk, P., Protozanova, E. & Frank-Kamenetskii, M. D. Base-stacking and base-pairing contributions into thermal stability of the DNA double helix. *Nucleic Acids Res.* **34**, 564–574 (2006).

81. Ball, P. Water is an active matrix of life for cell and molecular biology. *PNAS* **114**, 13327–13335 (2017).

82. Nakano, M. *et al.* Local thermodynamics of the water molecules around single- and double-stranded DNA studied by grid inhomogeneous solvation theory. *Chem. Phys. Lett.* **660**, 250–255 (2016).

83. Mcdermott, M. L., Vanselous, H., Corcelli, S. A. & Petersen, P. B. DNA ' s Chiral Spine of Hydration. *ACS Cent. Sci.* **3**, 708–714 (2017).

84. Feng, B. *et al.* Hydrophobic catalysis and a potential biological role of DNA unstacking induced by environment effects. *Proc. Natl. Acad. Sci. U. S. A.* **116**, 17169–17174 (2019).

85. Privalov, P. L. & Crane-Robinson, C. Forces maintaining the DNA double helix. *Eur. Biophys. J.* **49**, 315–321 (2020).

86. Hospital, A., Candotti, M., Gelpí, J. L. & Orozco, M. The Multiple Roles of Waters in Protein Solvation. *J. Phys. Chem. B* **121**, 3636–3643 (2017).

87. Duboue, E., Fogarty, A. C., Hynes, J. T. & Laage, D. Dynamical Disorder in the DNA Hydration Shell. *J. Am. Chem. Soc.* **138**, 7610–7620 (2016).

88. Baker, E. S. & Bowers, M. T. B-DNA Helix Stability in a Solvent-Free Environment. *J. Am. Soc. Mass Spectrom.* **18**, 1188–1195 (2007).

89. Miyoshi, D., Nakamura, K., Tateishi-Karimata, H., Ohmichi, T. & Sugimoto, N. Hydration of watson crick base pairs and dehydration of hoogsteen base pairs inducing structural

polymorphism under molecular crowding conditions. *J. Am. Chem. Soc.* **131**, 3522–3531 (2009).

90. Nakano, S. I., Karimata, H., Ohmichi, T., Kawakami, J. & Sugimoto, N. The effect of molecular crowding with nucleotide length and cosolute structure on DNA duplex stability. *J. Am. Chem. Soc.* **126**, 14330–14331 (2004).

91. Nakano, S., Miyoshi, D. & Sugimoto, N. Effects of Molecular Crowding on the Structures , Interactions , and Functions of Nucleic Acids. *Chem. Rev.* **114**, 2733–2758 (2014).

92. Khimji, I., Shin, J. & Liu, J. DNA duplex stabilization in crowded polyanion solutions. *Chem. Commun.* **49**, 1306–1308 (2013).

93. Carlon, E., Orlandini, E. & Stella, A. L. Roles of Stiffness and Excluded Volume in DNA Denaturation. *Phys. Rev. Lett.* **88**, 4 (2002).

94. Knowles, D. B., LaCroix, A. S., Deines, N. F., Shkel, I. & Record, M. T. Separation of preferential interaction and excluded volume effects on DNA duplex and hairpin stability. *Proc. Natl. Acad. Sci. U. S. A.* **108**, 12699–12704 (2011).

95. Estévez-Torres, A. & Baigl, D. DNA compaction: fundamentals and applications. *Soft Matter* **7**, 6746 (2011).

96. Lei, Q., Ren, C., Su, X. & Ma, Y. Crowding-induced Cooperativity in DNA Surface Hybridization. *Sci. Rep.* **5**, 9217 (2015).

97. Muhuri, S., Mimura, K., Miyoshi, D. & Sugimoto, N. Stabilization of three-way junctions of DNA under molecular crowding conditions. *J. Am. Chem. Soc.* **131**, 9268–9280 (2009).

98. Sugimoto, N. *Noncanonical structures and their thermodynamics of DNA and RNA under molecular crowding: Beyond the Watson-Crick double helix*. *International Review of Cell and Molecular Biology* **307**, (Elsevier Inc., 2014).

99. Yildirim, A., Sharma, M., Varner, B. M., Fang, L. & Feig, M. Conformational preferences of DNA in reduced dielectric environments. *J. Phys. Chem. B* **118**, 10874–10881 (2014).

100. Jaiswal, A. K., Srivastava, R., Pandey, P. & Bandyopadhyay, P. *Microscopic picture of water-ethylene glycol interaction near a model DNA by computer simulation: Concentration dependence, structure, and localized thermodynamics*. *PloS one* **13**, (2018).

101. Huey, R. & Mohr, S. C. Condensed states of nucleic acids. III. Ψ(+) and Ψ(−) Conformational transitions of DNA induced by ethanol and salt. *Biopolymers* **20**, 2533–2552 (1981).

102. Ke, F., Kim Luu, Y., Hadjiargyrou, M. & Liang, D. Characterizing DNA condensation and conformational changes in organic solvents. *PLoS One* **5**, 1–8 (2010).

103. Piškur, J. & Rupprecht, A. Aggregated DNA in ethanol solution. *FEBS Lett.* **375**, 174–178 (1995).

104. Sen, A. & Nielsen, P. E. On the stability of peptide nucleic acid duplexes in the presence of organic solvents. *Nucleic Acids Res.* **35**, 3367–3374 (2007).

105. Zhang, T. *et al.* Polar organic solvents accelerate the rate of DNA strand replacement reaction. *Analyst* **140**, 2023–2028 (2015).

106. Dave, N. & Liu, J. Fast molecular beacon hybridization in organic solvents with improved target specificity. *J. Phys. Chem. B* **114**, 15694–15699 (2010).

107. Lee, J., Vogt, C. E., McBrairty, M. & Al-Hashimi, H. M. Influence of dimethylsulfoxide on RNA structure and ligand binding. *Anal. Chem.* **85**, 9692–9698 (2013).

108. Zhou, W., Saran, R., Chen, Q., Ding, J. & Liu, J. A New Na+-Dependent RNA-Cleaving DNAzyme with over 1000-fold Rate Acceleration by Ethanol. *ChemBioChem* **17**, 159–163 (2016).

109. Dong, S. *et al.* Effect of organic solvents and biologically relevant ions on thelight-induced DNA cleavage by pyrene and its amino and hydroxy derivatives. *Int. J. Mol. Sci.* **3**, 937–947 (2002).

110. Cui, S. *et al.* Double-Stranded DNA Dissociates into Single Strands When Dragged into a Poor Solvent. *J. Am. Chem. Soc.* **129**, 14710–14716 (2007).

111. Ortega, G., Kurnik, M., Gautam, B. K. & Plaxco, K. W. Attachment of Proteins to a Hydroxyl-Terminated Surface Eliminates the Stabilizing Effects of Polyols. *J. Am. Chem. Soc.* **142**, 15349–15354 (2020).

112. Del Vecchio, P., Esposito, D., Ricchi, L. & Barone, G. The effects of polyols on the thermal stability of calf thymus DNA. *Int. J. Biol. Macromol.* **24**, 361–369 (1999).

113. Nakano, S. ichi & Sugimoto, N. The structural stability and catalytic activity of DNA and RNA oligonucleotides in the presence of organic solvents. *Biophys. Rev.* **8**, 11–23 (2016).

114. Kaiser, A., Ritter, M., Nazmutdinov, R. & Probst, M. Hydrogen Bonding and Dielectric Spectra of Ethylene Glycol-Water Mixtures from Molecular Dynamics Simulations. *J. Phys. Chem. B* **120**, 10515–10523 (2016).

115. Nelson, R. G. & Curtis Johnson, W. Conformation of DNA in ethylene glycol. *Biochem. Biophys. Res. Commun.* **41**, 211–216 (1970).

116. Nordstrom, L. J., Clark, C. A., Andersen, B., Champlin, S. M. & Schwinefus, J. J. Effect of Ethylene Glycol, Urea, and N-Methylated Glycines on DNA Thermal Stability: The Role of DNA Base Pair Composition and Hydration †. *Biochemistry* **45**, 9604–9614 (2006).

117. Beig, A., Miller, J. M. & Dahan, A. Accounting for the solubility-permeability interplay in oral formulation development for poor water solubility drugs: The effect of PEG-400 on carbamazepine absorption. *Eur. J. Pharm. Biopharm.* **81**, 386–391 (2012).

118. Ghoshdastidar, D., Ghosh, D. & Senapati, S. High Nucleobase-Solubilizing Ability of Low-Viscous Ionic Liquid/Water Mixtures: Measurements and Mechanism. *J. Phys. Chem. B* **120**, 492–503 (2016).

119. Lee, J. S. *et al.* Detection of nucleotides in hydrated ssDNA via 2D h-BN nanopore with ionic-liquid/salt–water interface. *Electrophoresis* elps.202000356 (2021). doi:10.1002/elps.202000356

120. Nishimura, N., Nomura, Y., Nakamura, N. & Ohno, H. DNA strands robed with ionic liquid moiety. *Biomaterials* **26**, 5558–5563 (2005).

121. Bottari, C. *et al.* Conformational stability of DNA in hydrated ionic liquid by synchrotron-based UV resonance raman. in *UV and Higher Energy Photonics: From Materials to Applications 2019* (eds. Lérondel, G., Cho, Y.-H., Kawata, S. & Taguchi, A.) 24 (SPIE, 2019). doi:10.1117/12.2529077

122. Bottari, C. *et al.* Base-specific pre-melting and melting transitions of DNA in presence of ionic liquids probed by synchrotron-based UV resonance Raman scattering. *J. Mol. Liq.* **330**, 115433 (2021).

123. Jumbri, K., Kassim, M. A. & Yunus, N. M. Fluorescence and Molecular Simulation Studies on the Interaction between Imidazolium-Based Ionic Liquids and Calf Thymus DNA.

124. Cardoso, L. & Micaelo, N. M. DNA molecular solvation in neat ionic liquids. *ChemPhysChem* **12**, 275–277 (2011).

125. Rezabal, E. & Schäfer, T. First principle approach to solvation by methylimidazolium-based ionic liquids. *J. Phys. Chem. B* **117**, 553–562 (2013).

126. Ding, Y., Zhang, L., Xie, J. & Guo, R. Binding characteristics and molecular mechanism of interaction between ionic liquid and DNA. *J. Phys. Chem. B* **114**, 2033–2043 (2010).

127. Wang, H., Wang, J. & Zhang, S. Binding Gibbs energy of ionic liquids to calf thymus DNA: a fluorescence spectroscopy study. *Phys. Chem. Chem. Phys.* **13**, 3906 (2011).

128. Mishra, A., Ekka, M. K. & Maiti, S. Influence of Ionic Liquids on Thermodynamics of Small Molecule-DNA Interaction: The Binding of Ethidium Bromide to Calf Thymus DNA. *J. Phys. Chem. B* **120**, 2691–2700 (2016).

129. Prajapati, R. S., Sirajuddin, M., Durani, V., Sreeramulu, S. & Varadarajan, R. Contribution of cation-π interactions to protein stability. *Biochemistry* **45**, 15000–15010 (2006).

130. Singh, P. K., Sujana, J., Mora, A. K. & Nath, S. Probing the DNA-ionic liquid interaction

using an ultrafast molecular rotor. *J. Photochem. Photobiol. A Chem.* **246**, 16–22 (2012).

131. Meng, Z., Kubar, T., Mu, Y. & Shao, F. A Molecular Dynamics-Quantum Mechanics Theoretical Study of DNA-Mediated Charge Transport in Hydrated Ionic Liquids. *J. Chem. Theory Comput.* **14**, 2733–2742 (2018).

132. Jumbri, K., Micaelo, N. M. & Abdul Rahman, M. B. Solvation free energies of nucleic acid bases in ionic liquids. *Mol. Simul.* **43**, 19–27 (2017).

133. Jumbri, K., Abdul Rahman, M. B., Abdulmalek, E., Ahmad, H. & Micaelo, N. M. An insight into structure and stability of DNA in ionic liquids from molecular dynamics simulation and experimental studies. *Phys. Chem. Chem. Phys.* **16**, 14036–46 (2014).

134. Jumbri, K., Ahmad, H., Abdulmalek, E. & Abdul Rahman, M. B. Binding energy and biophysical properties of ionic liquid-DNA complex: Understanding the role of hydrophobic interactions. *J. Mol. Liq.* **223**, 1197–1203 (2016).

135. Del Olmo, L., Lage-Estebanez, I., López, R. & García De La Vega, J. M. Understanding the Structure and Properties of Cholinium Amino Acid Based Ionic Liquids. *J. Phys. Chem. B* **120**, 10327–10335 (2016).

136. Pabbathi, A. & Samanta, A. Spectroscopic and Molecular Docking Study of the Interaction of DNA with a Morpholinium Ionic Liquid. *J. Phys. Chem. B* **119**, 11099–11105 (2015).

137. Vasudevamurthy, M. K., Lever, M., George, P. M. & Morison, K. R. Betaine structure and the presence of hydroxyl groups alters the effects on DNA melting temperatures. *Biopolymers* **91**, 85–94 (2009).

138. Stellwagen, E., Muse, J. M. & Stellwagen, N. C. Monovalent cation size and DNA conformational stability. *Biochemistry* **50**, 3084–3094 (2011).

139. Koumoto, K., Ochiai, H. & Sugimoto, N. Structural effect of synthetic zwitterionic cosolutes on the stability of DNA duplexes. *Tetrahedron* **64**, 168–174 (2008).

140. Fujita, K. *et al.* Solubility and stability of cytochrome c in hydrated ionic liquids: Effect of oxo acid residues and kosmotropicity. *Biomacromolecules* **8**, 2080–2086 (2007).

141. Domínguez de María, P. & Maugeri, Z. Ionic liquids in biotransformations: From proof-of-concept to emerging deep-eutectic-solvents. *Curr. Opin. Chem. Biol.* **15**, 220–225 (2011).

142. Lin, Y., Zhao, A., Tao, Y., Ren, J. & Qu, X. Ionic Liquid as an Efficient Modulator on Artificial Enzyme System: Toward the Realization of High-Temperature Catalytic Reactions. *J. Am. Chem. Soc.* **135**, 4207–4210 (2013).

143. Vijayaraghavan, R., Izgorodin, A., Ganesh, V., Surianarayanan, M. & MacFarlane, D. R. Long-term structural and chemical stability of DNA in hydrated ionic liquids. *Angew. Chemie - Int. Ed.* **49**, 1631–1633 (2010).

144. Mamajanov, I., Engelhart, A. E., Bean, H. D. & Hud, N. V. DNA and RNA in anhydrous media: Duplex, triplex, and G-quadruplex secondary structures in a deep eutectic solvent. *Angew. Chemie - Int. Ed.* **49**, 6310–6314 (2010).

145. Maity, A., Singh, A. & Singh, N. Differential stability of DNA based on salt concentration. *Eur. Biophys. J.* **46**, 33–40 (2017).

146. Tateishi-Karimata, H. & Sugimoto, N. Structure, stability and behaviour of nucleic acids in ionic liquids. *Nucleic Acids Res.* **42**, 8831–8844 (2014).

147. Francisco, M., González, A. S. B., García de Dios, S. L., Weggemans, W. & Kroon, M. C. Comparison of a low transition temperature mixture (LTTM) formed by lactic acid and choline chloride with choline lactate ionic liquid and the choline chloride salt: physical properties and vapour–liquid equilibria of mixtures containing water and ethanol. *RSC Adv.* **3**, 23553 (2013).

148. Miao, S., Atkin, R. & Warr, G. G. Amphiphilic nanostructure in choline carboxylate and amino acid ionic liquids and solutions. *Phys. Chem. Chem. Phys.* **22**, 3490–3498 (2020).

149. Bhatt, J., Pereira, M. M. & Prasad, K. Simultaneous morphological transformation of metal salt and conformations of DNA in a bio-based ionic liquid. *Int. J. Biol. Macromol.* **135**, 926–930 (2019).

150. Kohno, Y. & Ohno, H. Ionic liquid/water mixtures: from hostility to conciliation. *Chem Commun* **48**, 7119–7130 (2012).

151. Vijayaraghavan, R. *et al.* Biocompatibility of choline salts as crosslinking agents for collagen based biomaterials. *Chem. Commun. (Camb).* **46**, 294–6 (2010).

152. Sahoo, D. K., Jena, S., Dutta, J., Chakrabarty, S. & Biswal, H. S. Critical Assessment of the Interaction between DNA and Choline Amino Acid Ionic Liquids: Evidences of Multimodal Binding and Stability Enhancement. *ACS Cent. Sci.* acscentsci.8b00601 (2018). doi:10.1021/acscentsci.8b00601

153. Kobrak, M. N. & Li, H. Electrostatic interactions in ionic liquids: the dangers of dipole and dielectric descriptions. *Phys. Chem. Chem. Phys.* **12**, 1922 (2010).

154. Chen, W. *et al.* Investigation on the thermal stability of deep eutectic solvents. *Wuli Huaxue Xuebao/ Acta Phys. - Chim. Sin.* **34**, 904–911 (2018).

155. Ma, C., Laaksonen, A., Liu, C., Lu, X. & Ji, X. The peculiar effect of water on ionic liquids and deep eutectic solvents. *Chem. Soc. Rev.* **47**, 8685–8720 (2018).

156. Ohno, H., Fujita, K. & Kohno, Y. Is seven the minimum number of water molecules per ion pair for assured biological activity in ionic liquid–water mixtures? *Phys. Chem. Chem. Phys.* **17**, 14454–14460 (2015).

157. Tanner, E. E. L. *et al.* The Influence of Water on Choline-Based Ionic Liquids. *ACS Biomater. Sci. Eng.* **5**, 3645–3653 (2019).

158. Pal, S. & Paul, S. Understanding The Role of Reline, a Natural DES, on Temperature-Induced Conformational Changes of C-Kit G-Quadruplex DNA: A Molecular Dynamics Study. *J. Phys. Chem. B* acs.jpcb.0c00644 (2020). doi:10.1021/acs.jpcb.0c00644

159. Saha, D., Kulkarni, M. & Mukherjee, A. Water modulates the ultraslow dynamics of hydrated ionic liquids near CG rich DNA: consequences for DNA stability. *Phys. Chem. Chem. Phys.* **18**, 32107–32115 (2016).

160. Haque, A., Khan, I., Hassan, S. I. & Khan, M. S. Interaction studies of cholinium-based ionic liquids with calf thymus DNA: Spectrophotometric and computational methods. *J. Mol. Liq.* **237**, 201–207 (2017).

161. Tateishi-Karimata, H. & Sugimoto, N. A-T base pairs are more stable than G-C base pairs in a hydrated ionic liquid. *Angew. Chemie - Int. Ed.* **51**, 1416–1419 (2012).

162. Melchior, W. B. & Von Hippel, P. H. Alteration of the relative stability of dA-dT and dG-dC base pairs in DNA. *Proc. Natl. Acad. Sci. U. S. A.* **70**, 298–302 (1973).

163. Rees, W. A., Korte, J., Von Hippel, P. H. & Yager, T. D. Betaine Can Eliminate the Base Pair Composition Dependence of DNA Melting. *Biochemistry* **32**, 137–144 (1993).

164. Hong, J. *et al.* Preferential interactions of glycine betaine and of urea with DNA: Implications for DNA hydration and for effects of these solutes on DNA stability. *Biochemistry* **43**, 14744–14758 (2004).

165. Janosik, S. M. The thermal stability of oligonucleotide duplexes is sequence independent in tetraalkylammonium salt solutions: application to identifying recombinant DNA clones. *NASPA J.* **42**, 1 (1998).

166. Nakano, M., Tateishi-Karimata, H., Tanaka, S. & Sugimoto, N. Choline ion interactions with DNA atoms explain unique stabilization of A-T base pairs in DNA duplexes: A microscopic view. *J. Phys. Chem. B* **118**, 379–389 (2014).

167. Portella, G., Germann, M. W., Hud, N. V. & Orozco, M. MD and NMR analyses of choline and TMA binding to duplex DNA: On the origins of aberrant sequence-dependent stability by alkyl cations in aqueous and water-free solvents. *J. Am. Chem. Soc.* **136**, 3075–3086 (2014).

168. Sequeira, R. A., Bhatt, J. & Prasad, K. Recent Trends in Processing of Proteins and DNA in Alternative Solvents : A Sustainable Approach. 116–137 (2020).

169. El Achkar, T., Fourmentin, S. & Greige-Gerges, H. Deep eutectic solvents: An overview on their interactions with water and biochemical compounds. *J. Mol. Liq.* **288**, 111028 (2019).

170. Dai, Y. *et al.* Natural deep eutectic solvents as new potential media for green technology. *Anal. Chim. Acta* **766**, 61–68 (2013).

171. Wagle, D. V., Zhao, H. & Baker, G. A. Deep eutectic solvents: Sustainable media for nanoscale and functional materials. *Acc. Chem. Res.* **47**, 2299–2308 (2014).

172. Smith, E. L., Abbott, A. P. & Ryder, K. S. Deep Eutectic Solvents (DESs) and Their Applications. *Chem. Rev.* **114**, 11060–11082 (2014).

173. Perna, F. M., Vitale, P. & Capriati, V. Deep eutectic solvents and their applications as green solvents. *Curr. Opin. Green Sustain. Chem.* **21**, 27–33 (2020).

174. Perkins, S. L., Painter, P. & Colina, C. M. Experimental and Computational Studies of Choline Chloride-Based Deep Eutectic Solvents. *J. Chem. Eng. Data* **59**, 3652–3662 (2014).

175. Yusof, R., Jumbri, K., Ahmad, H., Abdulmalek, E. & Basyaruddin Abdul Rahman, M. Binding of Tetrabutylammonium Bromide based Deep Eutectic Solvent to DNA by Spectroscopic Analysis. *Spectrochim. Acta Part A Mol. Biomol. Spectrosc.* **253**, 119543 (2021).

176. De La Harpe, K., Kohl, F. R., Zhang, Y. & Kohler, B. Excited-State Dynamics of a DNA Duplex in a Deep Eutectic Solvent Probed by Femtosecond Time-Resolved IR Spectroscopy. *J. Phys. Chem. A* **122**, 2437–2444 (2018).

177. Zhang, Y., de La Harpe, K., Hariharan, M. & Kohler, B. Excited-state dynamics of mononucleotides and DNA strands in a deep eutectic solvent. *Faraday Discuss.* **207**, 267–282 (2018).

178. Gállego, I., Grover, M. A. & Hud, N. V. Folding and imaging of DNA nanostructures in anhydrous and hydrated deep-eutectic solvents. *Angew. Chemie - Int. Ed.* **54**, 6765–6769 (2015).

179. Shiu, S. C. C. *et al.* The Three S's for Aptamer-Mediated Control of DNA Nanostructure Dynamics: Shape, Self-Complementarity, and Spatial Flexibility. *ChemBioChem* **19**, 1900–1906 (2018).

180. Kosinski, R. *et al.* Sites of high local frustration in DNA origami. *Nat. Commun.* **10**, 1–12 (2019).

181. Rich, A. & Zhang, S. Z-DNA: The long road to biological function. *Nat. Rev. Genet.* **4**, 566–572 (2003).

182. Bhanjadeo, M. M., Nayak, A. K. & Subudhi, U. Cerium chloride stimulated controlled conversion of B-to-Z DNA in self-assembled nanostructures. *Biochem. Biophys. Res. Commun.* **482**, 916–921 (2017).

183. Bujold, K. E., Lacroix, A. & Sleiman, H. F. DNA Nanostructures at the Interface with Biology. *Chem* **4**, 495–521 (2018).

184. Ghoshdastidar, D. & Senapati, S. Dehydrated DNA in B-form: Ionic liquids in rescue. *Nucleic Acids Res.* **46**, 4344–4353 (2018).

185. Vieweg, P., Dreyer, F. & Berndt, D. What Do We Know So Far ? *Reading*

186. Garai, A., Ghoshdastidar, D., Senapati, S. & Maiti, P. K. Ionic liquids make DNA rigid. *J. Chem. Phys.* **149**, (2018).

187. Satpathi, S. *et al.* A Green Solvent Induced DNA Package. *Sci. Rep.* **5**, 9137 (2015).

188. Jeong, K. B. *et al.* Reduction of DNA Folding by Ionic Liquids and Its Effects on the Analysis of DNA–Protein Interaction Using Solid-State Nanopore. *Small* **14**, 1–8 (2018).

189. Sarkar, S., Rajdev, P. & Singh, P. C. Hydrogen Bonding of Ionic Liquids in the Groove Region of DNA Controls the Extent of Its Stabilization: Synthesis, Spectroscopic and Simulation Studies. *Phys. Chem. Chem. Phys.* **19**, (2020).

190. Chandran, A., Ghoshdastidar, D. & Senapati, S. Groove Binding Mechanism of Ionic Liquids: A Key Factor in Long-Term Stability of DNA in Hydrated Ionic Liquids? *J. Am. Chem. Soc.* **134**, 20330–20339 (2012).

191. Nikolova, E. N. *et al.* A historical account of hoogsteen base-pairs in duplex DNA. *Biopolymers* **23**, n/a-n/a (2013).

192. Duan, J., Wang, X. & Kizer, M. E. *Biotechnological and Therapeutic Applications of Natural Nucleic Acid Structural Motifs*. *Topics in Current Chemistry* **378**, (Springer International Publishing, 2020).

193. Ma, Y., Iida, K. & Nagasawa, K. Topologies of G-quadruplex: Biological functions and regulation by ligands. *Biochem. Biophys. Res. Commun.* **1051**, (2020).

194. Haider, S., Parkinson, G. N. & Marsh, T. C. G-Quadruplexes (GQU). *J. Nucleic Acids* **2018**, 1–2 (2018).

195. Tateishi-Karimata, H. & Sugimoto, N. Chemical biology of non-canonical structures of nucleic acids for therapeutic applications. *Chem. Commun.* **56**, 2379–2390 (2020).

196. Alberti, P. & Mergny, J.-L. DNA duplex-quadruplex exchange as the basis for a nanomolecular machine. *Proc. Natl. Acad. Sci. U. S. A.* **100**, 1569–1573 (2003).

197. Boersma, A. J., Zuhorn, I. S. & Poolman, B. A sensor for quantification of macromolecular crowding in living cells. *Nat. Methods* **12**, 227–229 (2015).

198. Renaud De La Faverie, A. *et al.* Nucleic acids targeted to drugs: SELEX against a quadruplex ligand. *Biochimie* **93**, 1357–1367 (2011).

199. Deore, P. S., Gray, M. D., Chung, A. J. & Manderville, R. A. Ligand-Induced G-Quadruplex Polymorphism: A DNA Nanodevice for Label-Free Aptasensor Platforms. *J. Am. Chem.*

Soc. jacs.9b06533 (2019). doi:10.1021/jacs.9b06533

200. Guo, Y. *et al.* Multiple types of logic gates based on a single G-quadruplex DNA strand. *Sci. Rep.* **4**, 7315 (2014).

201. Kankia, B. & Kankia, B. Quadruplex-Based Reactions for Dynamic DNA Nanotechnology. *J. Phys. Chem. B* **124**, 4263–4269 (2020).

202. Ebrahimi, A., Ravan, H. & Khajouei, S. DNA nanotechnology and bioassay development. *TrAC - Trends Anal. Chem.* **114**, 126–142 (2019).

203. Gray, R. D. & Chaires, J. B. Linkage of cation binding and folding in human telomeric quadruplex DNA. *Biophys. Chem.* **159**, 205–209 (2011).

204. Bončina, M., Lah, J., Prislan, I. & Vesnaver, G. Energetic basis of human telomeric DNA folding into G-quadruplex structures. *J. Am. Chem. Soc.* **134**, 9657–9663 (2012).

205. Nakano, S., Ayusawa, T., Tanino, Y. & Sugimoto, N. Stabilization of DNA Loop Structures by Large Cations. (2019). doi:10.1021/acs.jpcb.9b06074

206. Marchand, A. *et al.* Sequence and Solvent Effects on Telomeric DNA Bimolecular G-Quadruplex Folding Kinetics. *J. Phys. Chem. B* **117**, 12391–12401 (2013).

207. Satpathi, S., Kulkarni, M., Mukherjee, A. & Hazra, P. Ionic liquid induced G-quadruplex formation and stabilization: spectroscopic and simulation studies. *Phys. Chem. Chem. Phys.* **18**, 29740–29746 (2016).

208. Di Antonio, M. *et al.* Single-molecule visualization of DNA G-quadruplex formation in live cells. *Nat. Chem.* (2020). doi:10.1038/s41557-020-0506-4

209. Miyoshi, D., Nakao, A. & Sugimoto, N. Molecular crowding regulates the structural switch of the DNA G-quadruplex. *Biochemistry* **41**, 15017–15024 (2002).

210. Xue, Y. *et al.* Human telomeric DNA forms parallel-stranded intramolecular G-quadruplex in K+ solution under molecular crowding condition. *J. Am. Chem. Soc.* **129**, 11185–11191 (2007).

211. Fujimoto, T., Nakano, S.-I., Miyoshi, D. & Sugimoto, N. The effects of molecular crowding on the structure and stability of g-quadruplexes with an abasic site. *J. Nucleic Acids* **2011**, 857149 (2011).

212. Nishio, M., Tsukakoshi, K. & Ikebukuro, K. G-quadruplex: Flexible Conformational Changes by Cations, pH, Crowding and Its Applications to Biosensing. *Biosens. Bioelectron.* 113030 (2021). doi:10.1016/j.bios.2021.113030

213. Gilbert, D. E. & Feigon, J. Multistranded DNA structures Dara E Gilbert and Juli Feigon*. *Curr. Opin. Struct. Biol.* **9**, 305–314 (1999).

214. Teng, Y., Pramanik, S., Tateishi-Karimata, H., Ohyama, T. & Sugimoto, N. Drastic stability change of X-X mismatch in d(CXG) trinucleotide repeat disorders under molecular crowding condition. *Biochem. Biophys. Res. Commun.* **496**, 601–607 (2018).

215. Miyoshi, D., Karimata, H. & Sugimoto, N. Hydration regulates thermodynamics of G-quadruplex formation under molecular crowding conditions. *J. Am. Chem. Soc.* **128**, 7957–7963 (2006).

216. Matsumoto, S. & Sugimoto, N. New Insights into the Functions of Nucleic Acids Controlled by Cellular Microenvironments. *Top. Curr. Chem.* **379**, (2021).

217. Xiao, F., Chen, Z., Wei, Z. & Tian, L. Hydrophobic Interaction: A Promising Driving Force for the Biomedical Applications of Nucleic Acids. *Adv. Sci.* **7**, 1–34 (2020).

218. Zhou, H.-X., Rivas, G. & Minton, A. P. Macromolecular crowding and confinemment: biochemical, biophysical, and potential physiological consequences. *Annu Rev Biophys* **37**, 375–397 (2008).

219. Hall, D. & Minton, A. P. Macromolecular crowding: Qualitative and semiquantitative successes, quantitative challenges. *Biochim. Biophys. Acta - Proteins Proteomics* **1649**, 127–139 (2003).

220. de Xammar Oro, J. R. & Grigera, J. R. On the thermal stability of DNA in solution of mixed solvents. *J. Biol. Phys.* **21**, 151–154 (1995).

221. Bonner, G. & Klibanov, A. M. Structural stability of DNA in nonaqueous solvents. *Biotechnol. Bioeng.* **68**, 339–344 (2000).

222. Nowak, E., Wisła-Świder, A., Khachatryan, G., Fiedorowicz, M. & Danel, K. Possible sensor applications of selected DNA–surfactant complexes. *Eur. Biophys. J.* (2019). doi:10.1007/s00249-019-01367-2

223. Chakraborty, G. *et al.* Electrostatically PEGylated DNA enables salt-free hybridization in water. *Chem. Sci.* **10**, 10097–10105 (2019).

224. Abe, H. *et al.* Structure formation and catalytic activity of DNA dissolved in organic solvents. *Angew. Chemie - Int. Ed.* **51**, 6475–6479 (2012).

225. Behera, A. K. *et al.* Enhanced deoxyribozyme-catalyzed RNA ligation in the presence of organic cosolvents. *Biopolymers* **99**, 382–391 (2013).

226. Tateishi-Karimata, H., Nakano, M. & Sugimoto, N. Comparable stability of Hoogsteen and Watson-Crick base Pairs in ionic liquid choline dihydrogen phosphate. *Sci. Rep.* (2014). doi:10.1038/srep03593

227. Marušič, M., Tateishi-Karimata, H., Sugimoto, N. & Plavec, J. Structural foundation for DNA behavior in hydrated ionic liquid: An NMR study. *Biochimie* **108**, 169–177 (2015).

228. Nakano, M., Tateishi-Karimata, H., Tanaka, S. & Sugimoto, N. Affinity of molecular ions for DNA structures is determined by solvent-accessible surface area. *J. Phys. Chem. B* **118**, 9583–9594 (2014).

229. Fujita, K. & Ohno, H. phosphatStable G-quadruplex structure in a hydrated ion pair: cholinium cation and dihydrogen e anion. *Chem. Commun. (Camb).* **48**, 5751–3 (2012).

230. Tateishi-Karimata, H., Nakano, M., Pramanik, S., Tanaka, S. & Sugimoto, N. I-Motifs are more stable than G-quadruplexes in a hydrated ionic liquid. *Chem. Commun.* **51**, 6909–6912 (2015).

231. Seviour, T. *et al.* The biofilm matrix scaffold of Pseudomonas aeruginosa contains G-quadruplex extracellular DNA structures. *npj Biofilms Microbiomes* **7**, 27 (2021).

232. Hall-Stoodley, L., Costerton, J. W. & Stoodley, P. Bacterial biofilms: From the natural environment to infectious diseases. *Nat. Rev. Microbiol.* **2**, 95–108 (2004).

233. Bryan, T. M. & Baumann, P. G-quadruplexes: From guanine gels to chemotherapeutics. *Mol. Biotechnol.* **49**, 198–208 (2011).

234. Pandey, P. K., Rawat, K., Aswal, V. K., Kohlbrecher, J. & Bohidar, H. B. Imidazolium based ionic liquid induced DNA gelation at remarkably low concentration. *Colloids Surfaces A Physicochem. Eng. Asp.* **538**, 184–191 (2018).

235. Mohamed, S. M. K. *et al.* Facile preparation of biocompatible and transparent silica aerogels as ionogels using choline dihydrogen phosphate ionic liquid. *Appl. Sci.* **11**, 1–16 (2020).

236. Bose, K., Lech, C. J., Heddi, B. & Phan, A. T. High-resolution AFM structure of DNA G-wires in aqueous solution. *Nat. Commun.* **9**, (2018).

237. Gu, C. *et al.* Supramolecular G4 Eutectogels of Guanosine with Solvent-Induced Chiral Inversion and Excellent Electrochromic Activity. *Angew. Chemie Int. Ed.* **59**, 18768–18773 (2020).

238. Zhao, C., Ren, J. & Qu, X. G-quadruplexes form ultrastable parallel structures in deep eutectic solvent. *Langmuir* **29**, 1183–1191 (2013).

239. Mertens, K. N. *et al.* Alteration ofthe groove width ofDNA induced by the multimodal hydrogen bonding of denaturants with DNA bases in its grooves affects their stability. *Mar. Micropaleontol.* 101773 (2019). doi:10.1016/j.marmicro.2019.101773

240. Aslanyan, L. *et al.* Effect of Urea on G-Quadruplex Stability. *J. Phys. Chem. B* **121**, 6511–6519 (2017).

241. Li, W. *et al.* Effect of Water and Organic Solvents on the Ionic Dissociation of Ionic Liquids. *J. Phys. Chem. B* **111**, 6452–6456 (2007).

242. Monhemi, H., Housaindokht, M. R., Moosavi-Movahedi, A. A. & Bozorgmehr, M. R. How a protein can remain stable in a solvent with high content of urea: insights from molecular dynamics simulation of Candida antarctica lipase B in urea : choline chloride deep eutectic solvent. *Phys. Chem. Chem. Phys.* **16**, 14882–93 (2014).

243. Lannan, F. M., Mamajanov, I. & Hud, N. V. Human telomere sequence DNA in water-free and high-viscosity solvents: G-quadruplex folding governed by Kramers rate theory. *J. Am. Chem. Soc.* **134**, 15324–15330 (2012).

244. Rajagopal, S. K. & Hariharan, M. Non-natural G-quadruplex in a non-natural environment. *Photochem. Photobiol. Sci.* **13**, 157–161 (2014).

245. Pal, S. & Paul, S. Effect of Hydrated and Nonhydrated Choline Chloride–Urea Deep Eutectic Solvent (Reline) on Thrombin-Binding G-quadruplex Aptamer (TBA): A Classical Molecular Dynamics Simulation Study. *J. Phys. Chem. C* **123**, acs.jpcc.9b01111 (2019).

246. Chang, T., He, S., Amini, R. & Li, Y. Functional Nucleic Acids Under Unusual Conditions. *ChemBioChem* cbic.202100087 (2021). doi:10.1002/cbic.202100087

247. Munzar, J. D., Ng, A. & Juncker, D. Duplexed aptamers: history, design, theory, and application to biosensing. *Chem. Soc. Rev.* (2019). doi:2019/CS/C8CS00880A

248. Moutsiopoulou, A., Broyles, D., Dikici, E., Daunert, S. & Deo, S. K. Molecular Aptamer Beacons and Their Applications in Sensing, Imaging, and Diagnostics. *Small* **15**, 1902248 (2019).

249. Komarova, N. & Kuznetsov, A. Inside the black box: What makes Selex better? *Molecules* **24**, (2019).

250. Huizenga, D. E. & Szostak, J. W. A DNA Aptamer That Binds Adenosine and ATP. *Biochemistry* **34**, 656–665 (1995).

251. Machado, I., Özalp, V. C., Rezabal, E. & Schäfer, T. DNA aptamers are functional molecular recognition sensors in protic ionic liquids. *Chem. Eur. J.* **20**, 11820–11825 (2014).

252. Chaou, T., Vialet, B. & Azéma, L. DNA aptamer selection in methanolic media: Adenine-aptamer as proof-of-concept. *Methods* **97**, 11–19 (2016).

253. Stanlis, K. K. H. & McIntosh, J. R. Single-strand DNA aptamers as probes for protein localization in cells. *J. Histochem. Cytochem.* **51**, 797–808 (2003).

254. Arcella, A. *et al.* Structure and properties of DNA in apolar solvents. *J. Phys. Chem. B* **118**, 8540–8548 (2014).

255. Svigelj, R. *et al.* Selection of Anti-gluten DNA Aptamers in a Deep Eutectic Solvent. *Angew. Chemie - Int. Ed.* **57**, 12850–12854 (2018).

256. Ferreira, E. S. C., Voroshylova, I. V., Pereira, C. M. & D. S. Cordeiro, M. N. Improved Force Field Model for the Deep Eutectic Solvent Ethaline: Reliable Physicochemical Properties. *J. Phys. Chem. B* acs.jpcb.6b07233 (2016). doi:10.1021/acs.jpcb.6b07233

257. Lapeña, D., Lomba, L., Artal, M., Lafuente, C. & Giner, B. Thermophysical characterization of the deep eutectic solvent choline chloride:ethylene glycol and one of its mixtures with water. *Fluid Phase Equilib.* **492**, 1–9 (2019).

258. Chidchob, P. & Sleiman, H. F. Recent advances in DNA nanotechnology. *Curr. Opin. Chem. Biol.* **46**, 63–70 (2018).

259. Damase, T. R. & Allen, P. B. Designed and Evolved Nucleic Acid Nanotechnology: Contrast and Complementarity. *Bioconjug. Chem.* **30**, 2–12 (2019).

260. Shing Ho, P. Structure of the Holliday junction: applications beyond recombination. *Biochem. Soc. Trans.* **45**, 1149–1158 (2017).

261. Seeman, N. C. DNA engineering and its application to nanotechnology. *Trends Biotechnol.* **17**, 437–443 (1999).

262. Hong, F., Zhang, F., Liu, Y. & Yan, H. *DNA Origami: Scaffolds for Creating Higher Order Structures*. *Chemical Reviews* **117**, (2017).

263. Rothemund, P. W. K. Folding DNA to create nanoscale shapes and patterns. *Nature* **440**, 297–302 (2006).

264. Kwon, P. S. *et al.* Designer DNA architecture offers precise and multivalent spatial pattern-recognition for viral sensing and inhibition. *Nat. Chem.* **12**, (2019).

265. Kallenbach, N. R., Ma, R. I. & Seeman, N. C. An immobile nucleic acid junction constructed from oligonucleotides. *Nature* **305**, 829–831 (1983).

266. Gosse, C., Strick, T. R. & Kostrz, D. Molecular scaffolds: when DNA becomes the hardware for single-molecule investigations. *Curr. Opin. Chem. Biol.* **53**, 192–203 (2019).

267. Jahanban-Esfahlan, R. *et al.* Static DNA nanostructures for cancer theranostics: Recent progress in design and applications. *Nanotechnol. Sci. Appl.* **12**, 25–46 (2019).

268. Tapio, K. & Bald, I. The potential of DNA origami to build multifunctional materials. (2020).

269. Pan, M. *et al.* Programming DNA Nanoassembly for Enhanced Photodynamic Therapy. *Angew. Chemie Int. Ed.* 1897–1905 (2019). doi:10.1002/anie.201912574

270. Liu, K. *et al.* Detecting topological variations of DNA at single-molecule level. *Nat. Commun.* **10**, 3 (2019).

271. Scalise, D. & Schulman, R. Controlling Matter at the Molecular Scale with DNA Circuits.

Annu. Rev. Biomed. Eng. **21**, 469–493 (2019).

272. He, L. *et al.* Fluorescence Resonance Energy Transfer-Based DNA Tetrahedron Nanotweezer for Highly Reliable Detection of Tumor-Related mRNA in Living Cells. *ACS Nano* **11**, 4060–4066 (2017).

273. Erbas-Cakmak, S. *et al.* Molecular logic gates: The past, present and future. *Chem. Soc. Rev.* **47**, 2228–2248 (2018).

274. Song, T. *et al.* Fast and compact DNA logic circuits based on single-stranded gates using strand-displacing polymerase. *Nat. Nanotechnol.* **14**, 1075–1081 (2019).

275. Jue, Y. I. N. *et al.* DNA Nanotechnology-based Biocomputing. (2020). doi:10.1007/s40242-020-9086-5

276. Perez Sirkin, Y. A., Tagliazucchi, M. & Szleifer, I. Transport in nanopores and nanochannels: some fundamental challenges and nature-inspired solutions. *Mater. Today Adv.* **5**, 100047 (2020).

277. Zhang, Y. *et al.* Dynamic DNA Structures. *Small* **1900228**, 1900228 (2019).

278. Turner, A. P. F. Biosensors: sense and sensibility. *Chem. Soc. Rev.* **42**, 3184–3196 (2013).

279. Ye, T. *et al.* An All-in-One Aptasensor Integrating Enzyme Powered Three-Dimensional DNA Machine for the Antibiotic Detection An All-in-One Aptasensor Integrating Enzyme Powered Three- Dimensional DNA Machine for the Antibiotic Detection. (2020). doi:10.1021/acs.jafc.9b08143

280. Hu, Y. *et al.* Dynamic DNA Assemblies in Biomedical Applications. **2000557**, (2020).

281. Sameiyan, E. *et al.* DNA origami-based aptasensors. *Biosens. Bioelectron.* **143**, 111662 (2019).

282. Chen, Y. J., Groves, B., Muscat, R. A. & Seelig, G. DNA nanotechnology from the test tube to the cell. *Nat. Nanotechnol.* **10**, 748–760 (2015).

283. Huo, S., Li, H., Boersma, A. J. & Herrmann, A. DNA Nanotechnology Enters Cell Membranes. *Adv. Sci.* **1900043**, 1900043 (2019).

284. Yang, J., Jiang, S., Liu, X., Pan, L. & Zhang, C. Aptamer-Binding Directed DNA Origami Pattern for Logic Gates. *ACS Appl. Mater. Interfaces* **8**, 34054–34060 (2016).

285. Mastronardi, E., Foster, A., Zhang, X. & DeRosa, M. Smart Materials Based on DNA Aptamers: Taking Aptasensing to the Next Level. *Sensors* **14**, 3156–3171 (2014).

286. Luo, Z. *et al.* A rapid, adaptative DNA biosensor based on molecular beacon-concatenated dual signal amplification strategies for ultrasensitive detection of p53 gene and cancer cells. (2020). doi:10.1016/j.talanta.2019.120638

287. Hollenstein, M. DNA catalysis: The chemical repertoire of DNAzymes. *Molecules* **20**, 20777–20804 (2015).

288. Berg, K., Magbanua, E. & Hahn, U. *Nucleic Acid Aptamers*. **1380**, (Springer New York, 2016).

289. Guan, B. & Zhang, X. Aptamers as Versatile Ligands for Biomedical and Pharmaceutical Applications. (2020).

290. Brody, E. N. & Gold, L. Aptamers as therapeutic and diagnostic agents. *Rev. Mol. Biotechnol.* **74**, 5–13 (2000).

291. Schafer, T. & Ozalp, V. C. DNA-aptamer gating membranes. *Chem. Commun.* **51**, 5471–5474 (2015).

292. Fan, H. *et al.* A Smart DNAzyme-MnO2 nanosystem for efficient gene silencing. *Angew. Chemie - Int. Ed.* 4883–4887 (2015). doi:10.1002/anie.201411417

293. Wang, J., Mao, S., Li, H. F. & Lin, J. M. Multi-DNAzymes-functionalized gold nanoparticles for ultrasensitive chemiluminescence detection of thrombin on microchip. *Anal. Chim. Acta* **1027**, 76–82 (2018).

294. Sakai, Y. *et al.* DNA Aptamers for the Functionalisation of DNA Origami Nanostructures. *Genes (Basel).* **9**, 571 (2018).

295. Krishnan, Y. & Simmel, F. C. Nucleic acid based molecular devices. *Angew. Chemie - Int. Ed.* **50**, 3124–3156 (2011).

296. Rizzuto, F. J., Trinh, T. & Sleiman, H. F. Molecular Printing with DNA Nanotechnology. *Chem* **6**, 1560–1574 (2020).

297. Darley, E., Kaur, J., Singh, D., Surace, N. & Wickham, S. F. J. The fusion of lipid and DNA nanotechnology. 1–21 (2019). doi:10.3390/genes10121001

298. Kahn, J. S., Hu, Y. & Willner, I. Stimuli-Responsive DNA-Based Hydrogels: From Basic Principles to Applications. *Acc. Chem. Res.* **50**, 680–690 (2017).

299. Bae, S. W., Lee, J. S., Harms, V. M. & Murphy, W. L. Dynamic , Bioresponsive Hydrogels via Changes in DNA Aptamer Conformation. **1800353**, 1–6 (2018).

300. Jorge, A. & Eritja, R. Overview of DNA Self-Assembling: Progresses in Biomedical Applications. *Pharmaceutics* **10**, 268 (2018).

301. Le, J. *et al.* One nanometer self-assembled aptamer-DNA dendrimers carry 350. *Chem. Eng. J.* 124170 (2020). doi:10.1016/j.cej.2020.124170

302. Yadav, S., Sharma, A. K. & Kumar, P. Nanoscale Self-Assembly for Therapeutic Delivery. **8**, 1–24 (2020).

303. Asiri, A. M., Agarwal, S. & Gupta, V. K. Dynamic DNA nanostructures in biomedicine: beauty, utility and limits. *J. Mol. Liq.* 111484 (2019). doi:10.1016/j.molliq.2019.111484

304. Burns, J. R. & Howorka, S. Structural and functional stability of DNA nanopores in biological media. *Nanomaterials* **9**, (2019).

305. Dunn, K. E. The business of DNA nanotechnology: Commercialization of origami and other technologies. *Molecules* **25**, (2020).

306. Steinhauer, C., Jungmann, R., Sobey, T. L., Simmel, F. C. & Tinnefeld, P. DNA origami as a nanoscopic ruler for superresolution microscopy. *Angew. Chemie - Int. Ed.* **48**, 8870–8873 (2009).

307. Wang, D. *et al.* Design and operation of reconfigurable two-dimensional DNA molecular arrays. *Nat. Protoc.* **13**, 2312–2329 (2018).

308. Huang, Y. H. *et al.* Delivery of Therapeutics Targeting the mRNA Binding Protein HuR Using 3DNA Nanocarriers Suppresses Ovarian Tumor Growth. *Cancer Res.* **76**, 1549–1559 (2016).

309. Madsen, M. & Gothelf, K. V. Chemistries for DNA Nanotechnology. *Chem. Rev.* **119**, 6384–6458 (2019).

310. Ventura, S. P. M. *et al.* Ionic-Liquid-Mediated Extraction and Separation Processes for Bioactive Compounds: Past, Present, and Future Trends. *Chem. Rev.* (2017). doi:10.1021/acs.chemrev.6b00550

311. Freire, M. G. *et al.* Aqueous biphasic systems: a boost brought about by using ionic liquids. *Chem. Soc. Rev.* **41**, 4966 (2012).

312. Martzy, R. *et al.* Simple lysis of bacterial cells for DNA-based diagnostics using hydrophilic ionic liquids. 1–10 (2019). doi:10.1038/s41598-019-50246-5

313. Khimji, I. *et al.* Extraction of DNA staining dyes from DNA using hydrophobic ionic liquids. *Chem. Commun. (Camb).* **49**, 4537–9 (2013).

314. Xu, P. *et al.* A novel aqueous biphasic system formed by deep eutectic solvent and ionic liquid for DNA partitioning. *Talanta* **189**, 467–479 (2018).

315. Zoia, L. *et al.* Integrated biological and chemical characterisation of a pair of leonardesque canal lock gates. *PLoS One* **16**, e0247478 (2021).

316. Neves, M. C. *et al.* Improved ionic-liquid-functionalized macroporous supports able to purify nucleic acids in one-step. *Mater. Today Bio* 100086 (2020). doi:10.1016/j.mtbio.2020.100086

317. Peng, X. *et al.* Coupling oligonucleotides possessing a poly-cytosine tag with magnetic

ionic liquids for sequence-specific DNA analysis. *Chem. Commun.* **54**, 10284–10287 (2018).

318. Santra, K., Clark, K. D., Maity, N., Petrich, J. W. & Anderson, J. L. Exploiting Fluorescence Spectroscopy to Identify Magnetic Ionic Liquids Suitable for the Isolation of Oligonucleotides. *J. Phys. Chem. B* **122**, 7747–7756 (2018).

319. Clark, K. D. *et al.* Extraction of DNA by magnetic ionic liquids: Tunable solvents for rapid and selective DNA analysis. *Anal. Chem.* **87**, 1552–1559 (2015).

320. Ding, X., Clark, K. D., Varona, M., Emaus, M. N. & Anderson, J. L. Magnetic ionic liquid-enhanced isothermal nucleic acid amplification and its application to rapid visual DNA analysis. *Anal. Chim. Acta* **1045**, 132–140 (2019).

321. Emaus, M. N. & Anderson, J. L. Allelic discrimination between circulating tumor DNA fragments enabled by a multiplex-qPCR assay containing DNA-enriched magnetic ionic liquids. *Anal. Chim. Acta* **1124**, 184–193 (2020).

322. Shi, Y. *et al.* Ionic liquids promote PCR amplification of DNA. *Chem. Commun.* **48**, 5325 (2012).

323. Sivapragasam, M., Moniruzzaman, M. & Goto, M. Recent advances in exploiting ionic liquids for biomolecules: Solubility, stability and applications. *Biotechnol. J.* **11**, 1000–1013 (2016).

324. Zhao, H. DNA stability in ionic liquids and deep eutectic solvents. *J. Chem. Technol. Biotechnol.* **90**, 19–25 (2015).

325. Tateishi-Karimata, H. & Sugimoto, N. Biological and nanotechnological applications using interactions between ionic liquids and nucleic acids. *Biophys. Rev.* **10**, 931–940 (2018).

326. Abo-Hamad, A., Hayyan, M., AlSaadi, M. A. & Hashim, M. A. Potential applications of deep eutectic solvents in nanotechnology. *Chem. Eng. J.* **273**, 551–567 (2015).

327. Kist, J. A., Mitchell-koch, K. R. & Baker, G. A. The study and application of biomolecules in deep eutectic solvents. (2020). doi:10.1039/d0tb01656j

328. Gomes, J. M., Silva, S. S. & Reis, R. L. Biocompatible ionic liquids: Fundamental behaviours and applications. *Chem. Soc. Rev.* **48**, 4317–4335 (2019).

329. Menhaj, A. B., Smith, B. D. & Liu, J. Exploring the thermal stability of DNA-linked gold nanoparticles in ionic liquids and molecular solvents. *Chem. Sci.* **3**, 3216–3220 (2012).

330. Nimse, S. B., Song, K., Sonawane, M. D., Sayyed, D. R. & Kim, T. Immobilization techniques for microarray: Challenges and applications. *Sensors (Switzerland)* **14**, 22208–22229 (2014).

331. Patterson, A. *et al.* Using triplex-forming oligonucleotide probes for the reagentless, electrochemical detection of double-stranded DNA. *Anal. Chem.* **82**, 9109–9115 (2010).

332. Tateishi-Karimata, H., Pramanik, S. & Sugimoto, N. DNA sensor's selectivity enhancement and protection from contaminating nucleases due to a hydrated ionic liquid. *Analyst* **140**, 4393–4398 (2015).

333. Huang, Y. *et al.* Task-specific ionic liquid-enabled mercury sensor for sensitive detection of total mercury in food digestion solution. *Sensors Actuators B Chem.* **285**, 62–67 (2019).

334. Kosman, J. & Juskowiak, B. Peroxidase-mimicking DNAzymes for biosensing applications: A review. *Anal. Chim. Acta* **707**, 7–17 (2011).

335. Svigelj, R. *et al.* Truncated aptamers as selective receptors in a gluten sensor supporting direct measurement in a deep eutectic solvent. *Biosens. Bioelectron.* 112339 (2020). doi:10.1016/j.bios.2020.112339

336. Hansen, B. B. *et al.* Deep Eutectic Solvents: A Review of Fundamentals and Applications. *Chem. Rev.* acs.chemrev.0c00385 (2020). doi:10.1021/acs.chemrev.0c00385

337. Kong, D. M., Wang, N., Guo, X. X. & Shen, H. X. 'Turn-on' detection of Hg2+ ion using a peroxidase-like split G-quadruplex-hemin DNAzyme. *Analyst* **135**, 545–549 (2010).

338. O'Reilly, R. K., Turberfield, A. J. & Wilks, T. R. The Evolution of DNA-Templated Synthesis as a Tool for Materials Discovery. *Acc. Chem. Res.* **50**, 2496–2509 (2017).

339. Wang, L. & Arrabito, G. Hybrid, multiplexed, functional DNA nanotechnology for bioanalysis. *Analyst* **140**, 5821–5848 (2015).

340. Núñez-Pertíñez, S. & Wilks, T. R. Deep Eutectic Solvents as Media for the Prebiotic DNA-Templated Synthesis of Peptides. *Front. Chem.* **8**, 1–11 (2020).

341. Teng, Y., Tateishi-karimata, H. & Tsuruoka, T. Fluorescence of DNA-Templated Silver Nanoclusters via Unique Interactions of a Hydrated Ionic Liquid. (2018). doi:10.3390/molecules23112889

342. Chen, Z., Liu, C., Cao, F., Ren, J. & Qu, X. DNA metallization: Principles, methods, structures, and applications. *Chem. Soc. Rev.* **47**, 4017–4072 (2018).

343. Li, N. *et al.* Fabrication of Metal Nanostructures on DNA Templates. *ACS Appl. Mater. Interfaces* **11**, 13835–13852 (2019).

344. Kumar, V., Parmar, V. S. & Malhotra, S. V. Structural modifications of nucleosides in ionic liquids. *Biochimie* **92**, 1260–1265 (2010).

345. Mondal, D., Bhatt, J., Sharma, M., Chatterjee, S. & Prasad, K. A facile approach to prepare a dual functionalized DNA based material in a bio-deep eutectic solvent †. *Chem.*

Commun. **50**, 3989–3992 (2014).

346. Bhatt, J., Mondal, D., Devkar, R. V. & Prasad, K. Synthesis of functionalized N-doped graphene DNA hybrid material in a deep eutectic solvent. *Green Chem.* **18**, 4297–4302 (2016).

347. Chakraborty, S. *et al.* Facile Process for Metallizing DNA in a Multitasking Deep Eutectic Solvent for Ecofriendly C–C Coupling Reaction and Nitrobenzene Reduction. *ACS Sustain. Chem. Eng.* **7**, 14225–14235 (2019).

348. Rivilla, I. *et al.* Catalysis of a 1,3-dipolar reaction by distorted DNA incorporating a heterobimetallic platinum (II) and copper (II) complex. *Chem. Sci.* **8**, 7038–7046 (2017).

349. Silverman, S. K. DNA as a Versatile Chemical Component for Catalysis. *Angew Chem Int Ed Engl* **49**, 7180–7201 (2010).

350. Usselman, C. W. N. S. S. J. R. B. Catalytic DNA: Scope, Applications, and Biochemistry of Deoxyribozymes. *Physiol. Behav.* **176**, 139–148 (2017).

351. Rivilla, I. *et al.* Catalysis of a 1,3-dipolar reaction by distorted DNA incorporating a heterobimetallic platinum(II) and copper(II) complex. *Chem. Sci.* **8**, 7038–7046 (2017).

352. Boersma, A. J., Megens, R. P., Feringa, B. L. & Roelfes, G. DNA-based asymmetric catalysis. *Chem. Soc. Rev.* **39**, 2083–2092 (2010).

353. Roelfes, G. & Feringa, B. L. DNA-based asymmetric catalysis. *Angew. Chemie - Int. Ed.* **44**, 3230–3232 (2005).

354. Boersma, A. J. *et al.* Catalytic enantioselective syn hydration of enones in water using a DNA-based catalyst. *Nat. Chem.* **2**, 991–995 (2010).

355. Rioz-Martínez, A. & Roelfes, G. DNA-based hybrid catalysis. *Curr. Opin. Chem. Biol.* **25**, 80–87 (2015).

356. Zhao, H. & Shen, K. DNA-based asymmetric catalysis: role of ionic solvents and glymes. *RSC Adv.* **4**, 54051–54059 (2014).

357. Itoh, T. Ionic liquids as tool to improve enzymatic organic synthesis. *Chem. Rev.* **117**, 10567–10607 (2017).

358. Schindl, A., Hagen, M. L., Muzammal, S., Gunasekera, H. A. D. & Croft, A. K. Proteins in ionic liquids: Reactions, applications, and futures. *Front. Chem.* **7**, 1–31 (2019).

359. Lai, J.-Q. *et al.* Specific ion effects of ionic liquids on enzyme activity and stability. *Green Chem.* **13**, 1860 (2011).

360. Tan, J.-N. & Dou, Y. Deep eutectic solvents for biocatalytic transformations: focused lipase-catalyzed organic reactions. *Appl. Microbiol. Biotechnol.* (2020).

doi:10.1007/s00253-019-10342-y

361. Pätzold, M. *et al.* Deep Eutectic Solvents as Efficient Solvents in Biocatalysis. *Trends Biotechnol.* **37**, 943–959 (2019).

362. Molina-Espeja, P. *et al.* Beyond the outer limits of nature by directed evolution. *Biotechnol. Adv.* **34**, 754–767 (2016).

363. Yum, J. H., Park, S. & Sugiyama, H. G-quadruplexes as versatile scaffolds for catalysis. *Org. Biomol. Chem.* **17**, 9547–9561 (2019).

364. Mansuriya, B. D. & Altintas, Z. Applications of graphene quantum dots in biomedical sensors. *Sensors (Switzerland)* **20**, (2020).

365. Shen, J., Zhu, Y., Yang, X. & Li, C. Graphene quantum dots: Emergent nanolights for bioimaging, sensors, catalysis and photovoltaic devices. *Chem. Commun.* **48**, 3686–3699 (2012).

366. Nishimura, N. & Ohno, H. Design of successive ion conduction paths in DNA films with ionic liquids. *J. Mater. Chem.* **12**, 2299–2304 (2002).

367. Morimitsu, Y. *et al.* Mechanical Stabilization of Deoxyribonucleic Acid Solid Films Based on Hydrated Ionic Liquid. *Biomacromolecules* **21**, 464–471 (2020).

368. Mahmoudi-Moghaddam, H., Tajik, S. & Beitollahi, H. A new electrochemical DNA biosensor based on modified carbon paste electrode using graphene quantum dots and ionic liquid for determination of topotecan. *Microchem. J.* 104085 (2019). doi:10.1016/j.microc.2019.104085

369. Huang, J. Y. *et al.* A high-sensitivity electrochemical aptasensor of carcinoembryonic antigen based on graphene quantum dots-ionic liquid-nafion nanomatrix and DNAzyme-assisted signal amplification strategy. *Biosens. Bioelectron.* **99**, 28–33 (2018).

370. Shahdost-fard, F., Salimi, A., Sharifi, E. & Korani, A. Fabrication of a highly sensitive adenosine aptasensor based on covalent attachment of aptamer onto chitosan-carbon nanotubes-ionic liquid nanocomposite. *Biosens. Bioelectron.* **48**, 100–107 (2013).

371. Xu, S. *et al.* Real-time reliable determination of binding kinetics of DNA hybridization using a multi-channel graphene biosensor. *Nat. Commun.* **8**, 1–10 (2017).

372. Ke, G. *et al.* An accurate, high-speed, portable bifunctional electrical detector for COVID-19. *Sci. China Mater.* **64**, 739–747 (2021).

373. Sharma M., Mondal D., Singh N., Trivedi N., B. J. and P. K. High concentration DNA solubility in bio ionic liquids with long lasting chemical and structural stability at room temperature. *RSC Adv.* **5**, 40546–40551 (2015).

374. Rizan, N. *et al.* Effect of ionic liquid on the long-term structural and chemical stability of basidiomycetes DNAs integrated within Schottky-like junctions. *Appl. Phys. A* **127**, 142 (2021).

375. Clark, K. D., Sorensen, M., Nacham, O. & Anderson, J. L. Preservation of DNA in nuclease-rich samples using magnetic ionic liquids. *RSC Adv.* **6**, 39846–39851 (2016).

376. Mazid, R. R. *et al.* Enhanced enzymatic degradation resistance of plasmid DNA in ionic liquids. *RSC Adv.* **5**, 43839–43844 (2015).

377. Xin, Y. *et al.* Cryopreservation of DNA Origami Nanostructures. *Small* **16**, (2020).

378. Sharma, G. *et al.* Are ionic liquids and deep eutectic solvents the same?: Fundamental investigation from DNA dissolution point of view. *J. Mol. Liq.* **328**, 115386 (2021).

379. Singh, N., Sharma, M., Mondal, D., Pereira, M. M. & Prasad, K. Very high concentration solubility and long-term stability of DNA in an ammonium-based ionic liquid: A suitable medium for nucleic acid packaging and preservation. *ACS Sustain. Chem. Eng.* **5**, 1998–2005 (2017).

380. Mondal, D. *et al.* Improved solubility of DNA in recyclable and reusable bio-based deep eutectic solvents with long-term structural and chemical stability †. *Chem. Commun.* **49**, 9606–9608 (2013).

381. Mukesh, C. & Prasad, K. Formation of multiple structural formats of DNA in a bio-deep eutectic solvent. *Macromol. Chem. Phys.* **216**, 1061–1066 (2015).

382. Pedro, A. *et al.* Cholinium-based Good's buffers ionic liquids as remarkable stabilizers and recyclable preservation media for recombinant small RNAs. *ACS Sustain. Chem. Eng.* acssuschemeng.8b03900 (2018). doi:10.1021/acssuschemeng.8b03900

383. Mazid, R. R. *et al.* Biological stability and activity of siRNA in ionic liquids. *Chem. Commun.* **50**, 13457–13460 (2014).

384. Quental, M. V. *et al.* Integrated Extraction-Preservation Strategies for RNA Using Biobased Ionic Liquids. *ACS Sustain. Chem. Eng.* **7**, 9439–9448 (2019).

385. Mirjafari, A. Long-term DNA preservation and storage at ambient temperature. (2020). doi:US20200080131A1

386. Bisht, M. *et al.* Long-term protein packaging in cholinium-based ionic liquids: improved catalytic activity and enhanced stability of cytochrome c against multiple stresses. *Green Chem.* **19**, 4900–4911 (2017).

387. Weaver, K. D. *et al.* Cyto-toxicity and biocompatibility of a family of choline phosphate ionic liquids designed for pharmaceutical applications. *Green Chem.* **12**, 507 (2010).

388. Agatemor, C., Ibsen, K. N., Tanner, E. E. L. & Mitragotri, S. Ionic liquids for addressing unmet needs in healthcare. *Bioeng. Transl. Med.* **3**, 7–25 (2018).

389. Ventura, P. M., Gonçalves, F. J. M., Jeremias, G., Asselman, J. & Pereira, J. L. New insights on the effects of ionic liquid structural changes at the gene expression level : Molecular mechanisms of toxicity in Daphnia magna. (2020). doi:10.1016/j.jhazmat.2020.124517

390. Sarker, S. R., Ball, A. S., Bhargava, S. K. & Soni, S. K. Evaluation of plasmid DNA stability against ultrasonic shear stress and its: In vitro delivery efficiency using ionic liquid [Bmim][PF6]. *RSC Adv.* **9**, 29225–29231 (2019).

391. Sarkar, S. & Chandra Singh, P. Anions of Ionic Liquids Are Important Players in the Rescue of DNA Damage. *J. Phys. Chem. Lett.* **11**, 10150–10156 (2020).

392. Tanner, E. E. L., Wiraja, C., Curreri, C. A. & Xu, C. Stabilization and Topical Skin Delivery of Framework Nucleic Acids using Ionic Liquids. **2000041**, 1–9 (2020).

393. Mandal, A. *et al.* Treatment of psoriasis with NFKBIZ siRNA using topical ionic liquid formulations. *Sci. Adv.* **6**, eabb6049 (2020).

394. Vermeij, P., Kets, E., Dirks, C. & Piest, M. Liquid vaccines of live enveloped viruses. (2020).

395. Singh, S. K. & Savoy, A. W. Ionic liquids synthesis and applications: An overview. *J. Mol. Liq.* **297**, 112038 (2020).

396. Ramón, D. J. & Guillena, G. *Deep Eutectic Solvents: Synthesis, Properties, and Applications*. (John Wiley & Sons, 2020).

397. Diedenhofen, M. & Klamt, A. COSMO-RS as a tool for property prediction of IL mixtures-A review. *Fluid Phase Equilib.* **294**, 31–38 (2010).

398. Egorova, K. S., Posvyatenko, A. V, Larin, S. S. & Ananikov, V. P. Ionic liquids: prospects for nucleic acid handling and delivery. *Nucleic Acids Res.* **49**, 1201–1234 (2021).

CHAPTER 2

Materials and Methods

2.1 Materials (General)

2.1.1 Aqueous solutions and mixed solvents

All aqueous solutions were prepared with ultrapure water (18 MΩ) from Ultra Clear TWF with EI-Ion CEDI electro deionization system. The Tris Buffered Saline (**TBS**) aqueous buffer used mainly in Chapter 3-6 was prepared using powder from foil pouches (Sigma-Aldrich, T6664) that solvated in one liter consists in 50 mM Tris, 140 mM NaCl and 2.7 mM KCl. Then, 5 mM $MgCl_2$ were added using magnesium chloride hexahydrate (Sigma-Aldrich, M2670). The pH of the buffer was adjusted to 7.4 at 25 °C with HCl or NaOH. The rest of buffered solutions containing only water as solvent, were prepared with the corresponding amount of salts (sodium chloride, choline chloride, sodium lactate, etc.) or urea, and a mixture of Trizma HCl (Sigma-Aldrich, T3253) and Trizma Base (Sigma-Aldrich, T1503) using the quantities indicated by the manufacturer (Supelco, Spain). Once being prepared, the aqueous buffered solutions were filtered and stored at 6-8 °C.

Molecular solvents such as ethanol, ethylene glycol, triethylene glycol, glycerol or lactic acid were purchased from Sigma-Aldrich and used without further purification. In case of deep eutectic solvents, firstly, the hygroscopic reagent choline chloride was dehydrated under high vacuum and then, its hydration level was determined by Karl Fischer Titration. Afterwards, it was mixed within the corresponding hydrogen bond donor group at 80 °C for two hours. Before storing the solution at 6-8 °C they were filtrated and the water amount was measured again. While storing the almost anhydrous solutions for long periods (few months), it was extremely

important to heat them up to 80 °C for an hour, because precipitation of choline chloride was detected visually and using ^{1}H-NMR. This did not happen when deep eutectic solvents contained more than five wt. percentage of water. All ionic liquids were purchased directly from the manufacturer (Solvionic, Toulouse, France), and then their water amount was determined prior usage.

2.1.2 Chemicals

Table 2.1. Manufacturers of chemicals used throw the whole thesis and not mentioned elsewhere.

Name	Purchased from
Adenosine	≥99%. Sigma-Aldrich. Catalog Nº A9251
Agarose	BioReagent. Sigma-Aldrich. Catalog Nº A9539
Alexa Fluor 488	Termo Scientific. Catalog Nº A20000
AMP	≥97%, from yeast. Sigma-Aldrich. Catalog Nº A2252
APS	97%. Sigma-Aldrich. Catalog Nº 281778
ATP	Grade I, ≥99%, from microbial. Sigma-Aldrich. Catalog Nº A2383
Atto 488	≥90% (HPCE). Sigma-Aldrich. Catalog Nº 41051
Gluteraldehyde	Grade II, 25% in H_2O. Sigma-Aldrich. Catalog Nº G6257
GMP	≥99%, from yeast. Sigma-Aldrich. Catalog Nº G8377
Guanosine	≥98%. Sigma-Aldrich. Catalog Nº G6752
Hydrochloric acid	ACS reagent, 37%. Sigma-Aldrich. Catalog Nº 320331
SDS	BioReagent, ≥98.5% (GC). Catalog Nº L3771
Sodium hydroxide	BioUltra, 10 M in H_2O. Sigma-Aldrich. Catalog Nº 72068
TECP	Hydrochloride, ≥98%. Millipore. Catalog Nº 580560
Tween 20	Sigma-Aldrich. Catalog Nº P9416

2.1.3 DNA

All modified and non-modified DNA oligonucleotides used in Chapter 3, 4, 7 and 8 were ordered in Biomers GmbH (Munich, Germany) purified with HPLC. After being solvated, usually in ultrapure water, their concentration was calculated using UV-Vis Spectroscopy and the molar absorptivity indicated by the manufacturer. In case of salmon testes used in Chapter 3, 6 and 8, the salmon sperm sodium salt, the "short" one, was purchased from Sigma-Aldrich (D1626) and the "long" one from Thermo Scientific (15632011). While solvating DNA in each media, it was firstly heated up to 60 °C for several minutes and then cooled down slowly to room temperature. If DNA was solvated in almost anhydrous media, it was let mixing for several days or weeks at 40 °C (until a constant absorbance value was obtained) prior usage.

2.2 Methods (General)

2.2.1 UV-Vis spectroscopy

The UV-Vis absorbance was measured with two different instruments. On the one hand, the concentration of DNA (A260) and proteins (A280) was always assessed using a Nanodrop 2000c Spectrophotometer (Thermo Scientific, Spain) with a 2 µL volume sample of the biomolecule previously dissolved in water. The molar absorptivity (ε) used was that indicated by the company.

On the other hand, in those measurements where a cuvette or a temperature control was required, the Evolution 201 UV-Vis Spectrophotometer (Thermo Scientific, Spain) was used with a PCB-PLUS 1500 Peltier-Controlled External Water Recirculator. Furthermore, due to the

strong absorption of certain compounds, it was necessary to use a quartz cuvette with 1 mm path length (Hellma 110-QS) for melting measurements unless stated otherwise.

To determine the baseline of UV-Vis measurements, each media was previously measured in absence of the solute (usually, DNA). As can be observed in Figure 2.1, lactate anion-based media absorbed light in the UV range of interest, therefore, this media was heated in absence of DNA in order to correct the baseline of melting curves.

2.2.2 Circular Dichroism (CD) spectroscopy

Secondary structure analysis was carried out using a J-815 CD spectrometer (Jasco) with a Peltier FDCD Attachment (PFD-425S/15) used to maintain the temperature at 25 °C in all measurements if another temperature is not mentioned. The equipment is located in Nanogune (San Sebastián, Spain). The CD spectra of DNA and proteins were recorded from 350 to 180 nm and using the corresponding solvent as baseline; the data gathered per spectrum were the average of 5 time scans at a scanning rate of 200 nm/min and a bandwidth of 5 nm to minimize the noise and to smooth the signal. In parallel, it was also possible to measure the UV/Vis absorbance. Due to the strong absorption of certain compounds, it was necessary to use a quartz cuvette with 1 mm path length (Hellma 110-QS) unless stated otherwise.

In order to determine the baseline of measurements, each media was previously measured in absence of the solute (usually, DNA). As can be observed in Figure 2.1, only choline lactate media showed strong ellipticity above 220 nm and in this case, the data analyzed was that above 260 nm. Certain DES and IL also showed ellipticity but could be baselined. In other

cases, there was no ellipticity but the huge absorption of light below certain wavelength made impossible to acquire the ellipticity data of the solutes.

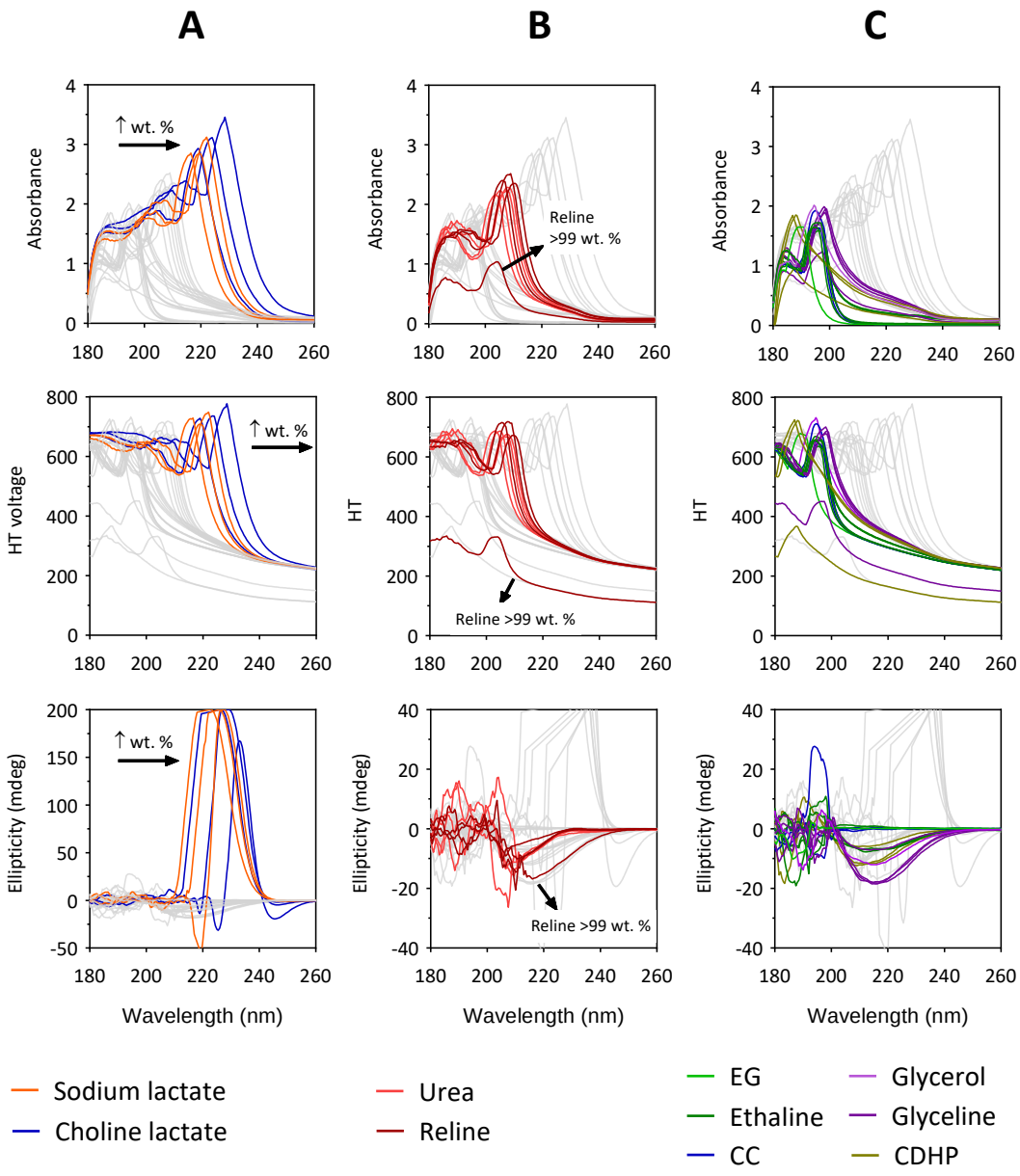

Figure 2.1. Absorbance, HT voltage and ellipticity data of different media. (A) Sodium lactate 11, 20 and 37 wt. percentage; Choline lactate 20, 37 and 71 wt. percentage. (B) Urea 10, 20, 40 and 50 wt. percentage; Reline 22, 53, 81 and >99 wt. percentage. (C) Ethylene glycol >99 wt. percentage; Glycerol >99 wt. percentage. Ethaline 23, 55, 85 and >99 wt. percentage; Glyceline 28, 66, 96 and >99 wt. percentage; Choline chloride 12, 30 and 45 wt. percentage; Choline dihydrogenphosphate 20, 37 and 66 wt. percentage. The data was acquired in circular dichroism instrument. The baseline was ultrapure water.

2.2.3 Karl Fischer titration

For the preparation of different media, it was necessary to assess accurately the water quantity, Karl Fischer Titration was used for this purpose, specifically the Mettler Toledo™ V20S Compact Volumetric KF Titrator (Thermo Scientific, Spain). The determined water content varied between 100 ppm and 50 wt. % and the sample volume used in each case varied according to the manufacturer recommendations. The reagents needed for the measurements were specifically adapted to dissolve the deep eutectic solvents and ionic liquids prepared: HYDRANAL-Titrant 5 and HYDRANAL-Solvent from Thermo Scientific (15634420 and 15674410, respectively). For instrument calibration after long periods without being used, it was necessary to use HYDRANAL-Water Standard 10.0 from Thermo Scientific (15644510).

2.2.4 Gel-electrophoresis

The length and double-strand formation of DNA oligonucleotides and salmon-sperm DNA were analyzed using the Bio-Rad equipment (excepting Chapter 6). Specifically an agarose (2-4 wt. %) gel-electrophoresis formed by TBE Running Buffer. The agarose gel experiments were carried out at 40-90V by 40-80 min, depending on the ionic strength of the media and DNA

length. GelRed™ Nucleic Acid Stain (10.000x in water) from Quimigen, Spain (41003) was used as staining dye (0.1 µL/g). As reference two ladder types were used, on the one hand the Gene Ruler Ultra Low Range DNA Ladder of 10-300 base pairs (Thermo Scientific, 11823983), and on the other hand the Gene Ruler 100 bp Plus DNA Ladder of 100-3000 base pairs (Thermo Scientific, 10309339).

2.2.5 Size-Exclusion Chromatography

The molecular weight (MW) and molar mass distribution (MWD) of DNA were analyzed by SEC/RI. The equipment was composed by a LC20 pump (Shimadzu, Spain) coupled to a Optilab T-Rex differential refractometer (λ=658 nm) (from Wyatt Technology Corp., USA). Separation was carried out using three columns in series (Ultrahydrogel 120, 250 and 2000; with pore sizes of 120, 250 and 2000 Å, respectively, all from Waters, Spain). The analyses were performed at 25 °C and the mobile phase had a flow rate of 0.6 mL/min. DNA oligonucleotides with different lengths (3930-616000 g/mol) were used to perform the calibration curve.

2.2.6 Nuclear Magnetic Resonance spectroscopy

Liquid ^{1}H NMR or ^{13}C NMR spectra were recorded at 400 or 500 MHz and 101 or 126 MHz for 13^{C} NMR, in a Bruker Advance spectrometer. At standard temperature and pressure, equipped with a z gradient BBOF probe, in $CDCl_3$ or D_2O. The data are reported as s = singlet, d = doublet, t = triplet, m = multiplet or unresolved, br s = broad signal, coupling constant(s) in Hz, integration. Data analysis was carried out with MestReNova software package.

2.2.7 Steady state and time-resolved fluorescence studies

Steady state measurements were conducted employing a FS920 single photon counting spectrofluorimeter from Edinburgh Instruments (Edinburgh, UK) equipped with a 450 W xenon arc lamp. The fluorophore-labelled samples were excited at 480 nm and fluorescence was monitored with the kinetic scan setup acquiring the emission at 525 nm, and a monochromatic bandwidth of 3 nm for excitation or 1 nm for emission. During measurements, the T-App Temperature Control Application software controlled the temperature.

Time-resolved measurements were done in the same equipment using the Time-Correlated Single Photon Counting (TCSPC) technique. The Pulsed Diode Laser from Edinburgh Instruments (Edinburgh, UK) had an excitation wavelength of 485 nm (linewidth <1.5 nm) and the emission bandwidth was set to 1 nm. The lifetime decays were acquired using pulses of 50 ns, 4096 channels and 5000 counts. In all cases, samples were measured into a quartz cuvette of 10 mm light path.

2.3 Materials and Methods (Chapter 3)

2.3.1 Density measurements

The density of solutions formed by molecular and deep eutectic solvents and different water quantities were measured using volumetric flasks. Great part of these values could be already found in the literature and they were corroborated with this method, on the other hand the densities of CC/EG (1:3) aqueous mixtures are not published yet in the literature. The volumetric flask used was of 1 mL and the calculated densities were the average of three independent measurements.

2.3.2 Viscosity measurements

The viscosity measurements were carried out with a controlled stress rheometer (AR-G2, TA Instruments). It was employed to analyse viscosities of different mixed solutions, using cone and plate geometry with 40 mm diameter. This rheometer is especially suitable for testing ionic liquids as it only requires a very small amount of sample (1–2 mL) to wet the whole cone surface. Samples were initially equilibrated for 5 min, and then the shear rate was exponentially increased from 10 to 8000 s^{-1} via stress controlled feedback over 5 minutes recording 10 points per decade.

Since studied DESs and ILs are highly hydrophilic and the solution measured contained already water, each independent measurement was performed with a new sample, discarding the volume used in previous ones. Repetitiveness was very good with root-mean square deviations (RMSD) less than 5% in all series. The temperature of viscosity measurement was

always assessed at 298 K employing a Peltier plate to set the temperature. All measurements were performed at atmospheric pressure.

2.3.3 Hybridization studies of DNA using steady state fluorescence

For hybridization studies, firstly, the Oligo1 labelled with Alexa Fluor 488 (17 nM) was solvated in the corresponding solvent and the fluorescence intensity was let stabilizing at 25 °C. Then an equivalent amount of Oligo2 labelled with Black Hole Quencher 1 was added to the solution and the fluorescence change was monitored, from which it was possible to obtain the hybridization percentages (Equation 2.1) and rates were obtained by fitting the experimental data with Equation 2.2 and using the value of b to resolve Equation 2.3.

$$\text{Hybridization } \% = 100 - (\mathrm{F_f} \cdot \frac{100}{\mathrm{F_0}}) \qquad \textit{Equation 2.1}$$

$$\mathrm{F(t)} = \mathrm{F_0} + \mathrm{a} \cdot \ \mathrm{e}^{-\mathrm{b} \cdot \mathrm{t}} \qquad \textit{Equation 2.2}$$

$$b = C_{oligo2} \cdot k_h \qquad \textit{Equation 2.3}$$

Where, $\mathrm{F_f}$ and $\mathrm{F_0}$ are the fluorescence values after and before hybridization, respectively and $\mathrm{F(t)}$ is the fluorescence at time t. a and b are constants obtained through curve fitting. Once knowing the value of constant b and the initial concentration of Oligo2 (17 nM), it is possible to obtain the hybridization rate between the two oligomers in each media. After hybridization, the sample was cooled to 0 °C and heated up to 80 °C at a rate of 1 °C/min, what allowed the calculation of the melting temperature from the first derivative. In general, the melting temperature was measured only once, because it was observed in several measurements that obtained values were highly accurate and reproducible (±0.5 °C) for the purpose of the study.

On the other hand, the fluorescence values of Oligo1-AF488 and Oligo2 in absence of BHQ-1 were also measured varying temperatures and media and were used to correct the baseline of melting curves.

Chapter 2

2.4 Materials and Methods (Chapter 4)

2.4.1 Procedure of *Ab Initio* calculations

Prior geometry optimizations and frequency calculations, the system was prepared with the Avogadro 1.2.0 open software. The Gaussian 16 (Gaussian, Inc., Wallingford CT, 2009) package[1] was used for Density Functional Theory (DFT) calculations and these were done in the Cluster Arina provided by SGIker (UPV/EHU/ ERDF, EU). Specifically, at the m062x/6-311+G** theory level was used for calculations. The aqueous environment was simulated with the iefpcm model. Geom=(connectivity) was included in the input, in order to avoid the angle errors during optimization (Code 2.1).

```
###
%mem=7520mb
%nprocshared=8
$RunGauss
#m062x/6-311+G** opt Freq SCRF(iefpcm,Solvent=Water)
…
###
```

Code 2.1

The changes in Enthalpy (ΔS) and Gibbs Free Energy (ΔG) were calculated from absolute values obtained with individual components or when they were solvated together. The ΔS and ΔG values are expressed in kcal/mol (1 Hartree = 627.41 kcal/mol).

2.4.2 Force Fields used in Molecular Dynamics calculations

The force field parameters of DNA, TIP3P water model, choline, glycerol, urea and metallic salts were obtained directly from the CHARMM36 Force Field. The force field of ethylene glycol was refined from CHARMM36 based-on a recently published article which is specially adapted to aqueous solutions[2]. On the other hand, the force fields of DESs were based in those of their separated compounds; this strategy has been approved in several articles[3–7]. However, for future works, it needs to be considered that rescaling the partial charges allows for proper sampling of the equilibrium properties of neat DESs as well as hydrated DESs[8,9]. Unfortunately, this article was posterior to simulations.

2.4.3 Procedure of Molecular Dynamics calculations

Firstly, in order to prepare the boxes (Figure 4.2), it was necessary to adjust the box size and it was found that 8.5 nm^3 were enough to prevent the interaction between nucleic acids in periodic boundary conditions. For the creation of the box, firstly, in packmol software[10], the HBA, HBD or DES molecules were randomly placed within 8.8 nm^3 (Code 2.2), slightly higher volume than desired. In presence of DNA, it was not filled with HBA, HBD or DES molecules in the space where DNA would be located (Code 2.3).

```
###
tolerance 2.0
filetype pdb
output thedesiredoutputname.pdb
structure theHBAorHBDmolecule.pdb
  resnumbers 2
```

```
  number thedesirednumberofmoleculesinthebox
  inside box -45. -45. -45. 45. 45. 45.
end structure
###
```

Code 2.2

```
###
…
  outside box -12.5 -12.5 -23.5 12.5 12.5 23.5
  inside box -45. -45. -45. 45. 45. 45.
…
###
```

Code 2.3

Then, DNA was placed in the box (if necessary) using solvate tool of VMD software[11]. Water was introduced using once again the solvate tool of VMD and finally metallic ions were added with add ions tool of VMD by replacing part of these water molecules, in this manner the boxes were ready for equilibration.

The equilibration calculations were done using NAMD 2.13 (University of Illinois) package and the Cluster Arina provided by SGIker (UPV/EHU/ ERDF, EU). When the box contained DNA, its atoms were labelled as 1 in the beta column in VMD (Code 2.4) and then frozen in equilibration input (Code 2.5). The box was firstly equilibrated for 2 ns at 800 K (nvt), and other 2 ns at 298 K and 1 atm (npt). Finally, DNA was unfrozen and all atoms were equilibrated for 15 ns at 298 K and 1 atm (npt conditions).

```
###
mol load psf thepsfstructure.psf pdb thepdbstructure.pdb
set all [atomselect top all]
set fix [atomselect top "nucleic"]
```

```
$all set beta 0
$fix set beta 1
$all writepdb theoutputpdbstructure.pdb
mol delete all
###
```

Code 2.4

```
###
if {1} {
fixedAtoms on
fixedAtomsFile theinputpdbstructure.pdb
fixedAtomsCol B
}
###
```

Code 2.5

In absence of DNA, all atoms were equilibrated for 2 ns at 800 K (nvt) and then for 12 ns at 298 K and 1 atm (npt). The systems were prepared for MD calculations by applying 10000 steps of energy minimization using the steepest descent method. Electrostatic interactions were evaluated using the particle-mesh-Ewald (PME) summation technique. The equations of motion were solved by using the leap-frog algorithm with 1 fs time step. The cut-off distance for the short-range interactions was set to 1.2 nm with a switching function used from 1.0 to 1.4 nm. The data used in analysis was that acquired in the last 10 ns in presence of DNA and 7 ns in its absence (with steps of 20 ps).

2.4.4 Analysis of Molecular Dynamics calculations

Prior analysing the output files, it was necessary, in presence of DNA, to use the PBC Wrap command in VMD in order to re-center the nucleic acid during the whole trajectory (Code 2.6).

```
###
pbc wrap -center com -centersel "nucleic" -compound residue -all
thedesiredtrajectoryoutputfile.dcd
###
```

Code 2.6

Then, different tools of VMD were used in the analysis of the last 10 ns of each calculation (with steps of 50 ps), i.e. they were used to calculate the densities, root mean square deviations (RMSD), radial distribution functions (RDF), and hydrogen bonding. The number of molecules were determined using Code 2.7. On the other hand, the atoms of minor and major grooves and backbone were selected using the three lines presented in Code 2.8.

```
###
set mol [molinfo top]
set sel [atomselect $mol {theatomormoleculetobecounted}]
set frames [molinfo $mol get numframes]
set fp [ open "theoutputfile.dat" w ]
for {set i 0} {$i < $frames} {incr i} {
    $sel frame $i
    $sel update
    set n [$sel num]
    puts $fp "$i $n"
}
```

```
$sel delete
close $fp
unset mol sel frames fp i n
###
```

Code 2.7

```
###
(resname GUA and not resid 14 and name N3 N2) or (resname CYT and not resid 5 and name O2) or (resname ADE and not resid 3 and name N3 H2) or (resname THY and not resid 16 and name O2) ### Selected atoms of minor groove without considering ending bases

(resname GUA and not resid 14 and name N7 O6) or (resname CYT and not resid 5 and name N4 H5) or (resname ADE and not resid 3 and name N7 N6) or (resname THY and not resid 16 and name O4 C5M) ### Selected atoms of major groove without considering ending bases
(backbone and resname ADE and not resid 3) or (backbone and resname GUA and not resid 14) or (backbone and resname THY and not resid 16) or (backbone and resname CYT and not resid 5) ### Selected atoms of phosphate backbone without considering ending bases
###
```

Code 2.8

However, for further structural analysis of DNA it was necessary to use the Curves+ and Canal software[12] in Linux using Fortran code. Firstly, the trajectories of DNA (dcd) were converted to crd in VMD and then the analysis of each step was done using Curves+ software (Code 2.9), with Canal it was possible to analyse the whole trajectory (Code 2.10) with the input created with Curves+. With these software it was possible to obtain the helical, backbone and groove parameters of DNA.

```
###
/Cur+executablelocation <<!
&inp     file=inputtrjfile.trj     ftop=inputtopfile.top,     lis=outputfilename, lib=/standardfilelocation, &end
```

```
2 1 -1 0 0
1:12
24:13
!
###
```

Code 2.9

```
###
/canalexecutablelocation <<!
&inp lis=outputfilename, lev1=2,lev2=11,histo=.t,corr=.t.,&end
curvesinputfilename AGGTTCCAGGTG
!
###
```

Code 2.10

2.5 Materials and Methods (Chapter 5)

2.5.1 Binding studies using Surface Plasmon Resonance

A Pioneer FE SPR System was used for analysing the affinity of the ATP DNA-aptamer towards different target molecules (ATP, AMP, adenosine and GMP) in different solvent mixtures. Firstly, the biotinylated DNA was immobilized on a SADH (Streptavidin) biosensor, with streptavidin immobilized in a dextran hydrogel. For the latter procedure, the running buffer was always TBS, with 0.05 wt. % of Tween 20. The DNA was injected until the surface of the sensorchip was saturated and response kept constant. Finally, before proceeding with the affinity studies, 20 mM of NaOH were used to clean the DNA bound non-specifically. Then, the media was changed to the desired media, and after obtaining a constant response, the target, solvated in each media, was injected at increasing concentrations. The flow rate was always of 25 µL/min.

2.5.2 Binding studies using Steady State Fluorescence

For molecular recognition studies, 50 nM of the ATP DNA-molecular beacon were solvated in the corresponding media. On the other hand, a 10 mM stock solution of the target (AMP or GMP) was prepared in the same solvent conditions. Then, the excitation at 525 nm was constantly acquired upon excitation at 480 nm and the target molecule was added at a constant temperature. The fluorescence intensity was let to stabilize before the addition of each target concentration. The intensity values were corrected depending on the concentration of the molecular beacon in each target addition.

2.5.3 Calculation of the dissociation constant from binding studies

The dissociation constant (K_d) was calculated from the mathematical fitting to one site binding saturation equation (Equation 2.4) using the response or fluorescence values obtained upon the addition of the different concentrations of target molecule.

$$f(C_{target})_N = \frac{B_{max} \cdot C_{target}}{K_d \cdot C_{target}} \qquad \textit{Equation 2.4}$$

Where B_{max} is a constant value obtained upon curve fitting, C_{target} is the concentration of the target in each step and $f(C_{target})_N$ is the response or fluorescence values obtained in each step minus the value obtained in absence of the target.

2.6 Materials and Methods (Chapter 6)

2.6.1 DNA Oligonucleotides and target molecules

The nucleic acids and molecular targets used in this chapter were ordered from Ella Biotech GmbH (Planegg, Germany) (Table 2.2), due to the close collaboration of Prof Mayer's group with this manufacturer. The initial population of single-stranded random-sequences was formed by a D3 DNA pool, the library had a randomized internal region of 43 nucleotides flanked by two primer regions with 18 and 19 nucleotides at the 5' and 3' ends. In addition, two primer sequences were designed for further amplification of eluted sequences, the reverse primer was 5'-phosphate labelled to make possible the later digestion by the lambda exonuclease. The target molecule of SELEX was 8-Amino-hexyl-adenosine triphosphate immobilized in sepharose-beads, and two other ATP and GTP beads were used in binding assays.

Table 2.2. Used starting library, primers and targets during SELEX and binding assays.

Name	Sequence 5' to 3'
Starting library	GCTGTGTGACTCCTGCAA**N43**GCAGCTGTATCTTGTCTCC
Fwd primer	GCT GTG TGA CTC CTG CAA
Rv primer	Phosphated-GGA GAC AAG ATA CAG CTG C

8-Amino-hexyl-ATP	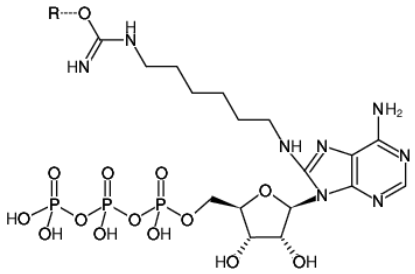
γ-Amino-hexyl-ATP	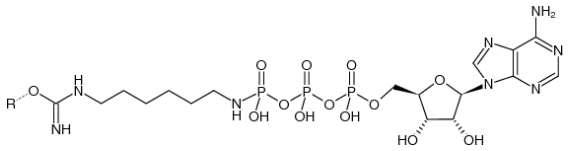
γ-Amino-hexyl-GTP	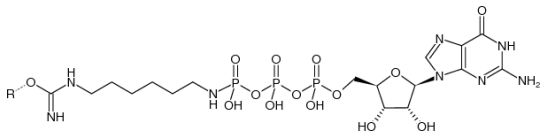

2.6.2 SELEX procedure

Incubation step. The first step of each round consists in incubating the starting library with the target. For that purpose, the beads were deposited in bio-spin chromatography columns with a porous 30 µm polyethylene bed support and 1,2 ml bed volume (Bio-Rad, France), 100 µL of suspension of target beads (≈ 5 µM) were firstly dried by centrifugation and then weighed to ensure always the same amount of them. Then, the column with beads was washed with 200 µL of the selection buffer three times and finally 200 µL of the selection buffer were added with the desired concentration of DNA. Salmon sperm DNA purchased from Thermo Fisher Scientific, Inc. (Karlsruhe, Germany), was used as a competitor and introduced in the

solvent matrix in each incubation step at a concentration of 1 mg/mL. The final mixture was incubated at 25 °C for the desired period of time. In order to separate unbound sequences from bound ones, the solution was taken out from the column by gravity and the flow through obtained was discarded.

Partitioning and elution steps. The remaining unbound or weakly bound DNA was washed off the column using 200 µL of selection buffer the desired amount of times, these solutions were discarded by gravity. The DNA that was strongly bound to the beads was separated using thermal elution strategy: 200 µL of pure water were added to the column and heated up to 95 °C for 2 minutes and the solution was recovered by centrifugation (30 sec. 12400 rpm) for further amplification of sequences.

Amplification and conditioning steps. Each PCR reaction was carried out in presence of 200 µM of A, G, C and T deoxynucleotides triphosphates (dNTPs) from Genaxxon (Ulm, Germany); 2 mM of $MgCl_2$ and 2.5 units of *Taq polymerase* per 100 µL of solution. The primers concentration was 1 µM for both of them and the thermal cycling was: 95 °C for 60 s, 64 °C for 30 s, 72 °C for 45 s (repeated the needed cycles) and 72 °C for 120 s in final extension step, then solution was cold down to 10 °C. Prior SELEX procedure, it was confirmed that residual amount of choline lactate did not affect the PCR reaction.

After amplification, the formation of double-stranded DNA (dsDNA) was confirmed by 4% agarose gel electrophoresis. Each electrophoresis experiment was carried out at 130-150 V by 10-15 min. As reference the Gene Ruler Ultra Low Range DNA Ladder (10-300 base-pairs) from Thermo Fisher Scientific was used. Then the dsDNA amplified was purified with a PCR

clean-up kit (Macherey-Nagel, Germany), and the phosphate complementary strand was digested by lambda exonuclease (Thermo Fisher Scientific) following a standard protocol, the completion of the reaction was verified by agarose gel electrophoresis. Finally, ssDNA was purified using the previous PCR clean-up kit. Purified sequences were used for the next SELEX round and all the previous steps were repeated the necessary number of rounds.

2.6.3 Cloning and sequencing

In order to split up the library members into single members, the final pool was cloned into a bacterial vector, obtaining single-member colonies. Then, the plasmids were extracted and Sanger sequencing was carried out. The analysis of obtained sequences was carried out using MUSCLE software and bioinformatic tools developed in Prof. Mayer's group.

2.6.4 Radioactive phosphorylation of sequences for binding studies

After SELEX steps and isolation of possible aptamer sequences, binding assays were performed labelling radioactively the DNA. For this purpose, firstly plasmid-DNA was amplified and purified using standard protocols.

Purified ssDNA was 5' labelled with ^{32}P from γ-ATP using T4 polynucleotide kinase (Thermo Fisher Scientific) by incubating 40 µl DNA solution (ca. 45 pmol) with 5 µl T4 PNK buffer, 2.5 µl T4 PNK (10 U/ µl) and 0.9 µl radioactive ATP (10 µCi/µl) (Perkin Elmer) for 40 min at 37 °C. The labelled DNA was purified from unreacted γ-ATP with G25 spin columns by centrifugation for 2 minutes (750 g) (GE Healthcare).

Finally, before performing binding assays, the successful labelling and removal of γ-ATP was confirmed by 10% polyacrylamide gel electrophoresis (PAGE). 0.5 µl of each ssDNA sample was inserted and carried out at 130-150 V by 10-15 min.

2.6.5 Binding studies using liquid scintillation counting (LSC)

Binding assays of radioactively labelled samples were done with the pool of 1st rounds as negative control and the pool of final rounds as positive control. Once the SELEX procedure validation assays finished, further binding assays of unique sequences were optimized and had few differences with the former: radioactive DNA amount was always 10 pmol (0.05 µM), the duration of incubation step was fixed to 30 minutes and solution was taken out by centrifugation (30 sec. 12400 rpm). Beads were washed twice and solutions were centrifuged as in incubation. In thermal elution step the column was heated up to 80 °C for 5 minutes and the solution was recovered by centrifugation (60 sec. 12400 rpm).

Radioactivity of obtained solutions were measured by LSC: one solution of incubation step (also called supernatant), several solutions in partitioning step (one per washing), one solution of elution step and another one of the beads (inserting directly the column in the eppendorf). Considering that the sum of the counts per minute (CPM) of the collected solutions plus the beads corresponded to 100% of radioactivity, it was possible to calculate the percentage of DNA found in each solution.

Chapter 2

2.7 Materials and Methods (Chapter 7)

2.7.1 Immobilization assay in Surface Plasmon Resonance

The Biacore T200 Surface Plasmon Resonance equipment was used for online monitoring the DNA nanostructure. A High-affinity Streptavidin (SA) Sensor Chip was used for the immobilization of the biotinylated DNA. This DNA was injected until surface saturation and then the non-specifically bound DNA was removed using 20 mM of NaOH. The flux rate was of 25 µL/min in immobilization experiments and further assays with DNA and molecular targets.

2.7.2 Immobilization assay in Quartz Crystal Microbalance

The QCM-D equipment was specifically the *Q-Sense E1*system (Biolin Scientific, Sweden). A standard gold sensor chip was used (QSX301, Q-Sense, Sweden) with the following specifications: frequency 4.95 MHz ± 50 kHz, diameter 14 mm, thickness 0.3 mm, RMS surface roughness of electrode <3 nm. Before usage, the sensor was cleaned with an UV cleaner for 10 min, thereafter with basic piranha (1:1:5 of H_2O_2, 25 wt. percentage ammonia solution and ultrapure water) at 80 °C for 5 min, and again with UV treatment for 10 min.

For the immobilization of DNA in the gold surface, an aqueous solution of the thiolated DNA (100 µM, 100 µL) was firstly pretreated with 100 µL of TECP disulfide reducing gel for 30 minutes. Next, the reducing gel was removed by centrifuging (12800 rpm). Using physiological media (TBS), the treated DNA solution was diluted to 10 µM and injected to the QCM-D containing the gold sensorchip. NaOH 20 mM was used to remove non-specifically bound DNA.

All QCM-D measurements were done at a stabilized temperature of 23 °C and the flux was 35 µL/min.

2.8 Materials and Methods (Chapter 8)

2.8.1 Scanning Electron Microscope (SEM) and Confocal Microscopy (CM)

After cleaning the empty AAO membranes using boiling water and a solution of 5 wt. percentage HCl, the SEM measurements were done by the General Research Services of UPV/EHU (SGIker) using a magnification of 100 kx. Then, the pictures were analyzed using FIJI/ImageJ Software (PixelSize=0.9921875 nm), obtaining an average Feret of 35 ± 10 nm.

Confocal microscopy studies were done using the Leica SP2 AOBS confocal microscope (Leica Microsystems, Wetzlar, Germany) with a lens that has 63x zoom and a numerical aperture of 1.4. The excitation wavelength was at 488 nm and the emission spectra were taken from 505 to 535 nm. The voltage 477 V was applied to obtain fluorescence intensity of the membrane surface. Two different pictures were obtained in the same time: the fluorescence and the reflection mode of the laser.

2.8.2 Immobilization of DNA on anodized aluminum oxide (AAO)

The DNA immobilization protocol on AAO surface was equal in the QCM-D sensorchip and isoporous membrane and was based-on a published protocol[13]. First, they were cleaned with boiling water for one hour and then they were immersed in HCl solution (5 wt. percentage) for 30 seconds. Then, they were washed with ultrapure water and were dried in nitrogen gas.

Second, they were immersed into an acetone solution containing 5 wt. % of APTES (Sigma-Aldrich, Catalogue Nº A3648) for 8 hours. Then, they were washed in acetone and baked at 120 °C for 2 hours. After that, they were left overnight in aqueous solution containing 25 wt. percentage of gluteraldehyde.

After thoroughly washing with ultrapure water and drying in nitrogen gas, the sensorchip or the membranes were modified with the amino-modified DNA by drop-coating using 100 µL of a physiological solution (TBS, pH 7.4) containing amino-modified DNA at 100 µM for 8 hours. Then the sensorchip or membranes were rinsed with hot ultrapure water until no DNA was detected in the washing solution. All procedures were done at 25 °C unless mentioned otherwise. Further layers of DNA or the one-step supersandwich were hybridized with the capture probe immersing the membranes in a salty solution (0.5 M NaCl) containing the DNA at 10 µM for 8 hours or injecting this DNA with a flux of 35 µL/min in QCM-D, in case of the sensorchip.

2.8.3 Side-Bi-Side diffusion cell

The diffusion cell was manufactured by PermeGear Inc. (Hellertown, USA) and had a capacity of 7 mL in each chamber (Figure 2.2). In order to do the permeation studies, the AAO membrane was placed between the two chambers using two black Viton® gaskets (Merck, Catalog Nº 27355) to avoid leakage. After filling both chambers with the corresponding media, the permeation of the erioglaucine disodium salt, also known as brilliant blue[14] (Merck, Catalogue Nº 861146), was monitored by UV-Vis (630 nm) in the spectrophotometer using a peristaltic tubing pump (Ismatec, Wertheim, Germany) and a flow-through cuvette from Hellma

GmbH (Müllheim, Germany). The stirring speed in the donor and receptor chambers was 1200 rpm and two small PTFE stirring bars were used in each side.

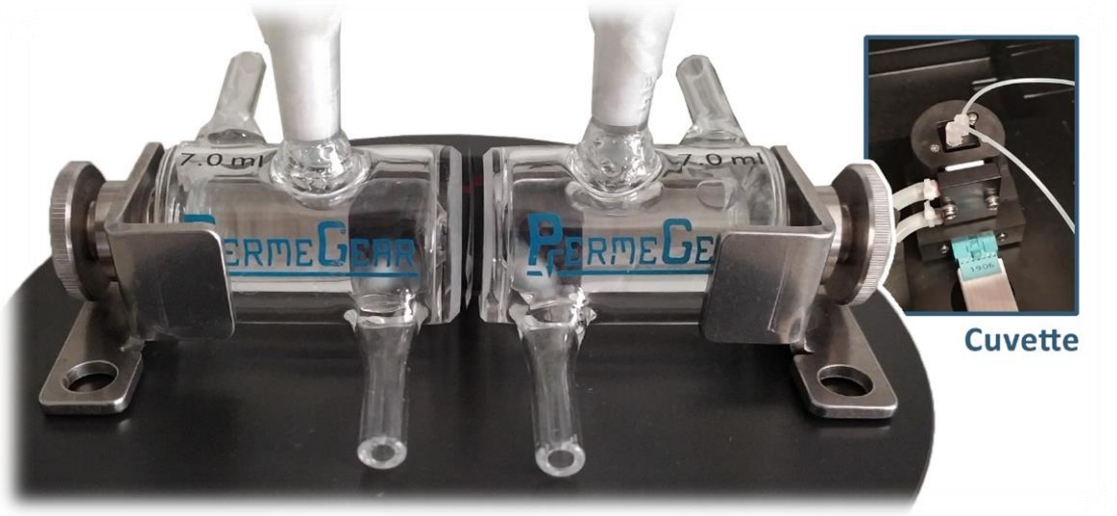

Figure 2.2. The Side-Bi-Side diffusion cell and a picture of the cuvette in the holder.

2.8.4 Custom-made microfluidic diffusion cell

The flow was in opposite directions to increase the transfer of matter and recirculated using a peristaltic tubing pump in case of aqueous solutions (Ismatec, Wertheim, Germany). While using organic solvents, the flow was recirculated with a ReaXus LD Class piston pump (Teledyne Isco, Lincoln, USA). The permeation of the dye was monitored inserting a cuvette (Hellma GmbH, Müllheim, Germany) in the circuit of the receiving channel and using the spectrophotometer.

The diffusion coefficient of the dye across the membrane was calculated using Equation 2.5, derived from Fick's first law of diffusion[15]. Where D is the diffusional coefficient (cm^2/s); C_i, C_t and C_f are the initial, intermediary and final concentrations of the dye (mol/L) in the receptor

channel, respectively. V_1 and V_2 are the volume of the liquid (cm^3) in the donor and receptor channels, respectively; L is the thickness of the dry membrane (cm); and A is the effective diffusion area of the membrane (cm^2). In all experiments, a plot of $\ln[(C_f\text{-}C_i)/(C_f\text{-}C_t)]$ *versus* time (t), showed a straight initial line. From this, the diffusion coefficient could be calculated using the Equation 2.6 where K is the gradient of the straight line.

$$D = \frac{V_1 \cdot V_2}{(V_1 + V_2)} \cdot \frac{L}{A} \cdot \frac{1}{t} \cdot \ln\left(\frac{C_f - C_i}{C_f - C_i}\right) \qquad \textit{Equation 2.5}$$

$$D = K \cdot \frac{V_1 \cdot V_2}{(V_1 + V_2)} \cdot \frac{L}{A} \qquad \textit{Equation 2.6}$$

2.8.5 Catalytic Diels-Alder reaction

The Diels-Alder reactions were done in aqueous solution containing 20 mM MOPS and a pH of 6.5. The DNA bound catalyst was prepared by mixing an aqueous solution of salmon-sperm DNA with an aqueous solution of catalyst [Cu(ligand)$(NO_3)_2$] 24 hours in advance. Then, an aliquot of a stock solution (0.5 M) of dienophile was added and the MOPS buffer was added achieving a final concentration of 20 mM MOPS, 1.3 mg/mL DNA, 0.39 mM of ligand, 0.3 mM of metal and 1 mM of dienophile. The mixture was cooled to 5 °C. The reaction started by addition of freshly refluxed cyclopentadiene (final concentration 15 mM) and was mixed at 1200 rpm for 5 days.

2.8.6 High Performance Liquid Chromatography (HPLC)

After extracting the reactants and products using dichloromethane (DCM), the DCM was evaporated and 2 mL of ethyl acetate were added to each sample. Then, the ethyl acetate

solutions were sonicated, filtered and injected in the HPLC vials. Ivan Rivilla, from the F. P. Cossio's group performed the HPLC measurements injecting 15 µL of sample and using an already published protocol[16]. The column consisted on a Daicel chiralcel-ODH (heptane/iPrOH 98:2, 0.5 ml/min).

The *endo* percentage (Equation 2.7) and the enantiomeric excess percentage of the *endo* isomer (Equation 2.8) were calculated with the areas of each product obtained at a wavelength of 266 nm using a HPLC with a UV-Vis spectrophotometer. On the other hand, calibration curves of the dienophile and products were done in each HPLC measurement round, in order to calculate the yield and conversion, this was done measuring the total area of products (≈10-16') or dienophile (≈16-21') at 313 and 266 nm, respectively (Figure 2.3).

$$endo\ \% = \frac{\mathrm{A}_{endo}}{(A_{exo}+A_{endo})} \cdot 100 \qquad \textit{Equation 2.7}$$

$$ee\ \% = [A_{endo(+)} - A_{endo(-)}] \cdot (\frac{100}{\mathrm{A}_{endo}}) \qquad \textit{Equation 2.8}$$

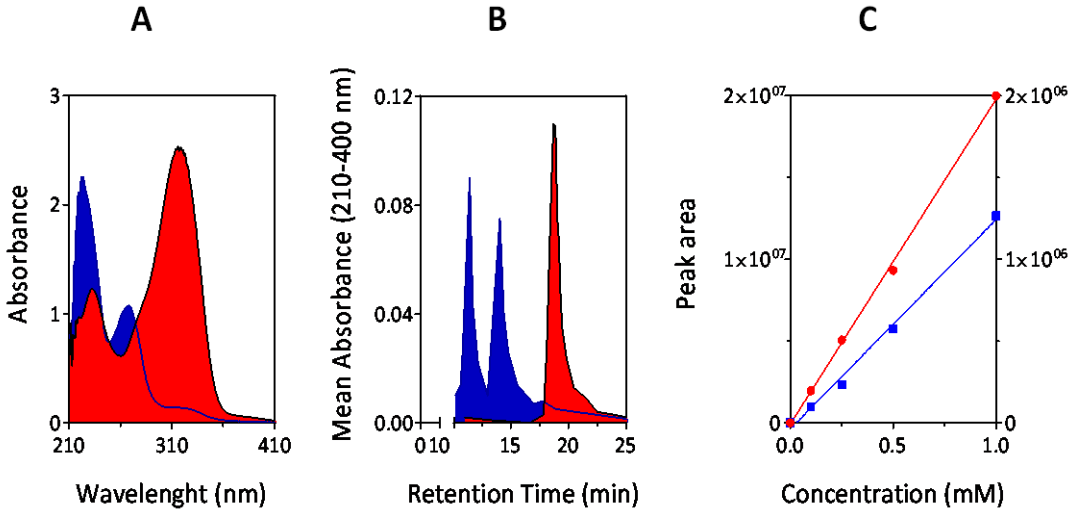

Figure 2.3. (A) The UV-Vis spectra of the dienophile (red) and product (blue). (B) The HPLC chromatogram of dienophile (red) and product (blue). (C) An example of the calibration curve obtained from the area of the peaks of HPLC chromatogram for dienophile (red, left Y-axis) and product (blue, right Y-axis).

2.9 References

1. Frisch, M. J.; Trucks, G. W.; Schlegel, H. B.; Scuseria, G. E.; Robb, M. A.; Cheeseman, J. R.; Scalmani, G.; Barone, V.; Petersson, G. A.; Nakatsuji, H.; Li, X.; Caricato, M.; Marenich, A. V.; Bloino, J.; Janesko, B. G.; Gomperts, R.; Mennucci, B.; Hratch, D. J. No Title. *Gaussian 16, Revis. C.01*
2. Kaur, S., Shobhna & Kashyap, H. K. Insights Gained from Refined Force-Field for Pure and Aqueous Ethylene Glycol through Molecular Dynamics Simulations. *J. Phys. Chem. B* **123**, 6543–6553 (2019).
3. Perkins, S. L., Painter, P. & Colina, C. M. Experimental and Computational Studies of Choline Chloride-Based Deep Eutectic Solvents. *J. Chem. Eng. Data* **59**, 3652–3662 (2014).
4. Kumari, P. & Kashyap, H. K. Influence of Hydration on the Structure of Reline Deep Eutectic Solvent: A Molecular Dynamics Study. *ACS Omega* **3**, 15246–15255 (2018).
5. Kaur, S., Malik, A. & Kashyap, H. K. Anatomy of Microscopic Structure of Ethaline Deep Eutectic Solvent Decoded through Molecular Dynamics Simulations. *J. Phys. Chem. B* **123**, 8291–8299 (2019).
6. Baz, J., Held, C., Pleiss, J. & Hansen, N. Thermophysical properties of glyceline–water mixtures investigated by molecular modelling. *Phys. Chem. Chem. Phys.* **21**, 6467–6476 (2019).
7. Weng, L. & Toner, M. Janus-faced role of water in defining nanostructure of choline chloride/glycerol deep eutectic solvent. *Phys. Chem. Chem. Phys.* **20**, 22455–22462 (2018).

8. Hansen, B. B. *et al.* Deep Eutectic Solvents: A Review of Fundamentals and Applications. *Chem. Rev.* acs.chemrev.0c00385 (2020). doi:10.1021/acs.chemrev.0c00385

9. Sapir, L. & Harries, D. Restructuring a Deep Eutectic Solvent by Water: The Nanostructure of Hydrated Choline Chloride/Urea. *J. Chem. Theory Comput.* **16**, 3335–3342 (2020).

10. Martínez, L., Andrade, R., Birgin, E. G. & Martínez, J. M. PACKMOL: A package for building initial configurations for molecular dynamics simulations. *J. Comput. Chem.* **30**, 2157–2164 (2009).

11. Humphrey, W., Dalke, A. & Schulten, K. VMD: Visual molecular dynamics. *J. Mol. Graph.* **14**, 33–38 (1996).

12. Lavery, R., Moakher, M., Maddocks, J. H. & Zakrzewska, K. Conformational analysis of nucleic acids revisited: Curves+. *Nucleic Acids Res.* **37**, 5917–5929 (2009).

13. Jiang, Y., Liu, N., Guo, W., Xia, F. & Jiang, L. Highly-Efficient Gating of Solid-State Nanochannels by DNA Supersandwich Structure Containing ATP Aptamers: A Nanofluidic IMPLICATION Logic Device. *J. Am. Chem. Soc.* **134**, 15395–15401 (2012).

14. Bişgin, A. A. Ta. Simultaneous preconcentration and determination of brilliant blue and sunset yellow in foodstuffs by solid-phase extraction combined UV-vis spectrophotometry. *J. AOAC Int.* **101**, 1850–1856 (2018).

15. Liu, Z., Wang, W., Xie, R., Ju, X.-J. & Chu, L.-Y. Stimuli-responsive smart gating membranes. *Chem. Soc. Rev.* **45**, 460–475 (2016).

16. Roelfes, G., Boersma, A. J. & Feringa, B. L. Highly enantioselective DNA-based catalysis. *Chem. Commun.* **6**, 635–637 (2006).

CHAPTER 3

Spectroscopic studies of DNA double helixes in mixed solvents

3.1 Introduction

The double helical DNA and nanostructures based on this secondary structure are usually solvated using physiological conditions, consisting in water molecules and inorganic ions that neutralize the negative charge of phosphate groups. These conditions are the most conventional liquid environment for DNA and are the ideal conditions for the thermal stabilization of Watson-Crick base-pairs, as explained in Chapter 1. However, the use of physiological media presents some challenges in technological designs. For example, when storing DNA in water hydrolytic reactions take place, which cause the degradation of DNA. Moreover, water can also easily evaporate in microfluidic systems or be a limitation to dissolve different target molecules[1]. This brought about the interest of studying the structure and stability of the double-helix in non-conventional media that could solve previous issues; molecular solvents, deep eutectic solvents (DESs) and ionic liquids (ILs) are the main alternative media.

So far, due to its time-cost, it is not possible to studies the solvation of the DNA sequence of interest in all media. Multiple fundamental studies have been made with the aim of being able to predict the thermal and conformational stability of the DNA double helix, but these have succeeded specially for physiological media[2–5], in contrast, very little is known yet about its thermal and conformational stability beyond those specific conditions with water as the unique solvent[6]. In this chapter, a systematic spectroscopic study was done about the structural and thermal stabilities of different double-helix structures, especially in molecular solvents and deep eutectic solvents in order to expand

and add new perspectives to the work done by Isabel Machado in her PhD thesis about the use of DNA in ionic liquids (2016, UPV/EHU).

During this work, apart from studying two salmon-sperm DNA (s-sDNA) with different average lengths, the greatest part of the studies have been done using short-DNA oligonucleotides (12 nucleotides) with well-defined sequences. These short sequences are in the length range of complementary oligonucleotides of the DNA-origami scaffolds, functional DNA or the sequences used for the SDR[7,8]. Therefore, the obtained data can be used directly in dynamic DNA nanostructures. On the other hand, the molecular solvents, ILs and DESs were mixed with water at different ratios, from diluted conditions to almost anhydrous ones. In this way it has been possible to understand how the stability of the double helix changes as the level of DNA hydration varies.

3.2 Results and Discussion

3.2.1 The thermal stability of a short double helix in deep eutectic solvents

Despite the systematic study of Isabel Machado about the double helical DNA solvation in several ionic liquids, the thermal and structural stabilities of this DNA in deep eutectic solvents are yet completely unknown. The latter media can offer some advantages compared with ionic liquids, being the most relevant ones their easy synthesis, natural source and their low-cost. In order to study how varies the thermal stability in the principal DESs[9], firstly, a short DNA duplex has been solvated at a great variety of concentrations of three DESs and their individual components (HBA and HBD groups), from diluted to almost anhydrous conditions. Choline chloride salt was selected as HBA group, in order to compare results with those obtained using choline-based ILs[6]. As HBD groups, urea and two different polyol molecules were chosen, which form reline, ethaline and glyceline, the most used DES in industry and technology[10–13]. On the other hand, another DES was added as a potential media with low viscosity and wide liquid temperature range, which is formed between choline chloride and ethylene glycol in a molar ratio of 1:3 (Figure 3.1).The DESs were synthesized using the protocol described in Section 2.1.1.

Hydrogen bond acceptor group

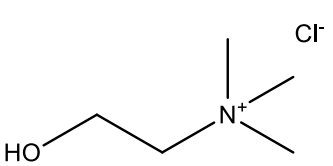

Choline chloride (CC)

Hydrogen bond donor groups

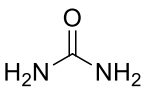

Urea

1:2

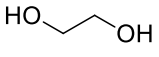

Ethylene glycol (EG)

1:2

1:3

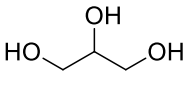

Glycerol (Gly)

1:2

Figure 3.1. The HBA group and different HBD groups used in the synthesis of DESs. Below of its HBD group is shown the molar ratio between HBA and HBD groups.

The thermal stabilities of the duplex formed between Oligo1 and Oligo2 were characterized using steady state fluorescence studies. For that purpose, the Oligo1 was modified with a fluorophore (Alexa Fluor 488) at the 5' position and the Oligo2 with a quencher (BHQ-1) at the 3' position. On the other hand, it was necessary to prepare the different media systematically. In order to do so, it was firstly necessary to elucidate if the introduction of metallic salts could improve the thermal stability of the short duplexes in presence of deep eutectic solvents. It is well known that metallic salts, until certain concentration (1-2 mol/L), increase the thermal stability of duplexes in water shielding the electrostatic repulsion between backbones, but as DESs are charged media, they could substitute the role of metallic salts.

In order to elucidate if it was necessary to introduce salts to enhance the stability of the double helix, the melting temperatures were evaluated in presence of different DES/water/salt mixtures using ethaline as DES and NaCl as salt. The ethaline/water mixtures were prepared in absence of NaCl, in presence of a constant concentration of NaCl and decreasing gradually the concentration of NaCl proportional to the decrease in water concentration. Moreover, as blank, water/NaCl mixtures were prepared reducing metallic salts concentration. The details can be found in Table 3.1 and calculated melting temperatures and hybridization percentages are shown in Figure 3.2.

Table 3.1. Prepared mixtures in water. (A) In absence of DES, varying NaCl concentration. (B) Substituting water with ethaline but maintaining NaCl concentration constant. (C) Substituting water with ethaline and reducing NaCl concentration. (D) In absence of NaCl, varying ethaline concentration.

Mixture	Compound	The concentration in each sample (M)							
A	NaCl	0.14	0.12	0.11	0.09	0.08	0.06	0.05	0.03
B	Ethaline	0	0.44	0.87	1.30	1.74	2.18	2.61	3.42
	NaCl	0.5	0.5	0.5	0.5	0.5	0.5	0.5	0.5
C	Ethaline	0	0.44	0.87	1.30	1.74	2.18	2.61	3.42
	NaCl	0.14	0.12	0.11	0.09	0.08	0.06	0.05	0.03
D	Ethaline	0	0.44	0.87	1.30	1.74	2.18	2.61	3.42

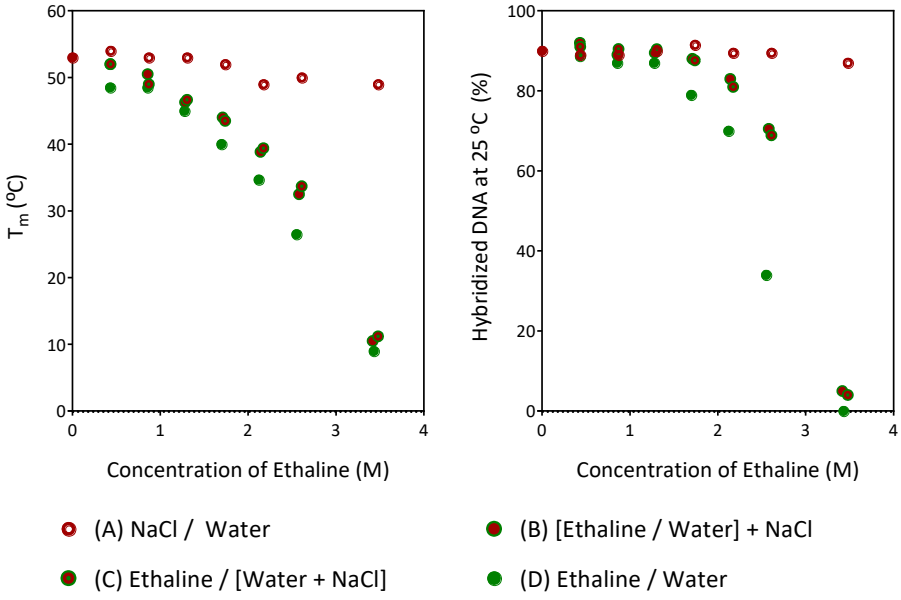

Figure 3.2. Melting temperatures and hybridized percentages at 25 °C of the duplexes formed between Oligo1 and Oligo2 in each mixture described in Table 3.1. The concentration of each DNA oligonucleotide was 17 nM.

As can be seen in Figure 3.2, it was found that the presence of metallic salts in ethaline DES enhanced the thermal stability of the duplex formed between Oligo1 and Oligo2. This enhancement was very significant while using ethaline at concentrations of 1.74, 2.18 and 2.61 M. But, at the highest concentration of ethaline (3.48 mol/L; ≈ 85 wt. %) the stabilization effect of metallic salts was almost lost. On the other hand, there were no significant differences between maintaining the original concentration of salts (B mixture) or reducing them gradually (A and C mixtures), probably because there were enough metallic cations in contact with DNA which was at a very low concentration (17 nM).

Considering that a minimum metallic salt concentration could be beneficial, the mixtures based-on DESs and their individual compounds were prepared using the same procedure of C mixture. The density of each solution was measured as explained in Section 2.3.1, in order to work not only in molar concentration but also in mass and molar fractions. The details of the different mixtures prepared are shown in Table S3.1 and in Figure 3.3 can be found all melting temperatures of the duplexes. For the best of our knowledge, this is the first systematic study about the thermal stability of a duplex in several deep eutectic solvents and their individual HBA and HBD groups and serves to understand how to design the solvent and choose the right water fraction. These data are discussed in more depth below.

In Figure 3.3A and 3.3B can be observed that at a same concentration or molar fraction, urea had the highest destabilization effect between the three HBD groups and the melting temperatures in the two polyol solvents were almost equal. On the other hand, the HBA group, choline chloride (Figure 3.3C and 3.3D), had certain thermal destabilization effect above 1 M.

These results were not surprising as urea is usually used at 8 M as denaturant and the similar effect of polyols has been already reported in the literature[14–16]. The destabilization capacity of salts above 1 or 2 M can be also found in the literature with other ions such as NaCl or $CaCl_2$[17].

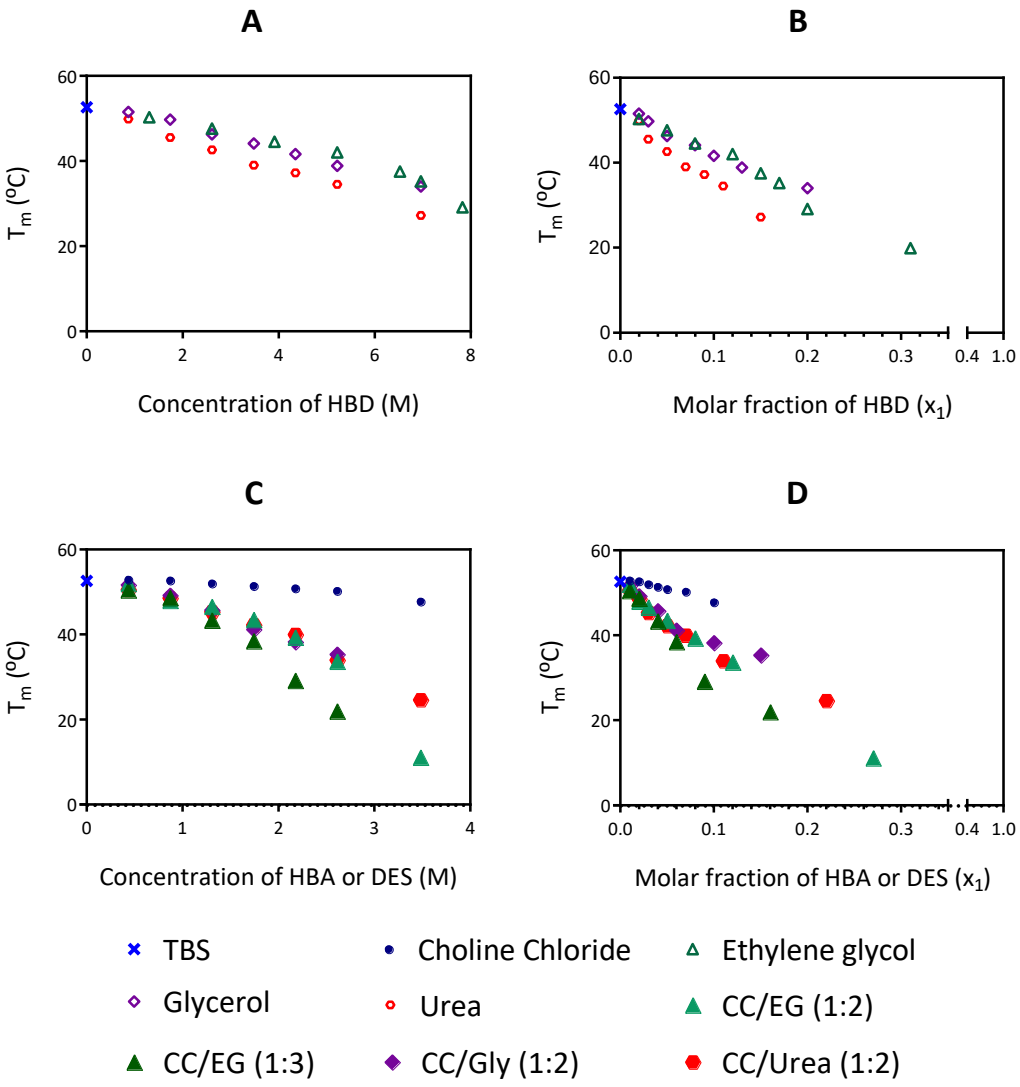

Figure 3.3. Melting temperatures of the duplexes formed between Oligo1 and Oligo2 in (A)(B) HBD groups and (C)(D) HBA group and DESs. The concentration of DNA oligonucleotides was 17 nM.

What remained unknown until now is the destabilization effect of DESs and the comparison with their individual components. In case of the most famous DESs, ethaline (CC/EG (1:2)), glyceline (CC/Gly (1:2)) and reline (CC/Urea (1:2)), they destabilized in a similar manner the duplex, at least until 2.61 M (64 – 77 wt. % DES). Then, in some cases there was a huge fall in the melting temperature that could not be measured with the equipment used (the minimum temperature that could be achieved was -10 °C). On the other hand, it was found that the molar ratio of HBD needs to be minimized as much as possible to maintain the duplex thermally stable, this was seen comparing between CC/EG (1:2) and CC/EG (1:3), where the latter destabilizes more the duplex than the rest of the DESs above 1 M or 0.05 molar fraction.

Curiously, as can be better observed in Figure S3.1, in case of reline, the DES destabilized less the duplex than the HBD group. This needs to be better studied but probably the hydrogen bonds that urea forms with the HBA group reduce the creation of hydroxide ions close to DNA. Furthermore, it is interesting that when represented *versus* molar concentration, the thermal destabilization fits a second order polynomial trend at least until 2.61 M in all cases (77 wt. % DES) and 3.48 M in others (≈ 85 wt. % DES). The latter could permit, in example with hairpin-based aptamers, to adjust the best DNA, DES and physiological media combination to achieve the desired trade-off between thermal stability, stimuli-responsiveness and solvent properties.

On the other hand, during the measurements, it was possible to calculate also the hybridization percentages and rates at 25 ^{o}C, shown in Figure S3.2. It can be observed that hybridization percentages also followed a second order polynomial curve. Unfortunately, in case of the hybridization rates, which have important implications in sensing and stimuli-responsive

designs, the values obtained did not follow any trend. With both, HBD groups and DESs, the hybridization rates decreased while increasing their concentration. This is contrary to the behaviour measured in ethanol or observed in other molecular solvents or ionic liquids in the literature[18,19]. One reason of the decrease in rates in DESs could be the increase in viscosity of solution (Figure S3.3). However, increasing concentration of ethylammonium nitrate ionic liquid accelerated the hybridization rates between two oligonucleotides[20] even if its viscosity also increased. Therefore, further studies are still needed to understand the kinetics of DNA in non-physiological media[21–23].

3.2.2 The nanoenvironment close to DNA *via* time-resolved fluorescence

Time-resolved fluorescence studies were done to gain insights about the interactions between solvent and DNA. Firstly, the lifetime of the hydrophilic and highly negatively charged Alexa Fluor 488[24] was measured in each mixture, while being linked to Oligo1 and also in its free state in presence of Oligo1. It was observed that there was only one lifetime decay in all cases, but first, a strong dynamic quenching occurred when AF488 was covalently attached to Oligo1 as has been already observed with other linked dyes[25,26]. The lifetime decreased from 4.3 to 3.31 ns from free to labelled-state in aqueous media. Second, the trend in lifetime values was very different if the fluorophore was free or linked to DNA: the lifetime of the free fluorophore decreased while increasing the concentration of HBA, HBD and DES media whereas the lifetime of AF488 attached to Oligo1 did not decrease in presence of HBA, HBD or DES media. It increased or maintained close to the value of 3.31 ns (Figure 3.4).

The different lifetime values of Alexa Fluor 488 (AF488) can vary due to multiple parameters such as changes in the nanoenvironment (viscosity, pH, polarity, solvation) or molecular interactions of the fluorophore with DNA, including dynamic quenching[27,28]. However, some of these could be discarded as main factors: it seems that viscosity did not influence the lifetime of free AF488, as it should lengthen it[29] but glycerol and glyceline had the shortest lifetime values. On the other hand, the fluorophore is pH insensitive between 4 and 10[30].

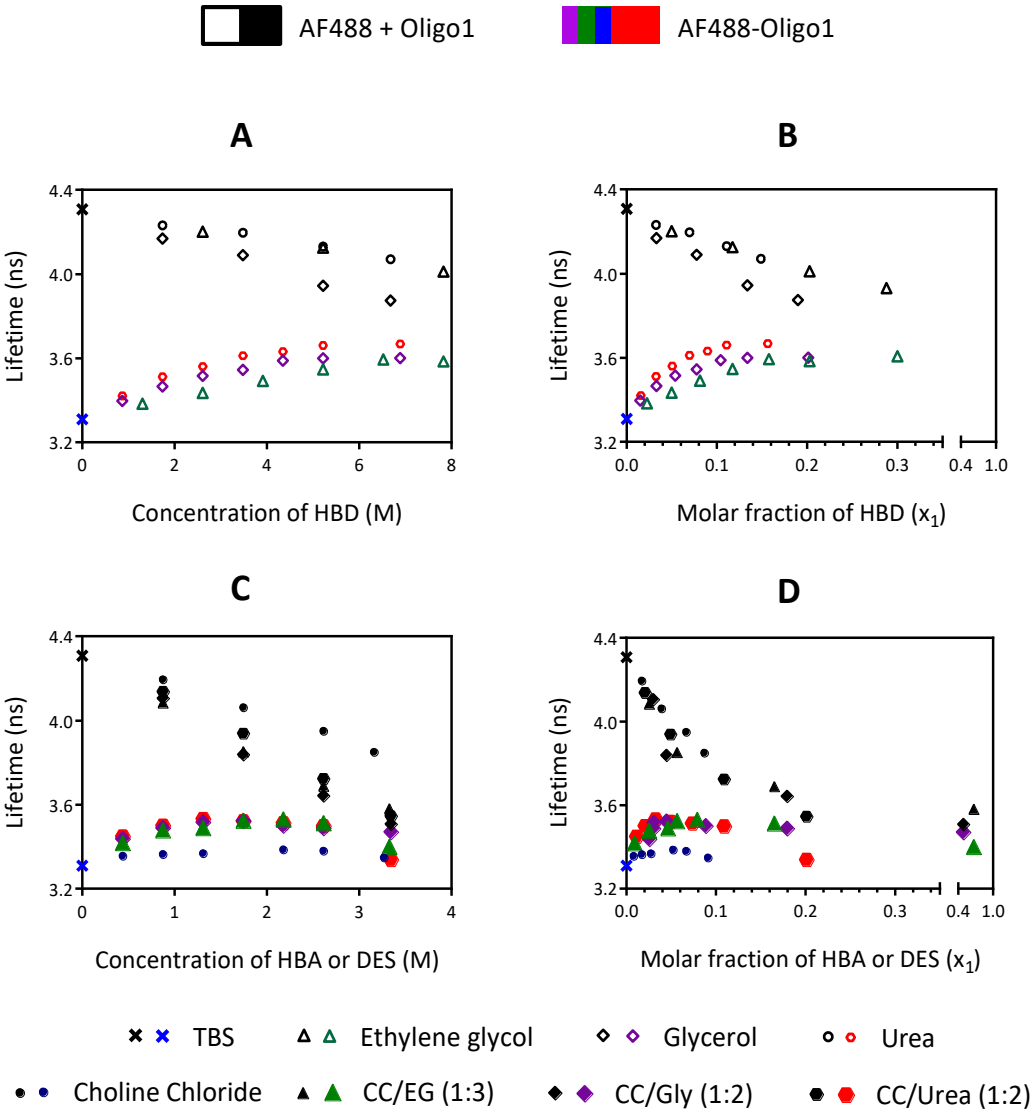

Figure 3.4. Lifetime values of Alexa Fluor 488 free in solution (black) and attached to Oligo1 (coloured) at 25 ^{o}C. (A)(B) In HBD media. (C)(D) In HBA and DES media. The concentration of the fluorophore and DNA oligonucleotide was 17 nM.

In case of polarity, the mixtures tend to be less polar while decreasing the concentration of water what could explain the linear decrease in lifetime of free AF488 while increasing HBA,

HBD and DES media concentration[31]. Contrary to free AF488 that showed a linear change in lifetime values, the changes in lifetime values of AF488 attached to Oligo1 might be influenced also by the interactions of the media with DNA. This could explain why these changes in lifetime followed a second or third order polynomial trend.

The initial lenghtening of the lifetime could be explained by a decrease in the dynamic quenching that DNA was causing[32]. This decrease can be due to structural changes on DNA, but it can be discarded that the lifetime depends on the non-covalent interactions with nucleotides of Oligo1, because upon addition of Oligo2 the lifetime maintained at 3.30 ns in TBS (data not shown). On the other hand, the lifetime values of the linked fluorophore in DES only increased linearly until a certain concentration or molar fraction then they decreased, differently to what occurred in HBD groups were they did not decrease. This might be due to the dynamic quenching that high salt concentration could provoke on the fluorophore[33] and therefore it means that the choline salt interacts strongly with ssDNA upon this concentration, independent of the HBD group. The characterization of interactions between solvent and DNA continues in the next section and in Chapter 4 using computational methods.

3.2.3 The secondary structure of DNA characterized by circular dichroism

Fluorescence studies allowed the accurate determination of the thermal stabilities of DNA in non-physiological media, apart from giving some clues about the microenvironment. However, those technics did not give information about possible changes in the secondary structure of the double helix. Characterizing the secondary structure of DNA it could be possible

to observe the structure of the melted sequences and minor changes in the hybridized helixes. For that purpose, circular dichroism studies were done to Oligo1 and the duplexes formed between both oligonucleotides.

Firstly, in physiological conditions (TBS), the circular dichroism (CD) spectra of Oligo1 and Oligo2 were measured separately or altogether (Figure 3.5A), including that of the duplex at different temperatures (Figure 3.5B). It can be observed that the spectra of each oligonucleotide in TBS are very similar to that of the duplex at 80 ^{o}C, what means that at 25 ^{o}C, Oligo1 and Oligo2 are in a random-coil form in absence of their complementary sequence, at least in physiological conditions. The red shift in the positive peak of the duplex from fully hybridized to denatured state (from 267 nm to 277 nm) and the disappearance of the negative peak denotes the loss of ellipticity.

On the other hand, it was possible to calculate the melting temperature of the duplex being of 56 ^{o}C, this was confirmed using UV-Vis, which gave a similar value (54 ^{o}C) (Figure S3.5). These values were slightly higher than the value of 52 ^{o}C found by spectrofluorimetry, the enhanced thermal stability of DNA at higher concentrations is due to the cooperative effect of DNA hybridization, the higher number of DNA molecules increases the probability of the

complementary base pairing. The concentration was 5 µM in CD or UV-Vis studies and 17 nM in fluorescence studies.

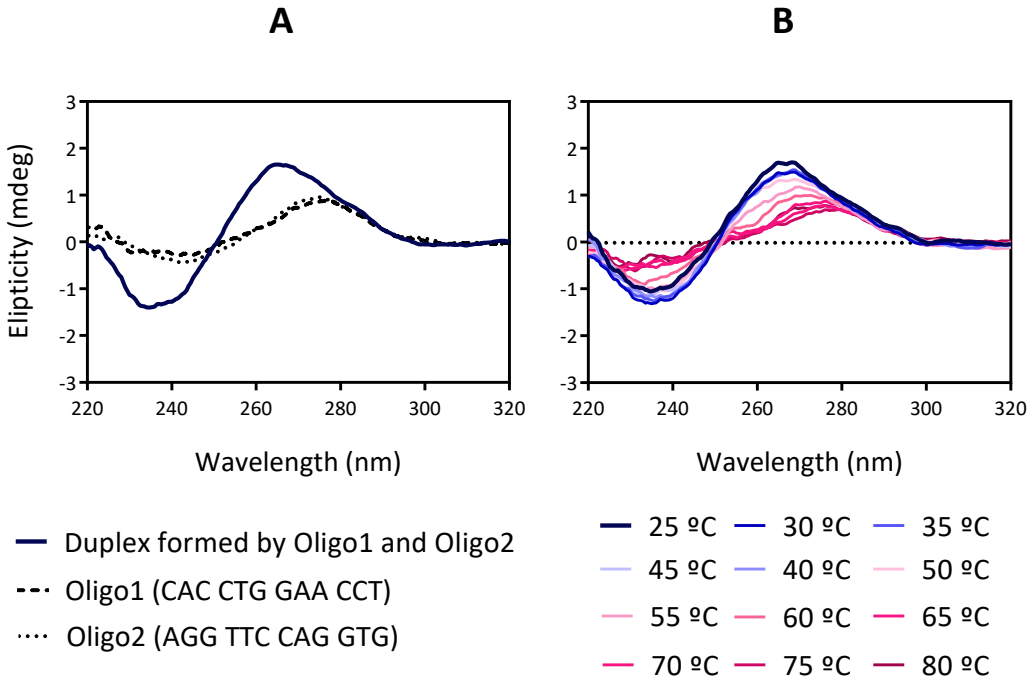

Figure 3.5. CD spectra of DNA oligonucleotides (5 µM) in TBS media. (A) The spectra of the duplex and individual oligonucleotides at 25 ^{o}C. (B) The spectra of the duplex at different temperatures.

Then, CD studies continued solvating the Oligo1 and duplexes at low (≈ 0.9 M) and high DES concentrations (≈ 3.4 M), plus the equivalent concentrations of their individual components. All CD spectra can be found in Figure S3.6-S3.9 separated by solvent type. All measurements were done at a constant temperature of 25 ^{o}C; therefore, some duplexes were partially or totally

Spectroscopic studies of DNA double helixes in mixed solvents denatured while using almost anhydrous conditions (≈ 3.4 M) according to the hybridization percentages calculated in fluorescence studies (Figure S3.4).

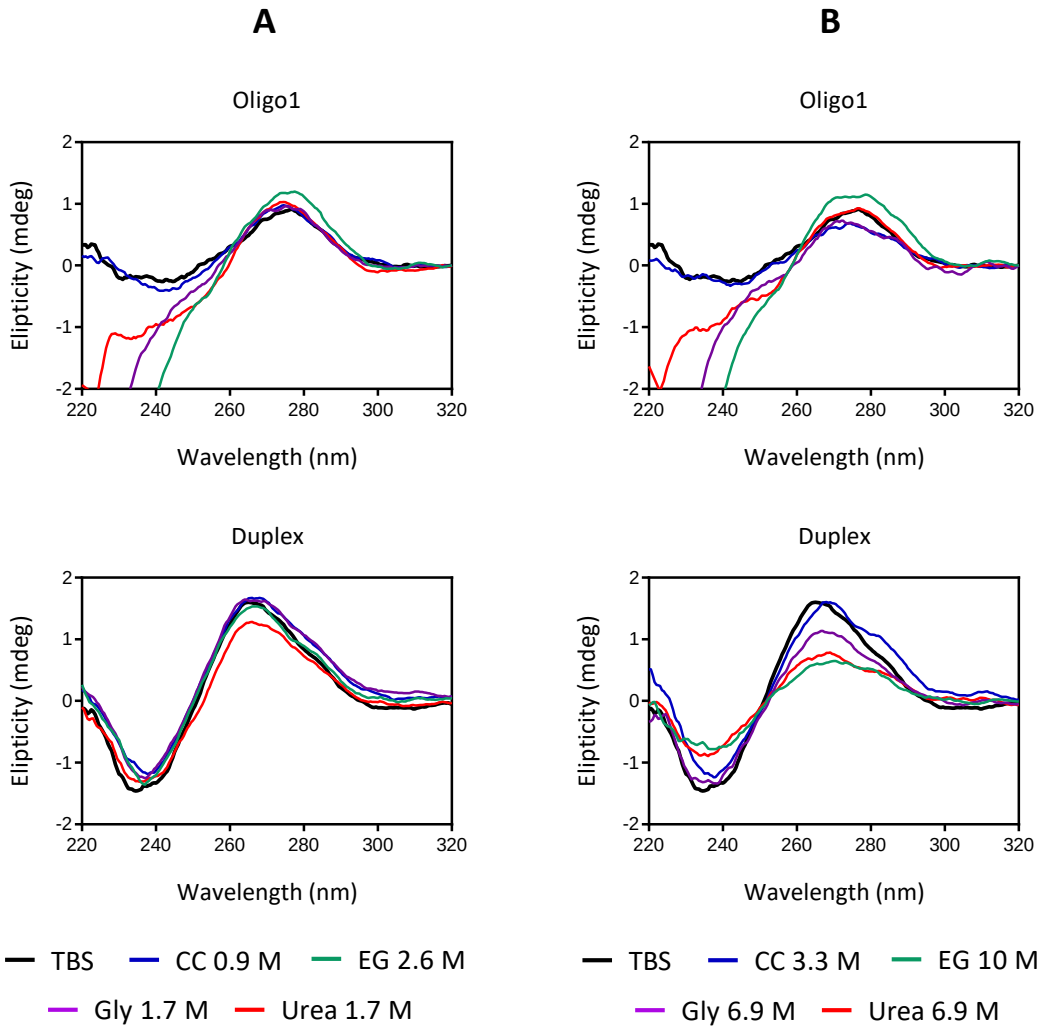

Figure 3.6. CD spectra of Oligo1 and duplex formed between Oligo1 and Oligo2 (5 µM) at (A) highly hydrated or (B) low hydrated HBA and HBD media.

As can be observed in measurements done to samples with HBA or HBD groups as solvent (Figure 3.6), at low concentrations there were already some differences from spectra

measured in physiological media (TBS). In case of Oligo1, the only spectra similar to TBS was that obtained in choline chloride at low concentrations, in others there was huge negative ellipticity what could mean that single-stranded DNA formed aggregates, but this should be further studied. In any case, this difference between HBD groups and choline chloride would explain why previously the lifetime of the fluorophore linked to Oligo1 changed drastically upon addition of HBD media but not upon addition of choline chloride (Figure 3.4).

In case of the duplex, at low concentrations, the only significant difference was found in the intensity reduction of the positive peak while solvating dsDNA in urea 1.74 M, this is in concordance with the hybridization percentages found at this concentration, lower in urea than in the rest of the media. On the other hand, it means that the possible aggregation of ssDNA is prevented while forming the dsDNA structure. Moreover, at higher concentrations, in choline chloride (3.3 M; ≈ 45 wt. %) the duplex showed a shoulder at 285 nm found also in TBS media but in a very small quantity what would mean that not all duplexes were in the classical Watson-Crick B-form. The shift in the positive peak from 265 to 270 nm that usually corresponds to the strong interaction of the media (choline in this case) with DNA bases, what would explain the dynamic quenching observed in the fluorophore. In HBD media, the intensity of the positive and negative peaks decreased equally, indicating the partial denaturation of the duplexes at high concentrations due to dehydration of bases.

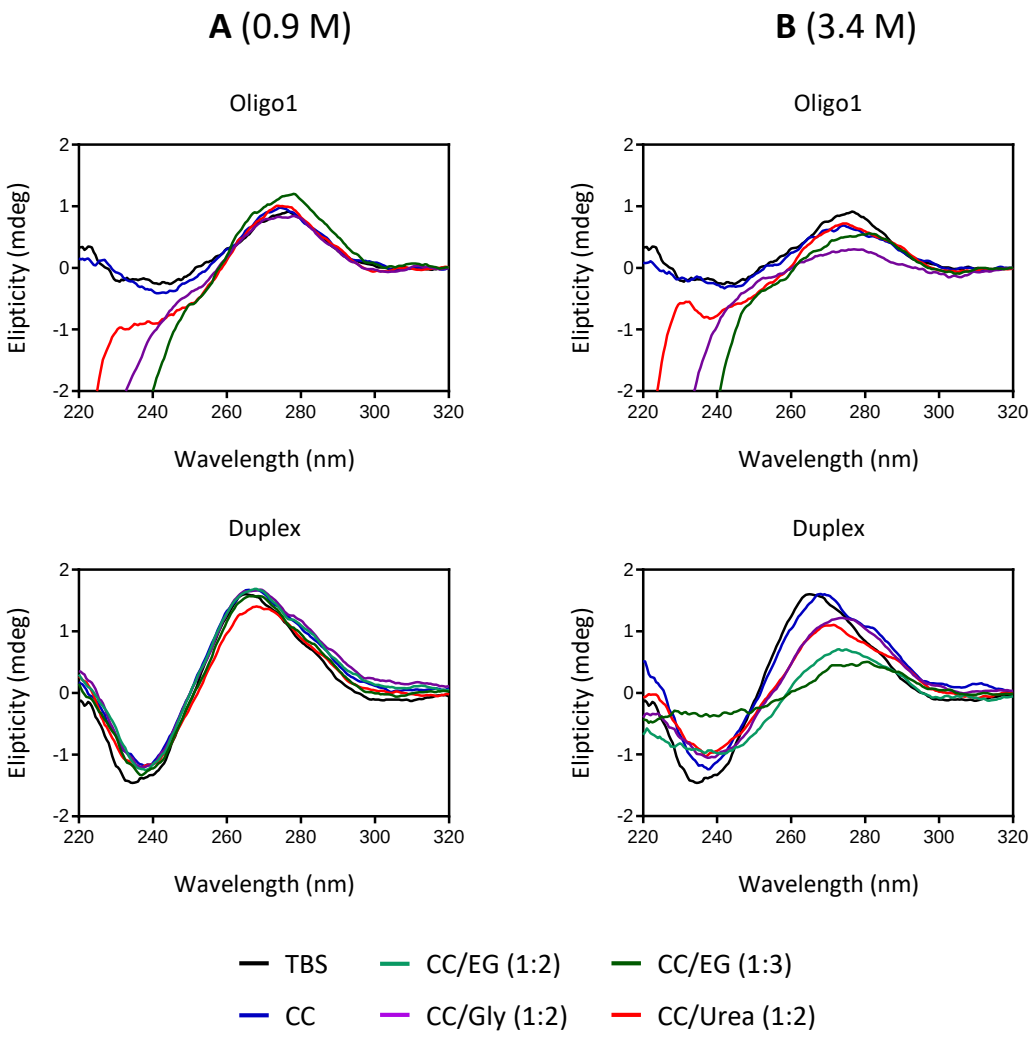

Figure 3.7. CD spectra of Oligo1 and duplex formed between Oligo1 and Oligo2 (5 µM) at (A) highly hydrated HBA and DES media and (B) low hydrated HBA and DES media.

In Figure 3.7, are shown the spectra obtained while solvating the DNA in DES media. At low concentrations, the spectra of Oligo1 in DESs were very similar to those in HBD groups, but they changed drastically at higher concentrations, the reduction in the positive peak usually means the loss of base stacking, probably due to DES that replaced water molecules. In the

spectra of the duplexes at low concentrations of DESs, once again that containing urea (reline) was the only one that decreased slightly the positive peak, due to a lower hybridization percentage in this media. At higher concentrations, the melting temperatures (Figure 3.3) and hybridization percentages (Figure S3.2) found in fluorescence studies matched the spectra obtained in almost anhydrous DES (3.4 M) where the duplex was destabilized following this order: CC/EG (1:3) > CC/EG (1:2) > CC/Urea (1:2) ≈ CC/Gly (1:2). The findings of this and previous section were further studied computationally in Chapter 4.

3.2.4 Base-pair percentage-dependent DNA solvation in mixed solvents

Combining the PhD Thesis of Isabel Machado (2016, UPV/EHU) and that presented so far in this chapter, it is already possible to predict how the most relevant ionic liquids and deep eutectic solvents affect the thermal and conformational stabilities of short DNA double helixes at different hydration levels. However, it is important to consider the variation on these stabilities while changing the sequence of the double helix. In physiological media these can be easily predicted but the site-specific binding of choline cation[34–36] could probably change the linear trend seen in aqueous solutions, proportional to G/C percentage. In order to elucidate the effect of choline, sodium and choline salts, two ionic liquids and a deep eutectic solvent were mixed with water to solvate short duplexes containing from 25 to 75 G/C percentage, including the duplex formed between Oligo1 and Oligo2 (58 G/C %) (Table S3.2). Then, these were studied using CD and UV-Vis. The most relevant information obtained from CD measurements correspond to the ellipticity of the positive peak and its wavelength, on the other hand the

melting temperature of the duplexes was calculated by UV-Vis. All spectra obtained are presented in the supplementary information (Figures S3.10-S3.15).

Firstly, the DNA was solvated in aqueous solutions containing sodium chloride. At 25 ^{o}C and 2 M concentration the duplexes were close to their maximum hybridization percentage but at 4 M they were partially denatured due to the excessive positive charge. This can be seen in the ellipticity values of the positive peaks (Figure 3.8A), which were higher at 2 M than 4 M. Moreover, there is a similar decrease in ellipticity in all duplexes because the thermal stability in physiological media is linearly dependant of the G/C percentage as mentioned before. On the other hand, the wavelength of positive peaks also varied between the different duplexes, those with less G/C percentage had the longest wavelength (≈ 276 nm) mainly due to the differences in A/T- and G/C-rich double helixes[37] (Figure 3.8B). Comparing between the influence of NaCl in each sequence, it seems that there were no huge differences in secondary structure of the duplexes at 2M or 4M, only varied their thermal stability. The lower melting temperature at 4 M compared with 2 M and the influence of the G/C percentage on the thermal temperature was confirmed by UV-Vis (Figure 3.8C).

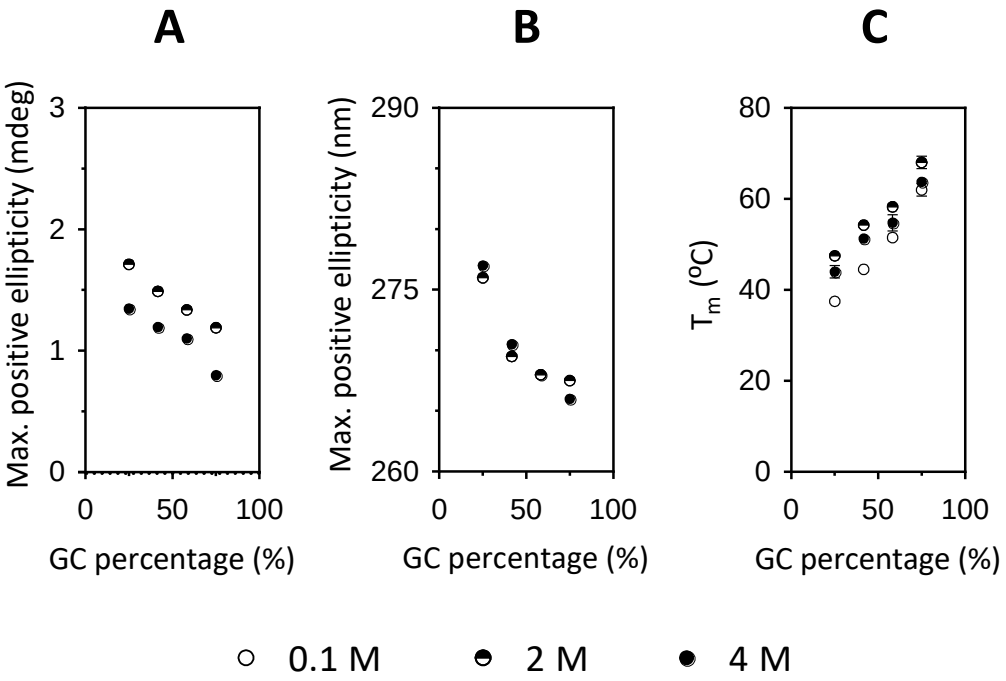

Figure 3.8. Measurements done in sodium chloride and water media. (A) Ellipticity of the positive peak in CD spectra. (B) Wavelength of the positive peak in CD spectra. (C) Melting temperature calculated by UV-Vis.

Then, the same experiment was repeated using choline chloride. There was a difference in the wavelength of the positive maximum at 75% G/C compared with that found in sodium chloride (Figure 3.9B) and a shoulder appeared at 285 nm (Figure S3.11), probably due to the creation of some G-quadruplexes. On the other hand, with sodium, the melting temperature changed proportionally in the four duplexes, whereas in case of choline chloride, the melting temperature was slightly higher at 0.5 M than 2.2 M for the sequence with 75% G/C and the contrary happened in the sequence with 25% G/C (Figure 3.9C). This is due the influence of specific site binding in the thermal stability of the duplexes: choline destabilized more G-C base

pairs and therefore, while increasing salt concentration, the thermal stability only increased in the 25% G/C duplex. The destabilization of these duplexes would favour the creation of G-quadruplexes explaining the shoulder found at 285 nm.

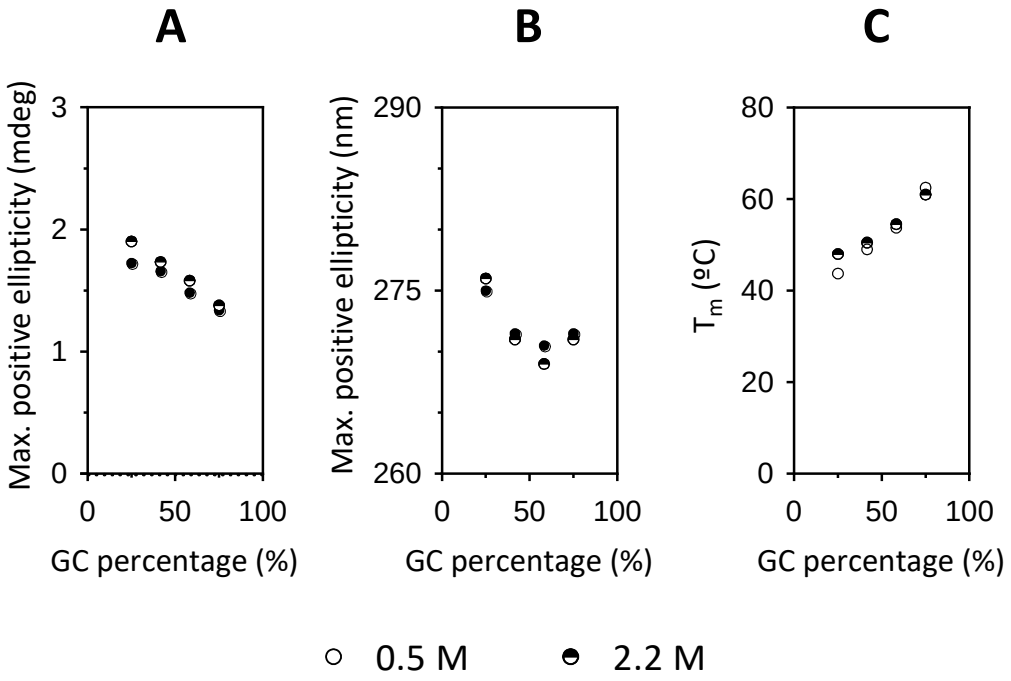

Figure 3.9. Measurements done in choline chloride and water media. (A) Ellipticity of the positive peak in CD spectra. (B) Wavelength of the positive peak in CD spectra. (C) Melting temperature calculated by UV-Vis.

Leaving the salts aside and studying the ethaline deep eutectic solvent, huger changes between the different duplexes appeared. In this solvent there are two ethylene glycol molecules per the previous choline chloride molecule and the presence of water is greatly reduced at 2.6 M concentration (Table S3.1). In circular dichroism spectra, the same trend seen in choline chloride appeared, with a huge red shift in G/C-rich sequence at 2.6 M of DES (Figure

3.10B). This would confirm that denatured duplexes with this high G/C percentage would be forming a kind of, probably, G-quadruplex structure not described in the literature.

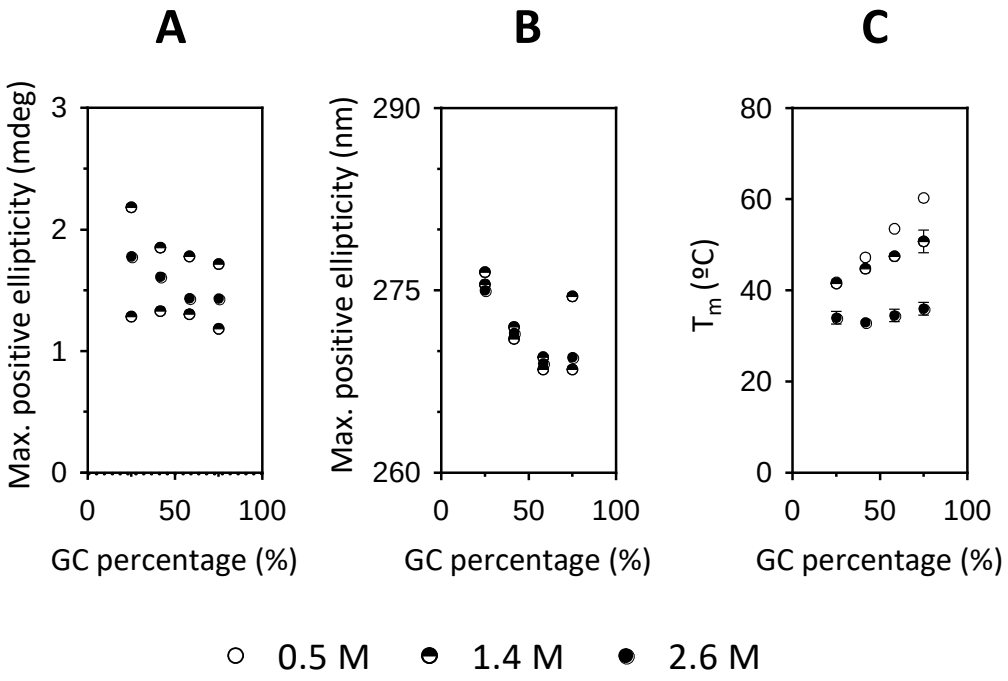

Figure 3.10. Measurements done in ethaline and water media. (A) Ellipticity of the positive peak in CD spectra. (B) Wavelength of the positive peak in CD spectra. (C) Melting temperature calculated by UV-Vis.

Regarding the thermal stability measured by UV-Vis, at 0.5 M concentration of ethaline, the duplexes had the same melting temperature as in choline chloride but then, their thermal stability decreased substantially at higher DES concentrations, especially in G/C-richest sequence, with a more significant change than that observed in choline chloride. On the other hand, the changes in melting temperatures of the duplex formed by Oligo1 and Oligo2 were in concordance with fluorescence studies (Figure 3.3). Interestingly, at 2.61 M, the thermal stability

was almost equal in all duplexes, it was independent of the DNA sequence what could be used for different technological designs[38] (Figure 3.10C).

Then, the duplexes were studied in two ionic liquids, being one of them choline lactate, the same used in SELEX of Chapter 6 with very interesting properties such as relative low viscosity, wide liquid range and chirality[39]. The lactate anion of this room temperature IL shows ellipticity below 260 nm and therefore it was not possible to obtain information from the negative peak of the spectra (Figure S3.13). The trend observed in CD is the same seen in choline chloride and ethaline, with a red shift in 75% G/C duplex compared but it seems that G-quadruplexes were already forming in a significant quantity with only 0.5 M of IL (Figure 3.11B), probably due to the slightly acid pH of the solution.

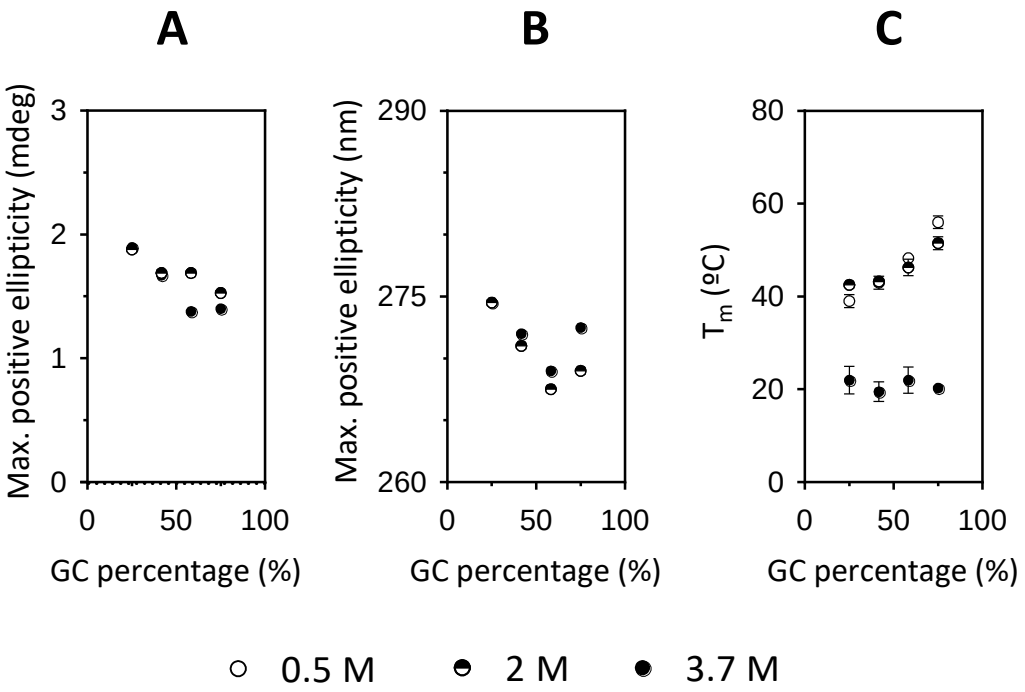

Figure 3.11. Measurements done in choline lactate and water media. (A) Ellipticity of the positive peak in CD spectra. (B) Wavelength of the positive peak in CD spectra. (C) Melting temperature calculated by UV-Vis.

On the other hand, at the lowest concentrations of choline lactate, 0.5 and 2 M, the thermal stability of the duplexes was very similar to those found in choline chloride, where the higher concentration of choline lactate destabilized specially G/C-rich sequences. At 3.7 M of choline lactate, all the melting temperatures decreased substantially and as found in ethaline the thermal stability was sequence independent (Figure 3.11C).

Then the same experiments were done using choline dihydrogenphosphate, the ionic liquid that appears in the majority of studies with DNA[40–42]. Results found were very different from those of ethaline and choline lactate. In CD, the ellipticity of the positive peak varied substantially in A/T-rich sequences between the two lowest and the highest concentration (Figure 3.12A). This shows the necessity of buffering this ionic liquid while using it at low concentrations with double helixes. On the other hand, the low ellipticity intensities and the huge red shift (from the usual 270-275 nm to 280-285 nm) of the G/C-rich duplexes in 0.5 M and 2 M could be due to a significant denaturation and the creation of G-quadruplexes (Figure 3.12B). The low thermal stability of G/C-rich duplexes in low concentrated IL (below 2 M) was found also using UV-Vis. It was below 10 ^{o}C at 0.5 and 1 M, not being possible to calculate it. Increasing the concentration of choline dihydrogenphosphate the thermal stability of the duplexes also increased. Contrary to what was found in previous media where all duplexes had

the same thermal stability, at 4 M of this IL the 25% G/C duplex was thermally more stable than the 75% G/C one (Figure 3.12C), confirming the observations found in a published article[36].

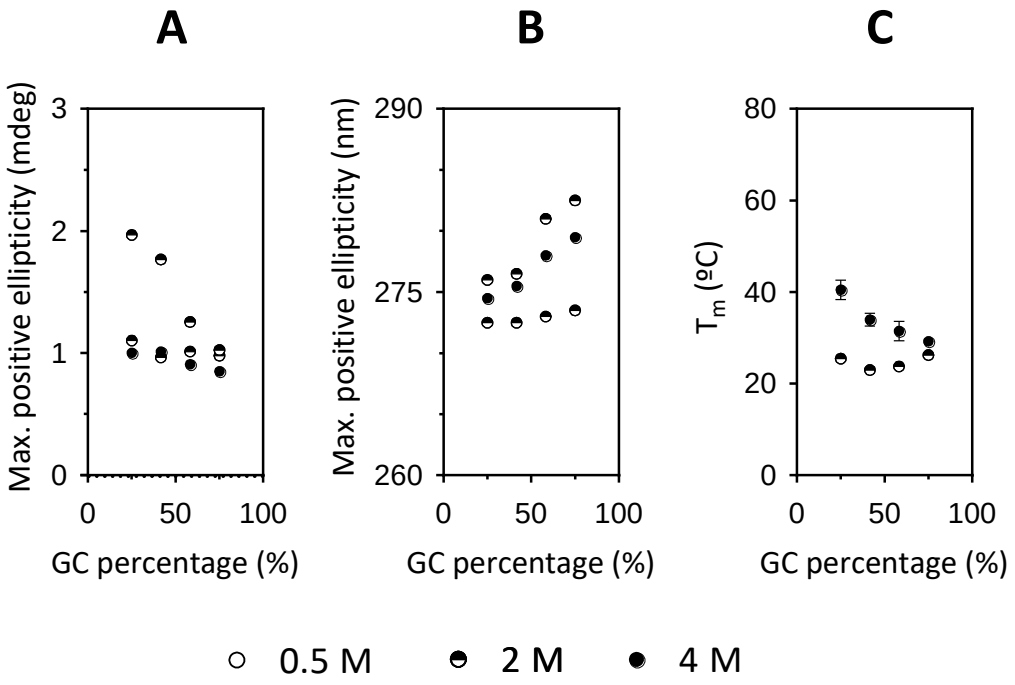

Figure 3.12. Measurements done in choline dihydrogenphosphate and water media. (A) Ellipticity of the positive peak in CD spectra. (B) Wavelength of the positive peak in CD spectra. (C) Melting temperature calculated by UV-Vis.

3.2.5 Length-dependent DNA solvation in mixed solvents

Apart from studying the short dsDNA with different G/C percentages, a brief study was done varying the length of the double helix, using for that purposes two salmon-sperm DNA samples. These nucleic acid samples are a low-cost material for many applications and therefore they might be useful to use them in non-physiological media, for example in DNA-based

catalysis[1]. The two samples were named as the "long" one, that consisted, first, in highly purified salmon-sperm DNA with a theoretical average base pair (bp) number of 2000. Second, the "short" one, commercially known as salmon-sperm sodium salt with a theoretical average bp number of 100 (Section 2.1.3) but calculated to be of 30 bp by gel-electrophoresis and GPC/SEC (Figure 3.13).

Gel-electrophoresis and GPC/SEC technics showed also that in both cases the s-sDNA were highly polidisperse. Despite this polidispersity, the great difference between mean sequence lengths (30 *vs* 2000 bp.) serve to elucidate if the cooperativity was still maintained in non-physiological media. If this cooperativity is maintained beyond aqueous environments, it would allow using almost anhydrous conditions because even if short duplexes were denatured, longer duplexes would have an increased thermal and structural stability in absence of water.

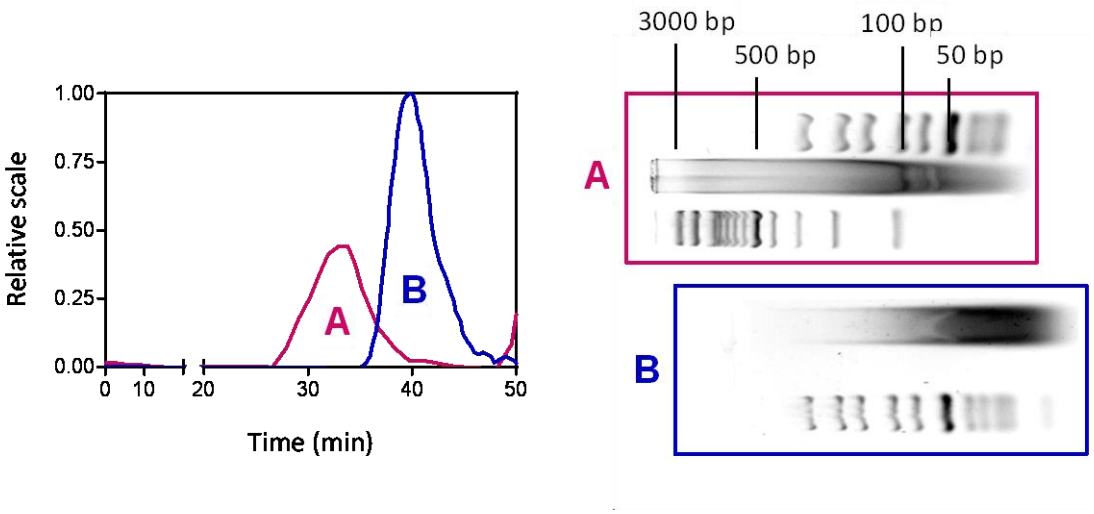

Figure 3.13. Left: GPC/SEC experiment of (A) "long" s-sDNA and (B) "short" s-sDNA. Right: Agarose gels after gel-electrophoresis of both s-sDNA with two different DNA ladders.

In order to prepare these experiments, both s-sDNA were solvated in physiological media (NaCl 100 mM, pH 7.4) and in different HBD groups, DES and ILs liquid at RT and at a final concentration of 95 v/v % (5 v/v % H_2O). The concentration of both s-sDNA in all samples was 0.5 mg/mL. All the spectra obtained by UV-Vis or circular dichroism at 25 ^oC and gel-electrophoresis data can be found in Figure S3.16-S3.17. It needs to be taken into account that whereas in previous experiments all sequences had a specific composition and lenght, in these salmon-sperm DNA samples there are a vast number of different sequences with an average G/C percentage close to 50%, indicated by the manufacturer.

In circular dichroism studies, in physiological media, the negative peaks were found at 243 and 244 nm for “short” and “long” s-sDNA, respectively. The positive peaks were at 279 and 275 nm for “short” and “long” s-sDNA, respectively. These are well-known values for the family of double helixes with Watson-Crick B-form. In case of ellipticity, in aqueous buffer the negative peak showed -4.5 and -11.5 mdeg for “short” and “long” s-sDNA respectively. The positive peak was at 8.3 and 10.7 mdeg for “short” and “long” s-sDNA. Usually, the B-form DNA shows similar intensities in both peaks, the lower intensity of the negative peak in the “short” s-sDNA sample could be due to impurities that absorb in that range (5 wt. % indicated by the manufacturer). Then, these CD values were compared to those obtained in the rest of the media; the results can be visualized in Figure 3.14 and 3.15.

On the one hand, there were significant differences in circular dichroism spectra between the DNA solvated in physiological medium (zeroed) and that in HBD media at 95 (v/v) % (Figure 3.14). Triethylene glycol and ethanol were used as solvents that are known to

condensate DNA. As can be observed, ellipticity of “short” and “long” s-sDNA decreases between 50 and 80% in these media. This decrease was also huge in the other two HBD media, ethylene glycol and glycerol, but the red shift of the CD minima indicated that instead of condensating, the DNA was solvated in its single-stranded form.

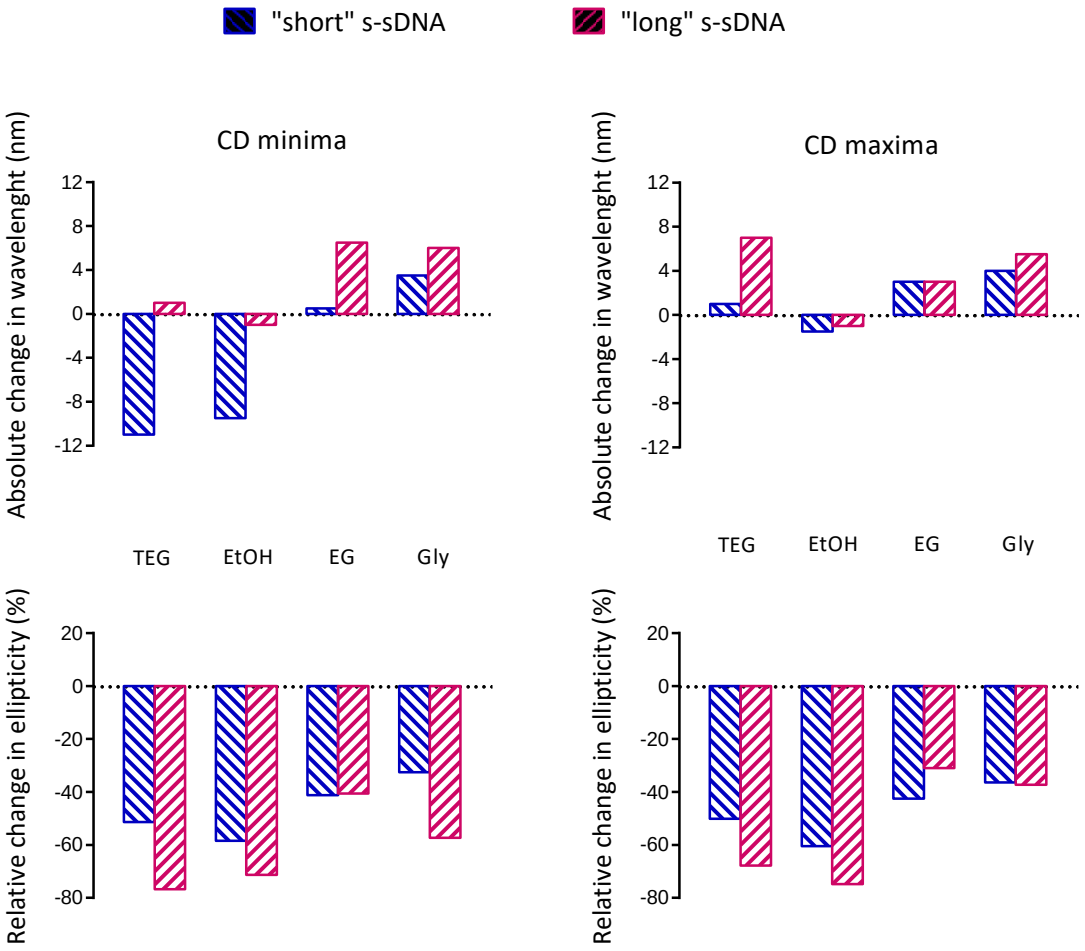

Figure 3.14. Differences in CD minima (top) and maxima (bottom) in HBD groups with 5 (v/v) % of water respect from the spectra obtained in physiological media.

On the other hand, in DES media, the decrease in ellipticity of the negative peak was only observed in “short” s-sDNA (Figure 3.15), what would mean that the cooperativity between DNA strands maintained the ellipticity of “long” s-sDNA. However, the intensities of positive peaks decreased in all cases, except for reline. In reline DES the conformation of the double helix of “long” s-sDNA suffered only minor changes. The ability of reline (CC/Urea (1:2)) DES to maintain DNA more stable than other DESs at very low hydration levels was also observed in duplexes formed between Oligo1 and Oligo2 (Figure 3.3), but in that case such high concentration of reline denatured partially the duplexes due to their shorter length.

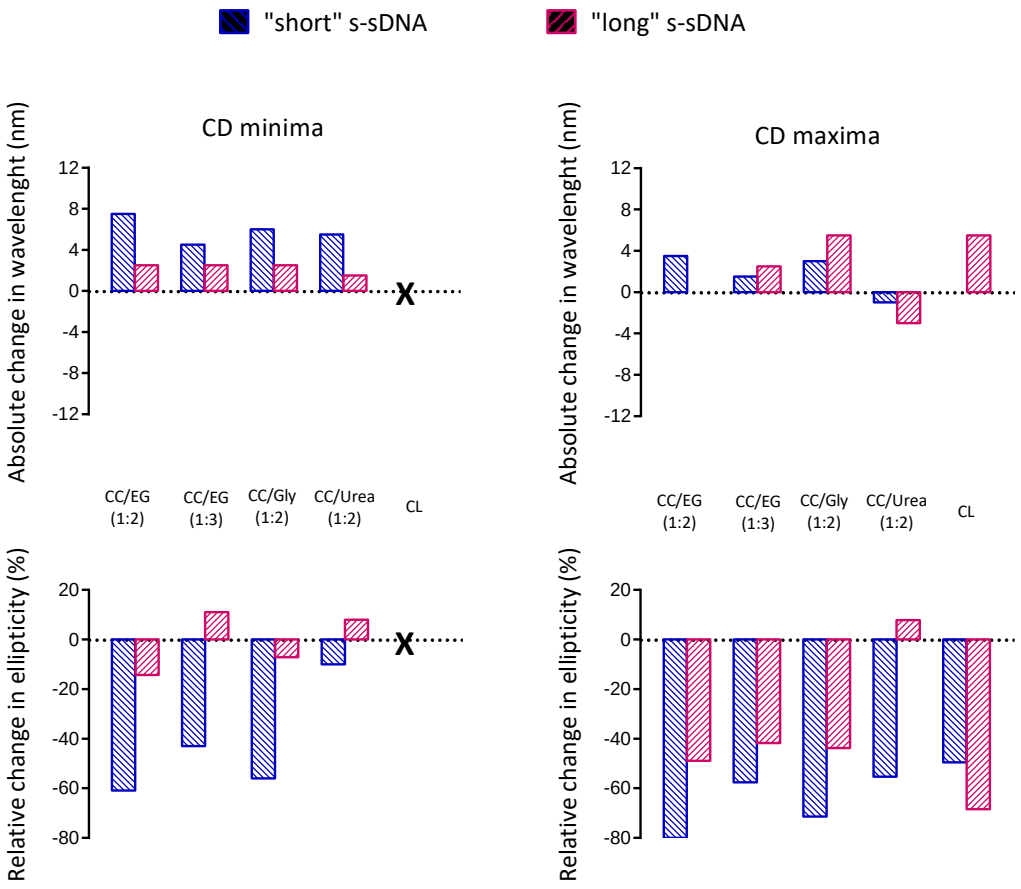

Figure 3.15. Differences in CD minima (top) and maxima (bottom) in DESs and an IL with 5 (v/v) % of water respect from the spectra obtained in physiological media.

Contrary to HBD media, in DESs, the intensity of the negative peak of "long" s-sDNA suffered minor changes, but the intensity of positive peak decreased significantly. Looking for an explanation, it might be attributed to an effect on DNA also observed in some ionic liquids or under molecular crowding conditions[43–46]: the DNA compacted *via* an axial compression respect from the usual B-form or the random-coil and some DNA bases no longer absorb light reducing the absorption intensity. In any case, this structural change needs to be better studied.

In resume, both types of s-sDNA were found to be highly soluble in non-physiological media with only 5 (v/v) % of water. The different results obtained between "short" and "long" s-sDNA samples indicate that the cooperativity between DNA strands exists also in DES close to anhydrous conditions. Unfortunately, most of the media destabilized the original Watson-Crick B-form secondary structure at room temperature but exceptionally, reline DES was able to maintain the thermal and structural stabilities of the "long" s-sDNA.

3.3 Conclusions

DNA duplexes have been systematically solvated in physiological media and a plethora of mixed solvents formed by molecular solvents, ILs and DESs. It was observed that the thermal stability of the short duplexes decreases following a polynomial trend while changing the water content. This allows the melting temperature to be adjusted adding specific amounts of water.

On the other hand, at an equal concentration, the DESs destabilized more the dsDNA than their corresponding molecular solvent, probably due to the reduction of water. Interestingly, reline DES was an exception, as it destabilized less the duplex than urea. In fact, thanks to the cooperativity in the double helix, the long salmon-sperm DNA maintained its B-form almost in anhydrous reline. The molecular mechanism of this event will be further studied in the following chapter.

Regarding the interactions of choline with DNA, it has been observed that this cation has different peculiarities: it displaces the metallic cations from DNA, avoids the aggregation of ssDNA, favors the formation of local secondary structures in DNA and destabilizes more the GC-rich duplexes than AT-rich ones.

In resume, this was the first systematic study of a double helix in presence of deep eutectic solvents. Moreover, it improves the knowledge about DNA solvation in molecular solvents and ionic liquids. All these media are of interest due to their liquid state in a wide range of temperatures, negligible volatility, ability to dissolve compounds or even their possible uses in catalysis. Therefore, the information obtained through these measurements can be used for new DNA nanotechnology designs that uses double-helixes.

3.4 References

1. Zhao, H. & Shen, K. DNA-based asymmetric catalysis: role of ionic solvents and glymes. *RSC Adv.* **4**, 54051–54059 (2014).

2. Tan, Z.-J. J. & Chen, S.-J. J. Nucleic acid helix stability: Effects of salt concentration, cation valence and size, and chain length. *Biophys. J.* **90**, 1175–1190 (2006).

3. Maity, A., Singh, A. & Singh, N. Differential stability of DNA based on salt concentration. *Eur. Biophys. J.* **46**, 33–40 (2017).

4. Baker, E. S. & Bowers, M. T. B-DNA Helix Stability in a Solvent-Free Environment. *J. Am. Soc. Mass Spectrom.* **18**, 1188–1195 (2007).

5. Koumoto, K., Ochiai, H. & Sugimoto, N. Structural effect of synthetic zwitterionic cosolutes on the stability of DNA duplexes. *Tetrahedron* **64**, 168–174 (2008).

6. Zhao, H. DNA stability in ionic liquids and deep eutectic solvents. *J. Chem. Technol. Biotechnol.* **90**, 19–25 (2015).

7. Rajendran, M. & Ellington, A. D. In vitro selection of molecular beacons. *Nucleic Acids Res.* **31**, 5700–5713 (2003).

8. Bidar, N. *et al.* Molecular Beacon Strategies for Sensing Purpose. *TrAC Trends Anal. Chem.* 116143 (2020). doi:10.1016/j.trac.2020.116143

9. Hansen, B. B. *et al.* Deep Eutectic Solvents: A Review of Fundamentals and Applications. *Chem. Rev.* acs.chemrev.0c00385 (2020). doi:10.1021/acs.chemrev.0c00385

10. Perna, F. M., Vitale, P. & Capriati, V. Deep eutectic solvents and their applications as green solvents. *Curr. Opin. Green Sustain. Chem.* **21**, 27–33 (2020).

11. Kist, J. A. *et al.* The study and application of biomolecules in deep eutectic solvents. *J. Mater. Chem. B* **9**, 536–566 (2021).

12. El Achkar, T., Fourmentin, S. & Greige-Gerges, H. Deep eutectic solvents: An overview on their interactions with water and biochemical compounds. *J. Mol. Liq.* **288**, 111028 (2019).

13. Hammond, O. Deep Eutectic Solvents : Structure , Solvation and Synthesis. (2019).

14. Jaiswal, A. K., Srivastava, R., Pandey, P. & Bandyopadhyay, P. *Microscopic picture of water-ethylene glycol interaction near a model DNA by computer simulation: Concentration dependence, structure, and localized thermodynamics*. *PloS one* **13**, (2018).

15. Nordstrom, L. J., Clark, C. A., Andersen, B., Champlin, S. M. & Schwinefus, J. J. Effect of Ethylene Glycol, Urea, and N-Methylated Glycines on DNA Thermal Stability: The Role of DNA Base Pair Composition and Hydration †. *Biochemistry* **45**, 9604–9614 (2006).

16. de Xammar Oro, J. R. & Grigera, J. R. On the thermal stability of DNA in solution of mixed solvents. *J. Biol. Phys.* **21**, 151–154 (1995).

17. Owczarzy, R., Moreira, B. G., You, Y., Behlke, M. A. & Wälder, J. A. Predicting stability of DNA duplexes in solutions containing magnesium and monovalent cations. *Biochemistry* **47**, 5336–5353 (2008).

18. Dave, N. & Liu, J. Fast molecular beacon hybridization in organic solvents with improved target specificity. *J. Phys. Chem. B* **114**, 15694–15699 (2010).

19. Zhang, T. *et al.* Polar organic solvents accelerate the rate of DNA strand replacement

reaction. *Analyst* **140**, 2023–2028 (2015).

20. Greaves, T. L., Weerawardena, A., Fong, C., Krodkiewska, I. & Drummond, C. J. Protic ionic liquids: Solvents with tunable phase behavior and physicochemical properties (vol 110B, pg 22479, 2006). *J. Phys. Chem. B* **110**, 26506 (2006).

21. Yin, Y. & Zhao, X. I. N. S. Kinetics and Dynamics of DNA Hybridization. *Acc. Chem. Res.* **44**, 1172–1181 (2011).

22. Gao, Y., Wolf, L. K. & Georgiadis, R. M. Secondary structure effects on DNA hybridization kinetics: A solution versus surface comparison. *Nucleic Acids Res.* **34**, 3370–3377 (2006).

23. Ouldridge, T. E., Šulc, P., Romano, F., Doye, J. P. K. & Louis, A. A. DNA hybridization kinetics: Zippering, internal displacement and sequence dependence. *Nucleic Acids Res.* **41**, 8886–8895 (2013).

24. Zanetti-Domingues, L. C., Tynan, C. J., Rolfe, D. J., Clarke, D. T. & Martin-Fernandez, M. Hydrophobic Fluorescent Probes Introduce Artifacts into Single Molecule Tracking Experiments Due to Non-Specific Binding. *PLoS One* **8**, (2013).

25. Heinlein, T., Knemeyer, J. P., Piestert, O. & Sauer, M. Photoinduced electron transfer between fluorescent dyes and guanosine residues in DNA-hairpins. *J. Phys. Chem. B* **107**, 7957–7964 (2003).

26. Stennett, E. M. S., Ciuba, M. A. & Levitus, M. Photophysical processes in single molecule organic fluorescent probes. *Chem. Soc. Rev.* **43**, 1057–1075 (2014).

27. Levitus, M. *Photophysics of single-molecule probes*. *Spectroscopy and Dynamics of Single Molecules* (Elsevier Inc., 2019). doi:10.1016/b978-0-12-816463-1.00001-8

28. Lakowicz, J. R. & Lakowicz, J. R. Time-Domain Lifetime Measurements. *Princ. Fluoresc. Spectrosc.* 95–140 (1999). doi:10.1007/978-1-4757-3061-6_4

29. Stsiapura, V. I., Kurhuzenkau, S. A., Kuzmitsky, V. A., Bouganov, O. V. & Tikhomirov, S. A. Solvent Polarity Effect on Nonradiative Decay Rate of Thioflavin T. *J. Phys. Chem. A* **120**, 5481–5496 (2016).

30. Invitrogen. Alexa Fluor Dyes - Simply the Best and Brightest Fluorescent Dyes and Conjugates. *Mol. Probes, Inc.* 1–36 (2005).

31. Pant, S., Tripathi, H. B. & Pant, D. D. Solvent polarity and viscosity effect on the fluorescence spectrum and excited state lifetime of quinine dication. *J. Photochem. Photobiol. A Chem.* **85**, 33–38 (1995).

32. Jean, J. M. & Hall, K. B. 2-Aminopurine fluorescence quenching and lifetimes: Role of base stacking. *Proc. Natl. Acad. Sci.* **98**, 37–41 (2001).

33. Adenier, A. & Aaron, J. J. A spectroscopic study of the fluorescence quenching interactions between biomedically important salts and the fluorescent probe merocyanine 540. *Spectrochim. Acta - Part A Mol. Biomol. Spectrosc.* **58**, 543–551 (2002).

34. Portella, G., Germann, M. W., Hud, N. V. & Orozco, M. MD and NMR analyses of choline and TMA binding to duplex DNA: On the origins of aberrant sequence-dependent stability by alkyl cations in aqueous and water-free solvents. *J. Am. Chem. Soc.* **136**, 3075–3086 (2014).

35. Nakano, M., Tateishi-Karimata, H., Tanaka, S. & Sugimoto, N. Choline ion interactions with DNA atoms explain unique stabilization of A-T base pairs in DNA duplexes: A

microscopic view. *J. Phys. Chem. B* **118**, 379–389 (2014).

36. Tateishi-Karimata, H. & Sugimoto, N. A-T base pairs are more stable than G-C base pairs in a hydrated ionic liquid. *Angew. Chemie - Int. Ed.* **51**, 1416–1419 (2012).

37. Urbanov, M. & Malo, P. Circular Dichroism Spectroscopy. in *Analytical Methods in Supramolecular Chemistry* **2**, 265–304 (Wiley-VCH Verlag GmbH & Co. KGaA, 2007).

38. Vasudevamurthy, M. K., Lever, M., George, P. M. & Morison, K. R. Betaine structure and the presence of hydroxyl groups alters the effects on DNA melting temperatures. *Biopolymers* **91**, 85–94 (2009).

39. Francisco, M., González, A. S. B., García de Dios, S. L., Weggemans, W. & Kroon, M. C. Comparison of a low transition temperature mixture (LTTM) formed by lactic acid and choline chloride with choline lactate ionic liquid and the choline chloride salt: physical properties and vapour–liquid equilibria of mixtures containing water and ethanol. *RSC Adv.* **3**, 23553 (2013).

40. Vijayaraghavan, R. *et al.* Biocompatibility of choline salts as crosslinking agents for collagen based biomaterials. *Chem. Commun. (Camb).* **46**, 294–6 (2010).

41. Menhaj, A. B., Smith, B. D. & Liu, J. Exploring the thermal stability of DNA-linked gold nanoparticles in ionic liquids and molecular solvents. *Chem. Sci.* **3**, 3216–3220 (2012).

42. Tateishi-Karimata, H., Pramanik, S. & Sugimoto, N. DNA sensor's selectivity enhancement and protection from contaminating nucleases due to a hydrated ionic liquid. *Analyst* **140**, 4393–4398 (2015).

43. Sikorav, J. L. & Church, G. M. Complementary recognition in condensed DNA: Accelerated

DNA renaturation. *J. Mol. Biol.* **222**, 1085–1108 (1991).

44. Ding, Y., Zhang, L., Xie, J. & Guo, R. Binding characteristics and molecular mechanism of interaction between ionic liquid and DNA. *J. Phys. Chem. B* **114**, 2033–2043 (2010).

45. Chandran, A., Ghoshdastidar, D. & Senapati, S. Groove Binding Mechanism of Ionic Liquids: A Key Factor in Long-Term Stability of DNA in Hydrated Ionic Liquids? *J. Am. Chem. Soc.* **134**, 20330–20339 (2012).

46. Sohrabi, B., Khani, V., Moosavi-Movahedi, A. A. & Moradi, P. Investigation of DNA-cationic bolaform surfactants interaction with different spacer length. *Colloids Surfaces B Biointerfaces* **110**, 29–35 (2013).

47. Agieienko, V. & Buchner, R. Densities, Viscosities, and Electrical Conductivities of Pure Anhydrous Reline and Its Mixtures with Water in the Temperature Range (293.15 to 338.15) K. *J. Chem. Eng. Data* **64**, 4763–4774 (2019).

48. Gygli, G., Xu, X. & Pleiss, J. Meta-analysis of viscosity of aqueous deep eutectic solvents and their components. *Sci. Rep.* **10**, 1–11 (2020).

3.5 Supplementary information

Table S3.1. Concentration of compound one in prepared mixtures in molar conc., mass and molar fractions. The solvent two was always physiological media (TBS).

M (mol/L)	x_1	m_1	M (mol/L)	x_1	m_1
Choline chloride			CC/EG (1:2) (Ethaline)		
0,44	0,01	0,06	0,44	0,01	0,11
0,87	0,02	0,12	0,87	0,02	0,23
1,31	0,03	0,18	1,31	0,03	0,34
1,74	0,04	0,24	1,74	0,05	0,45
2,18	0,05	0,29	2,18	0,08	0,55
2,61	0,07	0,35	2,61	0,12	0,66
3,48	0,10	0,46	3,48	0,27	0,85
Ethylene glycol			CC/EG (1:3)		
0,87	0,02	0,05	0,44	0,01	0,14
1,31	0,02	0,08	0,87	0,02	0,27
1,74	0,03	0,11	1,31	0,04	0,40
2,61	0,05	0,16	1,74	0,06	0,53
3,48	0,07	0,21	2,18	0,09	0,65
3,92	0,08	0,24	2,61	0,16	0,77
4,35	0,09	0,26	3,47	0,86	0,99
5,22	0,12	0,31	CC/Gly (1:2) (Glyceline)		
6,53	0,15	0,39	0,44	0,01	0,14
6,96	0,17	0,41	0,87	0,02	0,28
7,83	0,20	0,46	1,31	0,04	0,41
10,44	0,31	0,60	1,74	0,06	0,54
Glycerol			2,18	0,10	0,66
0,87	0,02	0,08	2,61	0,15	0,77
1,74	0,03	0,15	3,48	0,57	0,96
2,61	0,05	0,23	CC/Urea (1:2) (Reline)		
3,48	0,08	0,30	0,44	0,01	0,11
4,35	0,10	0,37	0,87	0,02	0,22
5,22	0,13	0,43	1,31	0,03	0,33
6,96	0,20	0,56	1,74	0,05	0,43
Urea			2,18	0,07	0,53
0,87	0,02	0,05	2,61	0,11	0,63
1,74	0,03	0,10	3,48	0,22	0,81
2,61	0,05	0,15			
3,48	0,07	0,20			
4,35	0,09	0,25			
5,22	0,11	0,29			
6,96	0,15	0,38			

Figure S3.1. Melting temperatures of the duplexes formed between Oligo1 and Oligo2. The second order polynomial fittings are detailed into the graphs, 52.6 was used as a constraint value for B0 in all of them. The concentration of DNA oligonucleotides was 17 nM.

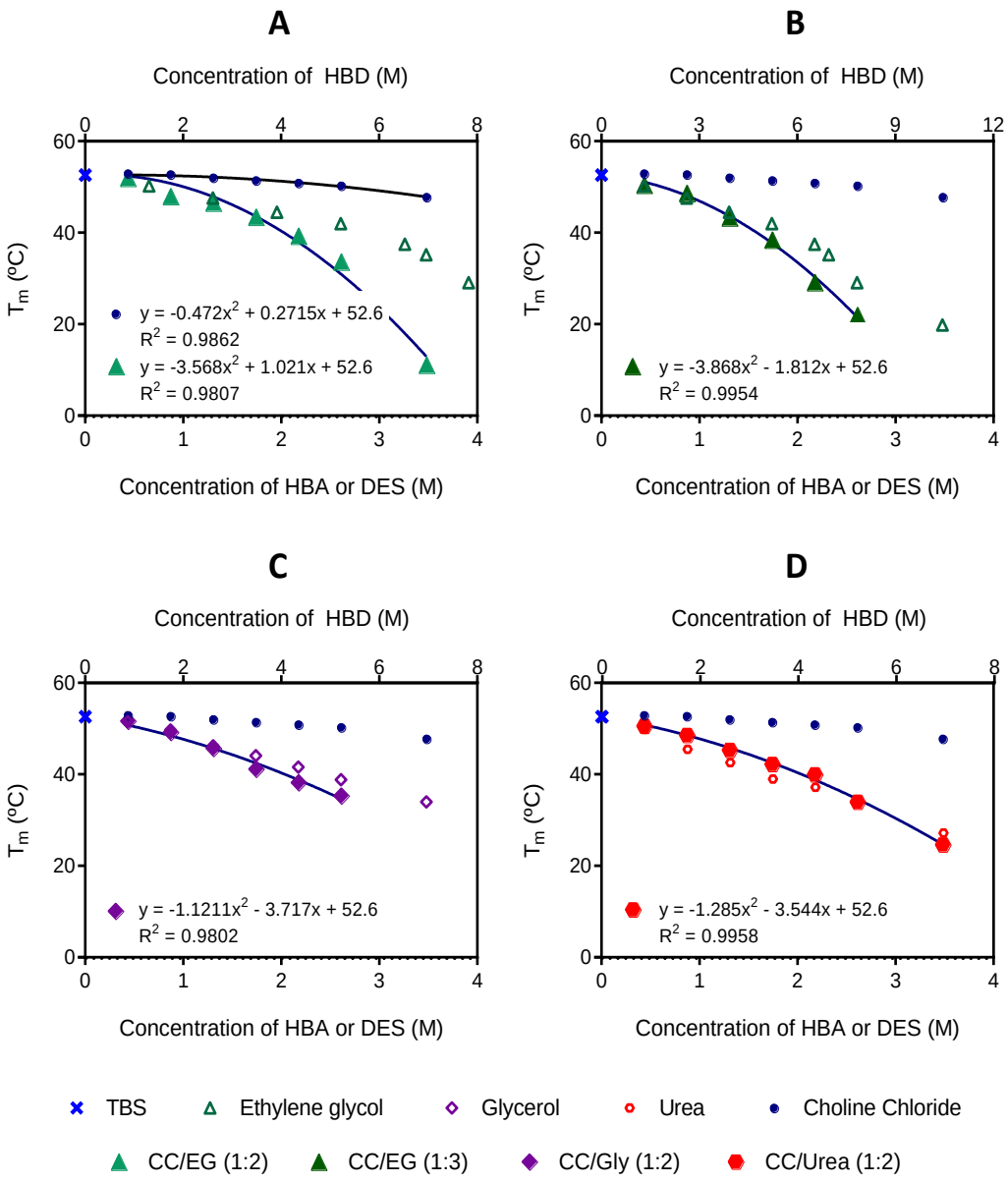

Figure S3.2. (A) Hybridization percentages of duplexes formed between Oligo1 and Oligo2 at 25 ºC. (B) Hybridization rates between Oligo1 and Oligo2 at 25 ºC. The concentration of DNA oligonucleotides was 17 nM.

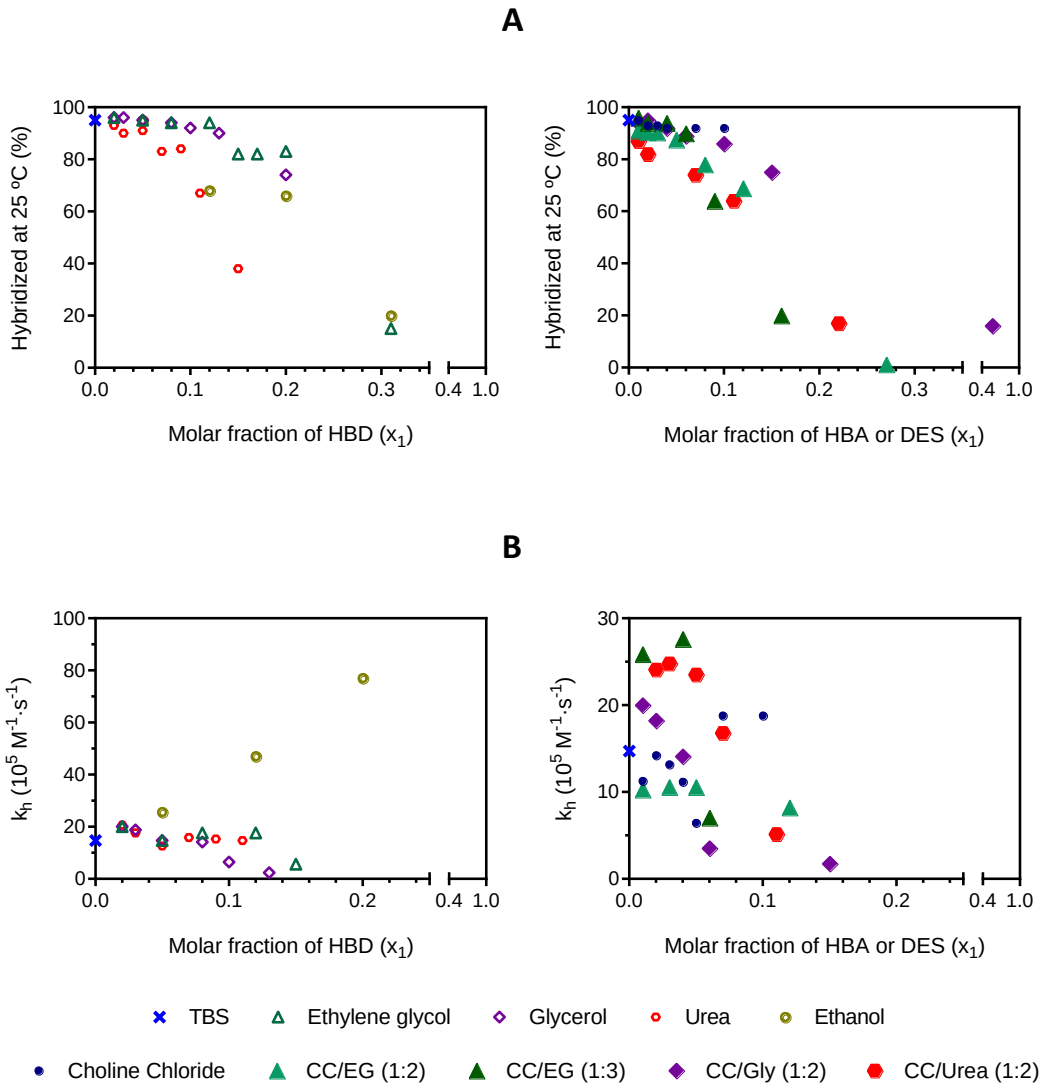

Figure S3.3. (A) Viscosities of different DES/TBS mixtures measured at room-temperature and atmospheric pressure. (B) Comparison with the published data of DES/H_2O mixtures at 25 ^oC and 0.1 MPa[47,48].

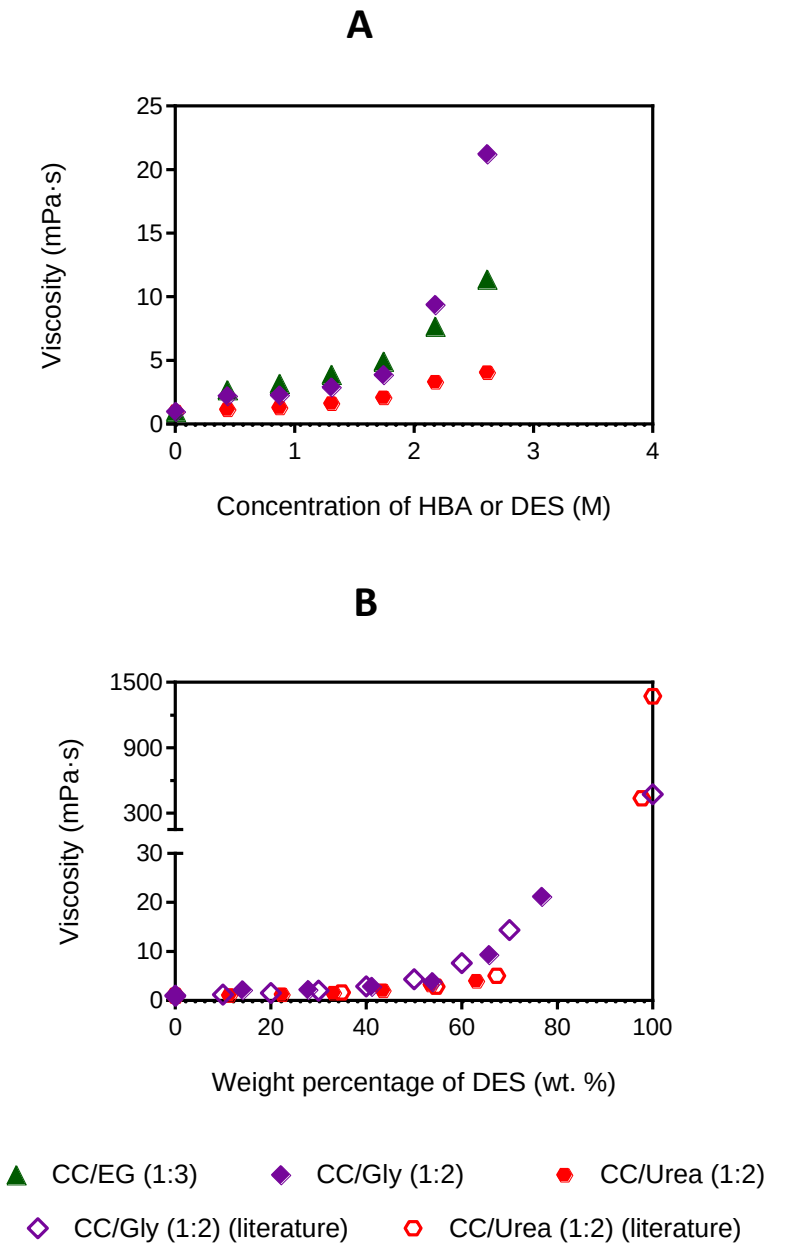

Figure S3.4. Lifetime values of Alexa Fluor 488 attached to Oligo1 at 25 ^{o}C prior hybridization. (A) In HBA and different DES media. (B) In HBA, ethylene glycol and CC/EG (1:3). (C) In HBA, glycerol and CC/Gly (1:2). (D) In HBA, urea and CC/Urea (1:2). The concentration of the fluorophore and DNA oligonucleotide was 17 nM.

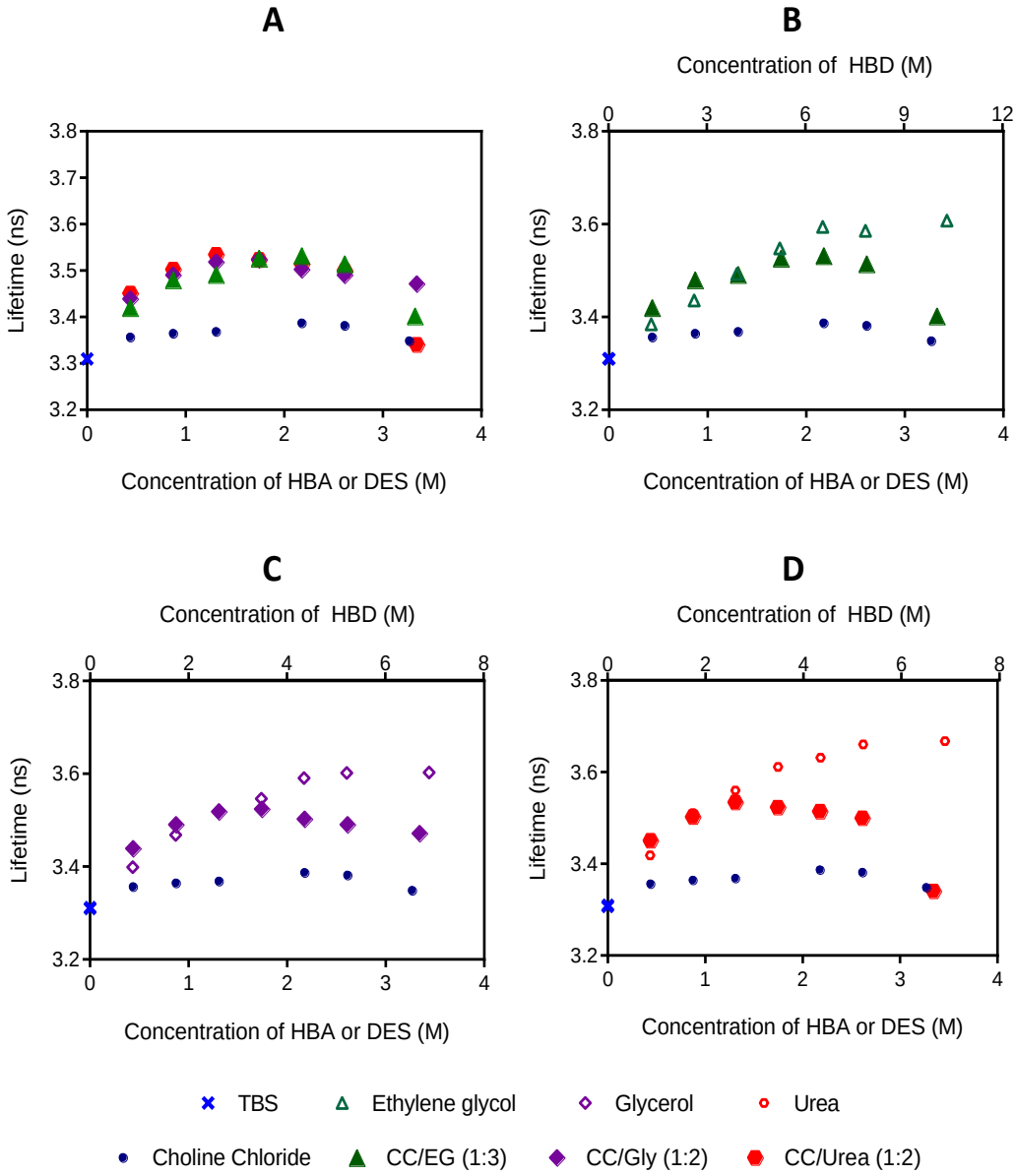

Figure S3.5. Melting temperature curves of the duplex formed between Oligo1 and Oligo2 measured in (A) circular dichroism and (B) UV-Vis. The concentration of DNA oligonucleotides was 5 µM.

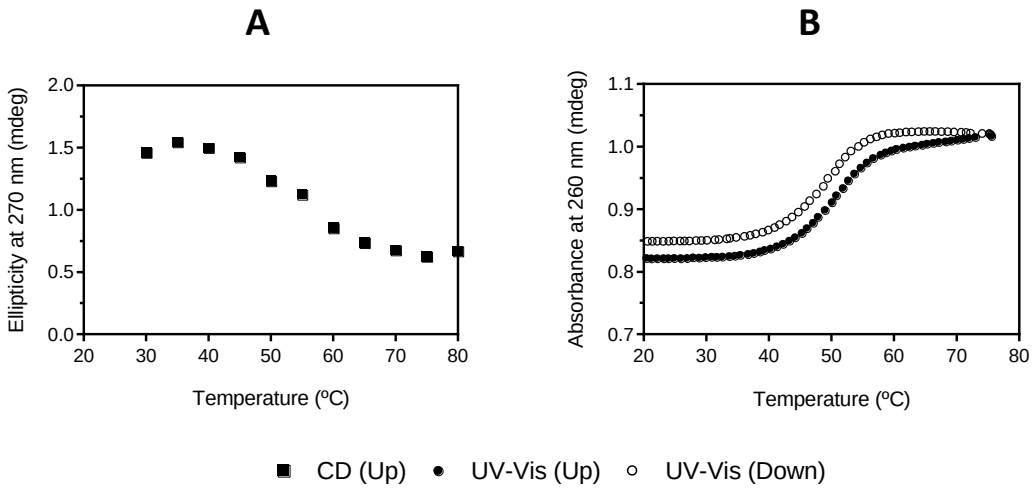

Figure S3.6. CD spectra of Oligo1 (5 µM) in different media. Below each concentration is shown the lifetime value of AF488 attached to Oligo1, calculated by spectrofluorimetry.

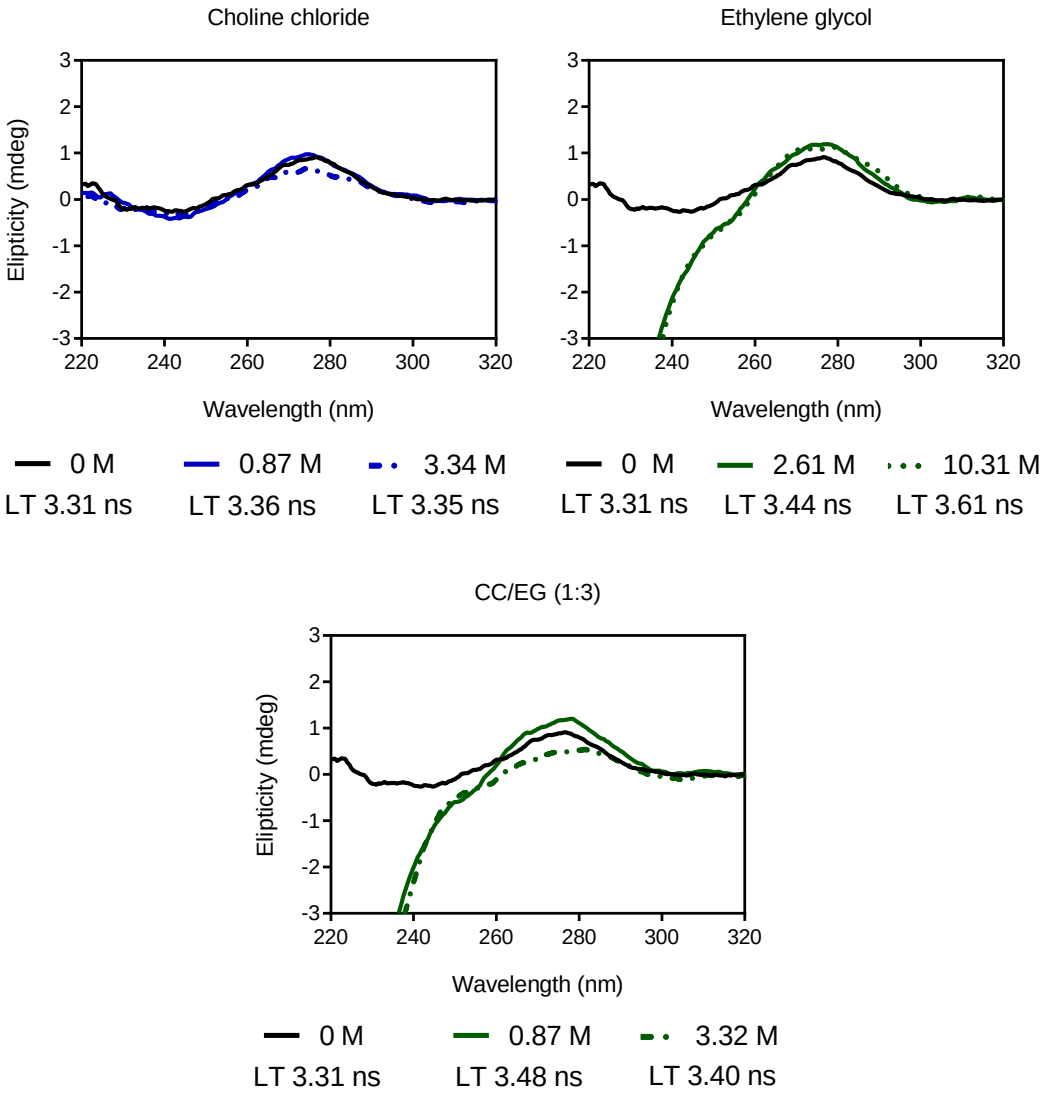

Figure S3.7. CD spectra of Oligo1 (5 µM) in different media. Below each concentration is shown the lifetime value of AF488 attached to Oligo1, calculated by spectrofluorimetry.

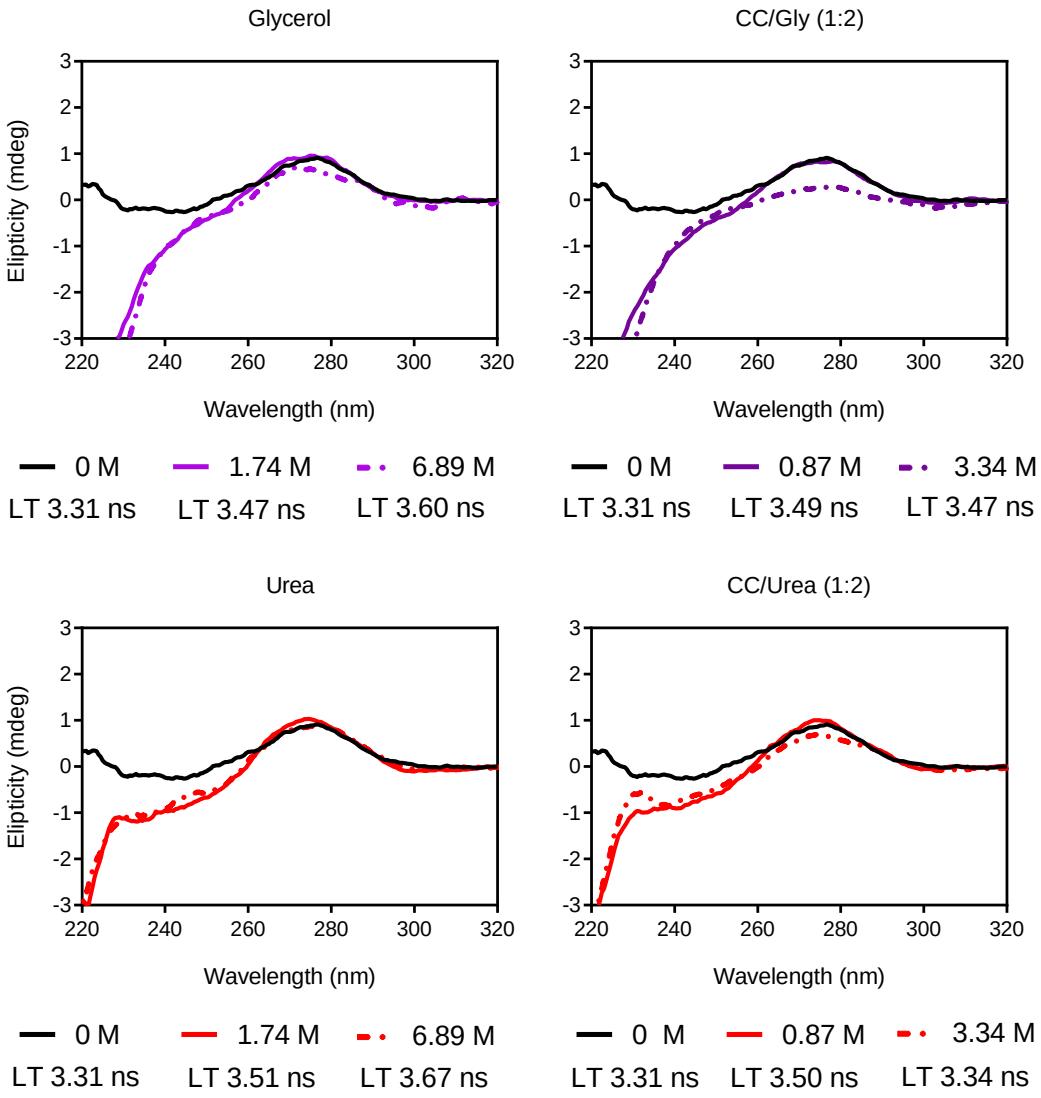

Figure S3.8. CD spectra of Oligo1 and Oligo2 (5 µM) in different media. Below each concentration is shown the hybridization percentage value calculated by spectrofluorimetry.

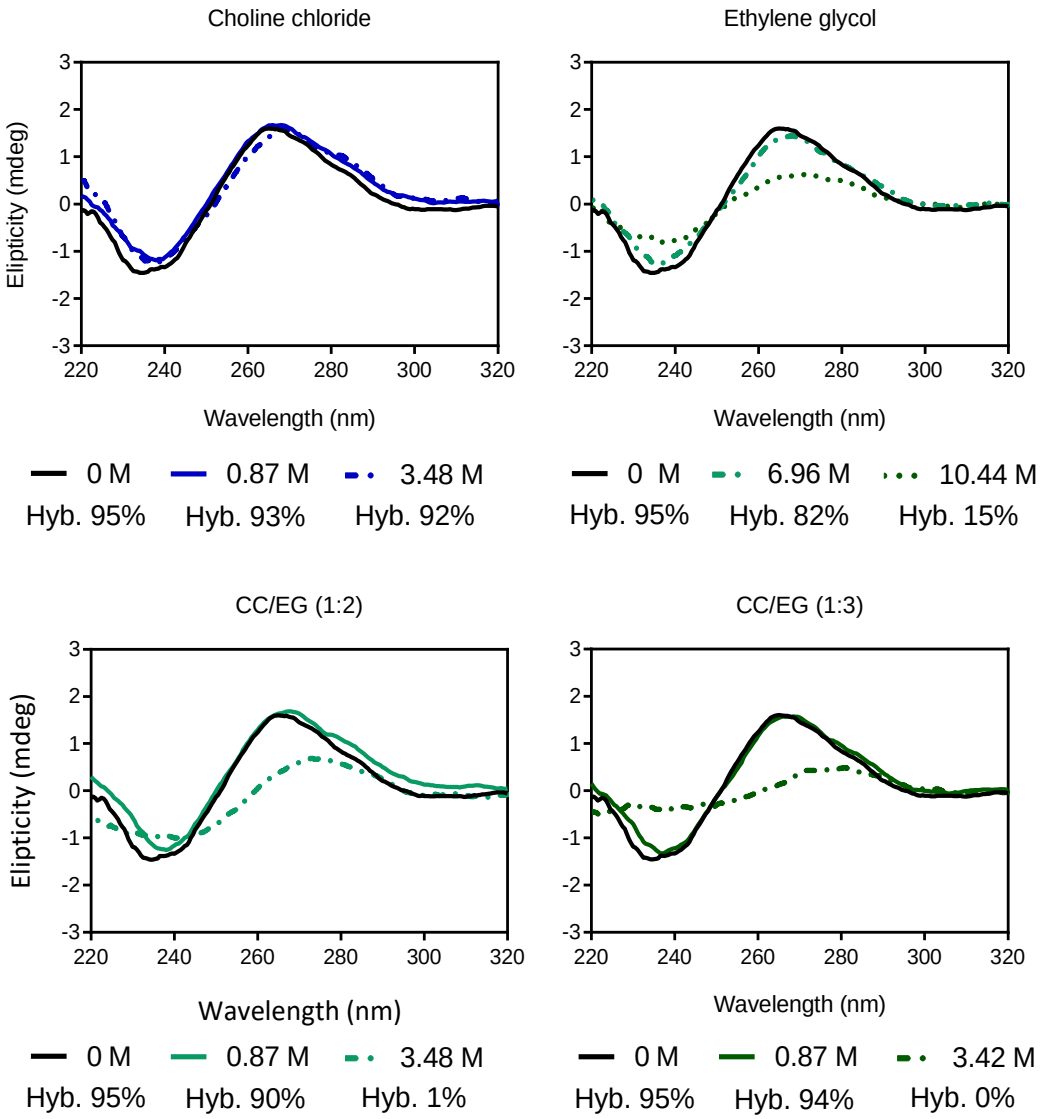

Figure S3.9. CD spectra of Oligo1 and Oligo2 (5 µM) in different media. Below each concentration is shown the hybridization percentage value calculated by spectrofluorimetry.

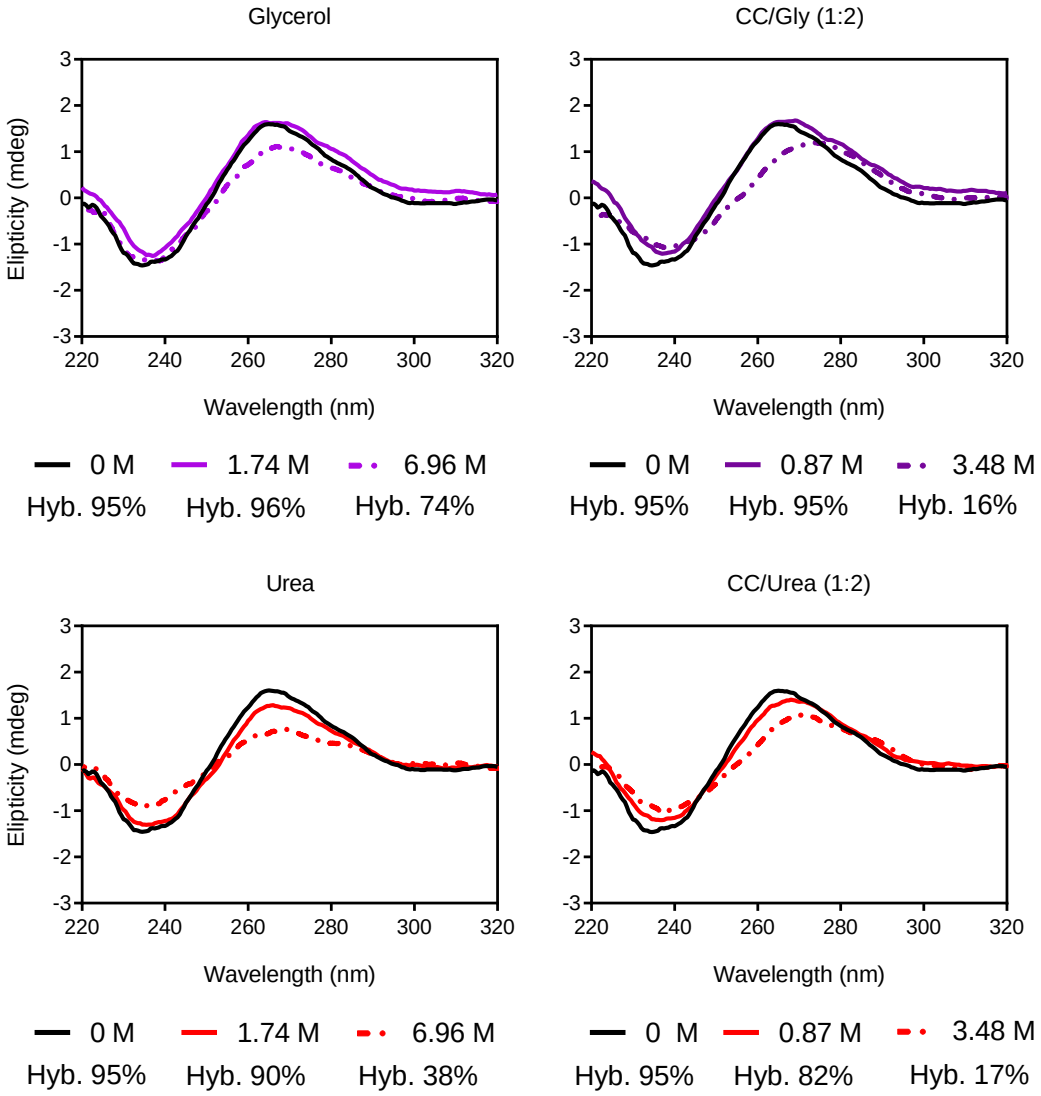

Table S3.2. Used DNA sequences.

Name	**Sequence 5' to 3'**	**G/C %**
Oligo1	CAC CTG GAA CCT	58
Oligo2	AGG TTC CAG GTG	
Oligo3	TAC CTG GAA CTT	41
Oligo4	AAG TTC CAG GTA	
Oligo5	TAC TTA GAA CTT	25
Oligo6	AAG TTC TAA GTA	
Oligo7	CAC CTG GCG CCT	75
Oligo8	AGG CGC CAG GTG	

Figure S3.10. Circular dichroism and UV-Vis spectra at 25 ^{o}C of duplexes in sodium chloride.

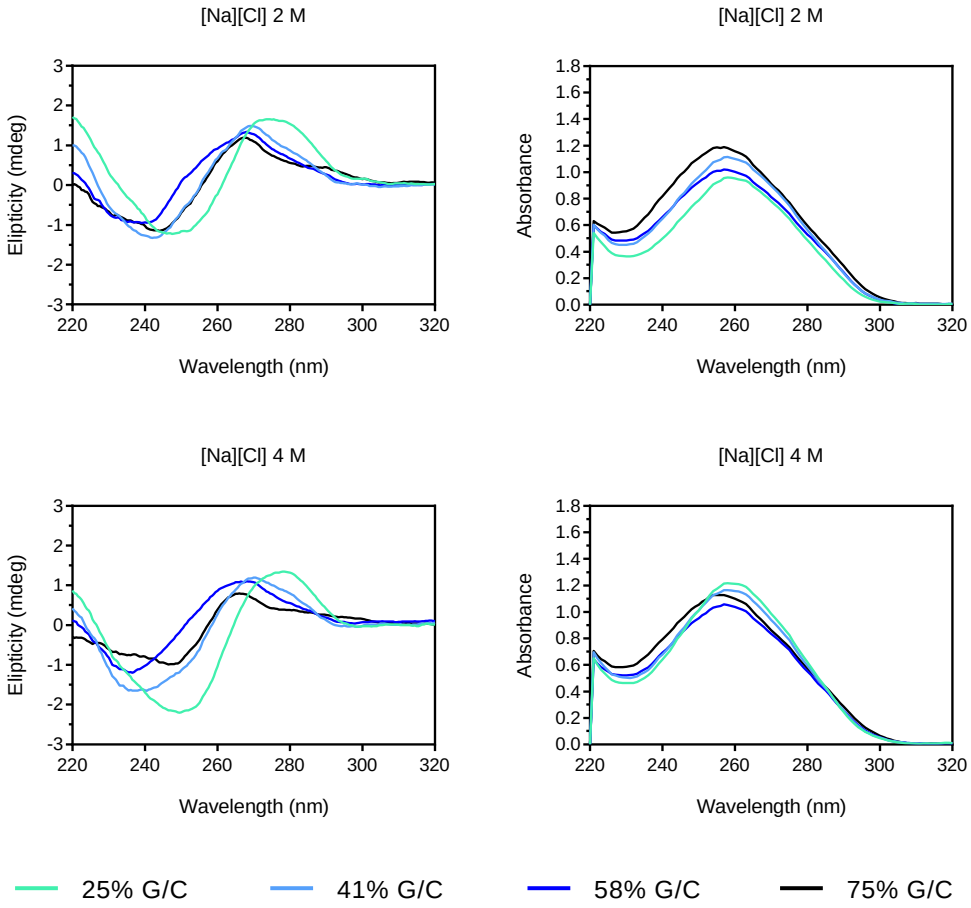

Figure S3.11. Circular dichroism and UV-Vis spectra at 25 ^{o}C of duplexes in choline chloride.

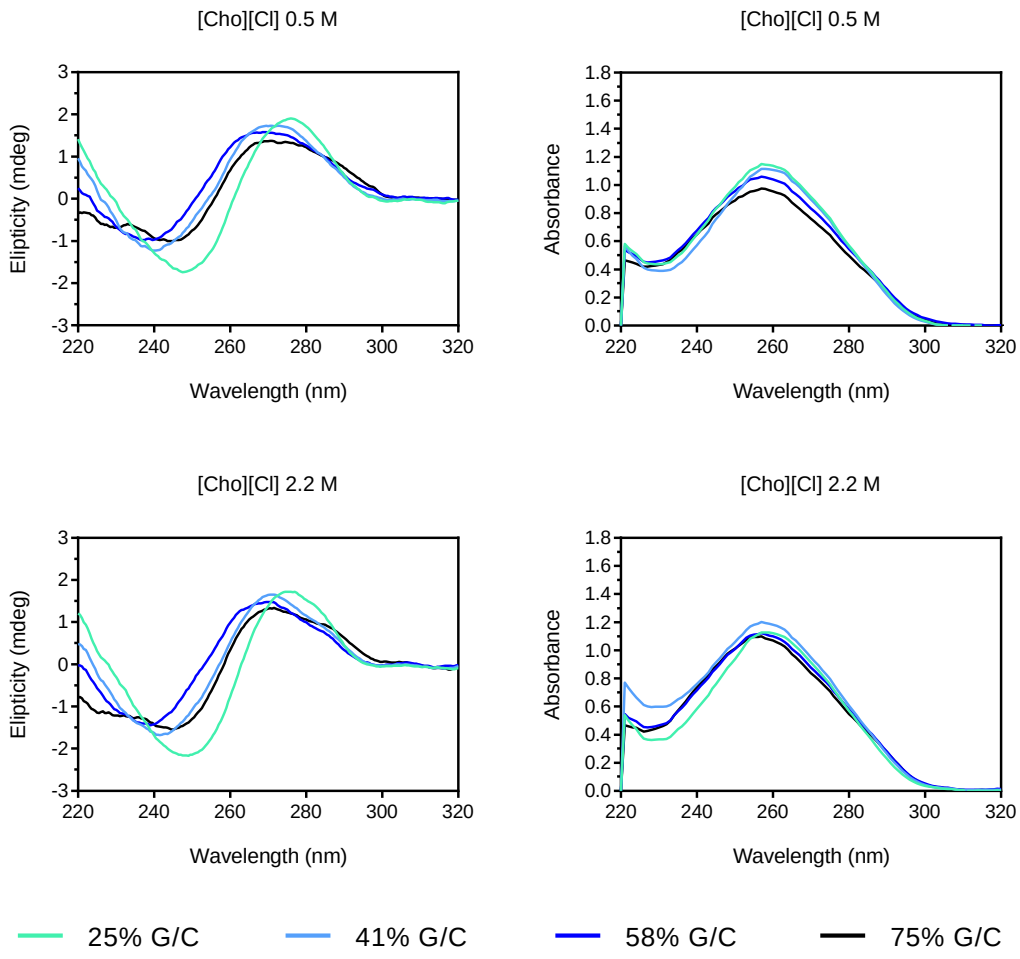

Figure S3.12. Circular dichroism and UV-Vis spectra at 25 ^{o}C of duplexes in ethaline.

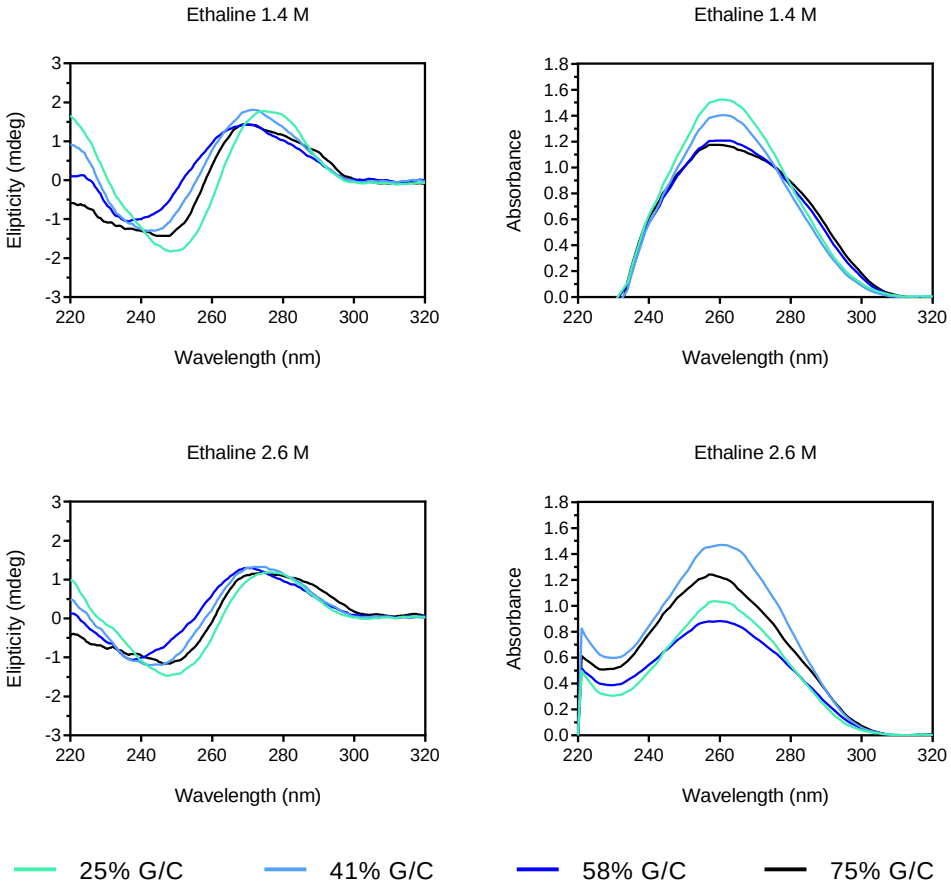

Figure S3.13. Circular dichroism and UV-Vis spectra at 25 ^{o}C of duplexes in choline lactate.

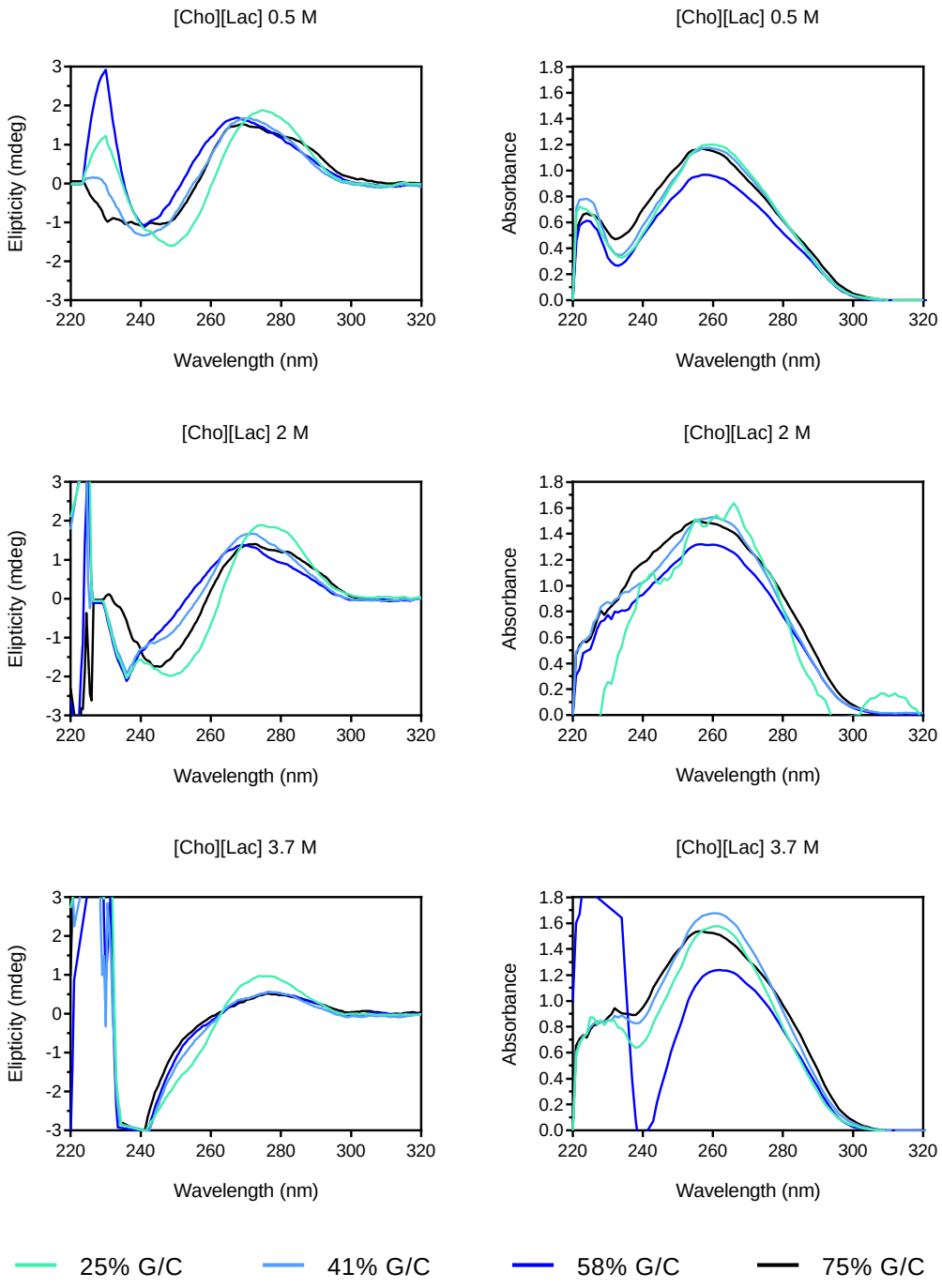

Figure S3.14. Circular dichroism and UV-Vis spectra at 25 ^{o}C of duplexes in choline dihydrogenphosphate.

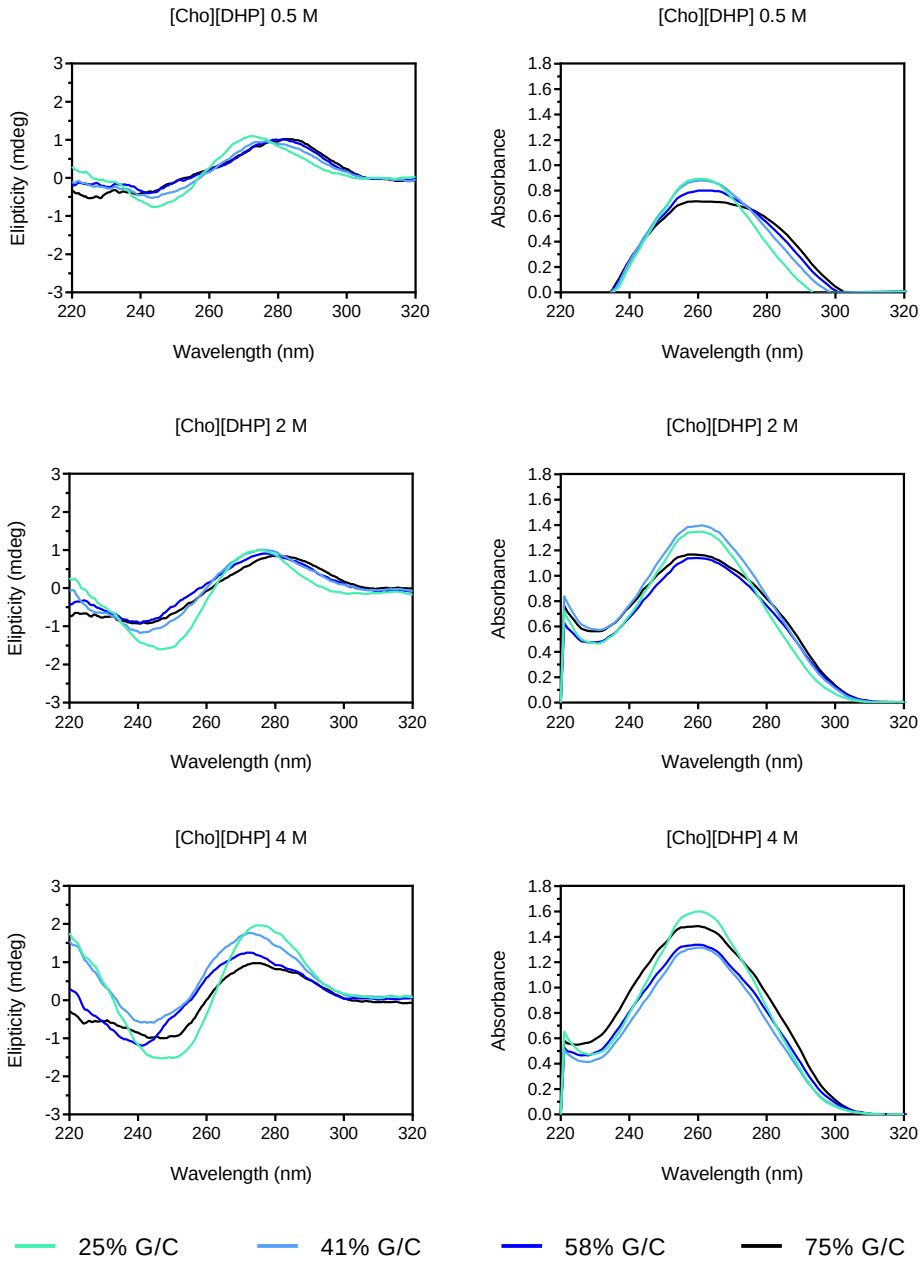

Figure S3.15. Normalized UV-Vis melting temperature curves.

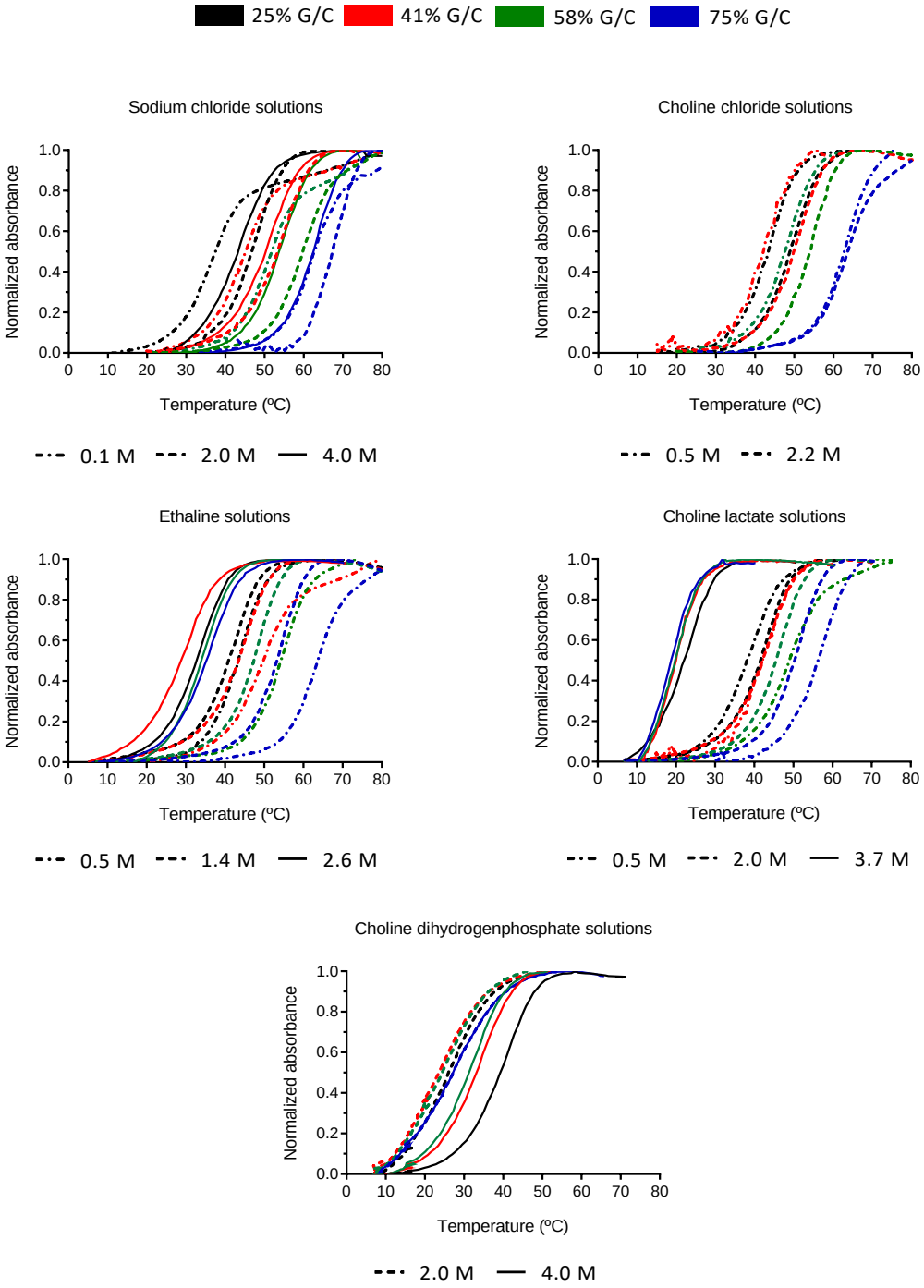

Figure S3.16. UV-Vis spectra of “short” and “long” s-sDNA solvated in different media.

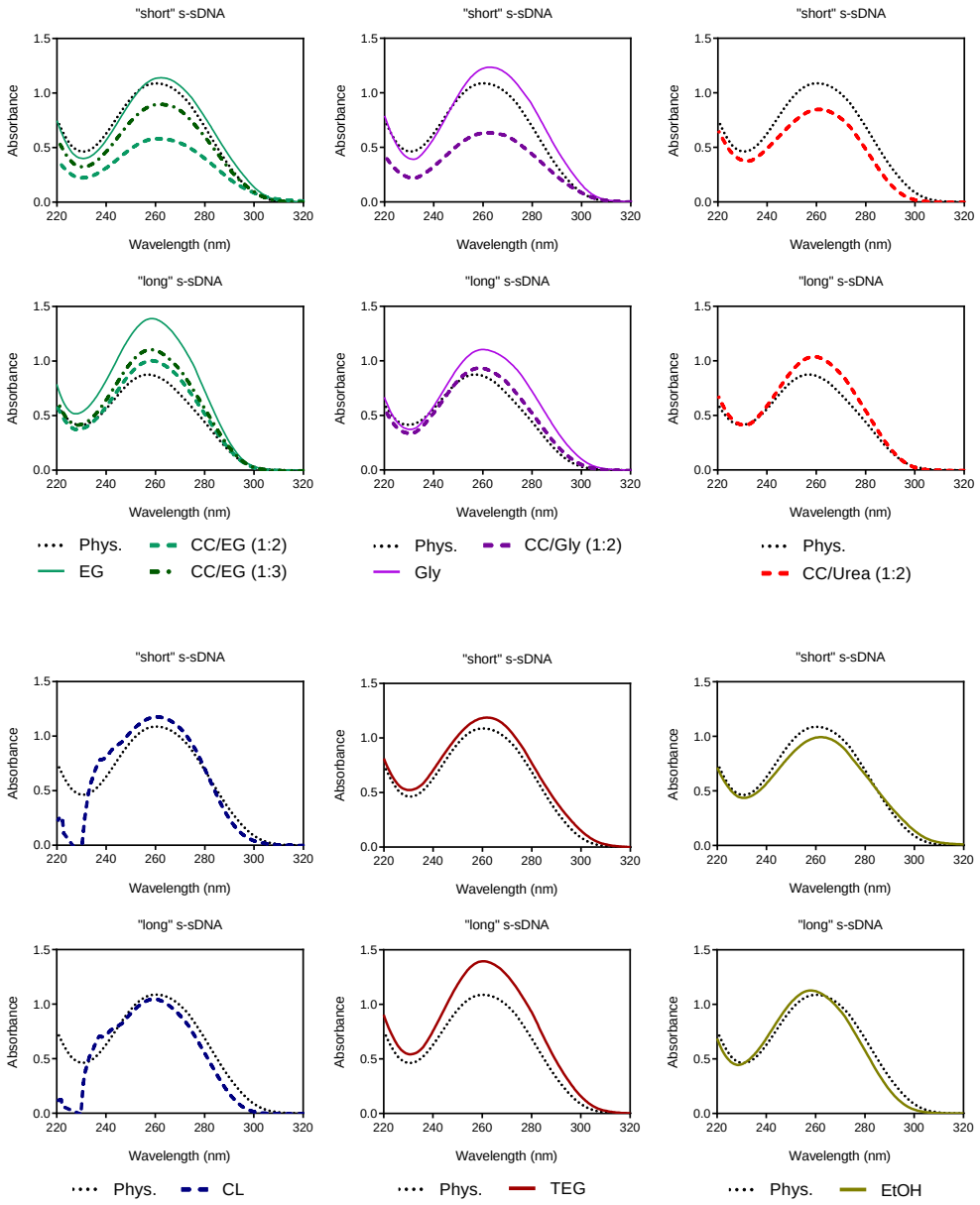

Figure S3.17. CD spectra of “short” and “long” s-sDNA solvated in different media.

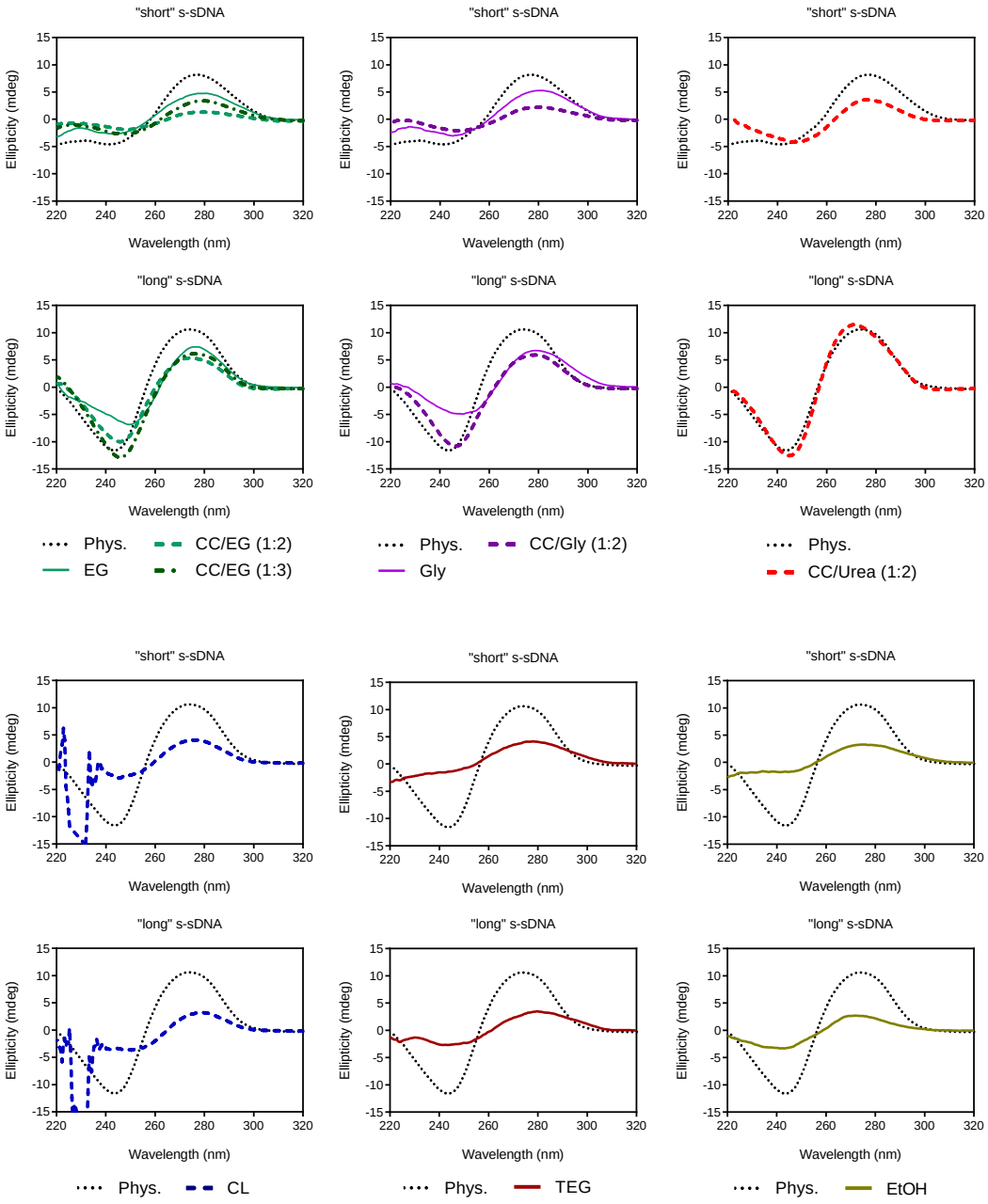

CHAPTER 4

Computational studies of a DNA double helix in mixed solvent

4.1 Introduction

The use of computational methods to model both, biomolecules and mixed solvents, is increasing rapidly since the last decades[1]. Therefore, in the near future, *in silico* studies could be the key to predict the effect of each media on the stability of DNA or to design the ideal solvent-DNA combination to detect a molecule of interest[2]. There are already huge advances in the development of reliable force fields for both, DNA[3,4] and solvents such as imidazolium-based ILs[5] or choline-based ILs[6] and DESs[7–9]. On the other hand, the peculiar effect of water in the nanostructure of these solvents is being studied also[10,11]. However, the results obtained with computer simulations must be carefully analyzed, especially when such complex systems as nucleic acids and mixed solvents are combined. In these mixtures, dispersion interactions, steric effects, or hydrogen bonding, among other events, play a non-negligible role for DNA solvation and solvent properties[12].

Unfortunately, very few studies about DNA solvation compare the results *in silico* and *in vitro* under the same conditions[13–15]. Leading in some cases in too hasty conclusions from the computer data related with the interactions, stability or conformation of DNA, which do not agree with other similar studies done in the laboratory. On the other hand, computationally it is not possible to study long DNA such as DNA-origami, salmon-sperm or calf-thymus DNA[16], and therefore a crystal structure of their average double helix is used, but only containing between 6 and 12 base pairs[17]. However, within its limits, while studying complex systems, computational methods could be used to understand different key-points in DNA solvation[18]. In general, comparison between values without considering the absolute numbers can be useful, in

example while analyzing the interactions between different molecules[19] and DNA or the conformational changes that it undergoes[20].

As mentioned in Chapters 1 and 3, there is still no theory or computational method to predict the behaviour of DNA in mixed solvents in detail[14,21]. This makes it impossible to use these techniques to quickly design a suitable solvent. A better understanding of what interactions between the solvent and the DNA affect the stability and conformation of the DNA will undoubtedly help to advance modelling strategies[22]. In this work, two classical computational methods have been used: the density functional theory (DFT) method and molecular dynamics (MD). The former case do not consider the whole experimental system, but it has been suggested to be useful while studying the interactions between mixed solvents and DNA[23], on the other hand MD allowed the creation of a box with the duplex formed between Oligo1 and Oligo2 (Chapter 3) solvated in mixed solvents. In this manner it was possible to replicate the same conditions studied *in vitro* but it was only possible to simulate it in the nanosecond scale.

4.2 Results and Discussion

4.2.1 Intermolecular interactions between solvent and DNA components

Ab initio methods were employed prior doing standard molecular dynamics calculations. Contrary to MD calculations, the whole DNA strands and solvent properties were not considered in DFT calculations because they would need too much computational time, however, the simulation of a concrete system gives interesting information about the preferential molecular interactions and the affinity of different solvent molecules towards DNA bases or backbone. The DFT calculations were carried out in the aqueous phase, on the one hand optimizing the previously studied solvent molecules and their individual components and on the other hand, DNA bases and backbone. All the energies found are listed in Table S4.1 and optimized structures are shown in Figure 4.1.

Then, the individual components of each solvent were optimized in contact with the DNA structures. This was done to elucidate the affinity and the molecular interactions between the different solvent molecules and those DNA sites that are usually exposed to the solvent. In Figure 4.2 are shown the different affinities and RMSD values calculated.

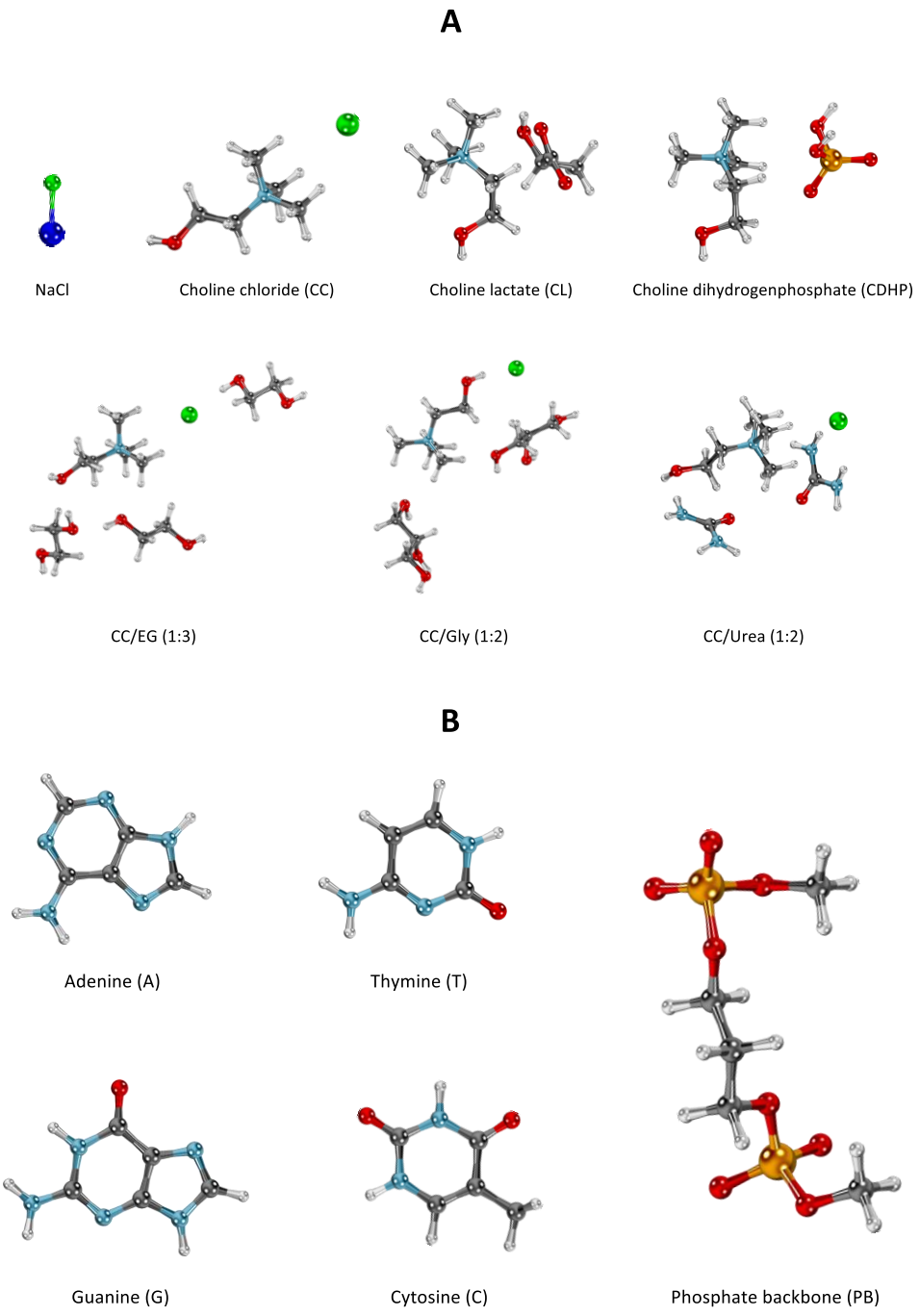

Figure 4.1. (A) Solvent and (B) DNA structures obtained using DFT methods.

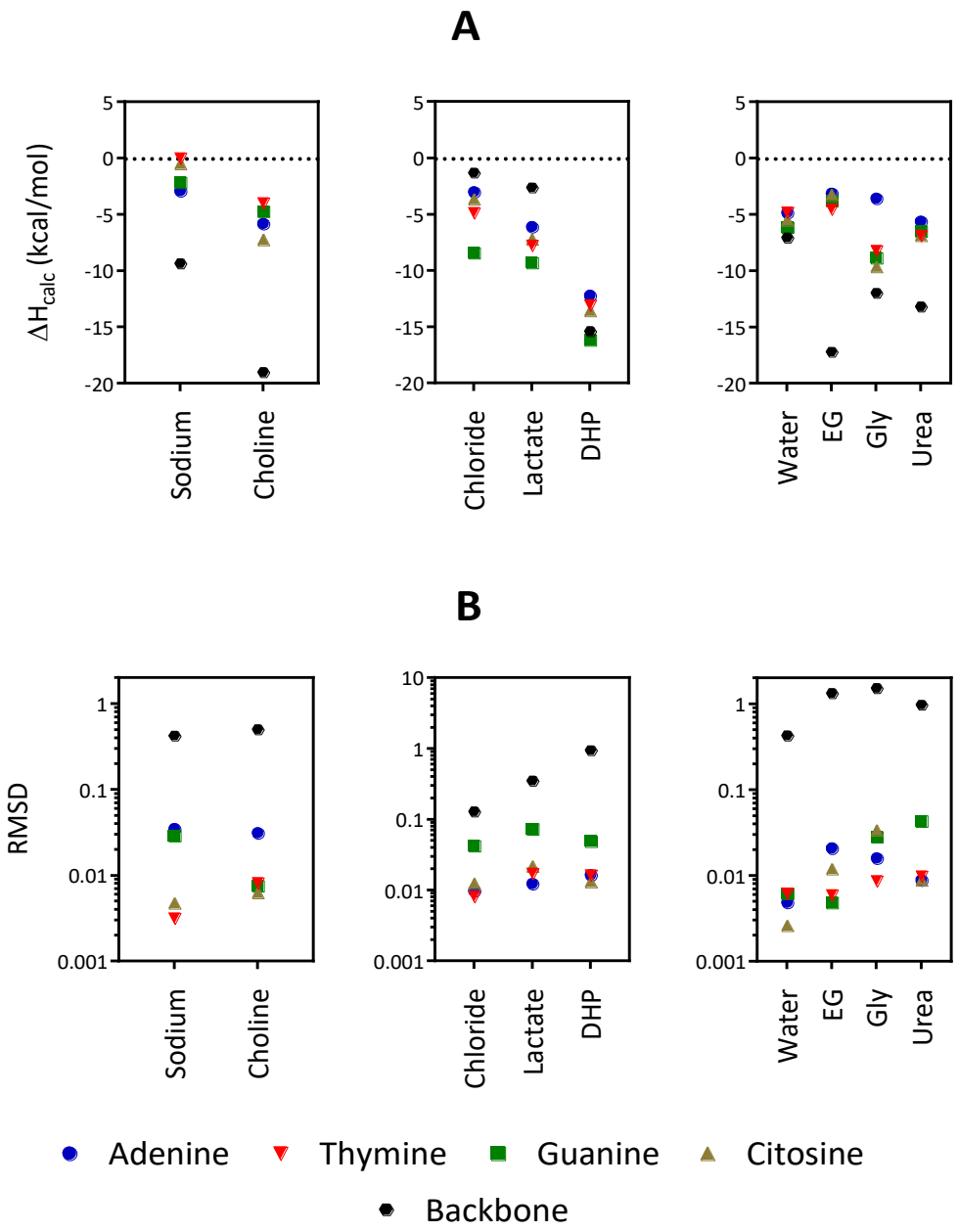

Figure 4.2. (A) Affinities for the bases of DNA and backbone. (B) RMSD values of DNA in presence of ions and molecules that are part of the mixed solvents.

These *ab initio* calculations are far from the experimental system, therefore the obtained affinity values (Figure 4.2A) are only indicative of the molecular interactions that could happen between DNA and the media and complement the molecular dynamics calculations shown in the next sections. On the other hand, the RMSD values (Figure 4.2B) indicate if the formed interactions suppose a huge change for the native conformation of DNA double helix.

From affinity results, it is possible to observe that choline has in general two times more affinity towards the bases than sodium; in fact, the former can create a greater number of interactions. In case of anions, chloride, lactate and dihydrogenphosphate (DHP) they seem to have slightly higher affinity towards guanine than other bases. DHP anion has a significantly higher affinity towards the bases and backbone compared with all other ions and despite of the electrostatic repulsion between phosphates.

Respect water and HBD groups, there were no significant differences between affinities towards the whole bases. As could be expected, glycerol can interact stronger with bases due to the extra hydrogen bond donor group, but interestingly ethylene glycol (EG) has higher affinity towards the backbone than glycerol. In order to understand better these differences, the different molecular structures were compared between each other (Figure S4.1 and S4.2). It can be observed that EG suits much better in the backbone and the extra hydroxyl group of glycerol does not form any interaction with it. Observing these optimized structures it was possible to observe how the different ions and molecules interact with the DNA atoms highlighted in Figure 4.3, the results are shown in Table 4.1.

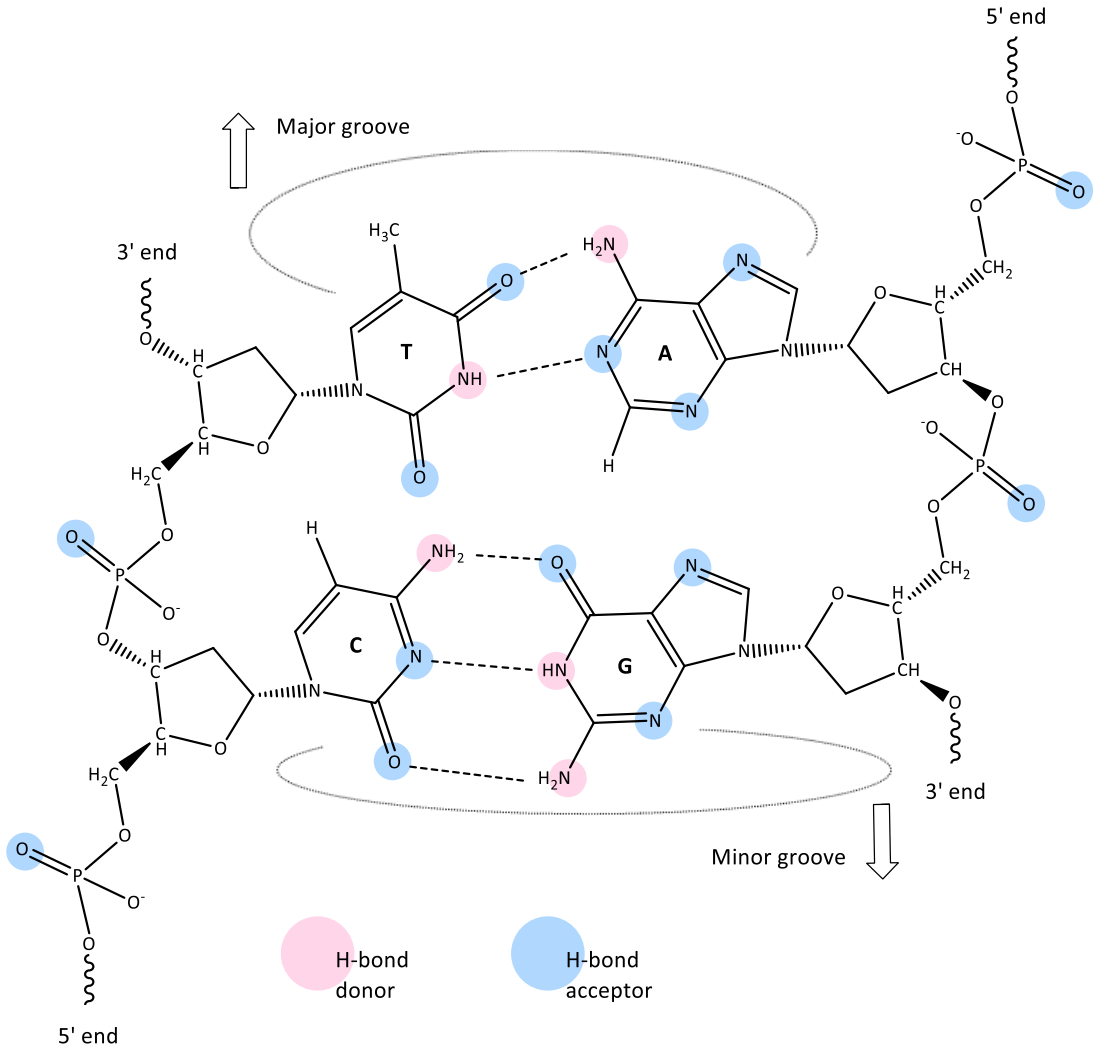

Figure 4.3. The DNA structure with the principal H-bonding donor and acceptor atoms.

Table 4.1. Number of H-bonding interactions formed between each solvent molecule or ion and DNA bases or backbone in optimized structures (Figures S4.1 and S4.2).

	Adenine		Thymine		Guanine		Cytosine		Backbone
	HB A	HB D	HB A	HB D	HB A	HB D	HB A	HB D	HB A
Sodium	1	0	0	0	1	0	0	0	1
Choline	1	1	1	0	1	0	1	0	1
Chloride	0	1	0	1	0	2	0	1	0
Lactate	1	1	1	1	0	2	1	1	1
DHP	1	1	1	1	1	1	2	1	2
Water	1	1	1	1	2	0	2	0	1
EG	0	1	0	1	1	0	0	1	2
Glycerol	1	1	1	1	2	2	2	1	2
Urea	1	1	1	1	0	2	1	1	3

The first column of Table 4.1 refers to adenine base. In example, sodium interacts strongly with the imine group of adenine, which is also involved in the Watson-Crick base pairing, but the hydroxyl group of the choline cation apart from interacting with that imine, also forms an H-bond with the amino group. This is why the RMSD of adenine while being solvated with choline is significantly higher than that of the other DNA bases. Regarding anions, chloride interacts with the amino group but it would not affect the base pairing. The hydroxyl and ketone groups of lactate and DHP anions interacts with the same amino and imine groups of choline, and the same happens with water, glycerol and urea. Ethylene glycol do not donate a hydrogen; only accept that of the amino group, what also occurs with cytosine. However, it would disrupt the base pairing due to its bulky nature.

In case of thymine, sodium almost does not interact strongly with this base, what can be observed also in the binding energy and RMSD values that are close to zero (Figure 4.2). In case of choline, it donates an H-bond, but do not creates any with an acceptor group of DNA, this also happens with guanine and cytosine. All the anions, glycerol and urea form an H-bond with the secondary amino that is involved in Watson-Crick base pairing but the other H-bond that they form is with the ketone not involved in the base-pairing. Water, differently from the rest of molecules, interacts preferentially with the ketone close to the methyl group.

Guanine forms more interactions with the solvent molecules than the rest of the DNA bases. Sodium interacts with the imine group of guanine not involved in the base pairing. In case of choline cation, it donates the HB to the ketone. The chloride and lactate anions are able to form two simultaneous hydrogen bonds with amino and secondary amino groups, but dihydrogenphosphate only forms one HB with this group. Water also donates two H-bonds but in contrast with chloride and lactate, one of these is with the imine group not involved in Watson-Crick base pairing. Glycerol forms the highest number of interactions with two simultaneous HB acceptor and donor groups.

In case of cytosine base, it does not interact with sodium, as happened with thymine. Dihydrogenphosphate donates two hydrogen bonds but to the same atom, that is why the affinity to this base is similar to the rest. In case of water, it donates two hydrogen bonds, but the RMSD of cytosine is almost zero, as happened also with other bases. Glycerol interacts with the three atoms that are involved in the Watson-Crick base pairing, whereas urea interacts with two and ethylene glycol only with one.

The H-bond interactions with the DNA backbone are quite different, principally due to its negative charged nature and the absence of hydrogen bond donor groups. As could be expected, sodium interacts strongly with the negatively charged oxygen. Interestingly, the positively charged alkylammonium group of choline that was far from DNA bases in this case is in parallel to the backbone, even if it does not directly interact with the oxygen, because the length of choline is insufficient to form the hydrogen bond with one phosphate group and neutralize effectively the adjacent one. In case of anions, chloride does not interact in any manner with the backbone, but lactate and DHP donate hydrogen bonds. Specially, DHP donates two hydrogen bonds, what can be observed in the high affinity and RMSD values.

Water only forms one hydrogen bond but its small size can allow many water molecules to interact with the rest of the backbone. In case of ethylene glycol and glycerol, they can form two hydrogen bonds with the two phosphate groups and the former alters less the conformation of the backbone than glycerol because it is longer. The interactions of urea with the backbone are quite special, because apart from donating a hydrogen bond to the ketone group, it also interacts with two ethers. As mentioned before these *ab initio* calculations reflect a system much simpler than the experimental one, but it will be interesting to know if the molecular dynamics results that are going to be presented in the next two sections match the behaviour observed here.

4.2.2 Solvation of a double helix in mixed solvents and their nanostructure

Between the innumerable events that could be studied with MD, in this chapter the main objective has been to deepening in the results found in Chapter 3. The MD simulations

Computational studies of a DNA double helix in mixed solvents were done in absence and presence of DNA oligonucleotides used in Chapter 3 (Oligo1 and Oligo2) (Table 4.2). The simulations in absence of DNA served to observe how the bulk media changes in presence of DNA but also to compare the obtained densities with experimental values. As can be observed in Figure 4.4, the obtained densities were slightly higher than experimental ones but followed the same trend excepting the highest concentration of glycerol-based media and reline, an artefact that has been recently related with the need of rescaling the partial charges[24,25]. However, even if they can be improved, the used force fields have been already validated as they have been published in leading journals (Section 2.4.2).

Table 4.2. The media simulated with molecular dynamics. The sodium atoms varied depending on the absence or presence of DNA oligonucleotides (n=11 boxes containing Oligo1 or Oligo2 and n=22 while containing both oligonucleotides). The media is equivalent to that used in Sections 3.2.1-3.2.3.

Medium		**Number of molecules or ions**					
HBA, HBD or DES	Molarity	HBA, HBD or DES	H_2O	Cl^-	Na^+	Mg^{2+}	K^+
	0	0	20484	56	51 + n	2	1
Choline chloride	0.44	161	19380	53	48 + n	2	1
	0.87	322	18276	50	46 + n	2	1
	1.31	483	17172	47	43 + n	2	1
	1.74	643	16089	44	40 + n	1	1
	2.18	804	14985	41	37 + n	1	1

	2.61	965	13881	38	35 + n	1	1
	3.48	1287	11693	32	29 + n	1	1
Ethylene glycol	1.74	643	18553	50	45 + n	1	2
	2.61	965	17593	48	43 + n	1	2
	6.96	2574	12724	35	32 + n	1	1
	10.44	3861	8751	24	22 + n	0	1
Glycerol	1.74	643	17952	49	44 + n	1	2
	6.96	2574	10254	28	26 + n	0	1
Urea	1.74	643	18900	51	46 + n	1	2
	6.96	2574	14063	38	35 + n	1	1
Ethaline	0.87	322	15950	43	40 + n	1	1
	2.18	804	9476	26	24 + n	0	1
	3.48	1287	3393	9	9 + n	0	0
Glyceline	0.87	322	15027	41	38 + n	1	1
	3.48	1287	962	3	3 + n	0	0
Reline	0.87	322	16184	44	41 + n	1	1
	3.48	1287	4476	12	12 + n	0	0
CC/EG (1:3)	0.87	322	15435	42	39 + n	1	1

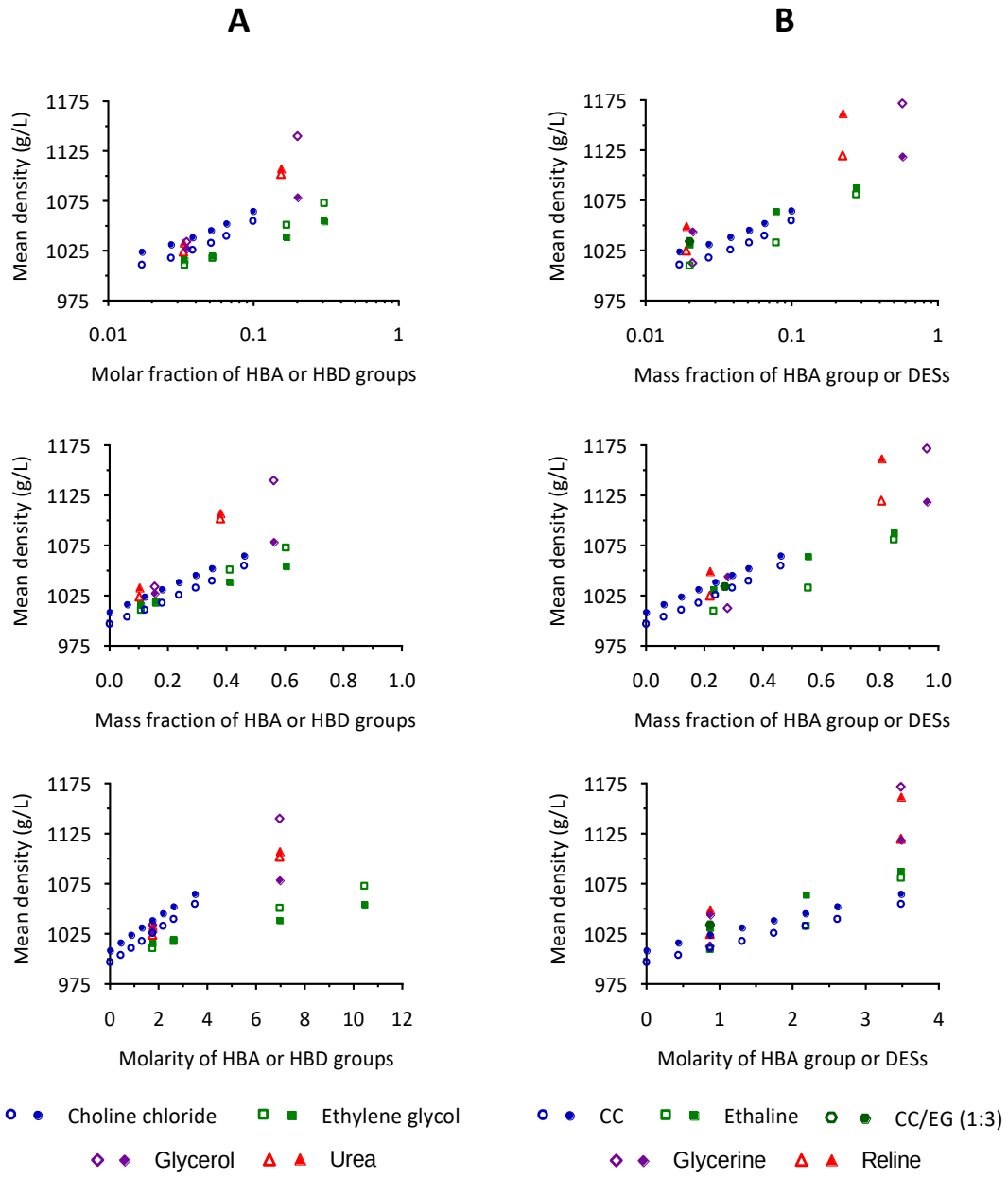

Figure 4.4. Experimentally (empty symbols) and computationally (filled symbols) calculated mean densities of mixtures based-on (A) HBA and HBD groups or (B) HBA group and DESs represented *vs.* mass fraction, molar fraction or molarity.

The first observation made in previous chapter was that sodium cations could enhance the stabilization of the double helix but only below a DES concentration (Figure 3.2). Therefore, it was studied if non-aqueous solvents were able to release sodium cations from DNA. For that purpose, the percentage of sodium cations close to DNA respect from the total sodium cations in the solvent was represented *vs.* the concentration of HBA, HBD groups or DESs (Figure 4.5).

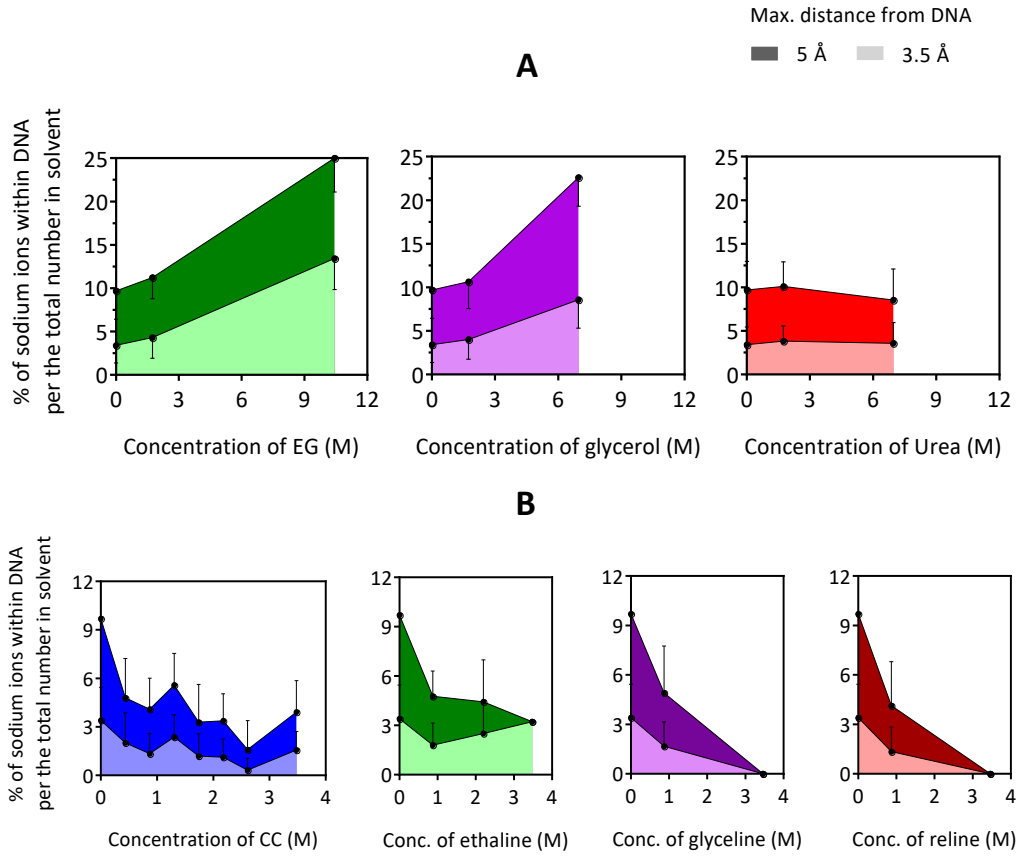

Figure 4.5. Relative number of sodium cations from DNA in different mixed solvents (A) HBD groups and (B) HBA group and deep eutectic solvents.

Interestingly, it was observed that whereas ethylene glycol and glycerol favoured the interactions between sodium and DNA, choline-based media had the ability to release sodium (Figure 4.5); this would explain why above certain concentration sodium was not able to enhance the stability of the double helix independent on the concentration used. It is curious the result found in mixture containing ethaline at 3.4 M concentration, whereas in glyceline and reline all sodium cations were released from DNA, in ethaline there was yet a single sodium close to DNA during the 10 ns. It can be observed that this sodium was trapped by three ethylene glycol molecules, which are also close to DNA over the whole simulation (Figure 4.6) contrary to the faster residence times found in ethylene glycol media at a same concentration (in absence of choline chloride).

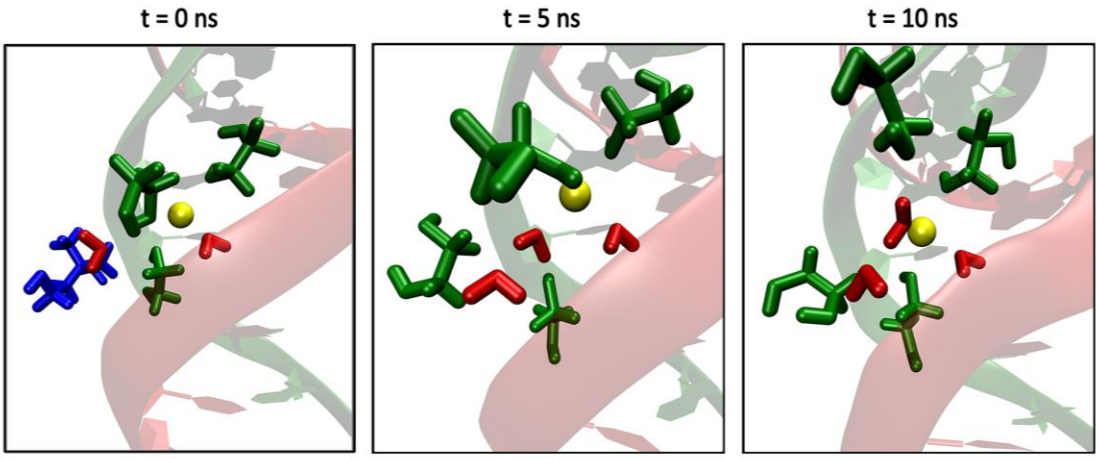

Figure 4.6. Snapshot taken from the trajectory analysed containing ethaline-based mixed solvent at 3.4 M and dsDNA (green EG; red water and yellow sodium).

The second observation in previous chapter was that reline destabilized less the duplex than urea, contrary to what happened with ethaline and glyceline that destabilized DNA more

than ethylene glycol and glycerol at a same concentration (Figure 3.3). Unfortunately, the denaturation of DNA cannot be measured in the nanosecond time-scale used in these simulations, but it is possible to observe the nanostructure of the solvent and elucidate if choline chloride prevents urea from interacting with DNA what could explain why it is more stable in reline[26]. The study about the effect of urea and reline started counting the number of atoms close to DNA as did with sodium, but as can be observed in Figure 4.7A there were only minor differences. In both media, urea and reline, there was a similar number of urea molecules close to DNA.

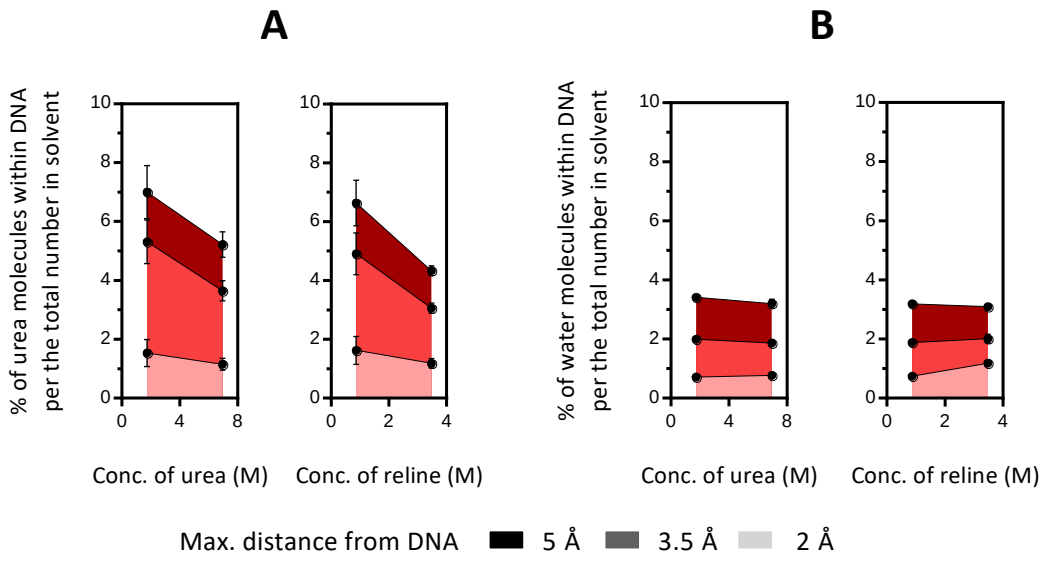

Figure 4.7. Relative number of (A) urea and (B) water molecules from DNA.

If the different behaviour of urea was not caused by a significant difference in number of molecules in close contact with the biomolecule, it must be related with a difference in their interactions. The radial distribution function (RDF) of urea from DNA was used in order to deepening in this matter. The data is shown in Figure 4.8.

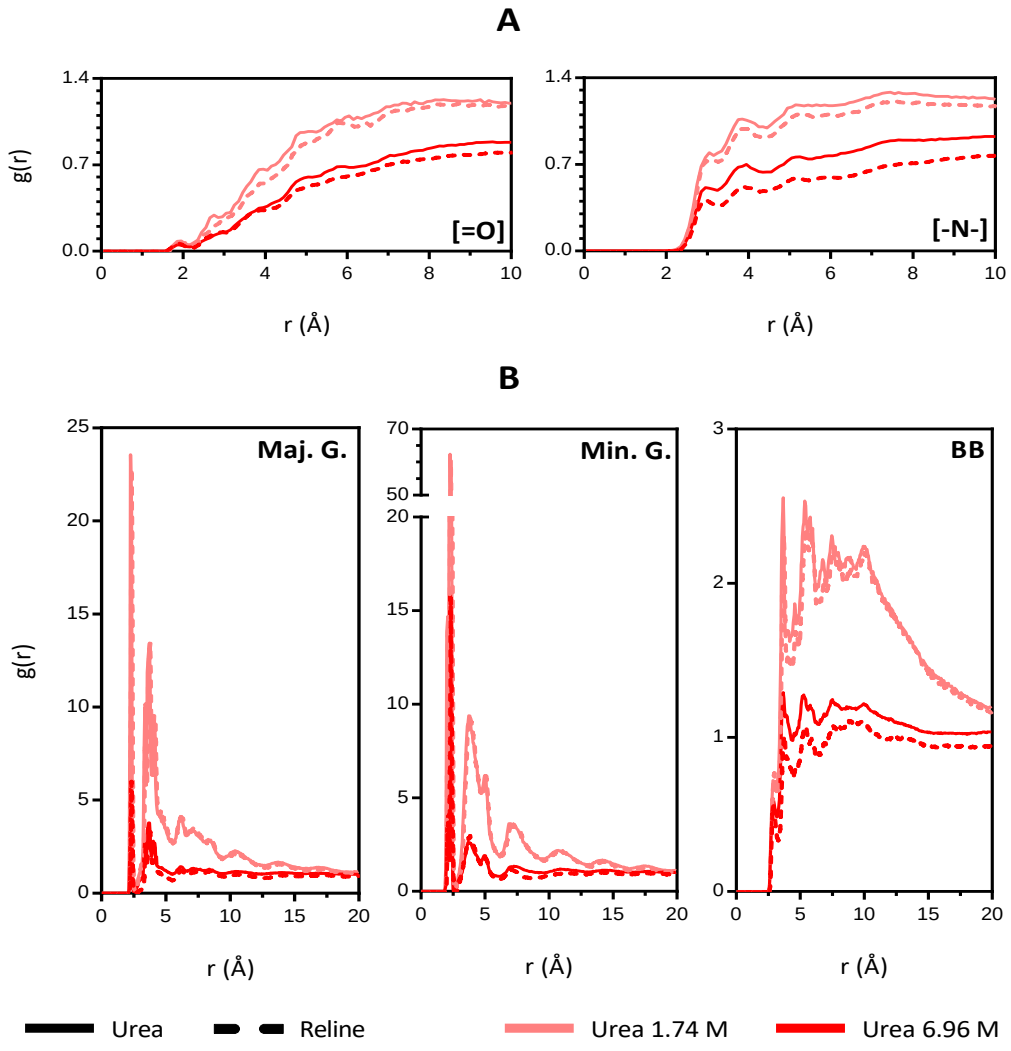

Figure 4.8. The RDF g(r) for (A) the oxygen or nitrogens of urea from DNA. (B) The nitrogens of urea from the major and minor grooves or backbone of DNA, except ends.

It can be observed that whereas the oxygen of the carbonyl group is located similarly from DNA in both concentrations of urea and reline, there were significantly less amine groups oriented towards DNA in case of reline at high concentrations (Figure 4.8A). In order to understand better this difference, the RDFs of nitrogens were calculated towards the whole backbone and the H-bonding atoms of the minor or major groove structures (Figure 4.8B). The latter atoms are highlighted in Figure 4.3. Once again, the amine groups of urea were less densely located close to DNA in presence of choline, especially at high DES concentrations. Therefore, the salt prevented urea from donning hydrogen bonds to DNA.

In order to quantify the number of H-bonds formed between urea and DNA, these were counted using VMD software (Table 4.3). Almost in all cases, the number of H-Bonds donned by urea to DNA was very similar in urea and reline. Except the number of H-Bonds donned in reline at 3.48 M (81 wt. %) to the major groove, this was significantly lower in absence of choline chloride (1.0 ± 0.6 *vs.* 4.4 ± 2.0). The same analysis was done with EG and glycerol-based solvents, and as can be observed in Table S4.2, ethylene glycol and glycerol donned more hydrogen bonds to DNA bases when they were part of a DESs, contrary to urea. On the other hand, it was observed that the interactions between water and DNA were promoted in reline, compared to the other media. As can be observed in Table S4.3, in general are formed between $4{\cdot}10^{-2}$ and $6{\cdot}10^{-2}$ hydrogen bonds between water and the major groove of DNA per water molecule within 3.5 Å from DNA. But, in case of reline at low hydration levels, this ratio increases significantly to $\approx 8.5{\cdot}10^{-2}$, therefore, the lack of interactions between urea and DNA in reline media, facilitates the hydration of the base-pairs. Although this needs to be studied further,

these results indicate that reduced interactions between urea and the major groove could be the cause of the higher stability of DNA in reline, compared to urea.

Table 4.3. The number of urea molecules within 3.5 Å of DNA and the number of H-Bonds donned by urea molecules to different DNA sites. In H-Bonding analysis the ending nucleotides were not considered.

Medium		**Urea molecules**	**Number of H-Bonds donned**		
		Within 3.5 Å	Maj. G.	Min. G.	Backbone
Urea	1.74 M	34 ± 5	1.6 ± 1.3	1.0 ± 1.0	10 ± 3
	6.96 M	94 ± 9	4.4 ± 2.0	3.1 ± 2.1	32 ± 6
Reline	0.87 M	32 ± 5	2.1 ± 1.6	1.0 ± 1.1	11 ± 4
	3.48 M	79 ± 4	1.0 ± 0.6	1.7 ± 1.3	29 ± 6

Related with the specific site-interactions between ions and DNA, in Section 3.2.4 it was found that choline cation, contrary to sodium, destabilized specifically G/C-rich duplexes. The molecular mechanism of this destabilization had already been experimentally and computationally explained in an ionic liquid-based solution[17,22,27], were choline interacted specifically with the minor groove of DNA and G/C base-pairing positions. In the previous chapter, it was found for the first time that this sequence specific destabilization also happened in deep eutectic solvents. In order to obtain some details at the molecular scale about these results, different studies were done about the interaction of choline chloride with DNA in single- and double-stranded form.

Using the RDF analysis, it was found that choline chloride apparently interacts very similarly with DNA in its single- or double-stranded form, contrary to chloride anion that lost the peak at 2.5 Å in presence of dsDNA. On the other hand, the previously observed ability of choline

to displace sodium cations from dsDNA was also observed in single-stranded (Figure S4.3). Then, the RDF analysis was done between the solvent and specific DNA regions, in order to detect the site-specific binding of choline (Figure 4.9).

From RDF spectra, it can be concluded that choline interacts preferentially with backbone throw the ammonium group (the peaks close to 5 Å), but forms strong hydrogen bonds with the hydroxyl group (the peak at 2.7 Å). In the major groove it interacts similarly with the hydroxyl and ammonium groups (there are similar intensities). Interestingly, in the minor groove, the g(r) values are significantly higher than in other regions showing a higher density of choline in this area compared with the major groove or backbone, these choline molecules are oriented towards DNA with their hydroxyl groups.

At 3.4 M concentration (46 wt. percentage of choline chloride), the g(r) value reduces significantly, probably because the minor groove was already saturated with choline and the density is lower than in the bulk media. In Figure 4.9C can be observed that the RDF spectra of water from DNA only changed in the minor groove region, what would mean that the site-specific binding of choline displaced water from the DNA bases of the minor groove.

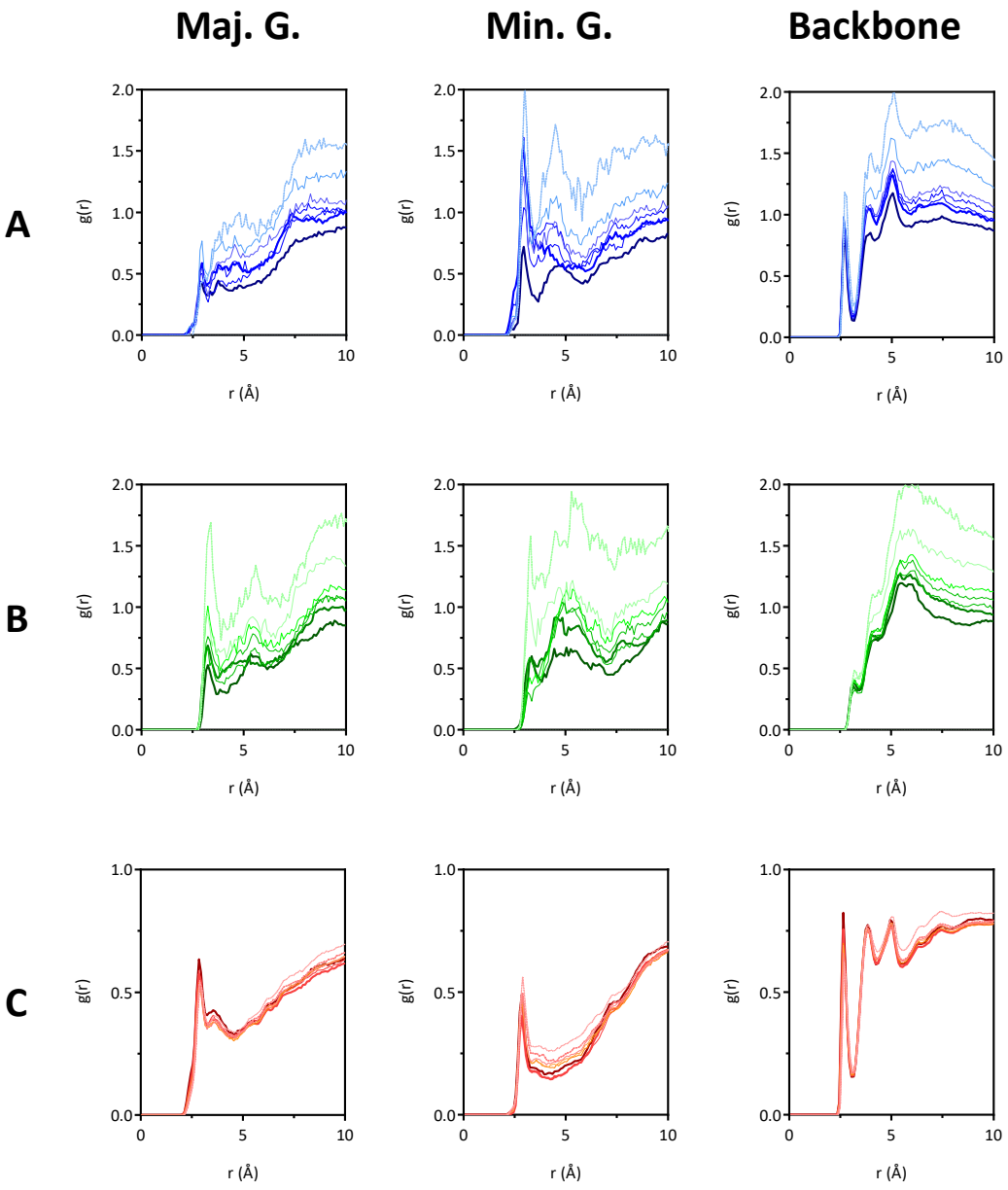

Figure 4.9. RDF curves of (A) oxygen of choline, (B) COM of choline and (C) oxygen of water from different DNA regions. The RDF analysis were done for different mixtures containing choline chloride at 0, 0.44, 0.87, 1.31, 1.74, 2.18, 2.61 and 3.4 M, represented from lighter to darker colors while increasing the choline concentration.

The site-specific interaction of choline was confirmed by a hydrogen-bonding analysis. When DNA acted as HB acceptor, there were almost no differences in the number of HBs donned by choline in the major and the minor groove per DNA HB acceptor atom (data not shown). However, when DNA was the HB donor, above 1.74 M or 4 molar percentage of choline chloride, the minor groove donned significantly more HBs than the major groove to choline (Figure 4.10A). Contrary to what happened with water that donned more HBs with the major groove (Figure 4.10B). The site-specific interactions found in urea and choline show that small differences in the interactions between media and DNA bases have significant impacts on the stability of the double-helix.

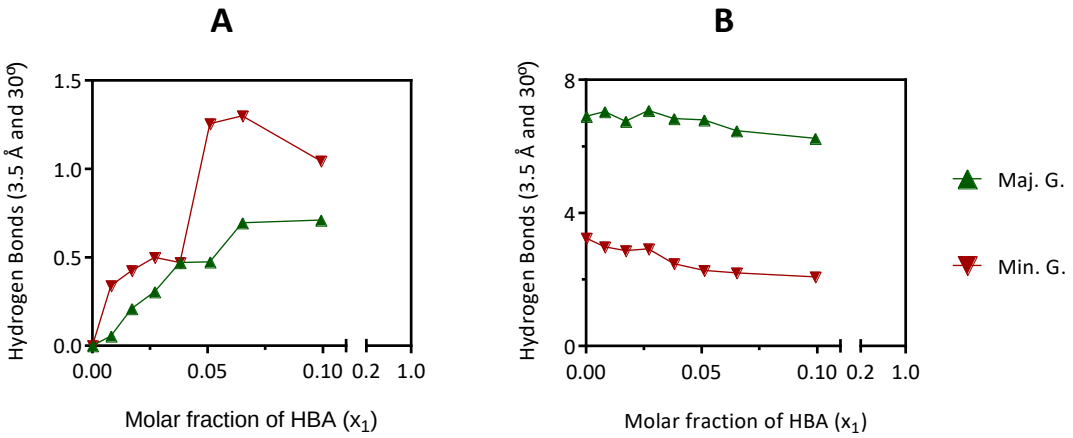

Figure 4.10. The number of hydrogen bonds donned by DNA to (A) choline cation or (B) water molecules in different DNA regions.

It was found also that choline forms a heterogeneous nanostructure around DNA not found in pure TBS and not mentioned in the literature. In Figure 4.11 can be seen that there was a major density of choline within 3.5 Å of DNA than within 2 or 5 Å, but in general the density of

choline within 5 Å of DNA was always higher than in the bulk media. Interestingly, the density of water molecules decreased significantly within 3.5 and 5 Å, but within 2 Å of DNA water had a higher density. This probably happened because the interactions of water with DNA prevented choline from displacing water as effectively as at longer distances.

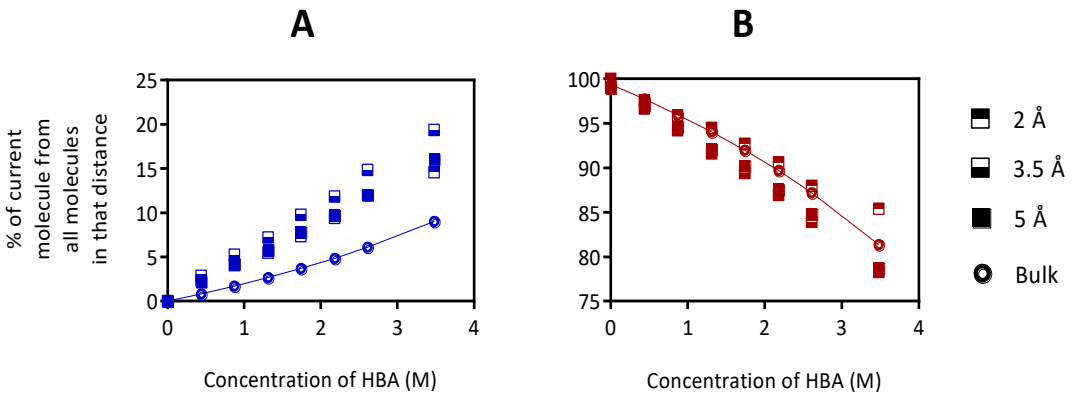

Figure 4.11. Percentage of (A) choline or (B) water within an specific distance of DNA from the total number of molecules and ions in that distance.

On the other hand, it was observed that choline had also the capacity to reduce effectively the water activity, responsible of DNA degradation, a matter that will be addressed in the next chapter. Choline chloride and DESs reduced the number of water-water interactions, more effectively than HBD groups at an equal water molar fraction (Figure S4.4). This might be directly related with the reduction of water activity, as it has been proposed that choline salt and DESs form aqueous electrolyte-like mixtures reducing the “free” water[25,28].

4.2.3 Intramolecular interactions and secondary structure of DNA

Leaving aside the interactions between DNA and its environment, it was also possible to study the intramolecular interactions of DNA using molecular dynamics and, although the simulation time was very short, to observe different behaviours of secondary structure. The unability to observe the denaturation event in the nanosecond scale can be observed in Figure 4.12, there were no significant variations in the intramolecular hydrogen bonds formed by DNA (without considering ending bases), whereas it was calculated in previous chapter that the hybridization percentage between Oligo1 and Oligo2 decreased substantially at 25 ^{o}C (Figure S3.2).

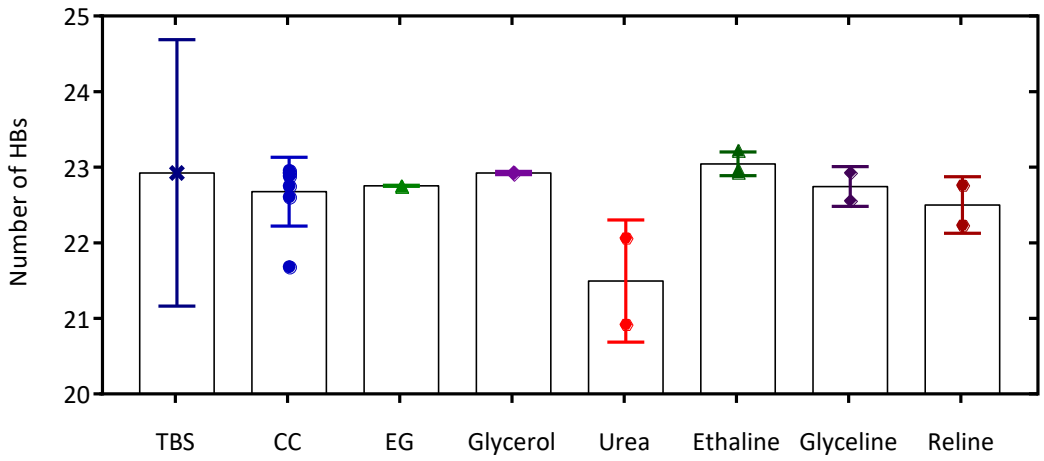

Figure 4.12. The number of hydrogen bonds formed between Oligo1 and Oligo2 in physiological media (TBS) and in each of the mixed solvents at different hydration levels. The height of the column represents the mean number obtained in each type of mixed solvent and the error bar is the standard deviation.

Contrary to the number of intramolecular hydrogen bonds of DNA, the 10-nanosecond time-scale allowed to observe significant differences in the secondary structure of double helix. As can be observed in Figure 4.13, the RMSD values of DNA in urea were significantly higher than those of DNA in physiological media. Therefore, even if in the simulation time-scale hydrogen bonds between bases did not move away longer than the 3.5 Å distance used as upper limit, the secondary structure suffered significant changes in 6.96 M urea.

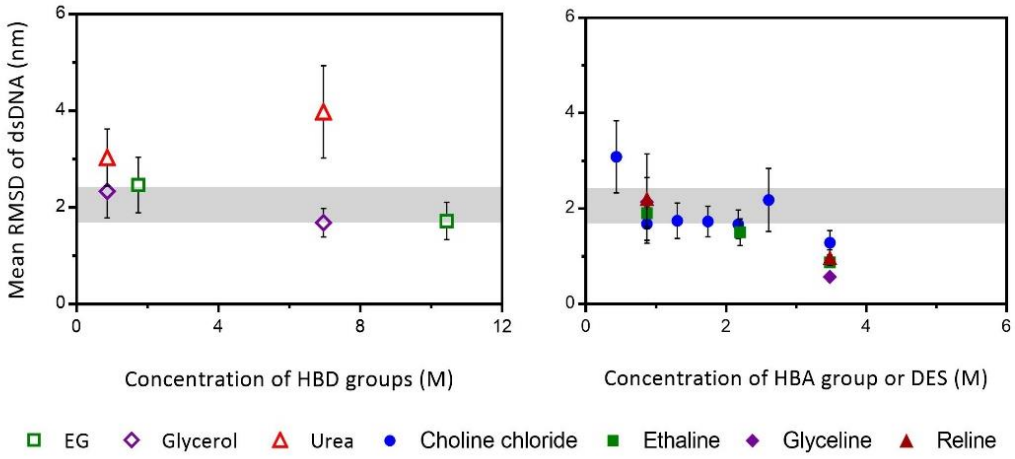

Figure 4.13. The mean RMSD values obtained. The grey line represents the value obtained in physiological media with its standard deviation.

The RMSD values at high DES concentration were also significantly different than those found in physiological media, but in this case, they were below that value. It was already observed in the previous section that DESs at this concentration can form a solvation shell around DNA slowing down molecular movements and trapping, in example, a sodium cation (Figure 4.6). Therefore, it is not surprising to find a slowdown in the molecular movements of DNA. In order to observe detailed variations in the secondary structure of the double helix, the

structural changes in each mixed solvent were analysed based-on 10 helical, backbone and groove parameters[29] (Figure S4.5 and S4.6).

Regarding the DNA grooves, the width of the major groove did not suffer significant changes in mixed solvents, compared to physiological media, but the width of the minor groove decreased significantly in presence of choline chloride, especially at low hydration levels (from 8.8 to almost 6 Å). It was observed in previous section that choline had a site-specific binding in this groove; therefore, it could the main responsible of this change. In the literature it is mentioned that minor groove compression is a mechanism used usually by nature to favour DNA-protein interaction, and this is achieved neutralizing the local phosphate groups[29]. Choline could act as a cation for phosphate neutralization, what would explain this behaviour. The depths of both, major and minor grooves increased significantly in all mixed solvents at low hydration levels, except in urea, where decreased. It was not possible to find an explanation for this in the literature (Figure S4.5).

Regarding the rotational and translational parameters of DNA parameters, the rise did not vary in the different systems, it maintained always close to 3.4 Å what equals the Van der Waals distance showing that all bases were coplanar and the pairs perpendicular to the helix axis. The roll, tilt and twist are correlated between each other, and it can be observed that there are significant differences in urea that increased their value, and minor differences in low hydrated DESs that decreased slightly their value. In case of slide and shift, no differences can be detected due to the huge variation of these values along the 10-nanosecond trajectory (Figure S4.6).

A more in-depth study of the influence of each solvent on these parameters would be of great interest, but is unfortunately outside the scope of this work. In any case, the parameters obtained show an interesting fact, which is that although the double helix denatures in both urea and deep eutectic solvents, the structural changes that lead to the separation between the strands seem to have different pathways.

4.3 Conclusions

Using *ab initio* methods and molecular dynamics it was possible to study the solvation of DNA in mixed solvents. Using the DFT methods it was possible to compare qualitatively the affinities of different media components towards DNA bases and phosphate backbone. It was also possible to observe the different interactions mechanisms. However, molecular dynamics calculations were much more valuable, as they permitted the comparison between the *in silico* results and those found experimentally in Chapter 3. Moreover, these simulations gave interesting information about different events observed in the previous chapter.

On the one hand, it has been possible to confirm that the presence of choline displaces metal cations from DNA. Interestingly, it has also been shown that at low hydration levels, these cations can be "trapped" by the solvent and their mobility is drastically reduced. The diffusion of water was also reduced and as well as the overall interactions formed by each water molecule, what would be related with the already reported decrease in water activity. On the other hand, it was also found that choline cation binds specifically to DNA, as demonstrated analyzing the H-bond interactions. This is in line with previously published results that use another type of demonstrations and is in line also with the melting studies of previous chapter, where ILs and DESs destabilized specifically the GC-rich duplexes.

Another observation in the previous chapter was that the reline DES destabilized DNA less than urea. By analyzing the water and urea molecules close to DNA in molecular dynamics simulations, it has been possible to see that in the presence of choline, urea interacts less with DNA, especially in the major groove. On the other hand, it was observed that the media

surrounding DNA has an “onion” structure, more pronounced for the distribution of choline chloride than water molecules. For the latter, the density of water was especially high within 2 Å of DNA.

Regarding the conformational stability of DNA, it was not possible to compare the results with those found using circular dichroism due to the short simulation time, but it was interesting that DESs decrease the RMSD of the double helix, contrary to urea. It was also observed that in presence of choline there were significant changes in the structural parameters of the double helix, especially in the width of the minor groove.

In resume, in a relative fast and cost-effective manner, the computational calculations allowed the detection of several key points that can explain the experimental results. However, it is necessary to check with experimental techniques that these events really happen. Further studies comparing experimental and computational results will allow us to conclude how well the simulations can predict and evaluate DNA solvation.

4.4 References

1. Oprzeska-Zingrebe, E. A. & Smiatek, J. Aqueous ionic liquids in comparison with standard co-solutes: Differences and common principles in their interaction with protein and DNA structures. *Biophys. Rev.* **10**, 809–824 (2018).

2. Dhahi, T. S., Adam, T. & Hashim, U. Interactive model for DNA specificity and selectivity and biosensor validation. *IOP Conf. Ser. Mater. Sci. Eng.* **917**, 012039 (2020).

3. Jeddi, I. & Saiz, L. Three-dimensional modeling of single stranded DNA hairpins for aptamer-based biosensors. *Sci. Rep.* **7**, 1–13 (2017).

4. Maffeo, C., Carr, R. & Aksimentiev, A. Introduction to MD simulation of DNA–protein systems. *Bionano.Physics.Illinois.Edu*

5. Bedrov, D. *et al.* Molecular Dynamics Simulations of Ionic Liquids and Electrolytes Using Polarizable Force Fields. *Chem. Rev.* **119**, 7940–7995 (2019).

6. Singh, A. P., Gardas, R. L. & Senapati, S. *How water manifests the structural regimes in ionic liquids*. *Soft Matter* **13**, (2017).

7. Perkins, S. L., Painter, P. & Colina, C. M. Experimental and Computational Studies of Choline Chloride-Based Deep Eutectic Solvents. *J. Chem. Eng. Data* **59**, 3652–3662 (2014).

8. Ferreira, E. S. C., Voroshylova, I. V., Pereira, C. M. & D. S. Cordeiro, M. N. Improved Force Field Model for the Deep Eutectic Solvent Ethaline: Reliable Physicochemical Properties. *J. Phys. Chem. B* acs.jpcb.6b07233 (2016). doi:10.1021/acs.jpcb.6b07233

9. Faraone, A. *et al.* Glycerol Hydrogen-Bonding Network Dominates Structure and Collective Dynamics in a Deep Eutectic Solvent. (2018). doi:10.1021/acs.jpcb.7b11224

10. Khan, I. *et al.* Assessing the activity coefficients of water in cholinium-based ionic liquids: Experimental measurements and COSMO-RS modeling. *Fluid Phase Equilib.* **361**, 16–22 (2014).

11. Hayes, R., Warr, G. G. & Atkin, R. Structure and Nanostructure in Ionic Liquids. *Chem. Rev.* **115**, 6357–6426 (2015).

12. Benedetto, A. & Ballone, P. Room Temperature Ionic Liquids Meet Biomolecules: A Microscopic View of Structure and Dynamics. *ACS Sustain. Chem. Eng.* **4**, 392–412 (2016).

13. Jumbri, K., Abdul Rahman, M. B., Abdulmalek, E., Ahmad, H. & Micaelo, N. M. An insight into structure and stability of DNA in ionic liquids from molecular dynamics simulation and experimental studies. *Phys. Chem. Chem. Phys.* **16**, 14036–46 (2014).

14. Garai, A., Ghoshdastidar, D., Senapati, S. & Maiti, P. K. Ionic liquids make DNA rigid. *J.*

Chem. Phys. **149**, (2018).

15. Sahoo, D. K., Jena, S., Dutta, J., Chakrabarty, S. & Biswal, H. S. Critical Assessment of the Interaction between DNA and Choline Amino Acid Ionic Liquids: Evidences of Multimodal Binding and Stability Enhancement. *ACS Cent. Sci.* acscentsci.8b00601 (2018). doi:10.1021/acscentsci.8b00601

16. Jumbri, K., Kassim, M. A. & Yunus, N. M. Fluorescence and Molecular Simulation Studies on the Interaction between Imidazolium-Based Ionic Liquids and Calf Thymus DNA.

17. Portella, G., Germann, M. W., Hud, N. V. & Orozco, M. MD and NMR analyses of choline and TMA binding to duplex DNA: On the origins of aberrant sequence-dependent stability by alkyl cations in aqueous and water-free solvents. *J. Am. Chem. Soc.* **136**, 3075–3086 (2014).

18. Tateishi-Karimata, H. & Sugimoto, N. Biological and nanotechnological applications using interactions between ionic liquids and nucleic acids. *Biophys. Rev.* **10**, 931–940 (2018).

19. Pabbathi, A. & Samanta, A. Spectroscopic and Molecular Docking Study of the Interaction of DNA with a Morpholinium Ionic Liquid. *J. Phys. Chem. B* **119**, 11099–11105 (2015).

20. Meng, Z., Kubar, T., Mu, Y. & Shao, F. A Molecular Dynamics-Quantum Mechanics Theoretical Study of DNA-Mediated Charge Transport in Hydrated Ionic Liquids. *J. Chem. Theory Comput.* **14**, 2733–2742 (2018).

21. Jumbri, K., Ahmad, H., Abdulmalek, E. & Abdul Rahman, M. B. Binding energy and biophysical properties of ionic liquid-DNA complex: Understanding the role of hydrophobic interactions. *J. Mol. Liq.* **223**, 1197–1203 (2016).

22. Nakano, M., Tateishi-Karimata, H., Tanaka, S. & Sugimoto, N. Choline ion interactions with DNA atoms explain unique stabilization of A-T base pairs in DNA duplexes: A microscopic view. *J. Phys. Chem. B* **118**, 379–389 (2014).

23. Gonfa, G., Muhammad, N. & Azmi Bustam, M. Probing the interactions between DNA nucleotides and biocompatible liquids: COSMO-RS and molecular simulation study. *Sep. Purif. Technol.* **196**, 237–243 (2018).

24. Baz, J., Held, C., Pleiss, J. & Hansen, N. Thermophysical properties of glyceline–water mixtures investigated by molecular modelling. *Phys. Chem. Chem. Phys.* **21**, 6467–6476 (2019).

25. Sapir, L. & Harries, D. Restructuring a Deep Eutectic Solvent by Water: The Nanostructure of Hydrated Choline Chloride/Urea. *J. Chem. Theory Comput.* **16**, 3335–3342 (2020).

26. Monhemi, H., Housaindokht, M. R., Moosavi-Movahedi, A. A. & Bozorgmehr, M. R. How a protein can remain stable in a solvent with high content of urea: insights from molecular dynamics simulation of Candida antarctica lipase B in urea : choline chloride

deep eutectic solvent. *Phys. Chem. Chem. Phys.* **16**, 14882–93 (2014).

27. Tateishi-Karimata, H. & Sugimoto, N. A-T base pairs are more stable than G-C base pairs in a hydrated ionic liquid. *Angew. Chemie - Int. Ed.* **51**, 1416–1419 (2012).

28. Nielsen, O. F., Bilde, M. & Frosch, M. Water Activity. *Spectrosc. An Int. J.* **27**, 565–569 (2012).

29. Blanchet, C., Pasi, M., Zakrzewska, K. & Lavery, R. CURVES+ web server for analyzing and visualizing the helical, backbone and groove parameters of nucleic acid structures. *Nucleic Acids Res.* **39**, W68–W73 (2011).

4.5 Supplementary information

Table S4.1. Absolute energies (Hartree) of the different optimizations.

	Sum of electronic and thermal Enthalpies	Sum of electronic and thermal Free Energies
Adenine	-467,167133	-467,206155
Guanine	-542,408724	-542,450822
Cytosine	-394,809383	-394,847814
Thymine	-453,983811	-454,024905
Phosphate backbone	-1482,468004	-1482,536479
Water	-76,403625	-76,425701
Sodium	-162,207239	-162,224028
Choline	-328,499234	-328,540928
Chloride	-460,377752	-460,395135
Lactate	-343,051314	-343,088321
Dihydrogenphosphate	-643,667977	-643,703165
Ethylene glycol	-230,144048	-230,178842
Glycerol	-344,641404	-344,680379
Urea	-225,198731	-225,229096
Sodium chloride	-622,594086	-622,62099
Choline chloride	-788,880968	-788,931052
Choline lactate	-671,556246	-671,623207
Choline dihydrogenphosphate	-972,178973	-972,238856
CC/EG (1:3)	-1479,338638	-1479,44311
CC/Gly (1:2)	-1478,179246	-1478,274979
CC/Urea (1:2)	-1239,294804	-1239,375729

Figure S4.1. Geometries obtained optimizing solvent compounds and DNA bases.

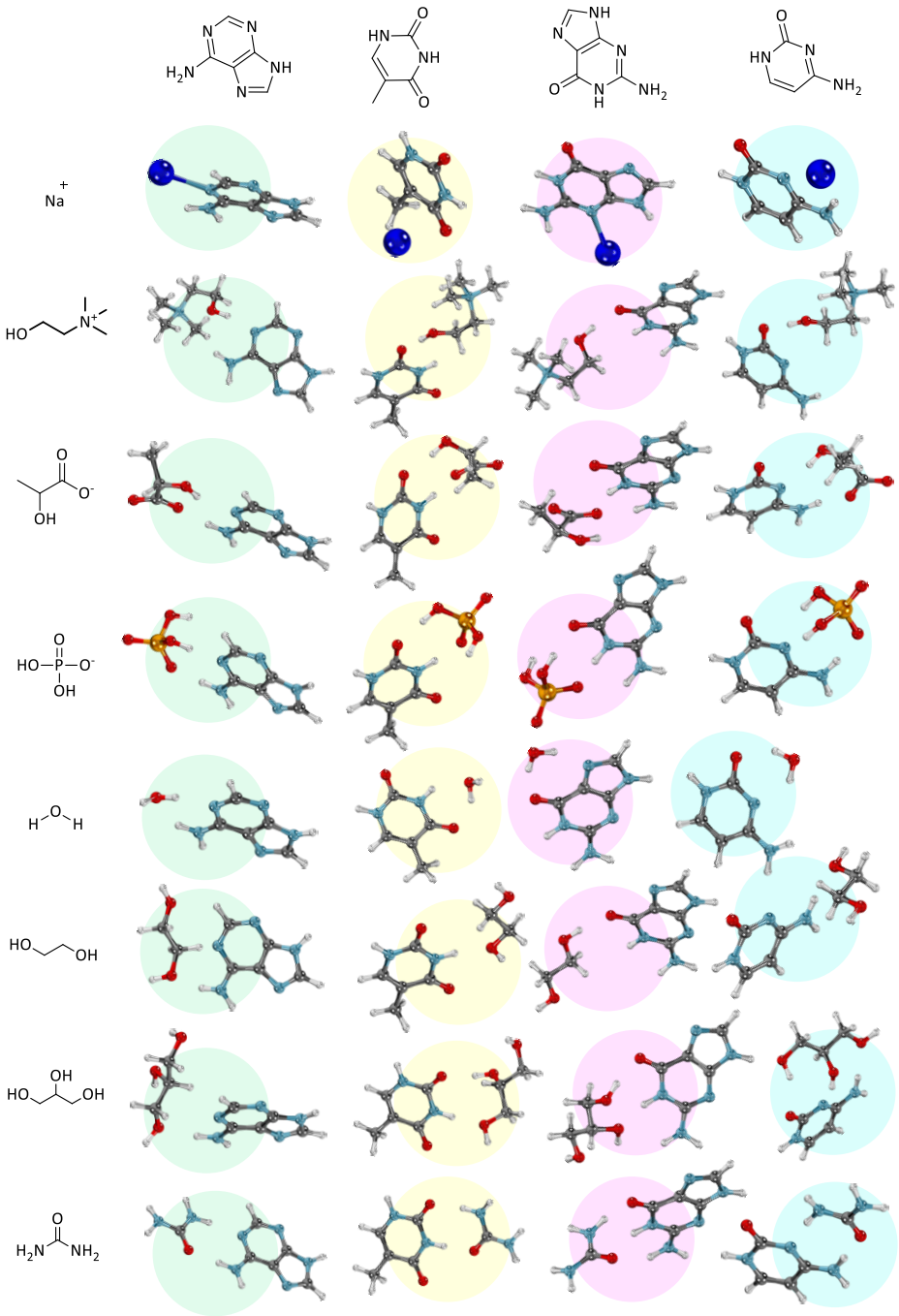

Figure S4.2. Geometries obtained optimizing solvent compounds and phosphate backbone.

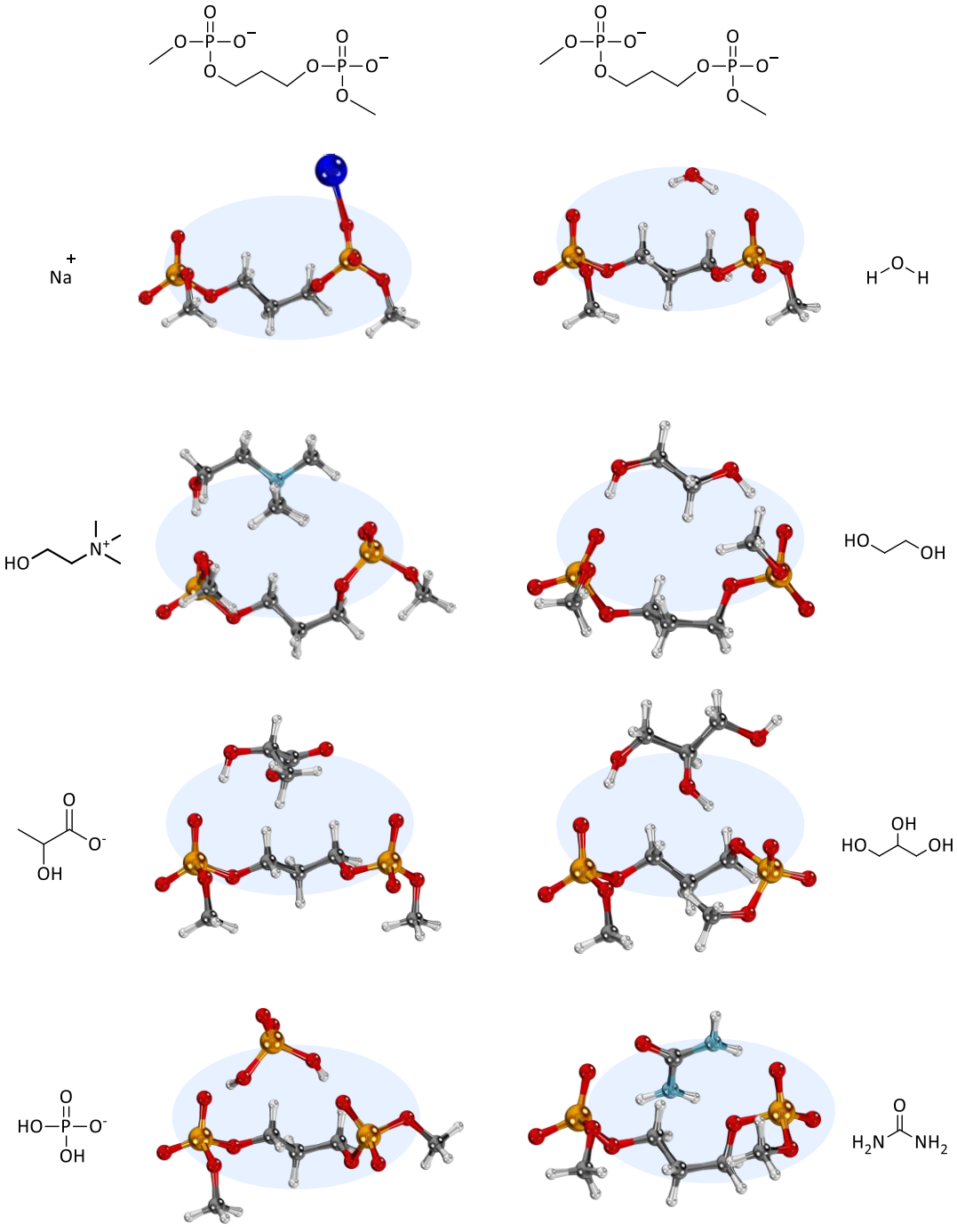

Table S4.2. The number of ethylene glycol or glycerol molecules within 3.5 Å of DNA and the number of H-Bonds donned by these molecules to different DNA sites. In hydrogen bonding analysis, the ending nucleotides were not considered.

Medium		**Ethylene glycol molecules**	**Number of H-Bonds donned**		
		Within 3.5 Å	Maj. G.	Min. G.	Backbone
EG	1.74 M	30.1 ± 5.7	0.5 ± 0.7	0.2 ± 0.4	7.2 ± 2.7
	6.96 M	76.4 ± 4.8	1.1 ± 1.0	0.8 ± 0.9	26.6 ± 4.9
Ethaline	0.87 M	32.7 ± 4.0	0.3 ± 0.6	0.2 ± 0.4	8.7 ± 3.3
	3.48 M	80.0 ± 2.9	1.8 ± 0.9	1.0 ± 0.9	30.3 ± 3.9
Medium		**Glycerol molecules**	**Number of H-Bonds donned**		
		Within 3.5 Å	Maj. G.	Min. G.	Backbone
Glycerol	1.74 M	35.4 ± 4.3	1.1 ± 1.1	0.3 ± 0.6	13.2 ± 3.9
	6.96 M	83.7 ± 6.0	2.3 ± 1.3	0.7 ± 0.8	35.3 ± 5.9
Glyceline	0.87 M	33.6 ± 4.3	0.9 ± 0.9	0.1 ± 0.4	13.1 ± 3.5
	3.48 M	73.6 ± 1.9	2.1 ± 1.0	1.0 ± 0.7	38.2 ± 2.7

Table S4.3. The number of water molecules within 3.5 Å of DNA and the number of H-Bonds donned and accepted between water, the selected molecules of the major groove of DNA and the relationship between these two values.

Medium		**Nº of H-Bonds between water and DNA**	**Nº of water**	**Division**
		Maj. G. as donor and acceptor	Within 3.5 Å of DNA	Nº of H-Bonds between water and DNA / Nº of water
TBS	-	17.5 ± 2.7	418.1 ± 10.7	0.042
CC	0.44 M	16.1 ± 2.6	382.5 ± 13.8	0.042
	0.87 M	14.9 ± 2.6	354.2 ± 8.6	0.042
	1.31 M	13.8 ± 2.7	332.8 ± 11.0	0.041
	1.74 M	13.1 ± 2.6	310.1 ± 10.5	0.042
	2.61 M	11.9 ± 2.5	266.2 ± 12.0	0.045
	3.48 M	11.0 ± 2.3	230.5 ± 11.5	0.048
EG	1.74 M	15.1 ± 2.9	359.2 ± 11.5	0.042
	10.44 M	11.3 ± 2.7	181.7 ± 9.6	0.062
Ethaline	0.87 M	14.4 ± 2.7	294.2 ± 12.0	0.048
	2.18 M	9.2 ± 2.5	155.0 ± 10.0	0.059
	3.48 M	3.8 ± 1.6	66.5 ± 4.3	0.058
Glycerol	1.74 M	14.7 ± 2.8	338.7 ± 13.4	0.043
	6.96 M	11.0 ± 2.6	215.3 ± 16.1	0.051
Glyceline	0.87 M	12.7 ± 2.6	283.9 ± 13.0	0.044
	3.48 M	0.7 ± 0.5	19.0 ± 1.6	0.039
Urea	1.74 M	15.8 ± 3.0	374.5 ± 13.5	0.042
	6.96 M	11.7 ± 2.5	260.0 ± 15.3	0.043
Reline	0.87 M	12.2 ± 2.9	303.7 ± 13.6	0.040
	3.48 M	7.4 ± 1.5	89 ± 6.9	0.084

Figure S4.3. RDF curves of choline, sodium and chloride from (A) Oligo1, (B) Oligo2 and (C) the dsDNA formed between Oligo1 and Oligo2. The RDF analysis were done for different mixtures containing choline chloride at 0, 0.44, 0.87, 1.31, 1.74, 2.18, 2.61 and 3.4 M (from light to darker colors).

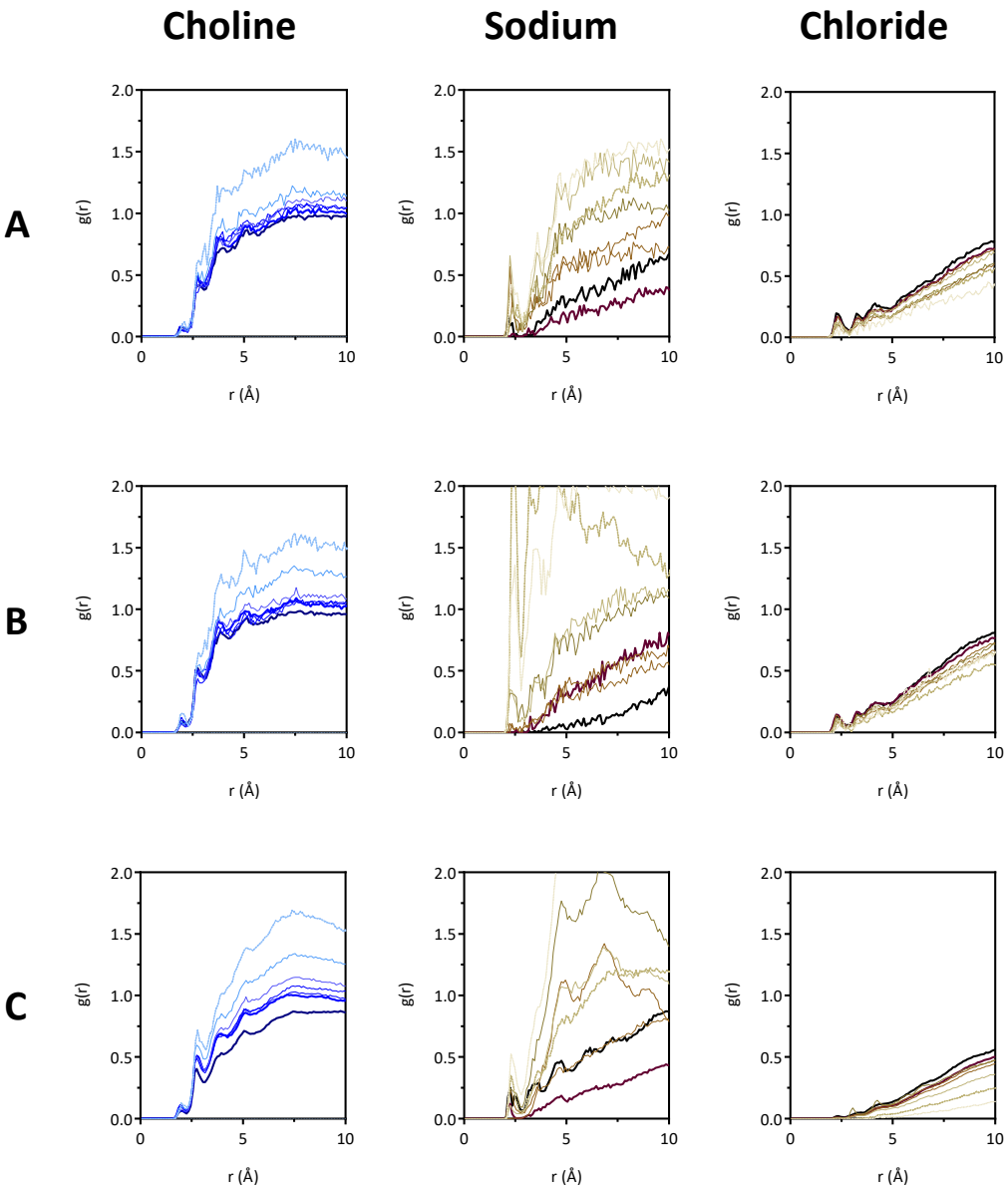

Figure S4.4. Number of hydrogen bonds detected per water molecule at different molar fractions. H-bonds formed between (A) water molecules (B) non-water molecules with water as donor and (C) non-water molecules with water as acceptor.

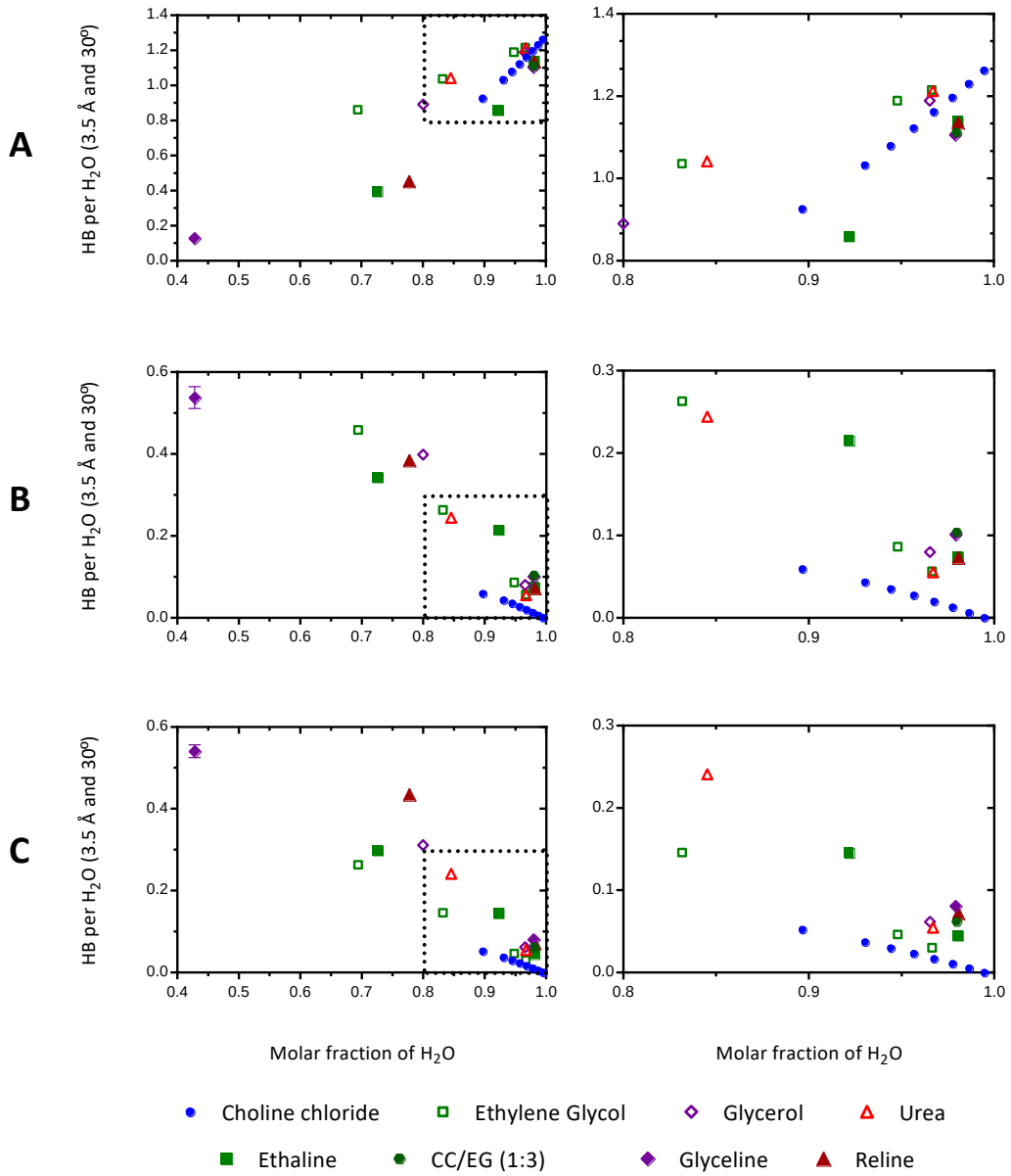

Figure S4.5. Mean values and standard deviation obtained for different structural parameters of DNA. The concentration of each mixed solvent increases from left to right.

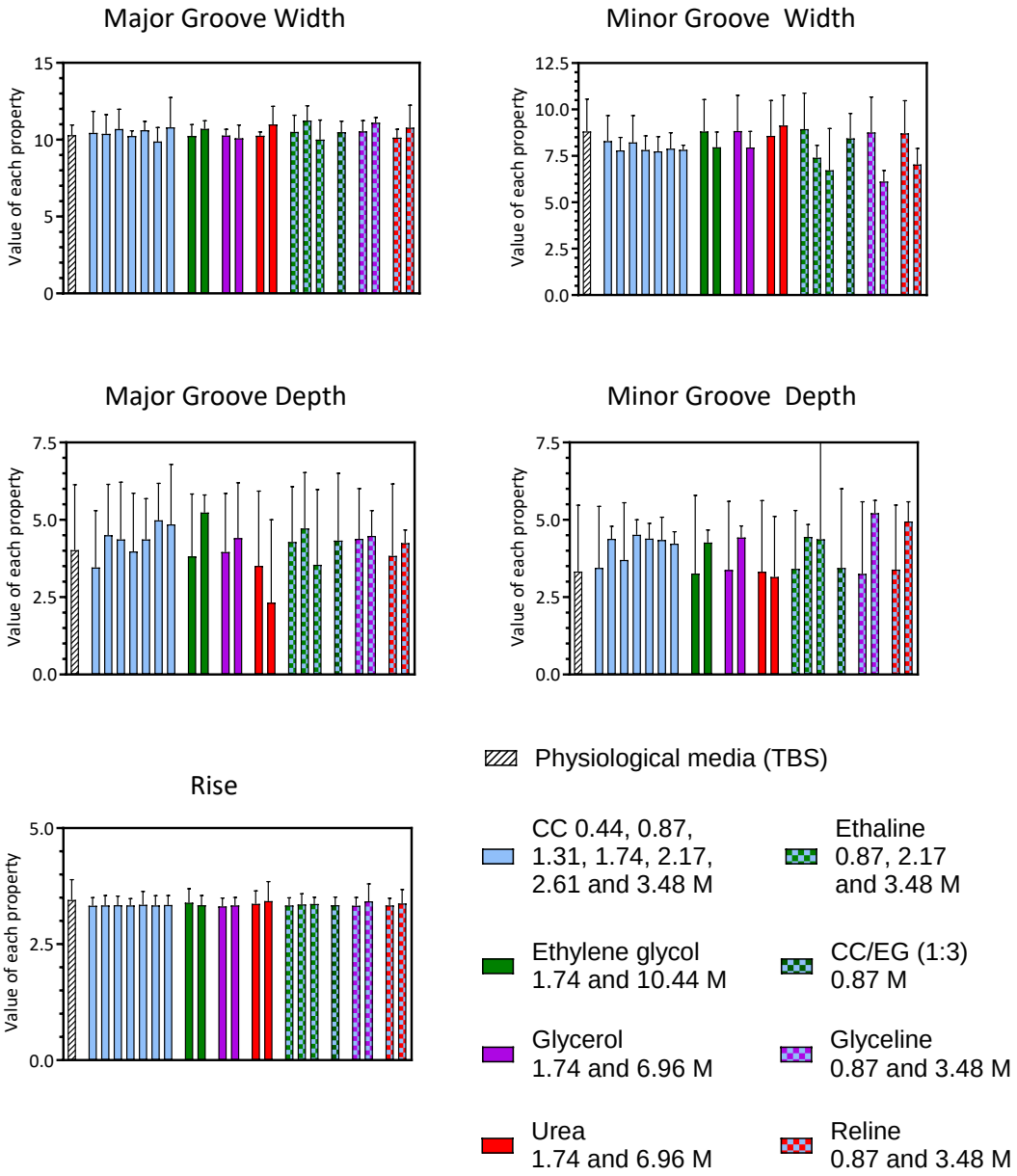

Figure S4.6. Mean values and standard deviation obtained for different structural parameters of DNA. The concentration of each mixed solvent increases from left to right.

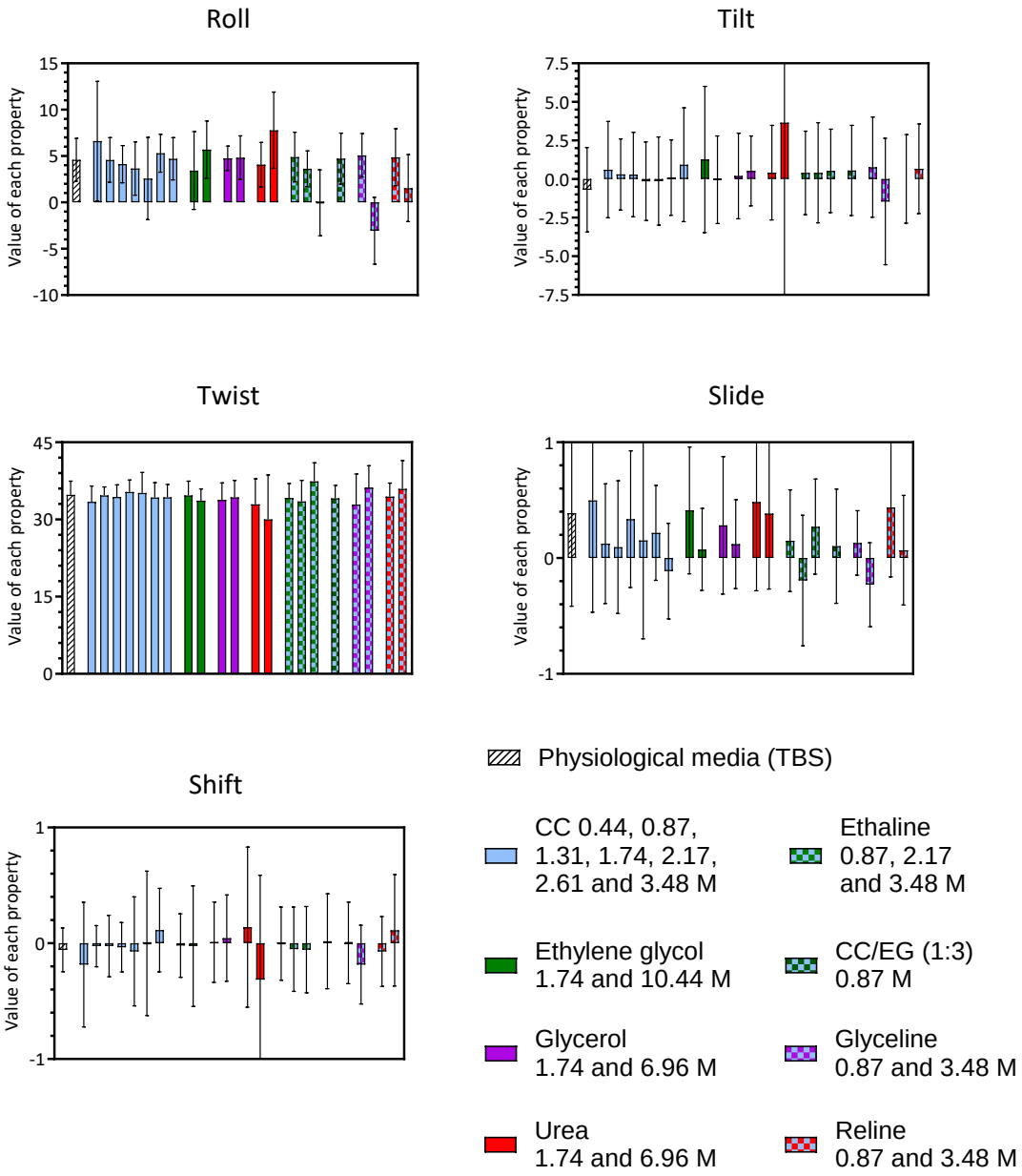

CHAPTER 5

Long-term use and function of DNA in deep eutectic solvents

5.1 Introduction

DNA-aptamers and DNAzymes usually have their best efficiency in selection conditions. But sometimes, even if there is a loss in sensitivity, the benefits may far outweigh the negatives. The solvation of DNA-aptamers or other nanostructures in ionic liquid o deep eutectic solvent present new opportunities, in example they could be in a liquid state in wide temperature ranges, support high vacuum conditions, acquire new kinetics and thermodynamics and they could be used for an extended period before degradation. This permitted the development of different applications as can be seen in Chapter 1. Moreover, it is possible to dilute a huge variety of molecular targets in them what lead to the very recent creation of the first gluten aptasensor in ethaline DES[1].

Most fundamental studies about DNA in non-physiological media are focused in understanding the thermal and structural stabilities, but the dynamic behaviour of DNA is not being studied even if it is of upmost importance. In example, DNA-aptamers make the recognition event upon a change in their secondary structure and forming specific interactions with their targets. Therefore, both, the static and the dynamic properties of DNA are necessary. The ATP DNA-aptamer[2,3] is a good proof-of-concept functional DNA because it recognizes the adenosine-based molecular targets using a hairpin loop based on a double helix and a guanine-rich binding pocket, two of the most common motifs present in functional DNA[4].

The ATP DNA-aptamer was originally selected in Tris-buffered Saline (TBS) aqueous solution (pH 7.4)[5,6]. There are no reports about the function of the native DNA in non-aqueous media, but recently, a chemically modified version of this aptamer has been characterized in an

ionic liquid. This modified structure contains a linker, a fluorophore and a quencher giving rise to the functional structure known as molecular beacon[7] that allows the monitoring of the recognition event by fluorescence methods[8]. In this work, the ATP DNA-molecular beacon was in a series of deep eutectic solvents and the original ATP DNA-aptamer was also studied beyond physiological media.

In this manner, it has been possible to understand the implications of using DNA-aptamer, based-on hairpin structures, beyond its selection media. Moreover, the structure of the aptamer has been monitored for several years at room temperature, from diluted to almost anhydrous conditions. This showed that molecular solvents and deep eutectic solvents can prevent the degradation of DNA.

5.2 Results and Discussion

5.2.1 Long-term secondary structure of the ATP DNA-aptamer

The ATP DNA-aptamer and molecular beacon (Table S5.1) adapt a hairpin structure with a double helix slightly shorter than that studied in the previous chapter. Therefore, the use of non-conventional media might affect greatly to its conformation and thermal stability. Before doing recognition assays, circular dichroism studies were done to understand how each environment could affect the conformation of the hairpin-loop and on the other hand, evaluate the long-term usability of the aptamer in non-physiological media.

New media replaced the original selection molecules (water, buffer and salts) systematically by HBA or HBD groups and DES molecules as in Chapters 3 and 4. The spectra of duplexes measured in Chapter 3 were used as comparison In order to understand if the differences were due to changes in the duplex structure or G-rich binding pocket. In the original selection media (TBS), the spectrum of the aptamer showed a maximum at 262 nm that had greater intensity than the minimum at 240 nm.

The difference between the aptamer and the duplex, which has similar intensities in negative and positive peaks, is due to the G-rich sites of the aptamer that increase the intensity of the positive band[9]. In presence of choline chloride, at low concentrations (0.9 M), the spectrum was equal to that found in physiological media, but there was a significant increase in the positive peak of the aptamer at the highest concentration (3.4 M; 45 wt. %) (Figure 5.1). A not depreciable positive band at 300 nm could indicate the formation of a completely new

secondary structure not found in physiological media. Comparing with the duplex, the red shift found in the latter at 3.4 M of choline chloride was not found in the aptamer, probably hindered by the ellipticity of the G-rich pocket that seems to be stabilized by choline.

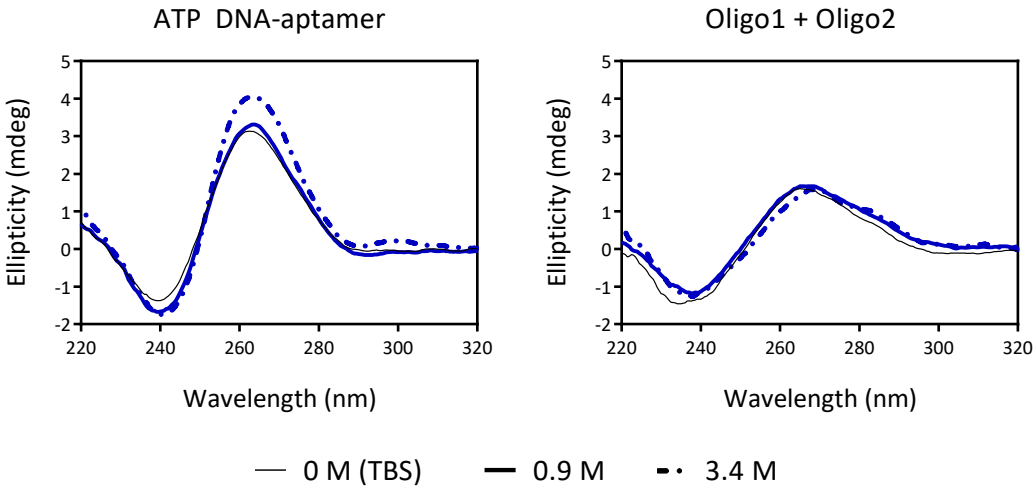

Figure 5.1. Circular dichroism measurements of DNA in presence of different concentrations of choline chloride. All the oligonucleotides were at 5 µM and the temperature was 25 ^{o}C.

Then, the aptamer was solvated in the different HBD groups: ethylene glycol, glycerol and urea (Figure 5.2). The ellipticity of positive peak increased again in presence of ethylene glycol and glycerol above 1.8 M what would surely affect the recognition capacity of the aptamer. In case of urea at low concentrations (1.74 M), the secondary structure of the aptamer did not seem to be altered and contrary to polyols, urea does not promote the formation of the G-quadruplex. At 6.96 M of urea the ellipticity decreased substantially and probably the double helixes were almost denatured as the ellipticity of the negative peak was close to zero.

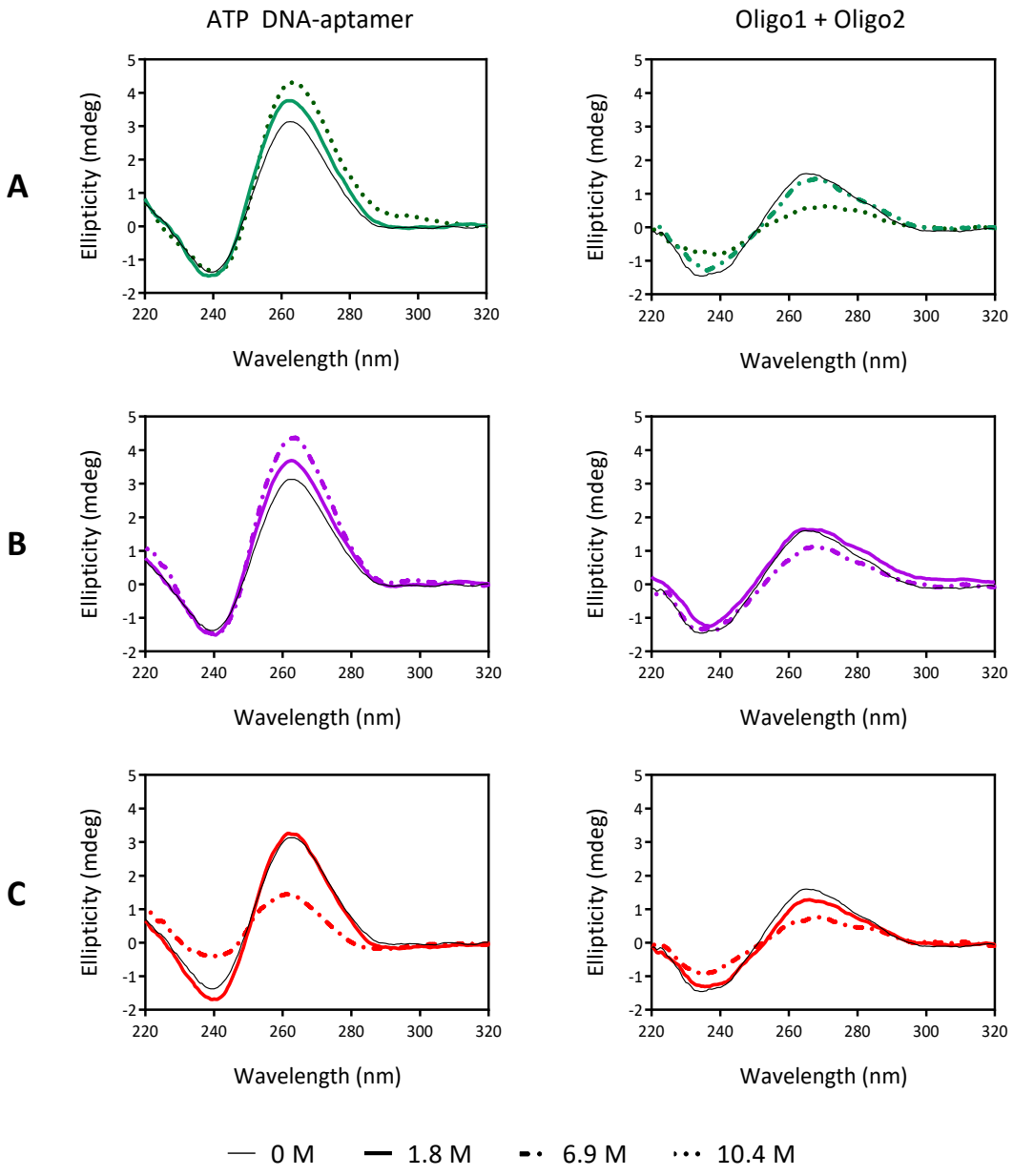

Figure 5.2. Circular dichroism measurements of DNA in presence of different concentrations of (A) ethylene glycol. (B) Glycerol. (C) Urea. All the oligonucleotides were at 5 µM and the temperature was 25 ºC.

Next, the aptamer was solvated in deep eutectic solvents (Figure 5.3). At 0.87 M, the only DES that seemed to alter the aptamer secondary structure was reline. It is curious that in ethylene glycol and glycerol based DESs at 0.87 M, there was no increase in the positive peak ellipticity as happened in equivalent concentrations of ethylene glycol and glycerol, probably because in DES solution, choline was preferentially occupying the positions close to the G-rich pocket. However, at 3.45 M (>85 wt. %), the spectra of the aptamer was altered drastically. At this concentration, it was seen in Chapter 3, that double helixes formed between Oligo1 and Oligo2 were highly denatured and as the hairpin has less base pairs, it could be expected that its double helix would be completely denatured, something that can be observed in the ellipticity of the negative peak that was almost zero. In case of the G-rich pocket, it seems that ethaline, glyceline and reline DESs greatly altered it, or annihilated in case of CC/EG (1:3) (3.42 M; 96 wt. %). In case of ethaline and glyceline, there was a peak at 300 nm, observed also in choline chloride. A spectrum with two positive peaks close to 260 and 300 nm has been reported previously as a G-quadruplex structure[10–12].

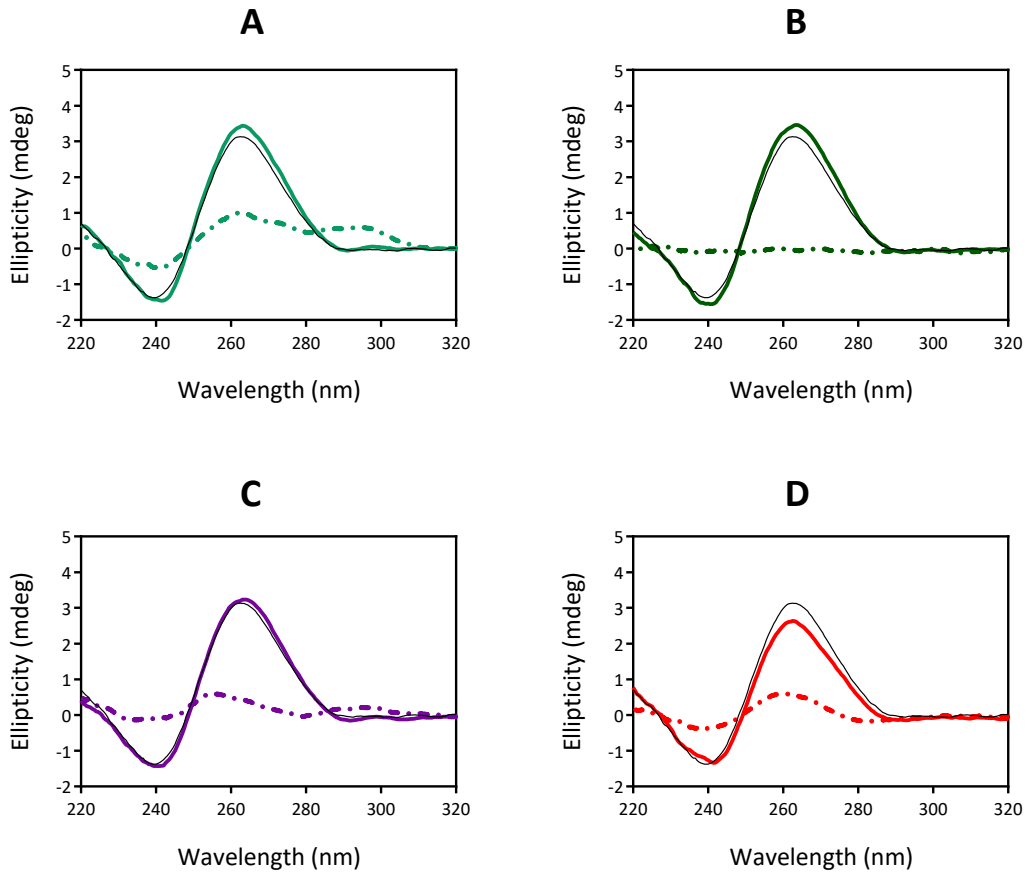

Figure 5.3. Circular Dichroism measurements of ATP DNA-aptamer in presence of different concentrations of (A) ethaline, (B) CC/EG (1:3), (C) glyceline and (D) urea. All the oligonucleotides were at 5 µM and the temperature was 25 ^{o}C.

So far, with circular dichroism technic it was possible to observe the secondary structure of the aptamer in absence of the target. The capacity of the aptamer to recognize the target with high sensitivity would then depend on the free energy change from these static structures to those acquired upon binding. The dissociation constants (K_d) of the aptamer is a good

parameter to know how these new environments would affect the recognition of ATP, AMP or adenosine and the specificity towards these molecules[3]. Circular dichroism can be used to monitor the structural change of the aptamer and calculate the K_d but unfortunately the adenosine targets also absorbs in the UV range and the HT voltage was saturated with a concentration of few hundred micromolar of ATP (Figure 5.4), therefore other methods were used to monitor the recognition event.

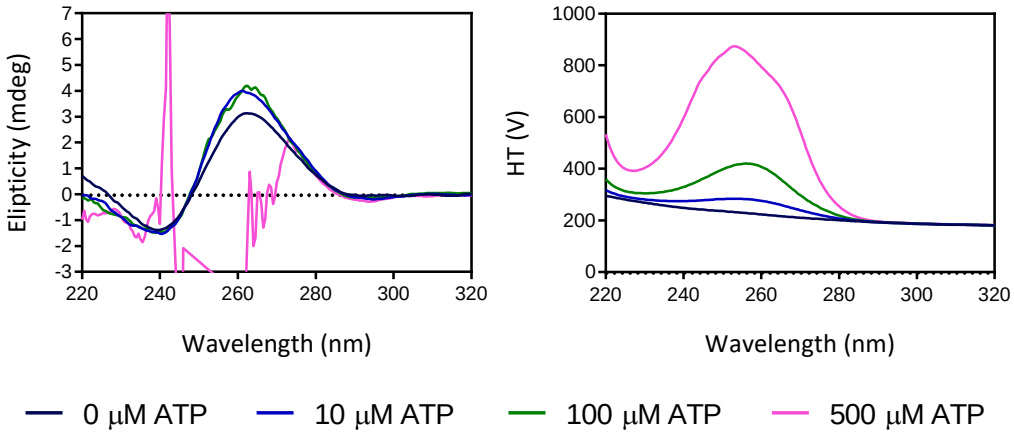

Figure 5.4. CD measurements of the ATP DNA-aptamer in TBS media and in presence of different concentrations of ATP molecule. The DNA concentration was 5 μM.

Despite the impossibility of monitoring the dynamic movements of the aptamer using circular dichroism, it is interesting to measure its secondary structure for long periods. One of the bottlenecks while using nanotechnological DNA designs is the fact that nucleic acids hydrolyse in presence of water. Therefore, reducing the activity of the latter by including inorganic salts or organic molecules is of great interest. In order to study if used DESs and their

individual components could reduce DNA degradation, the samples containing the duplex and the aptamer were stored at RT and characterized after 12 months.

In Figure S5.1-S5.4 are shown the whole spectra acquired at different periods, below are commented the most relevant results. It was found that the reduction of water activity using salts was the best manner to prevent DNA from hydrolysis and maintain at the same time a high hydration level. In example it can be observed in Figure 5.5 that the duplex of the ATP DNA-aptamer degraded after one year at 6.96 M of ethylene glycol but it did not at 0.87 M of choline chloride or CC/EG (1:3) DES. On the other hand, even if TBS media contained 0.14 M of NaCl, this was not enough salt concentration to prevent DNA degradation. The latter was also observed dissolving the duplex formed by Oligo1 and Oligo2 in ultrapure water or TBS media in presence or absence of choline chloride Figure 5.6.

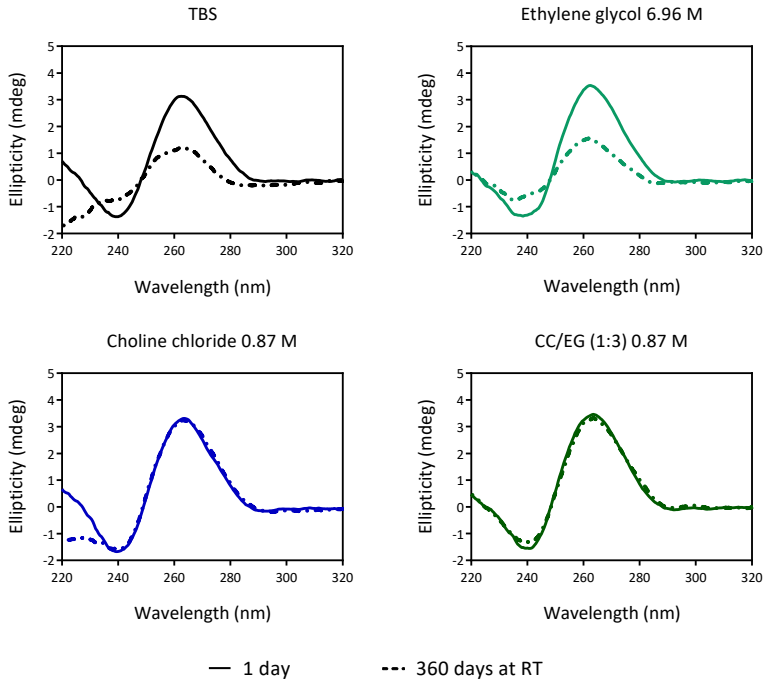

Figure 5.5. CD spectra of the ATP DNA-aptamer (5 µM) in different media and periods. The temperature of the measurement was 25 ^{o}C.

In measurements shown in Figure 5.6 it can be observed that physiological media maintained DNA stable for longer periods than ultra-pure water. In the latter, the duplex was almost lost after 112 days. However, in TBS media the duplex also degraded in less than a year. Only in presence of choline chloride at 0.87 M, it was possible to maintain the integrity of dsDNA at least for 16 months.

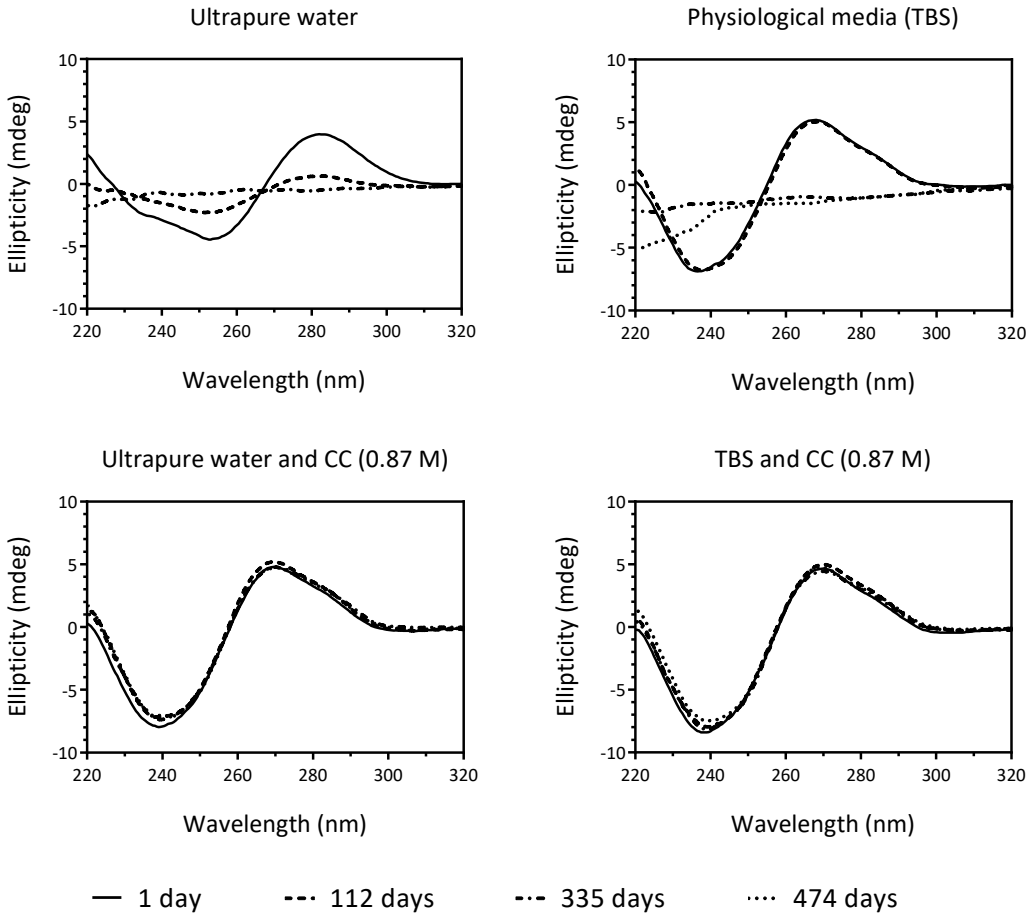

Figure 5.6. CD spectra of the duplex formed between Oligo1 and Oligo2 (5 µM) in different media and periods. In this particular case, the path lenght of the cuvette was 10 mm. The temperature of the measurement was 25 ^{o}C.

With the results obtained so far, it can be observed that 0.9 M of choline chloride were enough to preserve DNA for longer periods than in physiological media. A very positive aspect of these results is that at this concentration of deep eutectic solvents the double helix destabilizes very little thermally and structurally, as observed in Chapter 3. On the other hand, the studies were also conducted at a very low levels of hydration (3.4 M of DES). Interestingly, it was found that the ATP DNA-aptamer suffered significant changes in its secondary structure during the storage period (Figure 5.7). In ethylene glycol and glycerol based DESs, the ATP DNA-aptamer created a G-quadruplex structure that shows a maximum at 260 and 300 nm.

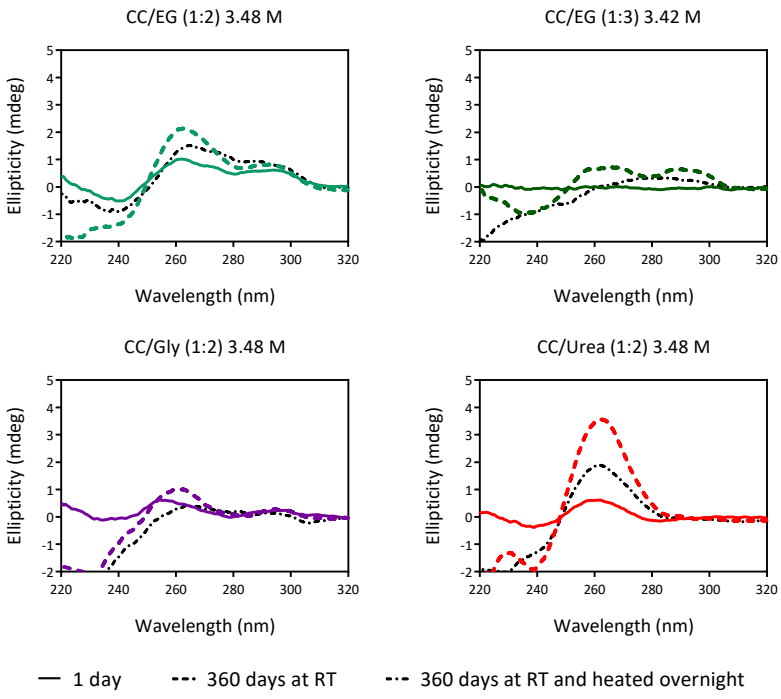

Figure 5.7. CD spectra of the ATP DNA-aptamer (5 μM) in different media and periods. The temperature of the measurement was 25 ^{o}C.

In case of reline DES, the aptamer passed from the denatured state to a secondary structure very similar to that of physiological media (Figure 5.7). Then, the four samples were heated up to 80 ^{o}C overnight in order to know if these structures could be reversible but as can be observed they were partially or totally annihilated and probably would need months to acquire those secondary structures again. The kinetically driven long-term changes did not form new conformations in samples containing Oligo1 and Oligo2 (Figure 5.8), probably because they had shorter sequences and could not found non-canonical stable conformations such as those found in the aptamer and maintained in a denatured state. The only difference was found in ethaline and glyceline samples where the duplex continued melting.

Furthermore, the samples containing Oligo1 and Oligo2 at low hydration levels were stored up to three years without observing degradation of DNA (Figure 5.8), but after 3 years the negative peaks were lost denoting aggregation of DNA or a kind of degradation that needs to be better understood. The loss of this peak was also observed in other samples of Oligo1 and Oligo2 solvated in HBD groups and DESs at lower concentrations (Figure S5.3 and S5.4). This aggregation was not observed in samples stored at -20 ^{o}C or stored at RT and containing choline chloride at 0.87 and 3.48 M.

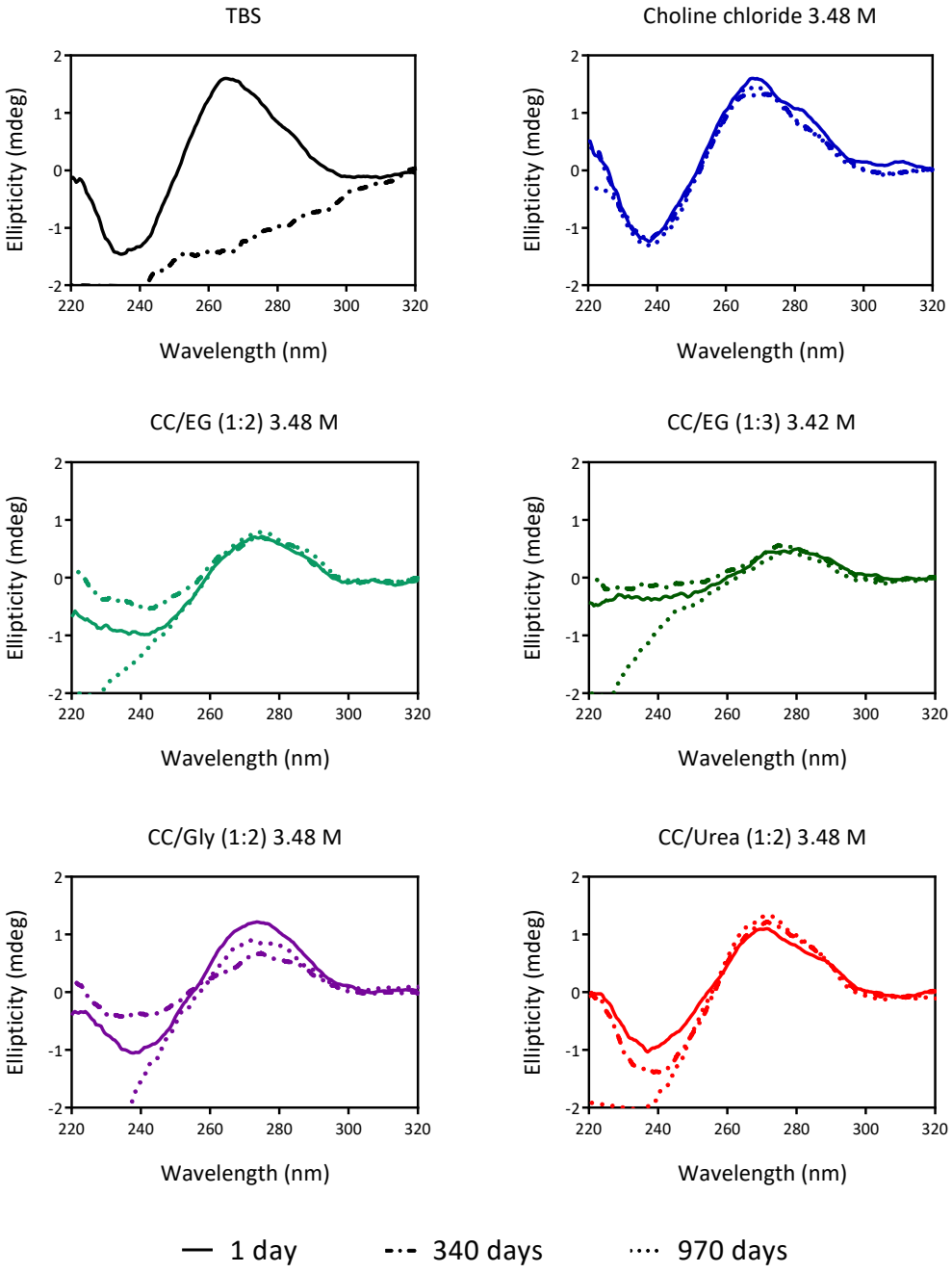

Figure 5.8. CD spectra of (A) the samples containing Oligo1 and Oligo2 (5 µM) in different media and periods. The temperature of the measurement was 25 ^{o}C.

5.2.2 The recognition capacity of the ATP DNA-aptamer

Surface Plasmon Resonance (SPR) is an optical technic able to monitor interactions at the nanoscale, based on changes in the refractive index of the media surrounding the immobilized sample[13]. In this case, the biotin-avidin interaction was used to immobilize the aptamer in the sensor surface, modifying its sequence in its 5' end with a biotinylated triethylenglycol (Table S5.1) (Section 2.5.1). This technic allows the on-line monitoring of the recognition event and the nanoscale accuracy permits to calculate in a precise way the affinity of the aptamer towards its target.

Unfortunately, SPR instruments are designed to be used in physiological conditions and they use great quantities of solvent per assay, in the range of 0.1 to 1 L. This could be a problem if ionic liquids are used as media due to their high cost of production, but in case of deep eutectic solvents, their cost is much lower. To the best of our knowledge, this is the first time that functional DNA is monitored in non-physiological media using surface plasmon resonance, therefore these experiments can serve also as a precedent for future studies of dynamic DNA nanostructures in these media.

Firstly, control experiments were done in physiological media. When ATP or AMP targets were injected in the channel (s 82), there was an increase in the response due to the target molecules that were captured by the aptamer (Figure 5.9A). Then, when the target injection stopped and there was only solvent (s 142), the aptamers released the target again, adopting a more energetically favourable conformation similar to that observed in CD studies. The K_{on} and K_{off} values could not be measured due to the fast kinetics, as has been already reported

previously[14]. The higher the concentration of the target the higher was the response, until a point in which all the aptamers were saturated.

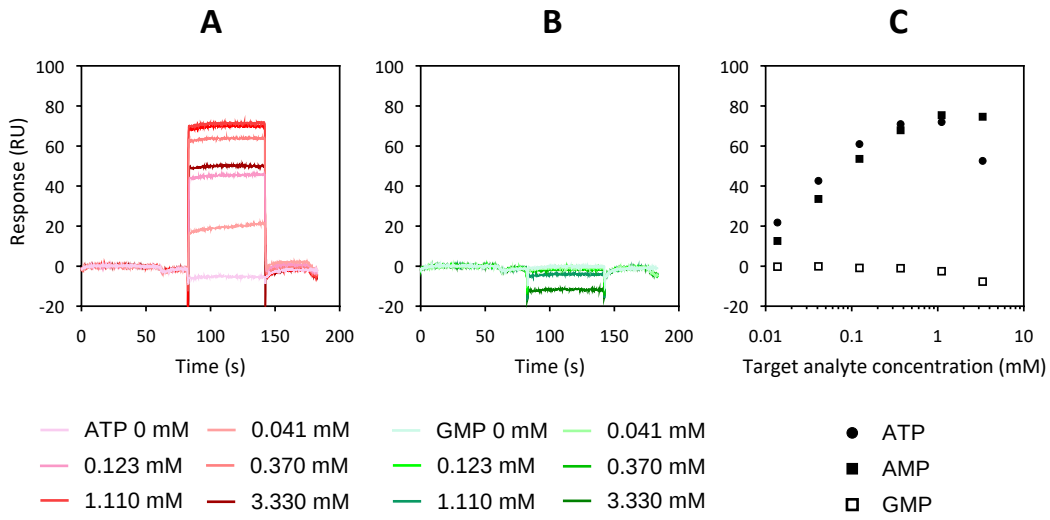

Figure 5.9. Response curves obtained from immobilized the biotinylated ATP DNA-aptamer while injecting (A) ATP or (B) GMP at different concentrations. (C) The response values represented *versus* the concentration of target molecule at 25 ^{o}C. The flux was 25 µL/min.

Above the saturation point, there was no increase in the response or there could be even a decrease because a very high concentration of the targets (>2 mM) decreased the pH and increased the electrostatic repulsions, affecting to the recognition capacity of the aptamer and causing huge changes on the local refractive index. On the other hand, contrary to ATP or AMP, when GMP was injected in the media, there was no increase in the response because the aptamers did not capture the molecule (Figure 5.9B). With the different responses upon target injection at multiple concentrations, it was possible to represent the graph shown in Figure 5.9C and calculate the dissociation constant (K_d) value.

Then, the same procedure was used but replacing the physiological media by deep eutectic solvents and their individual components. All the response values obtained are shown in Figure S5.5A-S5.12A. There is an absence of measurements at very high concentrations of DESs due to issues caused by huge changes in the refractive index. The measurement of the molecular adsorption kinetics in SPR is related with the changes in the local refractive index near the gold layer where the aptamer is immobilized; this at the same time changes the resonance angle and the SPR curve is calculated based-on the fit of the minimum angle. Usually, the angles that the instrument can monitor are limited; therefore, the local refractive index also needs to be in a determined range. In the used equipment, the range of the SPR minimum angle (dip) is between 64 and 76.

Due to the previous limitation, it was not possible to perform measurements at high concentrations because as can be seen in Figure 5.10A, at 2 M of glyceline, reline or CC/EG (1:3), the angular dip shift is already outside the limit. In Figure 5.10B are shown the dissociation constant values obtained in a reliable manner while using ATP as target, and in Table S5.2 are written with their standard deviation.

As shown in Figure 5.10B, already at 0.87 M of DES the recognition capacity of the aptamer decreased substantially. Compared with the original selection media where the K_d towards ATP was 32±2 μM, in glyceline the K_d value was 2.7 times higher (87±9 μM), in CC/EG (1:3) was 6.6 times higher (210±34 μM), in ethaline was 8.1 times higher (258±65 μM) and in reline was 32.8 times higher (1048±280 μM). It is curious that this decrease in sensitivity was not found in HBA or HBD groups at an equivalent concentration and in previous circular

dichroism spectra, DESs did not affect the secondary structure in a significant manner at 0.87 M. Moreover, there are huge differences between the K_d values of ethaline and glyceline DESs, even if solvent properties and interactions with DNA have shown to be similar.

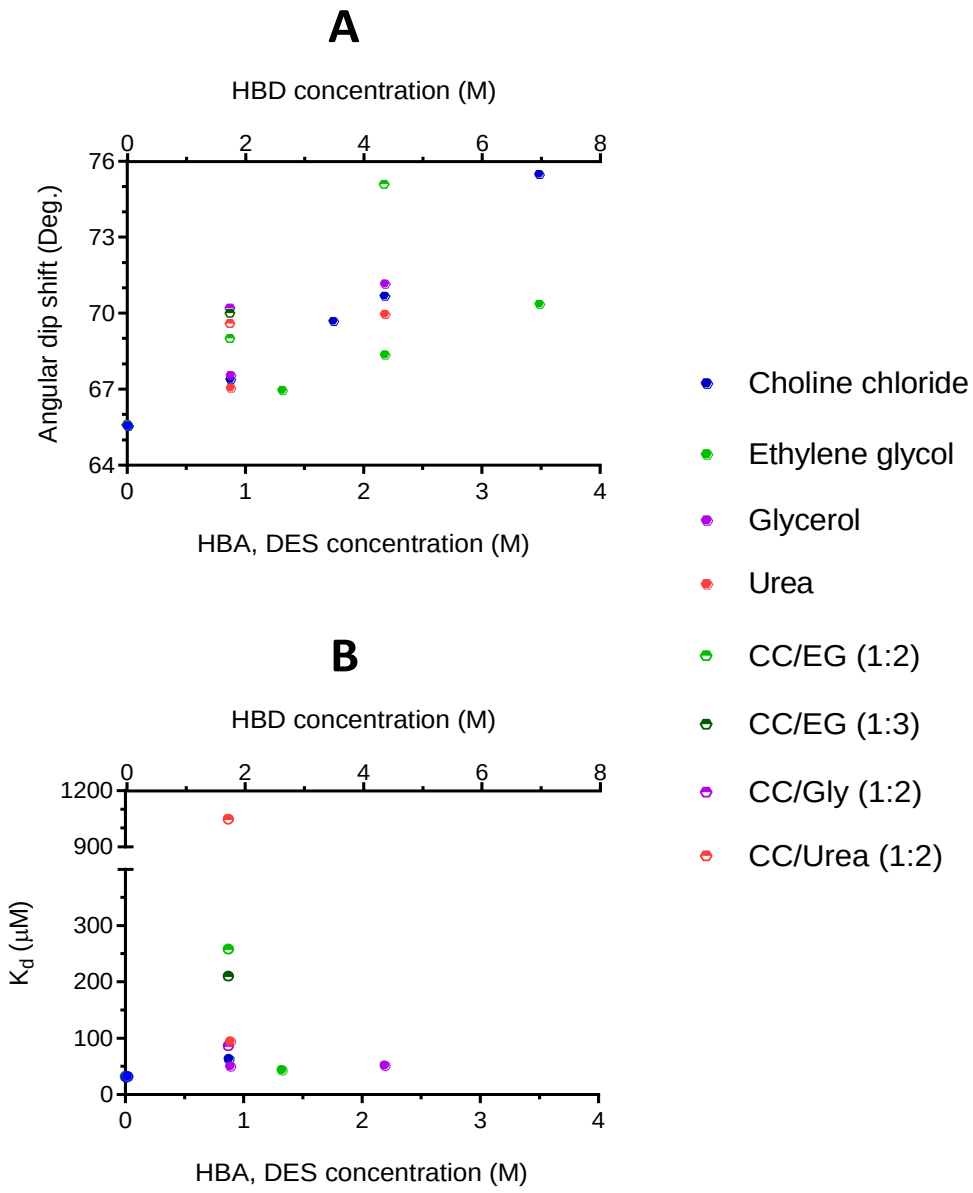

Figure 5.10. (A) The angular dip shift value found in its solution in absence of the target. (B) The dissociation constant values of the biotinylated aptamer towards ATP in different solutions.

Even if the sensitivity decreased substantially, the specificity of the aptamer towards adenosine-based molecules was maintained, recognizing other adenosine-based molecules such as AMP but not GMP. In order to understand better if changes in sensitivity were due to interaction of DESs with the double helix or the G-rich binding pocket, the assays were repeated using a DNA ATP-aptamer with a slightly larger double helix (ending with 8 base pairs instead of 4) (Table S5.1). The whole response values are shown in Figure S5.5B-S5.12B and dissociation constant values can be found in Figure 5.11 or with their standard deviation in Table S5.2.

As can be seen in Figure 5.11, while increasing the hairpin length of the aptamer in DES at 0.87 M, the recognition capacity was much better than that of the original ATP DNA-aptamer, which has a shorter duplex, probably because the longer hairpin favored the stability of the G-rich binding pocket. On the other hand, even if the sensitivity was much better in this second aptamer, it followed the same trend as before, the dissociation constant increased following this trend in all cases: glyceline < CC/EG (1:3) < ethaline << reline.

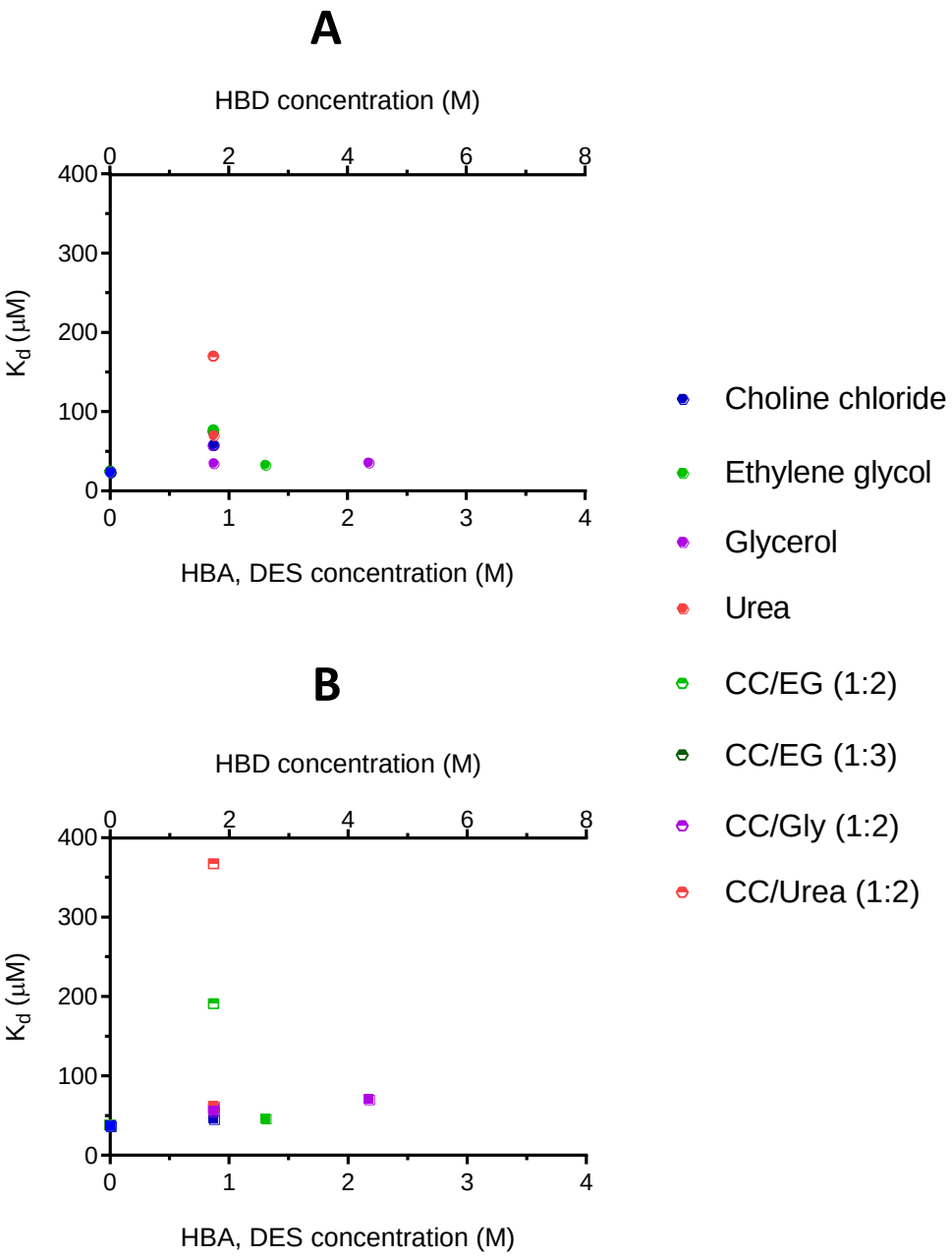

Figure 5.11. The dissociation constant values of the biotinylated aptamer (8 bp) towards (A) ATP and (B) AMP in different solutions.

5.2.3 The recognition capacity of the ATP DNA-molecular beacon

Further studies were done using an alternative technic to SPR and already used in Chapter 3: the steady state fluorescence. With this technic, the changes in refractive index of the media do not suppose and issue and therefore it could be possible to study the function in a wider concentration range. But prior using the aptamer in fluorescence studies, it was necessary to transform it into a molecular beacon[7]. It consists in a hairpin structure with a fluorophore attached to one end and a fluorescence quencher to the other. The proximity of the two ends results in Förster Resonance Energy Transfer (FRET) and hence the fluorescence emission when both ends are at the closest point is very low. Recognizing the target forces the hairpin to open and this event increases the fluorescence.

Contrary to SPR, in binding assays performed with the molecular beacon the concentration of the target was introduced in a summative manner, achieving the equilibrium in each step. As can be seen in the control experiment made in TBS the recognition of the target by molecular beacon was again too fast to measure the K_{on} (Figure 5.12A) and as expected, in case of GMP there was no recognition (Figure 5.12B). The curve used to calculate the dissociation constant is very similar to that obtained by SPR (Figure 5.12C).

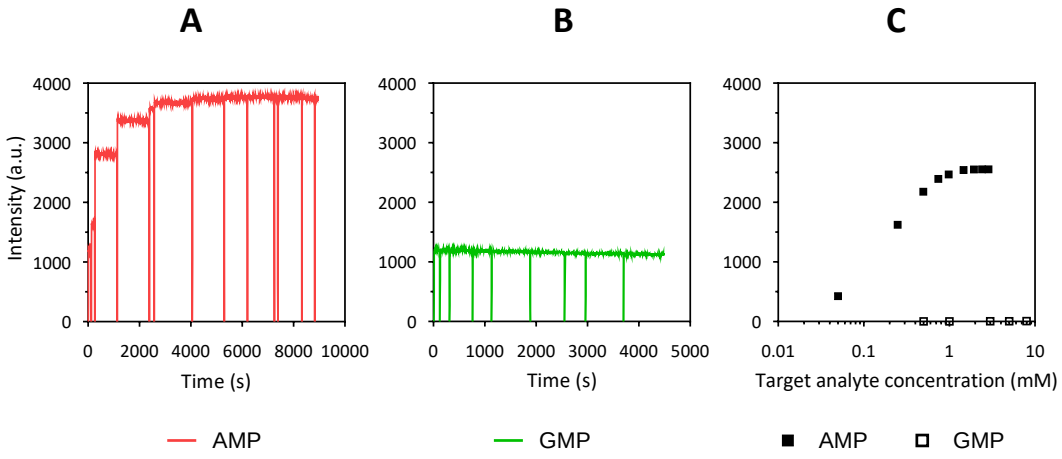

Figure 5.12. Spectra obtained in steady state fluorescence studies while adding increasing concentration (A) ATP or (B) GMP in presence of the ATP DNA-molecular beacon in physiological media at 25 ^{o}C. (C) The intensity values represented *versus* the concentration of target molecule. The DNA concentration was 25 nM.

In Figure 5.13A are represented the K_d values of the molecular beacon towards AMP and they appear with their standard deviation in Table S5.2. In Figure S5.5C-S5.12C are shown the different intensities obtained in each media upon target addition. The intensity in absence of target has been zeroed in order to calculate the K_d values, but it is a good indicator of the conformation of the beacon: it was observed that the initial fluorescence values were higher in non-physiological media at 0.87 M than in physiological media. What indicates that the quencher was already farther from the fluorophore than in pure TBS, probably it was due to the partial denaturation of the double helix. However, a small increase in the initial distance does not affect the accuracy of the measurement, because FRET was maintained even at the saturation point. Unfortunately, above 2.2 M of DES, the FRET was lost before saturation, and it was not possible to calculate the K_d values.

On the other hand, the absolute dissociation constant values obtained were different from those of the aptamer characterized by SPR, but this could be expected due to the modifications that have been made to the aptamer. Fortunately, with this technic, the refractive index of the solutions did not limit the measurements and contrary to SPR, it was possible to calculate the dissociation constant at multiple concentrations of choline chloride. It was seen that the aptamer efficiency decreased at the beginning but then it was maintained with a final increase at 3.47 M of CC (Figure 5.13A), probably due to the formation of the G-quadruplex structure observed in the peak at 300 nm in circular dichroism.

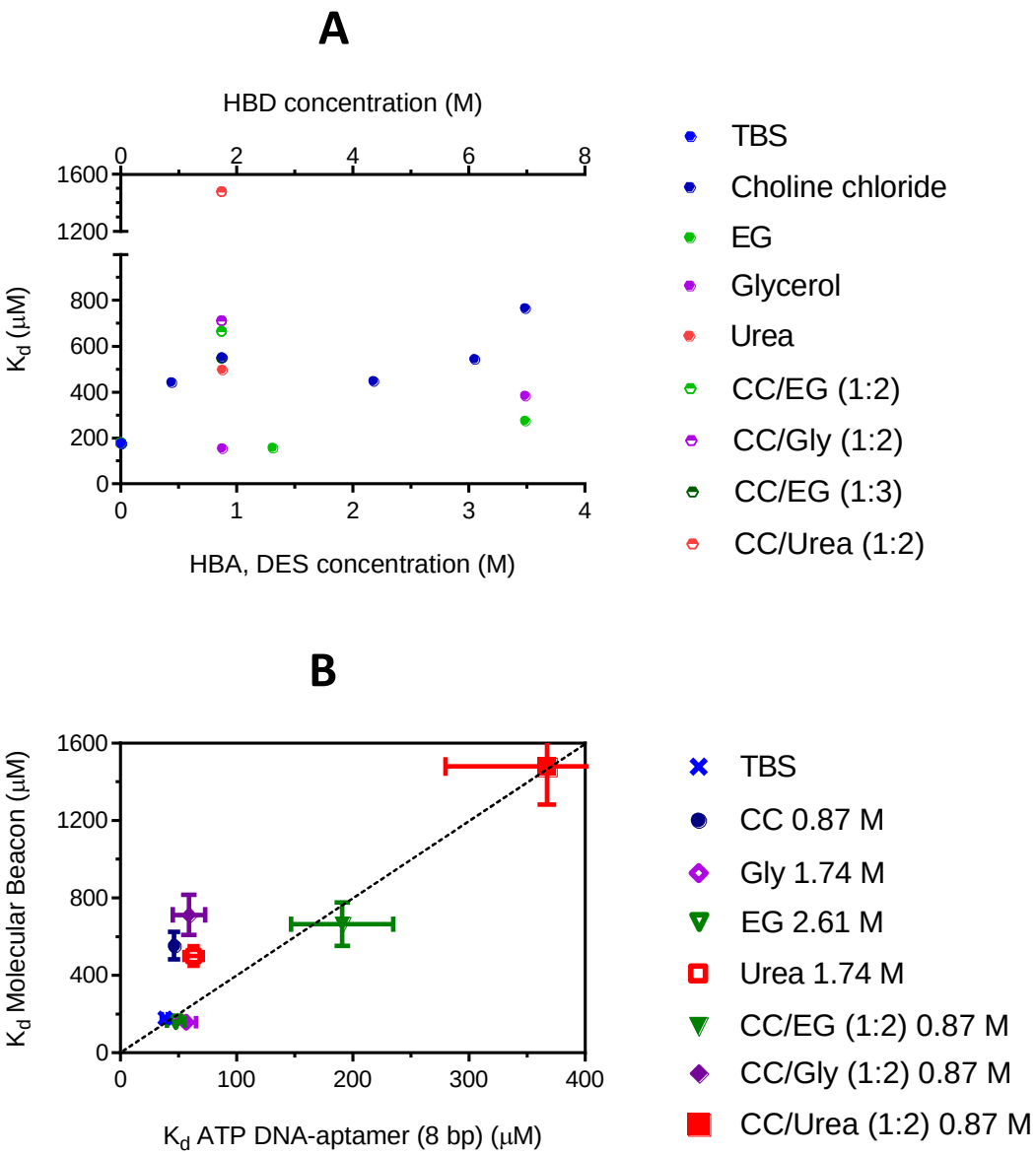

Figure 5.13. (A) The K_d of the ATP DNA-molecular beacon towards AMP. (B) The K_d of the ATP DNA-molecular beacon *versus* those of the biotinylated ATP DNA-aptamer (8 bp) towards AMP at 25 ^{o}C with their corresponding standard deviations.

In case of ethylene glycol and glycerol, it can be seen that they almost do not affect the sensitivity of the molecular beacon even at 6.96 M, where the positive peak of the aptamer increased substantially in CD spectra, related with the higher stability of the G-rich binding pocket. At 10.44 M of ethylene glycol, there were issues to dissolve high concentrations of AMP. On the other hand, urea affected the sensitivity of the aptamer at low concentrations, as found in SPR studies, even if it apparently did not alter the secondary structure of the aptamer at low concentrations according to circular dichroism (Figure 5.3). In case of the deep eutectic solvents, at 0.87 M, they affected the sensitivity more than the HBA and HBD groups, specially reline. At 0.87 M DES concentration, the K_d values of the molecular beacon were approximately at least 4 times higher than those found in SPR for the ATP DNA-aptamer with a large hairpin (Figure 5.13B), showing the huge influence of modifying chemically the aptamer.

As mentioned before, experiments were done also with DESs at a concentration above 2.2 M (≥65 wt. %), this was not possible with SPR technic due to the refractive index of the media. It was found that the fluorescence intensity of the molecular beacon did not increase upon AMP addition (Figure S5.5C-S5.8C). But it could not be stated if the absence of this increase was due to the loss of recognition ability or due to the denaturation of the double helix what would cause the loss of FRET. In order to be able to elucidate if the G-rich binding pocket was still capable of recognizing AMP in this media, the experiments were done at lower temperatures.

The melting temperature of the molecular beacon was calculated to be of 52 ^{o}C in TBS, and considering the destabilization effect on the double helix calculated in the Chapter 3, at 2.2

M concentration of DESs the molecular beacon should still be partially hybridized at 0 ºC. Therefore, if the intensity did not increase at this concentration it would be directly related with the recognition capacity of the G-rich pocket. The affinity studies done at this low temperature are shown in Figure 5.14.

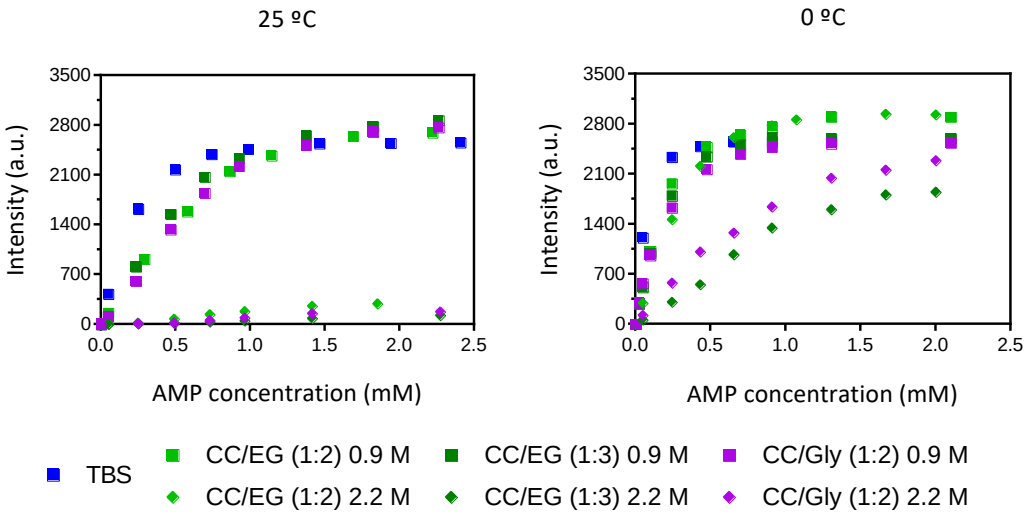

Figure 5.14. The intensity values represented *versus* the concentration of target molecule of the same recognition assays done at 25 or 0 ºC. The DNA concentration was 25 nM.

At zero degrees, the fluorescence intensities in absence of the target (F_0) were already higher than those found in TBS at this temperature (Table 5.1), indicating the partial denaturation of the duplex. However, the fluorophore-quencher pair were still close enough permitting the calculation of K_d values in all cases, this was not possible at 2.2 M of DES at 25 ºC due to the high denatured duplex. In all cases, the sensitivity of the molecular beacon was better at 0 than at 25 ºC, including physiological conditions where it showed a K_d of 65±7 µM at 0 ºC,

almost three times lower than at 25 ^{o}C. Therefore, the lower temperatures, apart from stabilizing the duplex, also improved the recognition capacity of the G-rich pocket.

Table 5.1. Data obtained from the steady state and time-resolved studies at 0 ^{o}C.

Media		**K_d towards AMP** (μM)	**F_0**	**Initial lifetimes** (ns)		τ_{av}	**Final lifetimes** (ns)		τ_{av}
TBS		65±7	1392	4.00	1.13	3.97	3.76	1.62	3.47
CC/EG (1:2)/TBS	0.87 M	215±22	1903	4.07	1.81	3.97	3.75	1.79	3.35
	2.175 M	402±72	2684	3.63	1.19	3.61	3.49	1.55	3.33
CC/EG (1:3)/TBS	0.87 M	202±24	2017	3.91	1.40	3.87	3.56	1.32	3.42
	2.175 M	2060±580	3410	3.52	1.20	3.50	3.40	1.43	3.33
CC/Gly (1:2)/TBS	0.87 M	205±12	1882	3.87	1.32	3.85	3.48	1.30	3.37
	2.175 M	1300±150	3039	3.61	1.66	3.56	3.27	1.26	3.22

Moreover, the molecular beacon was still functional and specific at 2.2 M DES concentration with its best performance in ethaline (402±72) μM, significantly better than in CC/EG (1:3) or glyceline. Considering that ethaline at 2.2 M can be liquid even at -60 ^{o}C[15], the possibility of using already selected hairpin- and G-quadruplex based aptamers in this media offers new opportunities for dynamic DNA nanostructures, but with the requirement of using them at low temperatures to achieve a good trade-off between structural stability and the recognition ability.

Within the binding studies at low temperatures, time-resolved studies were also done in order to gain insight about the nanoenvironment surrounding the molecular beacon. The lifetime values of the fluorophore were measured in absence and presence of the AMP target

(2 mM) (Table 5.1). The whole lifetime data can be found in Table S5.3. Differently from lifetime assays done in Chapter 3, in this case the fluorophore gave two lifetime components in all measurements even if they were done in equal solvent conditions. Looking for an explanation for the double-exponential decay fit, it was found that the new excitation state was detected due to the lower temperature. For an easier analysis, the two lifetime components were averaged to obtain a single lifetime value[16]. On the other hand, prior analysing the lifetime changes in DES media, different studies were done in TBS media in order to discard possible artefacts.

Firstly, the influence of the static quenching of the BMN-Q535 was confirmed measuring the lifetime of Atto 488 linked to Oligo1 in presence of Oligo2 with or without the quencher, the lifetime values were 3.58 and 3.79 ns, respectively. Therefore, the denaturation that DESs caused in the hairpin-loop of the molecular beacon should lengthen the lifetimes. On the other hand, the presence of AMP did not shorten the lifetime. In presence of 0, 0.5 and 5 mM of AMP the fluorophore linked to Oligo1 had a lifetime of 3.79, 3.80 and 3.77 ns at 0 ^{o}C, respectively. Therefore, differences in lifetime upon addition of AMP to the DNA-molecular beacon would be always related to changes in the secondary structure of DNA because an increase in AMP had no effect.

In TBS, upon addition of 2 mM of AMP to the DNA-molecular beacon the average lifetime shortened from 3.97 to 3.47 ns (Table 5.1), even if the static quenching of the BMN-Q535 reduced. This denoted the changes on the secondary structure of DNA upon target recognition. This reduction in lifetimes was also found in presence of DESs, confirming that the hairpin-loop

of the DNA-molecular beacon also behave dynamically in DESs at least up to 2.2 M. Moreover, it can be observed in lifetime values in absence of AMP that DESs at 2.2 M interacted with DNA and the fluorophore stronger than at 0.87 M.

5.3 Conclusions

By analyzing the aptamer by circular dichroism, it has been possible to observe how its double helix and recognition pocket are altered in a plethora of mixed solvents. The results are in agreement with the conformational and thermal stabilities of the duplexes of Chapter 3, what demonstrates the utility of the systematic studies. On the other hand, using this technique it was possible to see how 0.9 M choline chloride is sufficient to prevent DNA degradation for at least several years and even in the absence of salts, the mere fact of using solvents other than water has already reduced hydrolysis. The increase in the ellipticity of the negative peak after several months needs to be better studied as it could be due to DNA aggregation.

Circular dichroism has not been useful for monitoring aptamer binding to the target, so SPR and fluorescence techniques have been used. This is the first time that SPR has been used to study aptamer recognition in non-physiological solvents. It was possible to calculate the different K_d at low concentrations of mixed solvents, but unfortunately the refractive index has severely limited the range of mixed solvents that can be used.

Fluorescence was not affected by the refractive index of the solvent and it was possible to study aptamer recognition at all hydration levels. It has been observed that the capacity of the aptamer to recognize its target varies greatly with temperature, needing a temperature lower than 0 degrees for example, while using DESs above 2 M. Although this is a handicap in several cases, it also presents new opportunities for the use of functional DNA, as ethaline DES, for example, can be liquid at temperatures close to -80°C.

5.4 References

1. Svigelj, R. *et al.* Truncated aptamers as selective receptors in a gluten sensor supporting direct measurement in a deep eutectic solvent. *Biosens. Bioelectron.* 112339 (2020). doi:10.1016/j.bios.2020.112339

2. Slavkovic, S. *et al.* Thermodynamic analysis of cooperative ligand binding by the ATP-binding DNA aptamer indicates a population-shift binding mechanism. *Sci. Rep.* **10**, 1–11 (2020).

3. Xia, T., Yuan, J. & Fang, X. Conformational dynamics of an ATP-binding DNA aptamer: A single-molecule study. *J. Phys. Chem. B* **117**, 14994–15003 (2013).

4. Hernandez, L., Machado, I., Schafer, T. & Hernandez, F. Aptamers Overview: Selection, Features and Applications. *Curr. Top. Med. Chem.* **15**, 1066–1081 (2015).

5. Huizenga, D. E. & Szostak, J. W. A DNA Aptamer That Binds Adenosine and ATP. *Biochemistry* **34**, 656–665 (1995).

6. Lin, C. H. & Patel, D. J. Structural basis of DNA folding and recognition in an AMP-DNA aptamer complex: Distinct architectures but common recognition motifs for DNA and RNA aptamers complexed to AMP. *Chem. Biol.* **4**, 817–832 (1997).

7. Moutsiopoulou, A., Broyles, D., Dikici, E., Daunert, S. & Deo, S. K. Molecular Aptamer Beacons and Their Applications in Sensing, Imaging, and Diagnostics. *Small* **15**, 1902248 (2019).

8. Machado, I., Özalp, V. C., Rezabal, E. & Schäfer, T. DNA aptamers are functional molecular recognition sensors in protic ionic liquids. *Chem. Eur. J.* **20**, 11820–11825 (2014).

9. Özalp, V. C., Pinto, A., Nikulina, E., Chuvilin, A. & Schäfer, T. In situ monitoring of DNA-aptavalve gating function on mesoporous silica nanoparticles. *Part. Part. Syst. Charact.* (2014). doi:10.1002/ppsc.201300299

10. del Villar-Guerra, R. *et al.* G-Quadruplex Secondary Structure Obtained from Circular Dichroism Spectroscopy. *Angew. Chemie - Int. Ed.* **57**, 7171–7175 (2018).

11. Gattuso, H. *et al.* Circular Dichroism of DNA G-Quadruplexes: Combining Modeling and Spectroscopy to Unravel Complex Structures. *J. Phys. Chem. B* **120**, 3113–3121 (2016).

12. Antonio Randazzo, Gian Piero Spada, and M. W. da S. Circular Dichroism of Quadruplex Structures. (2012). doi:10.1007/128

13. Nguyen, H. H., Park, J., Kang, S. & Kim, M. Surface plasmon resonance: A versatile technique for biosensor applications. *Sensors (Switzerland)* **15**, 10481–10510 (2015).

14. Zhao, J. *et al.* Analysis of ATP and AMP binding to a DNA aptamer and its imidazole-tethered derivatives by surface plasmon resonance. *Analyst* **140**, 5881–5884 (2015).

15. Jani, A., Sohier, T. & Morineau, D. Phase behavior of aqueous solutions of ethaline deep eutectic solvent. *J. Mol. Liq.* **304**, 112701 (2020).

16. Li, Y. *et al.* Investigations on Average Fluorescence Lifetimes for Visualizing Multi-Exponential Decays. *Front. Phys.* **8**, (2020).

5.5 Supplementary information

Table S5.1. Used DNA sequences.

Name	**Sequence 5’ to 3’**
Oligo1	CAC CTG GAA CCT
Oligo2	AGG TTC CAG GTG
ATP-DNA aptamer	ACC TGG GGG AGT ATT GCG GAG GAA GGT
ATP-DNA aptamer Biotin (4 bp)	ACC TGG GGG AGT ATT GCG GAG GAA GGT (5’: Biotin-TEG)
ATP-DNA aptamer Biotin (8 bp)	CGG CAC CTG GGG GAG TAT TGC GGA GGA AGG TGC CG (5’: Biotin-TEG)
Molecular Beacon	CAC CTG GGG GAG TAT TGC GGA GGA AGG TTX XXX XXC CAG GTG (5’: Atto 488; 3’: BMN-Q535; X: Hexaethyleneglycol)

Figure S5.1. Circular dichroism spectra of the ATP DNA-aptamer stored at RT for different periods.

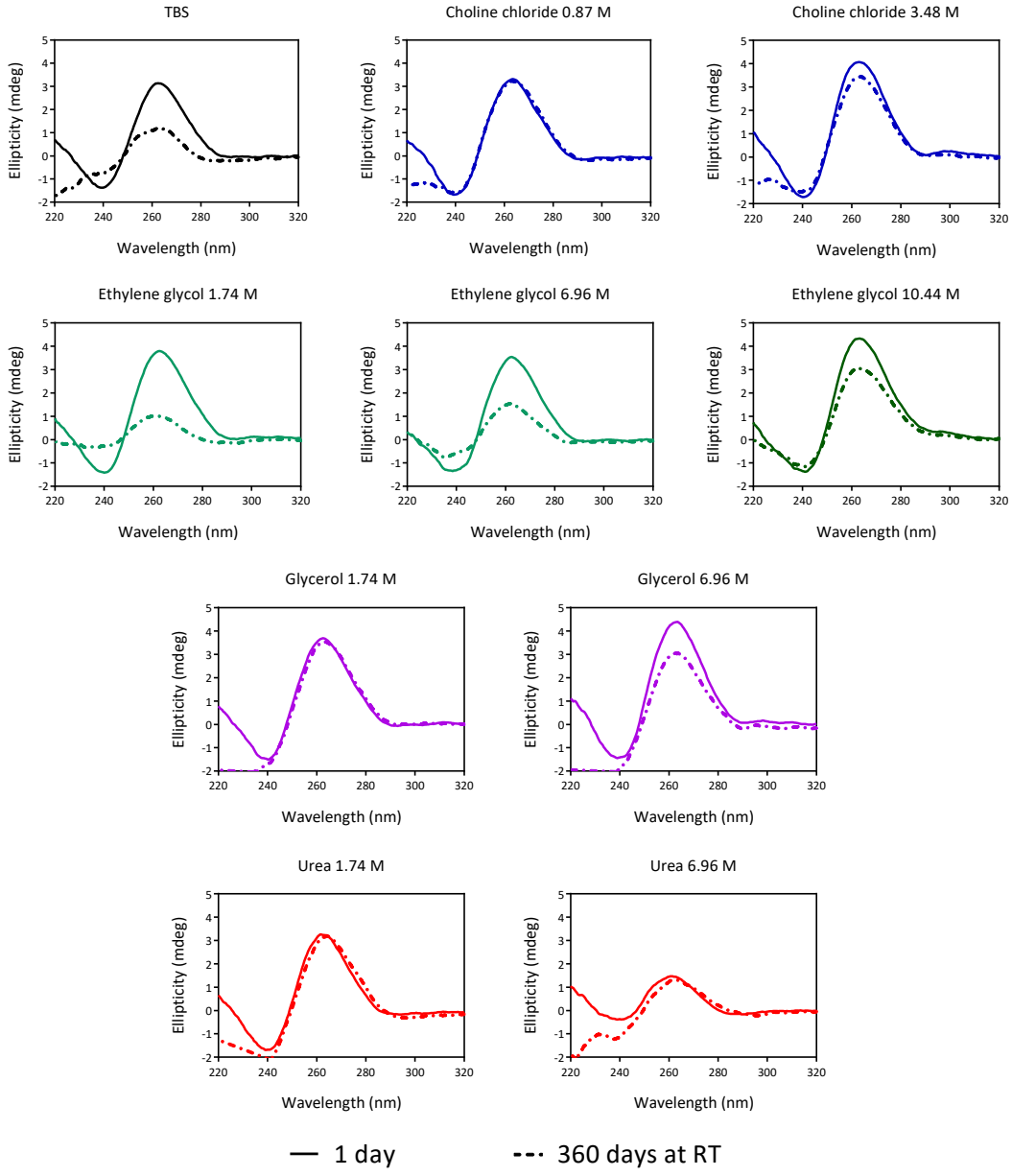

Figure S5.2. Circular dichroism spectra of the ATP DNA-aptamer stored at RT for different periods.

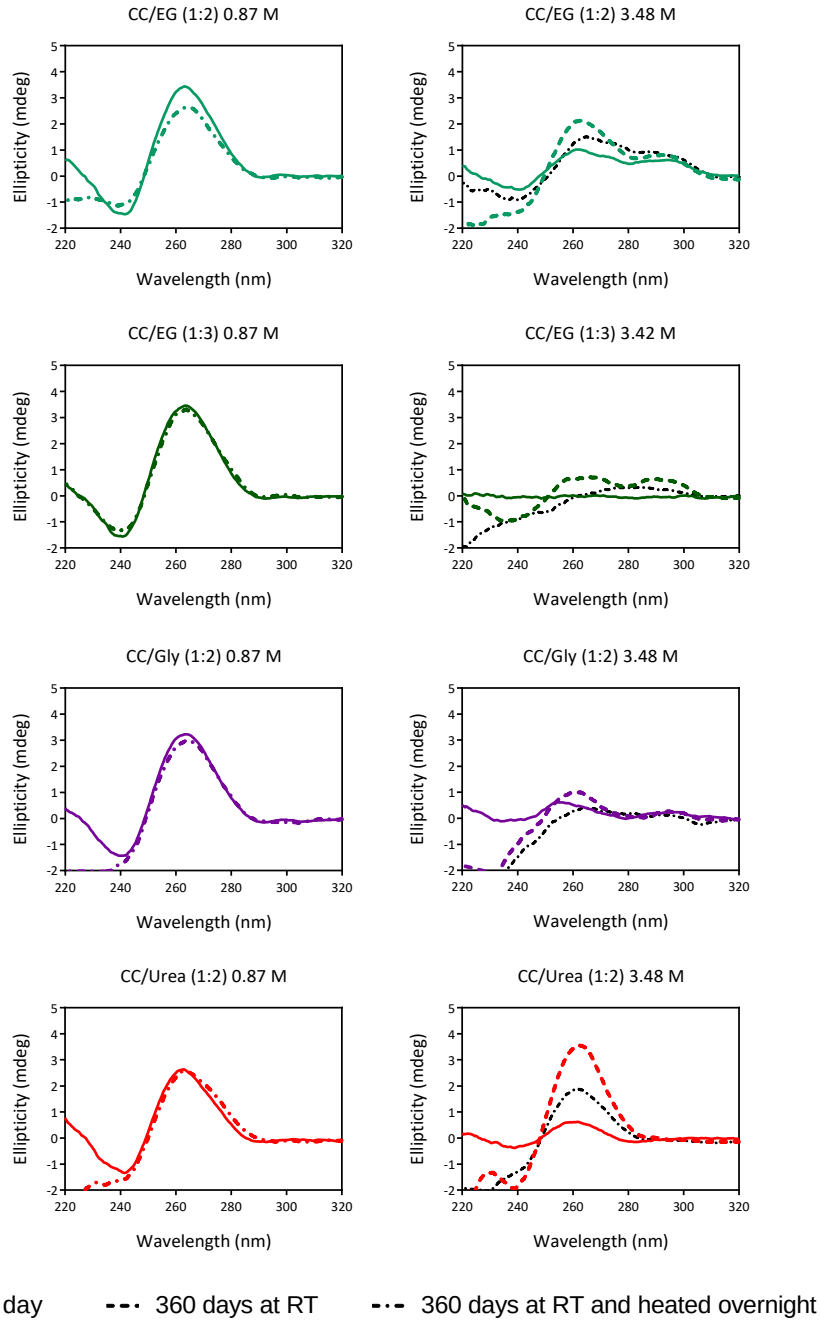

Figure S5.3. Circular dichroism spectra of solutions containing Oligo1 and Oligo2 during a period stored at RT or at -20 ºC.

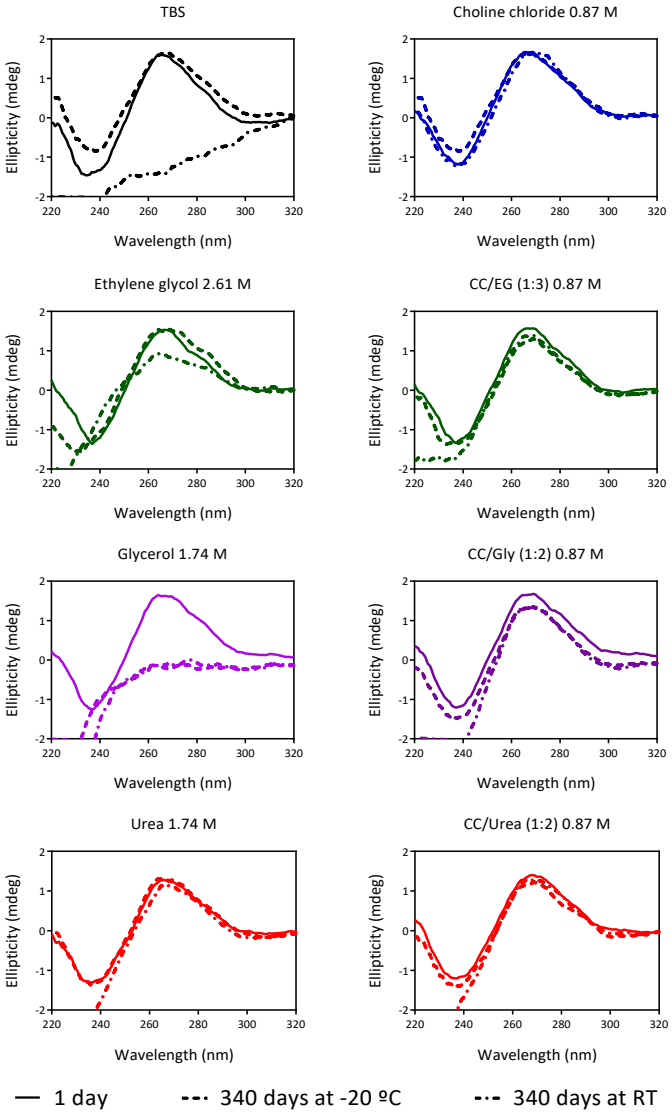

Figure S5.4. Circular dichroism spectra of solutions containing Oligo1 and Oligo2 during a period stored at RT.

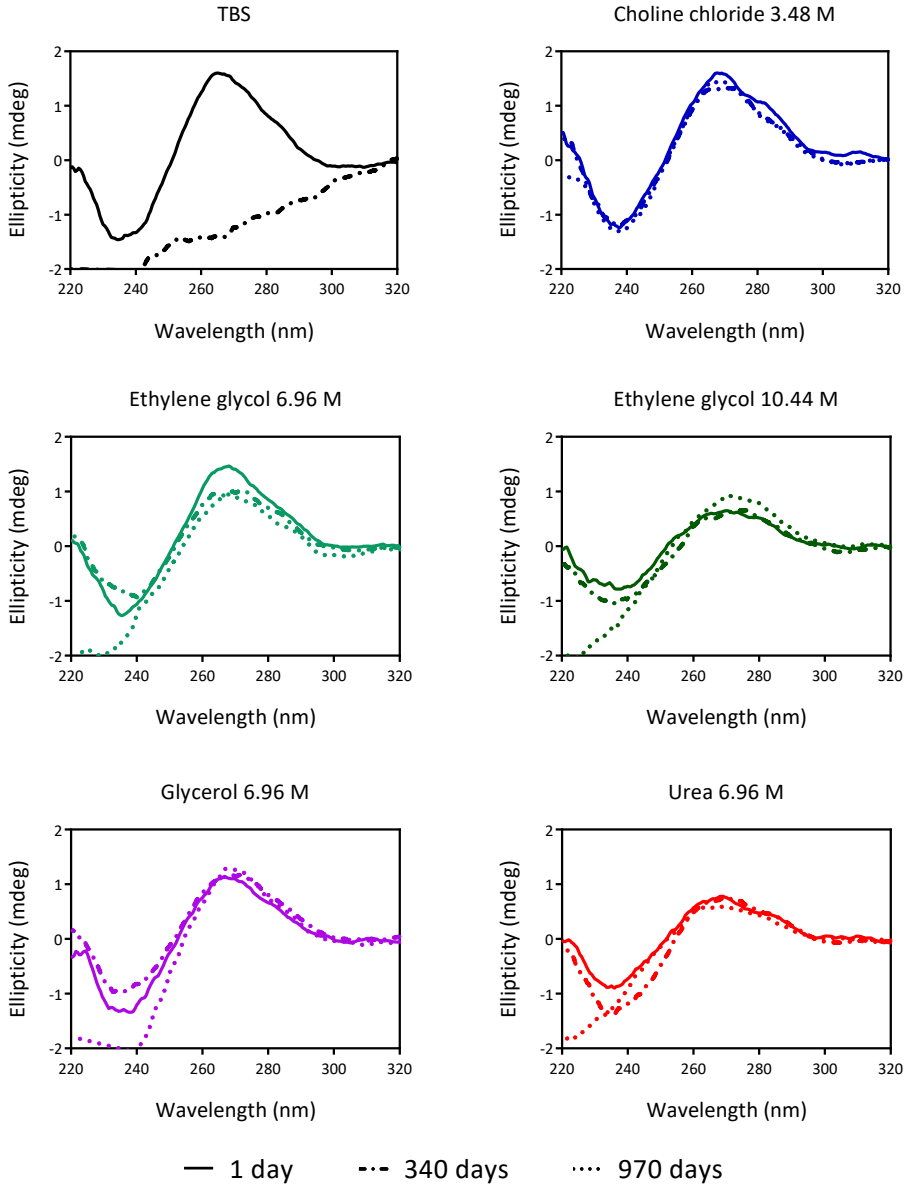

Figure S5.5. Mean response or intensity (zeroed) values obtained upon target addition at different conc. in presence of (A) ATP DNA-aptamer (4 bp), (B) ATP DNA-aptamer (8 bp) or (C) molecular beacon, while using choline chloride-containing media.

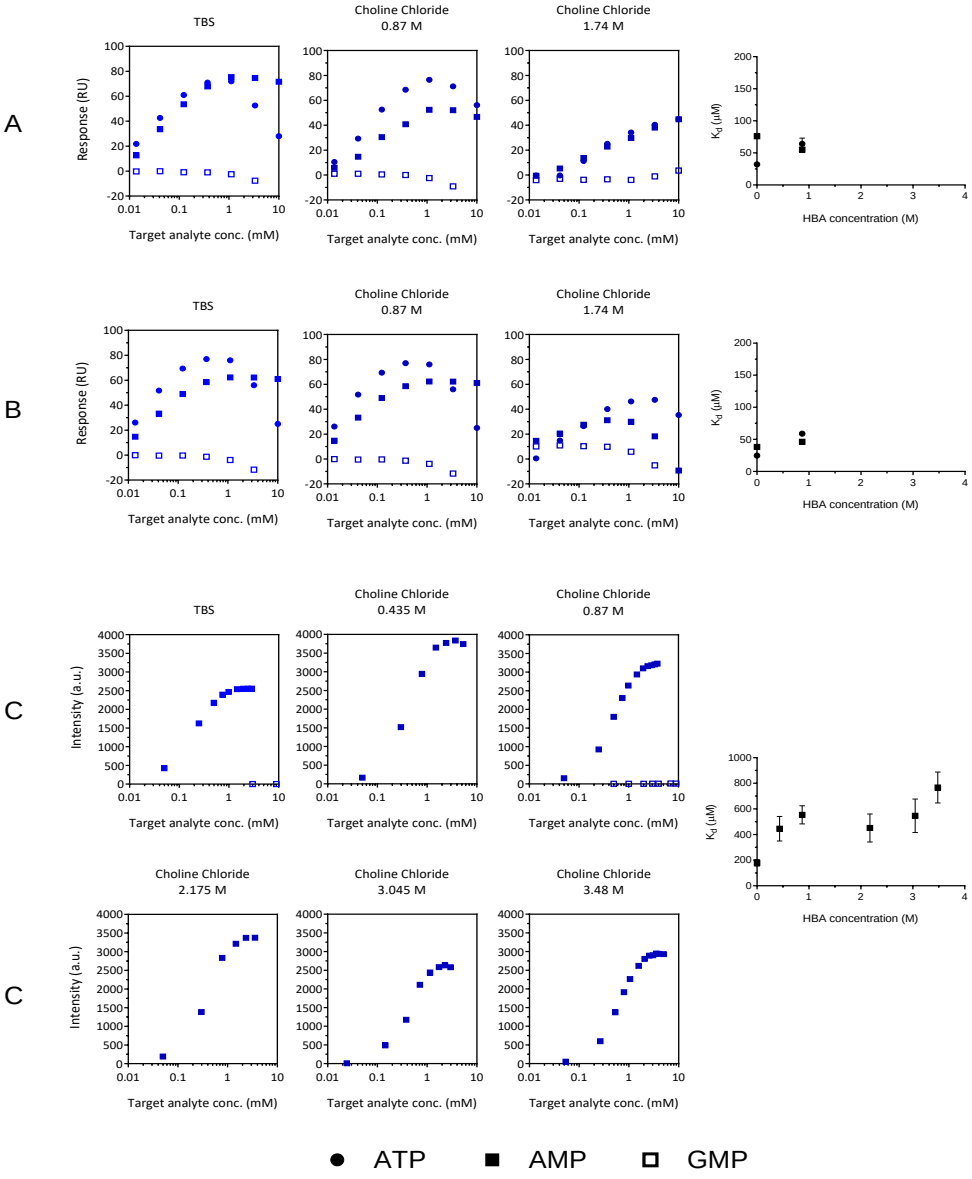

Figure S5.6. Mean response or intensity (zeroed) values obtained upon target addition at different concentrations in presence of (A) ATP DNA-aptamer (4 bp), (B) ATP DNA-aptamer (8 bp) or (C) molecular beacon, while using ethylene glycol-containing media.

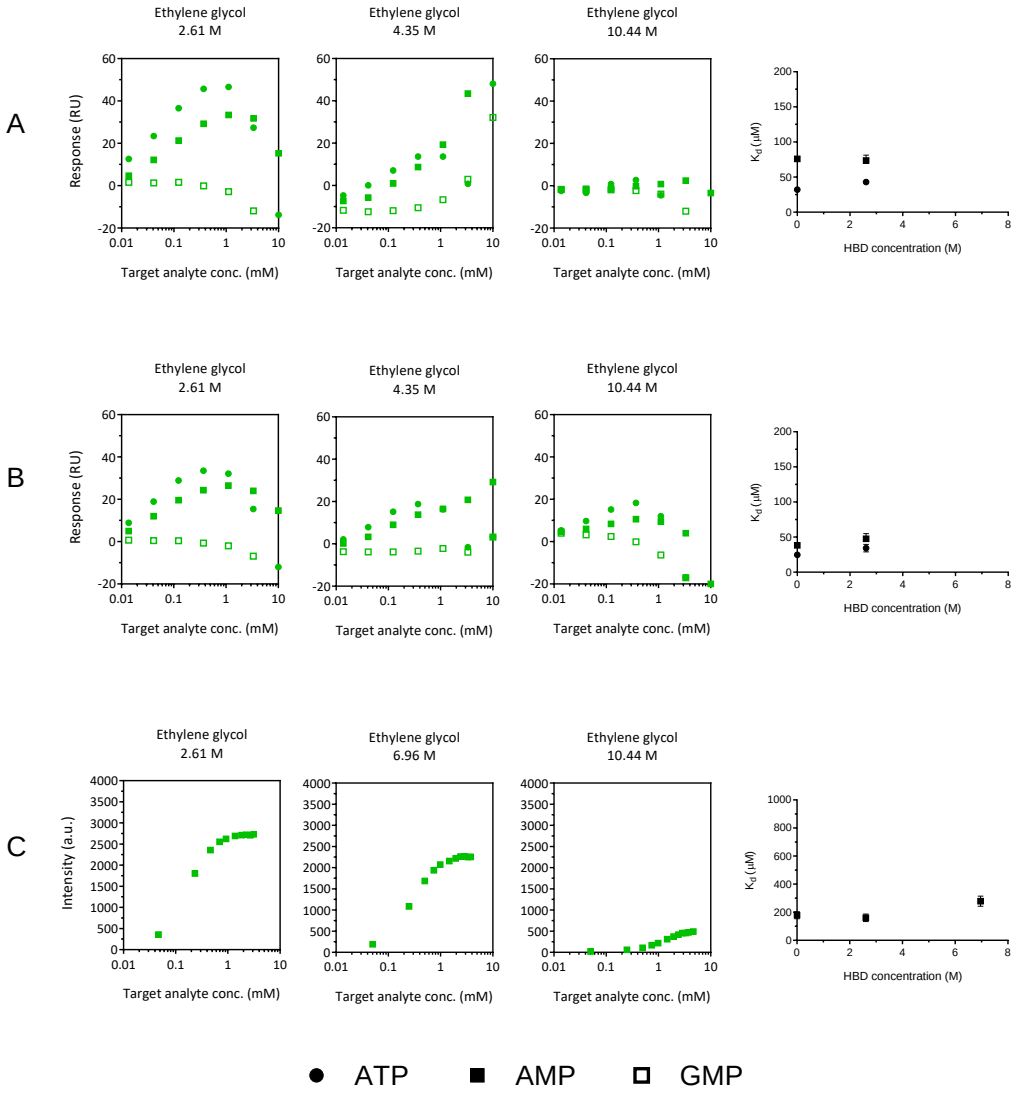

Figure S5.7. Mean response or intensity (zeroed) values obtained upon target addition at different concentrations in presence of (A) ATP DNA-aptamer (4 bp), (B) ATP DNA-aptamer (8 bp) or (C) molecular beacon, while using glycerol-containing media.

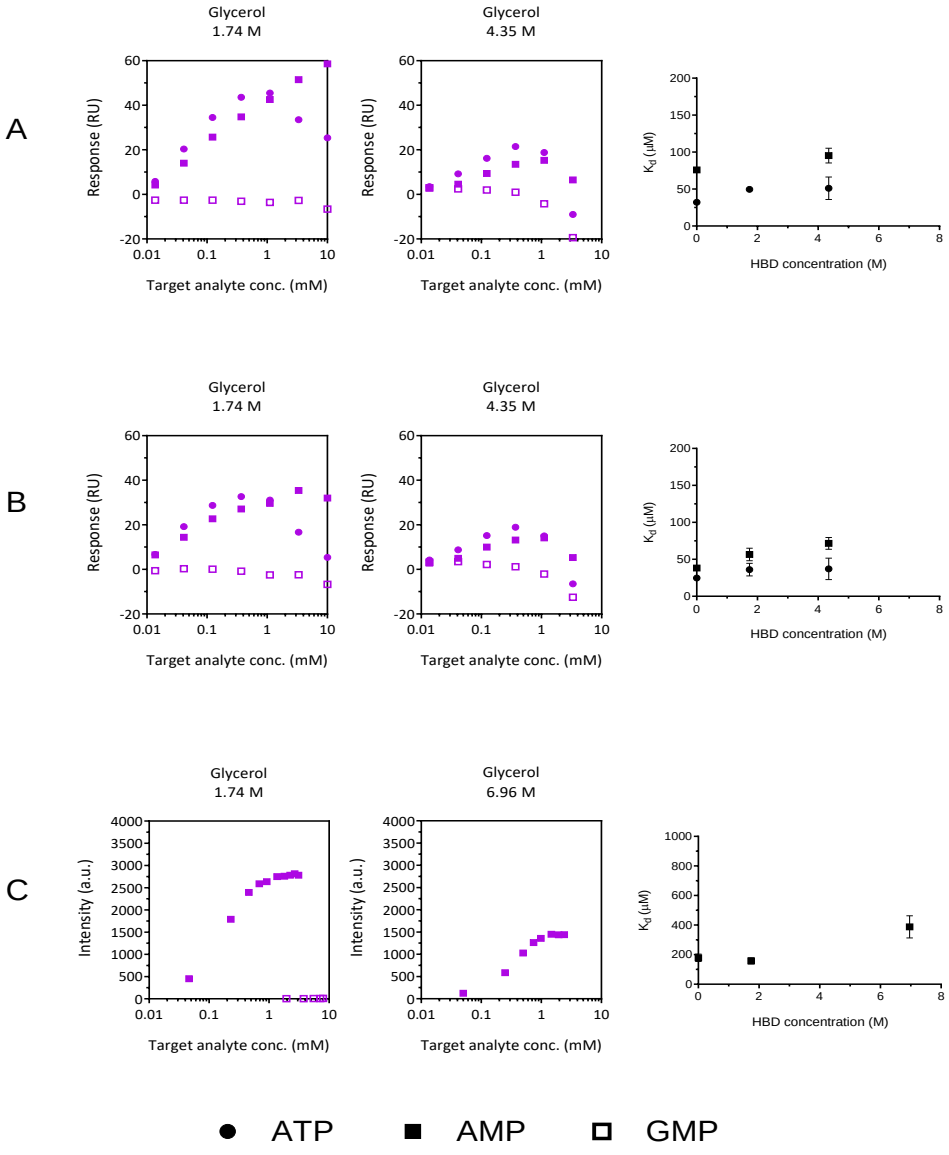

Figure S5.8. Mean response or intensity (zeroed) values obtained upon target addition at different concentrations in presence of (A) ATP DNA-aptamer (4 bp), (B) ATP DNA-aptamer (8 bp) or (C) molecular beacon, while using urea-containing media.

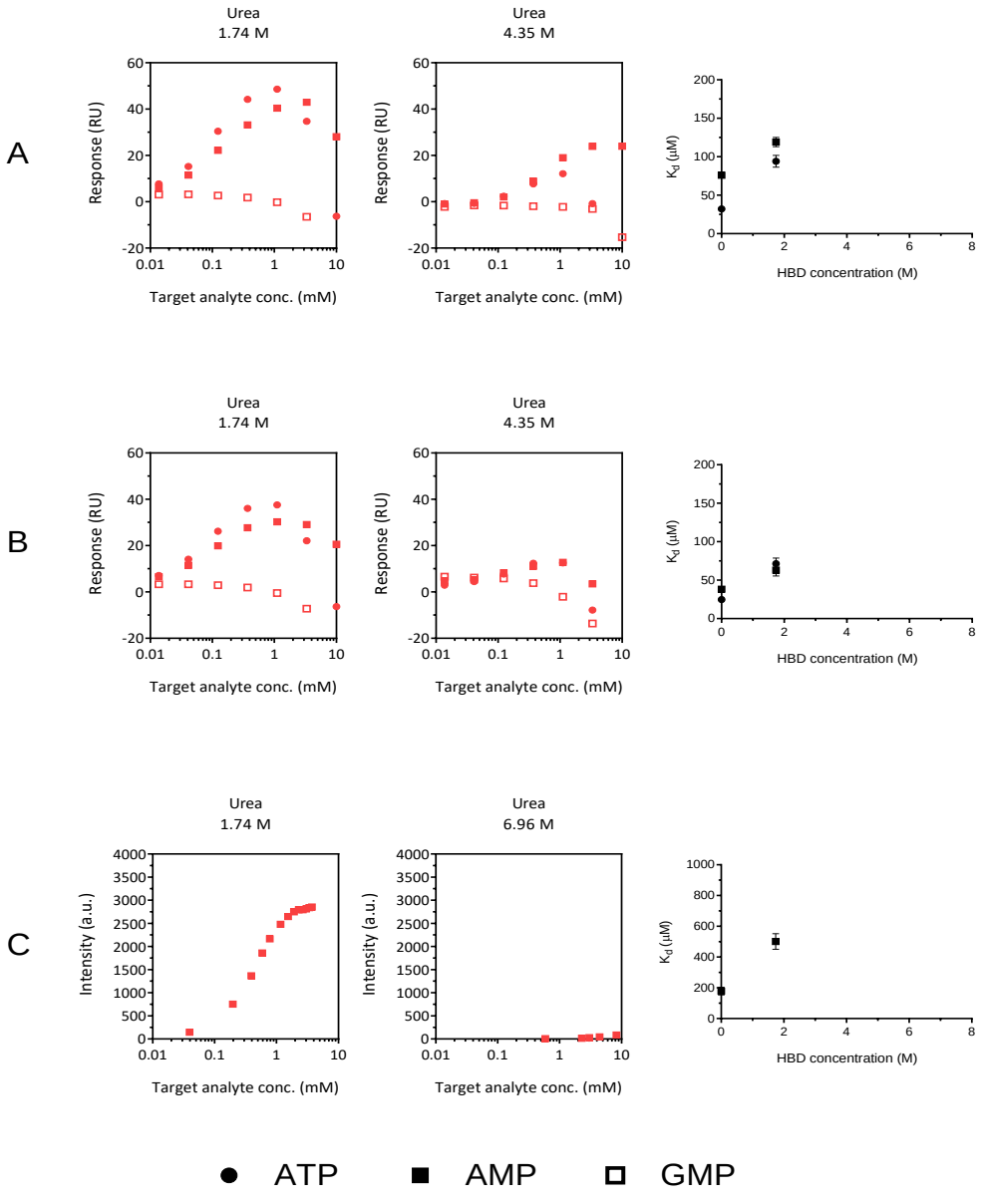

Figure S5.9. Mean response or intensity (zeroed) values obtained upon target addition at different concentrations in presence of (A) ATP DNA-aptamer (4 bp), (B) ATP DNA-aptamer (8 bp) or (C) molecular beacon, while using ethaline-containing media.

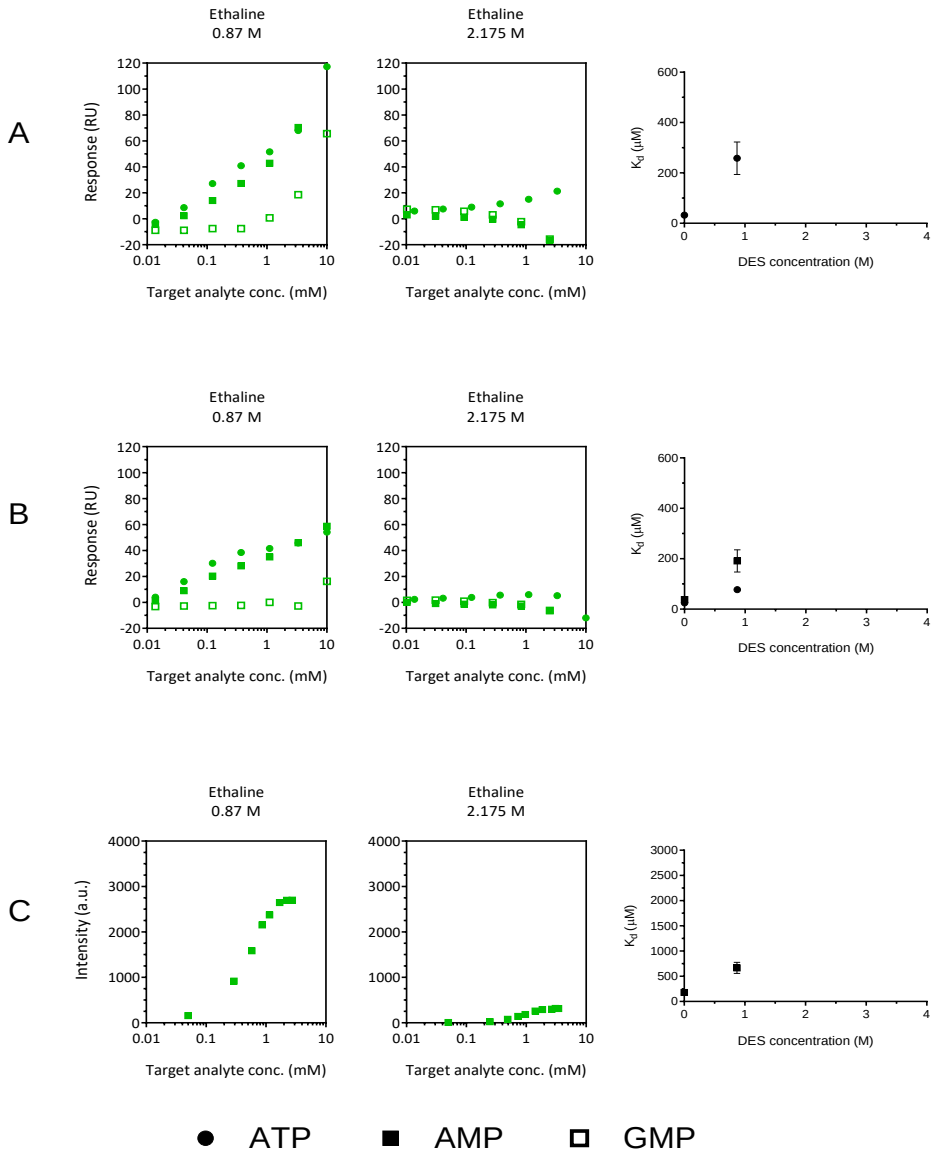

Figure S5.10. Mean response or intensity (zeroed) values obtained upon target addition at different conc. in presence of (A) ATP DNA-aptamer (4 bp), (B) ATP DNA-aptamer (8 bp) or (C) molecular beacon, while using CC/EG (1:3)-containing media.

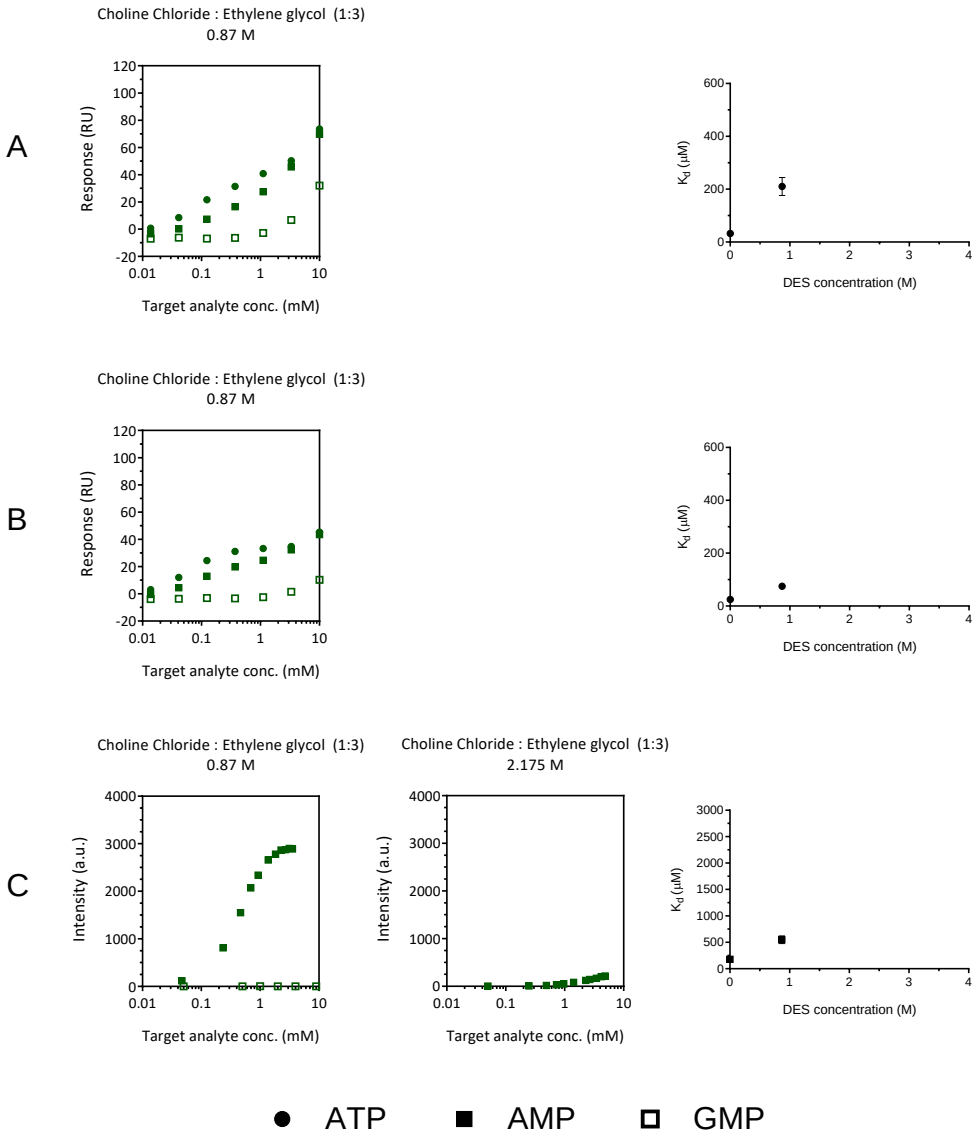

Figure S5.11. Mean response or intensity (zeroed) values obtained upon target addition at different conc. in presence of (A) ATP DNA-aptamer (4 bp), (B) ATP DNA-aptamer (8 bp) or (C) molecular beacon, while using glyceline-containing media.

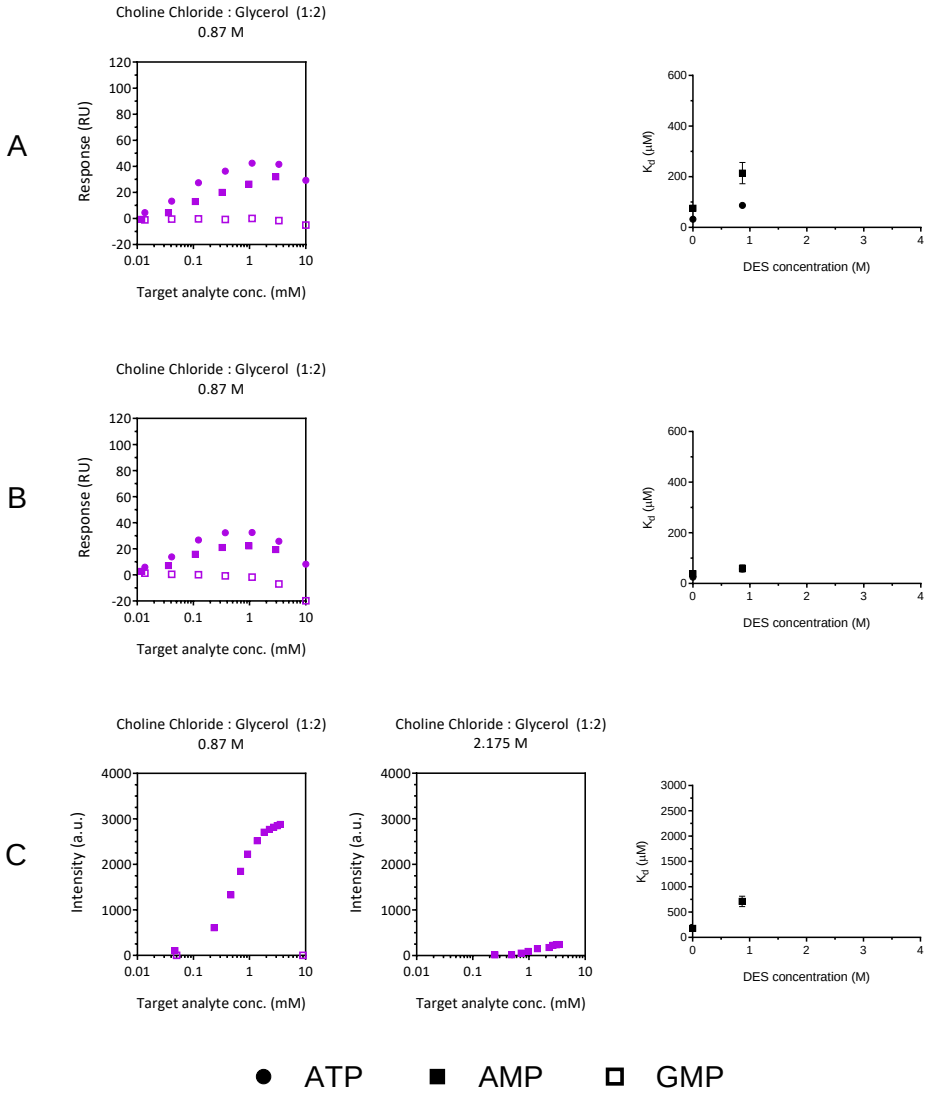

Figure S5.12. Mean response or intensity (zeroed) values obtained upon target addition at different conc. in presence of (A) ATP DNA-aptamer (4 bp), (B) ATP DNA-aptamer (8 bp) or (C) molecular beacon, while using reline-containing media.

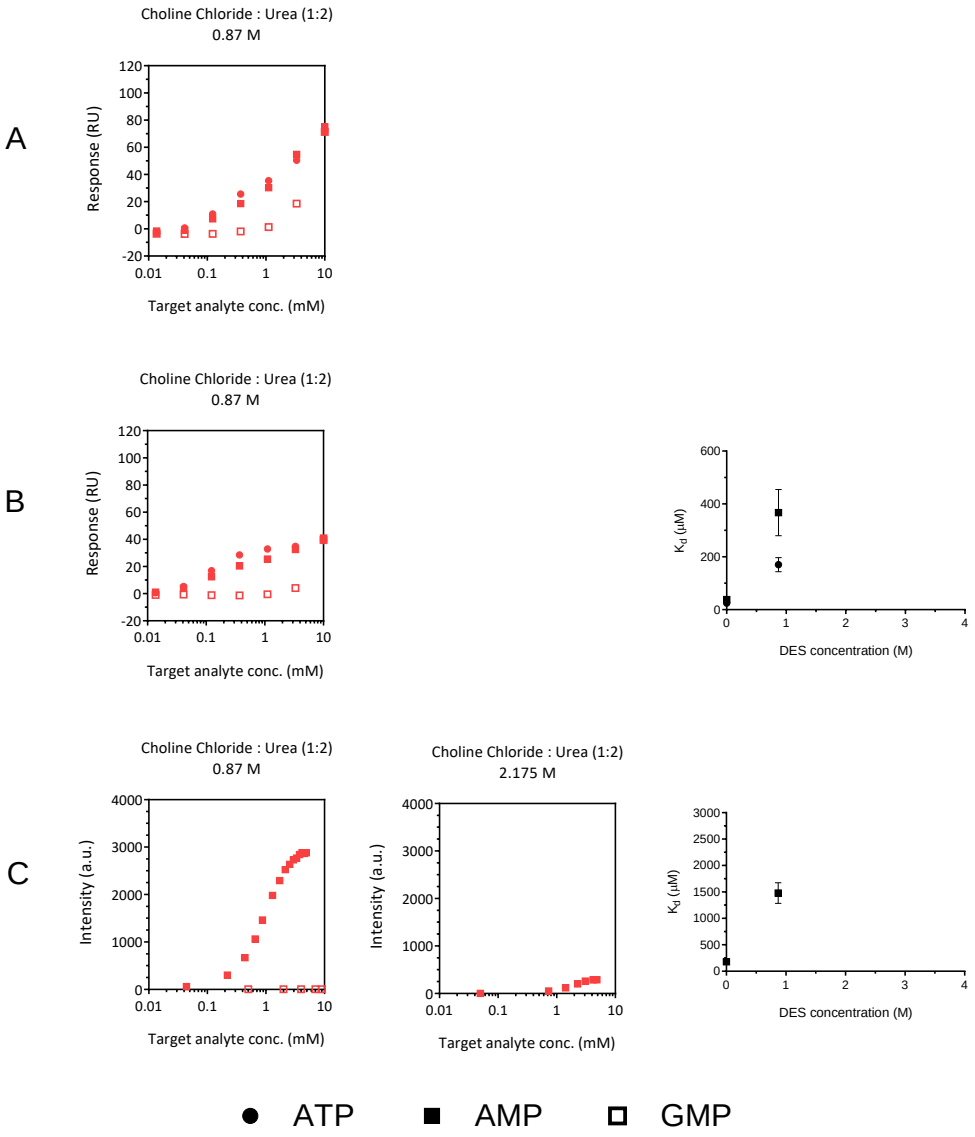

Table S5.2. Calculated dissociation constant values and their standard deviation.

Media	**ATP DNA-aptamer (4 bp)**				**ATP DNA-aptamer (8 bp)**				**Molecular beacon**	
	ATP		AMP		ATP		AMP		AMP	
	K_d (μM)	**SD**	**K_d** (μM)	**SD**	**K_d** (μM)	**SD**	**K_d** (μM)	**SD**	**K_d** (μM)	**SD**
TBS	32	2	76	1	25	3	38	3	179	25
CC/TBS 0.87 M	64	9	55	1	59	2	46	1	544	71
CC/TBS 2.175 M									451	110
CC/TBS 3.045 M									546	131
CC/TBS 3.48 M									767	121
EG/TBS 2.61 M	43	3	73	8	34	5	48	7	160	27
EG/TBS 6.96 M									279	36
Gly/TBS 1.74 M	50	2			36	9	57	9	158	21
Gly/TBS 4.35 M	51	15			37	15	72	8		
Gly/TBS 6.96 M									388	75
Urea/TBS 1.74 M	94	8	119	6	71	7	63	8	501	51
CC/EG (1:2)/TBS 0.87 M	258	65			77	10	191	44	665	112
CC/EG (1:3)/TBS 0.87 M	210	34			75	11			548	73
CC/Gly (1:2)/TBS 0.87 M	87	10	214	43	57	10	59	14	712	104
CC/Urea (1:2)/TBS 0.87 M	1048	280	1934	290	170	27	367	87	1479	196

Table S5.3. Values obtained from time-resolved experiments done in binding assays at 0 ^{o}C.

ATP DNA-molecular beacon (Atto 488 / BMN-Q535)								
Media		**AMP** (mM)	B_1	f_1	τ_1	B_2	τ_2	X^2
TBS		0	1149.55	89.994	4.003	452,91	1,13	1,104
		2	1022.01	71.629	3.757	941,1373	1,616	1,225
CC/EG (1:2)/TBS	0.9 M	0	1205.37	82.244	4.066	584,7709	1,809	1,167
		2	1009.03	66.216	3.751	1078,1292	1,791	1,248
CC/EG (1:3)/TBS	0.9 M	0	1483.85	89.975	3.905	464,0453	1,391	1,15
		2	1122.54	79.258	3.562	790,3657	1,324	1,142
CC/Gly (1:2)/TBS	0.9 M	0	1506,41	91.421	3.869	414,4933	1,319	1,215
		2	1203.83	81.734	3.478	719,4222	1,3	1,305
CC/EG (1:2)/TBS	2.2 M	0	695.87	92.083	3.626	182,9308	1,186	1,237
		2	1217.02	76.946	3.493	821,2333	1,551	1,201
CC/EG (1:3)/TBS	2.2 M	0	1249.55	90.933	3.524	367,2075	1,196	1,265
		2	1319.09	83.922	3.397	602,2201	1,425	1,258
CC/Gly (1:2)/TBS	2.2 M	0	1466.30	85.53	3.610	539,39	1,66	1,249
		2	1431.38	86.467	3.267	582,5009	1,256	1,26
Oligo1-Atto 488								
Media	**Oligo2** (nM)	**AMP** (mM)	B_1	f_1	τ_1	B_2	τ_2	X^2
TBS	0	0	818.43	93.31	3.81	177.13	1.26	1.22
	0	500	816.54	94.36	3.82	139.00	1.34	1.24
	0	5000	794.28	95.82	3.78	129.04	1.01	1.20
	17	0	849.52	95.52	3.79	122.84	1.23	1.24
	17 (BMN-Q535)	0	572.36	84.60	3.67	441.69	0.87	1.16

CHAPTER 6

Selection of functional DNA in a hydrated ionic liquid

6.1 Introduction

Nucleic acids are macromolecules possessing an unrivalled specificity of base pairing and molecular recognition capacity, which is the basis for their function as encoding and storing genetic information of all life forms. The function and interactions of nucleic acids are invariably associated with physiological solutions containing water as the abundant solvent. However, the bandwidth of applications of nucleic acids could be enhanced with changes in bulk aqueous phase properties[1], possibly similar to the development that biocatalysis underwent decades ago in organic solvents[2].

It is in this context that ionic liquids or deep eutectic solvents could match functional DNA in what regards versatility and yet overall similar physico-chemical properties: upon adjusting the functionalities of these media, their most prominent properties such as their charged nature and practical non-volatility remain unaltered. DNA-aptamers are ideal objects to be studied for this purpose as their function can rely on both conformational changes and the efficiency of molecular recognition event. In fact, an ATP DNA-aptamer selected in aqueous media and reported by Huizenga et al.[3,4] showed to maintain its function in a hydrated protic ionic liquid, although to a significantly reduced extent[5].

An intrinsic shortcoming from these studies was the fact that the aptamer had originally been selected in aqueous physiological conditions and the solvation in ionic liquids affected to its specificity and sensitivity. The alternative of doing a selection directly in the media of interest might solve this situation, and there are two previous studies that use

this approach[6,7]. However, the challenge has remained to prove that sequences of functional nucleic acids can exist which are different from those encountered in mainly aqueous solutions and which are particularly adapted to work in ionic liquid environments.

It has been found that the ILs and DESs that better solvate short-DNA are those based on tetraalkylammonium cations such as choline[8]. During the thesis of Isabel Machado (2016, UPV/EHU) and in the Chapter 3 of the present work, it was found that hydrated choline lactate (CL), a room temperature IL with relatively low viscosity, wide liquid range and low vapour pressure[9] could maintain multiple secondary structures of DNA stable. It was found also that the original ATP DNA-aptamer was able to recognize specifically the adenosine-based targets, but with a decreased efficiency when water was drastically reduced.

In this chapter, the SELEX of the ATP DNA-aptamer was *de novo* performed in presence of choline lactate ionic liquid, in order to elucidate if it would be possible to select DNA-aptamers better adapted to the non-physiological media. The original selection medium consisted in TBS, the aqueous buffer already used in previous chapters (50 mM Tris, 138 mM NaCl, 2.7 mM KCl and 5 mM $MgCl_2$ in H_2O, pH 7.4). In the new SELEX, this medium has been replaced partially with choline lactate, forming a hydrated ionic liquid called **2 M CL/TBS**, containing 40 wt. percentage of the IL and 60 wt. percentage of the aqueous buffer (2 M choline lactate, 30 mM Tris, 82.8 mM NaCl, 1.62 mM KCl and 3 mM $MgCl_2$ in H_2O, pH 5.6).

Apart from the new SELEX, a parallel one was done using TBS medium, in this manner it was possible to verify that the protocol was working fine. Isabel Machado did the main part of the work presented in Section 6.2.1 during her PhD thesis, but the work was stopped before starting with the binding studies and it has been continued in this thesis completing the Sections 6.2.2 and 6.2.3.

6.2 Results and Discussion

6.2.1 SELEX in non-physiological media

During SELEX procedures the parameters of the pool concentration, incubation time and the number of washing steps were changed in order to increase the stringency of the process (Table 6.1). In this manner, the specificity of the DNA pool towards the target increased and enrichment was more likely to be reached.

Table 6.1. Selection pressure applied in all SELEX procedures.

SELEX round	D3 DNA Pool (pmol)	Incubation time	Nº Washing steps
1	500	30	5
2-3	50	30	5
4	25	30	8
5	25	30	10
6-7	25	20	10
8-12	25	15	10

Based on the selection of the original ATP DNA-aptamer done in aqueous media[3], after eight rounds there should be enrichment of binding sequences. In order to probe if it happened, binding studies were done with pools of first and eighth rounds in both SELEX: the positive control in TBS with known results and the new one in presence of 2 M CL/TBS. In Liquid Scintillation Counting (LSC), it was seen that even at the first round, there were high binding values at the beads step (Figure 6.1A and 6.1B), when indeed no enrichment was expected to be observed at this round.

In order to overcome what was considered as a high degree of unspecific binding, salmon-sperm DNA (s-sDNA) was tested as a competitor. The concentration of s-sDNA was tried firstly with 0.1 mg/mL but it was not enough to avoid unspecific binding (Figure S6.1) and then it was adjusted to 1 mg/mL because at this concentration the amount of negative control in the beads was residual (Figure 6.1C and 6.1D).

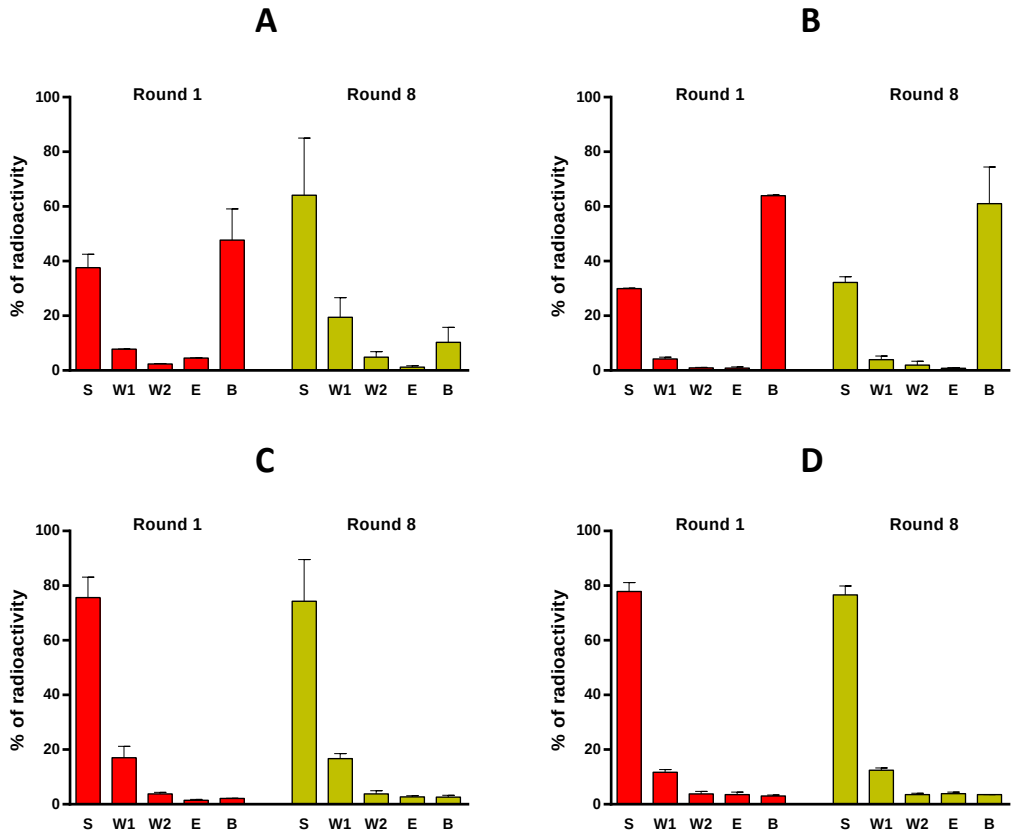

Figure 6.1. Enrichment studies of first SELEX done (A) in aqueous media and (B) in 2 M CL/TBS media. And using salmon-sperm DNA 1 mg/mL as competitor in these enrichment studies of first SELEX done (C) in aqueous media and (D) in 2 M CL/TBS media. Percentages of ^{32}P-DNA obtained in each step of the assay (**S**: Supernatant; **W1**: Washing 1; **W2**: Washing 2; **E**: Elution; **B**: Beads). All experiments were done in duplicate; the bars on top of the columns represent the error bar.

Based on previous observations, a SELEX was repeated in both solvents using 1 mg/mL of salmon-sperm DNA in each incubation step, and applying the same SELEX "pressure". To reduce working time, these new SELEX were continued from the second round of previous ones. After eight rounds (including first two of previous SELEX), enrichment was again verified with a considerable increase of possible specific DNA sequences in the SELEX done in aqueous media but yet no enrichment was observed in SELEX done in 2 M CL/TBS. Results of SELEX in aqueous selection media indicated that procedure was being done correctly.

In order to verify if finally, could be enrichment in 2 M CL/TBS SELEX, four more rounds were done obtaining a significant increase of DNA percentage in elution and beads solution (Figure 6.2). ssDNA bound in 12^{th} round yielded around 58% (≈ 31% elution and ≈ 27% beads+) of γ-^{32}P-DNA, that value is similar to the percentage obtained in the 8^{th} round of aqueous SELEX which was 51% (≈ 33% elution and ≈ 18% beads) and far above from negative control values. These results validated the SELEX procedures and the pools obtained in 8^{th} round for aqueous buffer and 12^{th} round for 2 M CL/TBS media were cloned and sequenced.

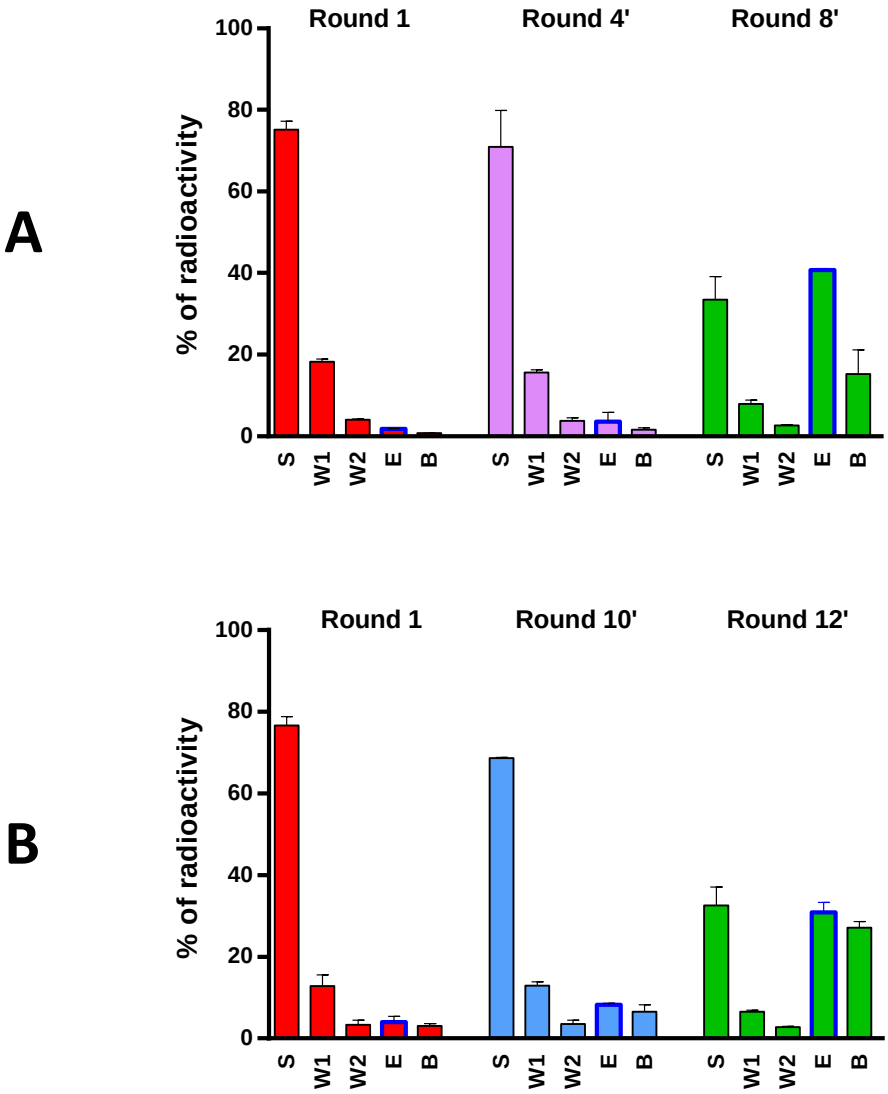

Figure 6.2. Enrichment studies of second SELEX done (A) in aqueous media and (B) in 2 M CL/TBS media.

6.2.2 Binding studies of potential aptamer sequences

Obtained sequences in both SELEX were analysed with MUSCLE and MEME tools and most sequences were found to be similar to motifs responsible for recognition in the original ATP DNA-aptamer SELEX: GGGGGA and GGAGGA (Figure S6.2), confirming that the control SELEX had worked properly and there were no systematic errors. Surprisingly, in the SELEX done in presence of 2 M CL/TBS, four sequences were found that had no similarity with those motifs and even more intriguing, there were no similarities between these four sequences (apart from their non-random region).

In order to clarify if these unique sequences were binding to the target and were not just bound non-specifically in some part of the beads, binding studies of each separated sequence were carried out. In Table 6.2, it can be seen the pools or sequences used in further binding studies: The original ATP DNA-aptamer (**ATPapt,** PDB: **1AW4**), and its mutated sequence that cannot recognize the target (**mut-ATPapt**)[10]. The pools of the 1st and 12th SELEX rounds (**R1** and **R12**) obtained in presence of 2 M CL/TBS, were used as negative and positive controls respectively. **CL1**, a sequence obtained in the novel SELEX which is very similar to those obtained in SELEX done in TBS, and finally, the four unique sequences obtained (**CL2**, **CL3**, **CL4**, **CL5**) to the target. Their truncated version of previous sequences without the non-random parts were also studied (**trun-CL1**, **-CL2**, **-CL3**, **-CL4**, **-CL5**).

Table 6.2. Names of the studied pools and oligomers with their sequences.

Name	Sequence 5' to 3'
ATPapt	ACCTGGGGGAGTATTGCGGAGGAAGGT
Mut-ATPapt	ACCTAGGAGAGTAATGCCGAGGAAGGT
R1	First round pool of first SELEX done in ionic liquid
R12'	Last round pool of second SELEX done in ionic liquid
trun-CL1	TTGCGGAGGAGAGTACTCGGGGGAGCAATTCCACGTAAGTCGA
trun-CL2	TACATCTATCCTTCTACTCTCACTTTTTAAGGGACCCCAAGTG
trun-CL3	GGTGGAGTCAGTCGCATCAGTCACTTTAGGAAGTTAC
trun-CL4	GATGTAAGCATAGTGAATAGAAACCACGTTGAGGACGCGGCGC
trun-CL5	TGACTCCAAGCCAGGGTGTTGCCGTAGTCGGCGCGTGTGAAAT
CL1-5	GCTGTGTGACTCCTGCAA**(trun-CL1-5)**GCAGCTGTATCTTGTCTCC

The protocol used in these binding studies was different from previous assays because they were optimized in order to increase the non-specific DNA recovery in incubation step and efficiency of thermal elution step (Section 2.6.2). After labelling radioactively the samples (Figure S6.3), the first binding assay was done in selection conditions; in elution step (Figure 6.3A), negative control (**R1**) and **CL2** gave similar results (≈ 11% and ≈ 14% respectively). However, in case of the others, the percentage was at least as high as in the positive control (**R12'**): ≈ 34% **R12'**, ≈ 35% **CL1**, ≈ 54% **CL3**, ≈ 37% **CL4** and ≈ 38% **CL5**. These results suggested that at least, three of the four sequences could be binding specifically to the target, and in case of **CL3** the binding would be higher in 2 M CL/TBS than that of the sequence with the well-known motif. All the percentages obtained in each step can be found in Table S6.1-S6.3.

Wondering if these sequences could be obtained in SELEX done in physiological media, or they only were specific in these non-conventional conditions, previous binding studies were repeated but instead of doing them in presence of ionic liquid, they were done in conditions used in the conventional SELEX (Figure 6.3B). The results showed that the final round pool (**R12'**) decreased slightly its binding and **CL1** was the only sequence with an increased recognition capacity in aqueous media, whereas the rest of them showed low (**CL4**) or no binding (**CL2**, **CL3** and **CL5**).

As in previous assay, almost all DNA was found in supernatant and elution solutions, comparing elution percentages with obtained ones in previous assay a clear solvent specificity can be observed in two unique sequences. In case of **CL3**, ≈54% of γ-^{32}P-DNA was eluted in ionic liquid presence and ≈4% in aqueous buffer (less than negative control); for **CL5**, ≈38% and ≈4% respectively.

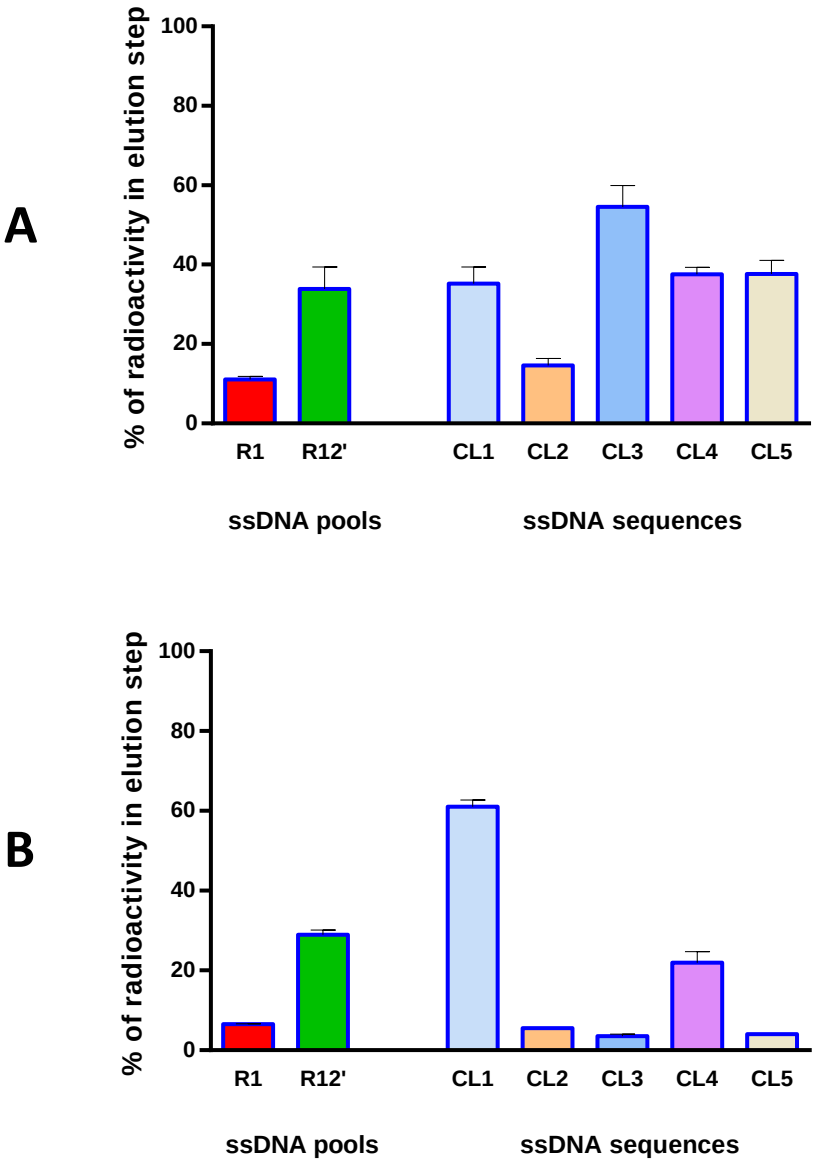

Figure 6.3. Binding assay towards immobilized 8-Amino-hexyl-ATP sepharose-beads (A) in 2 M CL/TBS (selection conditions) and (B) in aqueous media (not selection conditions). Only eluted solutions are shown for easier comparison.

In the light of the above, **CL3** and **CL5** needed the presence of the ionic liquid to recognize the target, but there was no similarity between the random parts of both sequences. In order to have a preliminary idea of the binding mechanism, truncated sequences (without the non-random parts) were studied in selection conditions. **ATPapt** and **mut-ATPapt** were used as positive and negative controls respectively. The binding assay showed a ≈ 24% of **ATPapt** in eluted percentage, and ≈ 5% in case of **mut-ATPapt**. In case of truncated unique sequences, it was seen that **trun-CL3** lost its recognition capacity (≈ 7%) but **trun-CL5** preserved it (≈ 43%). Furthermore, the solvent specificity was also maintained with a percentage of ≈ 5% for **trun-CL5** in physiological environment (Figure 6.4), whole data can be found in Table S6.3. The sequence **CL5** is the only one that has the motif "TGACTCC" in both, the random and non-random parts, but even if it could be a recognition site, there must be other causes that promote the recognition of the target and solvent specificity.

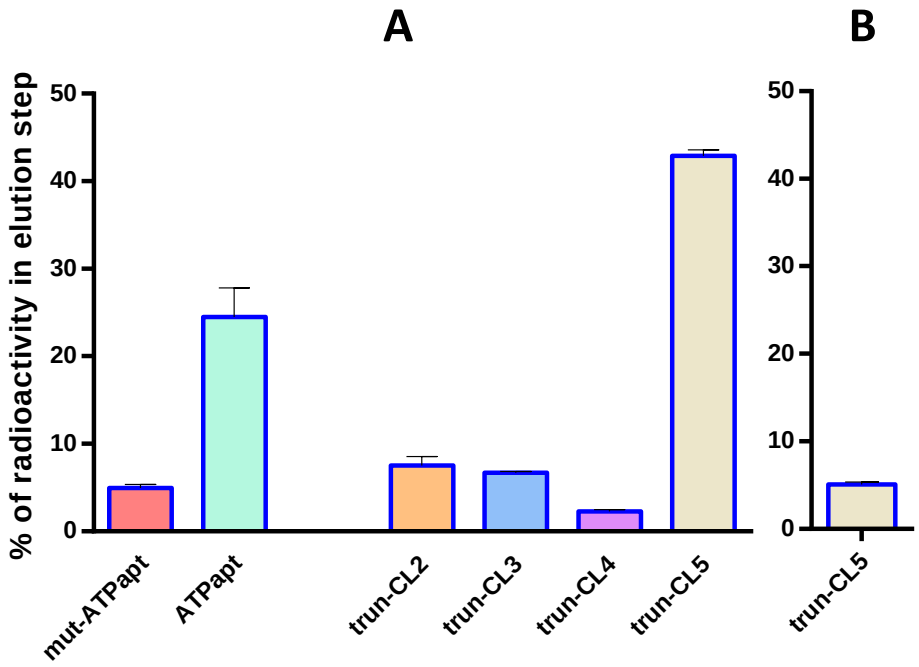

Figure 6.4. Binding assay of ATP DNA-aptamer, its mutated sequence and truncated sequences towards immobilized 8-Amino-hexyl-ATP sepharose-beads in (A) in 2 M CL/TBS (selection conditions) and (B) in TBS media (not selection conditions). Only eluted solutions are shown for easier comparison.

It is well known that the sequences with motifs similar to those of the original ATP DNA-aptamer are very likely to maintain their specificity towards adenosine-based molecules, not recognizing guanosine-based ones, but behaviour of new sequences with not known motifs is uncertain. It was checked if new motifs of **CL2 – CL5** could be also able to differentiate between those targets. In these assays GTP molecule was used but unfortunately, there was no market availability for immobilized 8-Amino-hexyl-guanosine triphosphate that would permit a direct comparison with SELEX target, but there were γ-Amino-

hexyl-ATP and –GTP sepharose-beads (Section 2.6.1) which were used as comparison. The risk of these new targets was that hydroxylation of the phosphate group could happen in 2 M CL/TBS media (pH 5.6), loosing part of them in the supernatant. In these studies, both elution and beads percentages were taken into account, because the radioactivity amount found in beads was significant.

In Figure 6.5, it can be seen that the positive control (**R12'**), **CL1** and **CL5** showed specificity towards ATP over GTP. This what was predictable for the **R12'** pool and **CL1** because have original ATP DNA-aptamer motifs but the target specificity found with **CL5** resulted very interesting. In case of **CL3**, in these assays did not show higher binding than the negative control for both, ATP and GTP beads, probably due to a recognition site hindered by the γ-Amino-hexyl linkage.

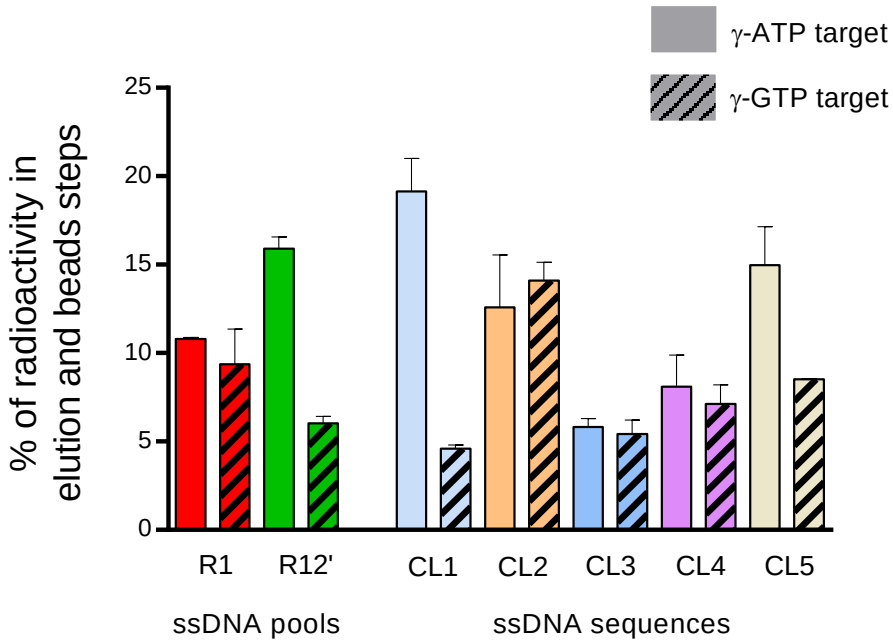

Figure 6.5. Binding assay towards immobilized γ-Amino-hexyl-ATP or -GTP sepharose-beads done in 2 M CL/TBS (selection conditions, with a different target). Only the sum of eluted and beads solutions percentages is shown for easier comparison.

6.2.3 Secondary structure of novel ATP DNA-aptamers

To the best of our knowledge, only two previous SELEX procedures used high volumes of non-conventional solvents. In one case, methanol in 25% (v/v) was used, and DNA was modified to increase its solubility in organic media but at the same time complicating the procedure and raising its cost[6]. In this study, they obtained an adenine aptamer with higher binding affinity in methanol than the original aptamer selected in aqueous media, however the aptamer needed a modified nucleotide to achieve that affinity and target specificity. Furthermore, the aptamer was not solvent specific, recognizing the target better in physiological media than in methanol containing media.

In the other case, published very recently, not-modified DNA-aptamers were selected using deep eutectic solvents[7], specifically ethaline solvent[11]. These selection was done towards a 33-mer peptide of gluten, which usually is recognized by antibodies but these have low efficiency in extraction media[12]. It was found that less rounds were necessary to achieve enrichment but a vast number of sequences were sequenced (around 830000). They also found, that most of these possible aptamers had the same recognition motif found in aqueous selection (the positive control); unfortunately, due to the vast number of sequences it was not possible to study the unique ones.

In this work, the two aptamers found had unique recognition motifs and specificity towards non-conventional conditions, probably due to a novel tertiary structure achieved in 2 M CL/TBS media. There are no similarities between random regions of new aptamer sequences found (**CL3** and **CL5**) and they neither have the well-known recognition motifs “GGGGG” and “GGAGG” that can be found in most part of the other sequences selected (Figure S6.2). Therefore, these two sequences are the first DNA-aptamers able to recognize the target specifically in non-physiological media, not recognizing it in purely aqueous medium. Understand why **CL3, CL5** and **trun-CL5** acquire this behaviour would serve to deepen in the capacity of non-aqueous media to tune DNA behaviour.

Circular Dichroism (CD) is commonly used to characterize the secondary structure of nucleic acids and proteins, in case of DNA it is possible, in example, to characterise the stacking of the guanines in a G-quadruplex, responsible of recognizing the ATP beads in the classic ATP DNA-aptamer[3]. Depending on the strand orientation the spectra of the G-quadruplex also varies: parallel G-quadruplexes are formed by anti-guanines and usually shows a maximum around 260 nm in the CD spectra. In case of antiparallel G-quadruplexes, the stacking of guanines is alternated leading to a maximum around 290 nm. Hybrid G-quadruplexes can have both types of stacking, and usually present two positive peaks around 270 and 290 nm. In some cases, two G-quadruplex antiparallel structures in the same strand can have hybrid-type CD spectra because other bases are stacking might be stacking on the main two quartets[13].

The CD spectra of three different truncated sequences were compared (specified in Table 6.2): **trun-CL1**, from the aptamer selected in original aqueous media and containing the classic recognition motifs. **trun-CL3**, from the novel **CL3** aptamer, which loses its recognition capacity while truncating it. **trun-CL5,** from the novel **CL5** aptamer, which maintains its recognition capacity and solvent specificity while truncating it. Due to the strong absorption of choline lactate, below 250 nm the noise of the spectra increases even if the solvent blank is subtracted (Figure 6.6).

In the circular dichroism spectra, it can be seen that **trun-CL1** shows the well-known G-rich binding pocket of the classic ATP DNA-aptamer and it seems that there is also a partial contribution of a duplex structure that shift the maximum from 260 to 268 nm. While solvating the aptamer in 2 M CL/TBS media, the intensity of the positive peak decreases, what could be due to a loss of the G-rich binding pocket structure and this event is in agreement with the reduction of sensitivity in hydrated ionic liquid media in sequences containing the "GGGGG" and "GGAGG" motifs observed during the binding assays.

In case of **trun-CL3**, it shows common spectra for duplex structures with a maximum at 273 nm but with very low intensities in aqueous and 2 M CL/TBS media, this could mean that the tertiary structure is not very stable. Different duplexes formed by two aptamer strands have been found using m-fold software, with Gibbs free energies (ΔG^o) varying between -3.5 and -2.5 kcal/mol in TBS conditions. The absence of a G-

quadruplex structure could explain the loss of the recognition function while truncating the **CL3** aptamer.

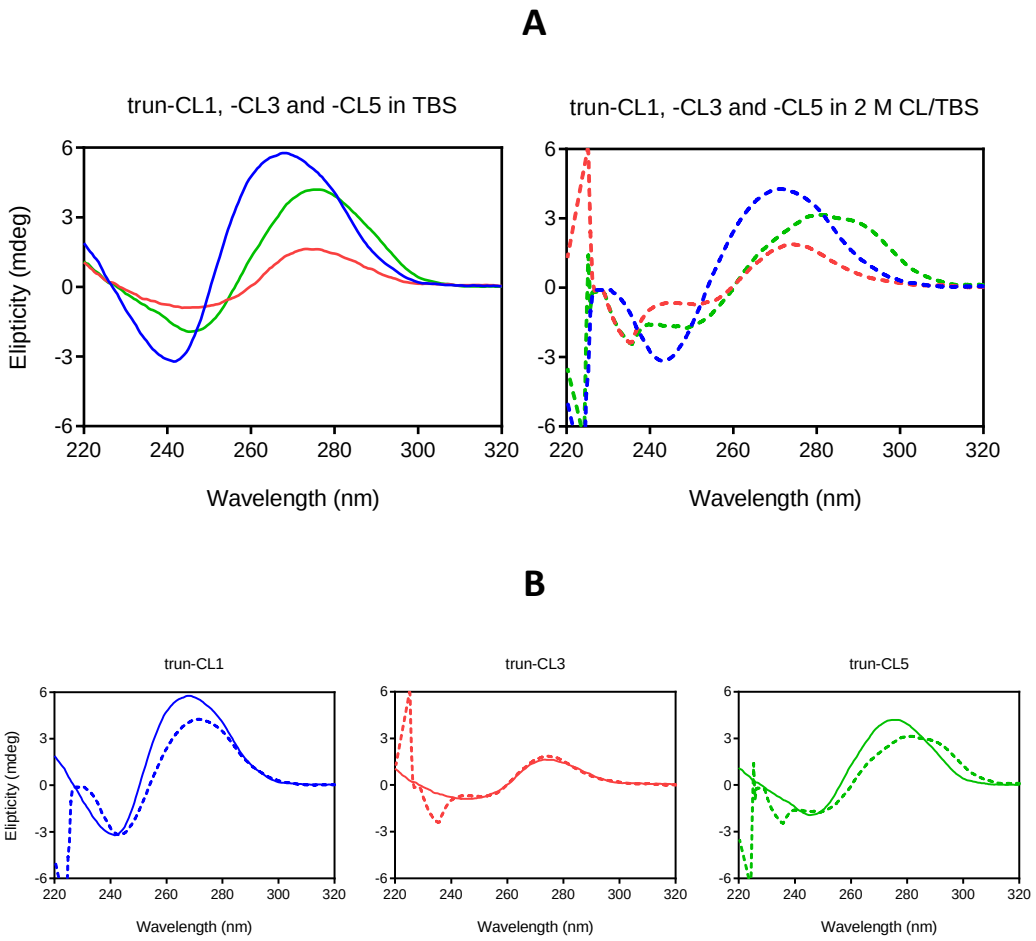

Figure 6.6. (A) CD spectra grouped by TBS or 2 M CL/TBS media. (B) CD spectra grouped by aptamer sequence (**trun-CL1**, **trun-CL3** and **trun-CL5**). DNA concentration in all cases was 5 µM and path length of the cuvette 1 mm, experiments were done in duplicate with negligible differences.

The **trun-CL5** aptamer gave different spectra in TBS media and 2 M CL/TBS media. In case of purely aqueous media, the maximum corresponds to that found in **trun-CL3**, probably due to a formation of a duplex. But when the aptamer is solvated in 2 M CL/TBS media two maxima seem to be overlapped, one at 280 and another one at 290 nm, an unusual spectra but similar to those found in this article[14] that contains an anti-parallel G-quadruplex conformation. Further studies using the individual components of the 2 M CL/TBS media, confirmed that these unusual peaks are only found in presence of the hydrated ionic liquid and moreover, the presence of certain metallic salts of TBS seems to be also necessary (Figure 6.7).

Then, **trun-CL5** was solvated in different media with low hydration levels and TBS components. This was done with the aim of elucidating if choline lactate was participating directly in the function of the new aptamer, or if it was functional due to the reduction of water activity and the presence of certain metallic salts. As can be observed in Figure S6.4, none of the alternative low-hydrated media was able to promote the secondary structure of the **trun-CL5** that was only found in 2 M CL/TBS. It can be observed that in choline chloride and reline the **trun-CL5** formed a double helix that was not perturbed even at very high concentrations, but in ethaline it was partially denatured at 3.4 M, following the thermal stability trend observed in Chapter 3. In case of sodium lactate, probably due to the acidic pH the aptamer did not acquire the same secondary structure as in choline chloride, reline or ethaline media.

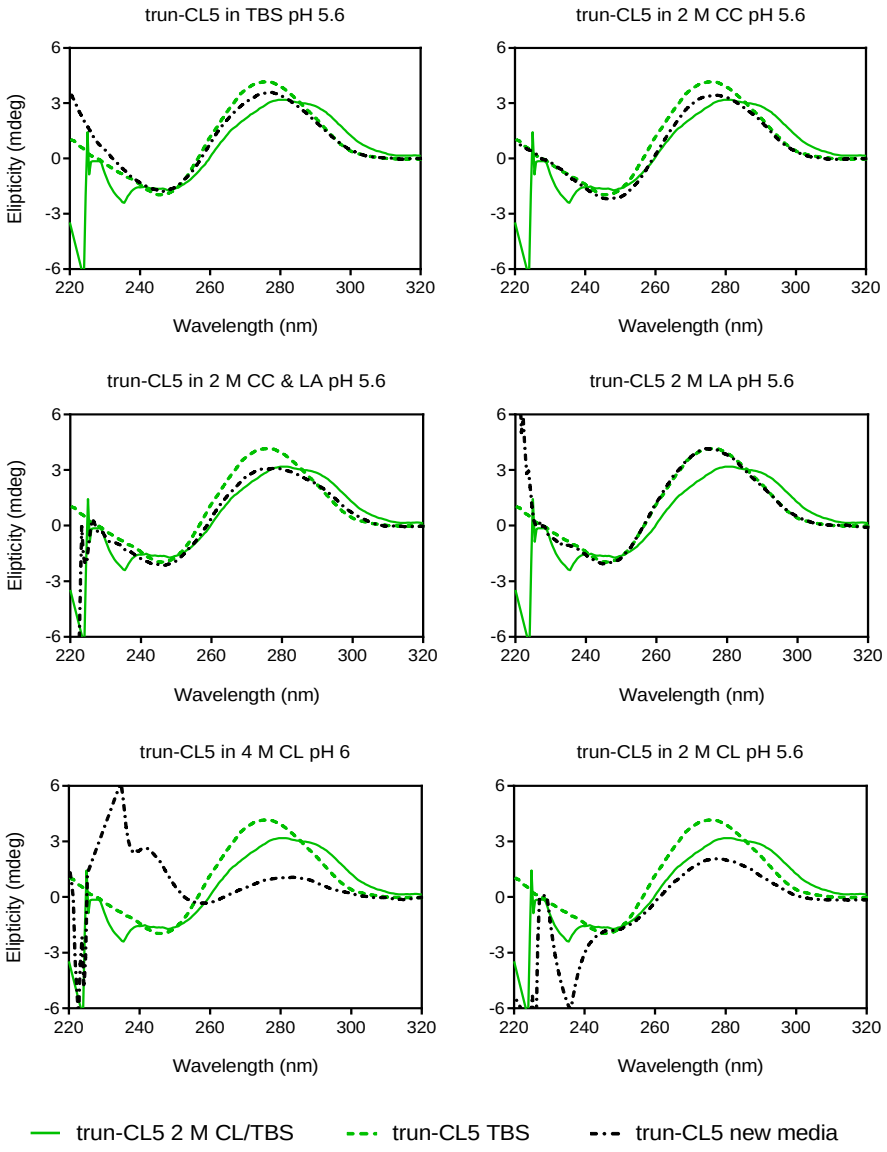

Figure 6.7. CD spectra of trun-CL5 solvated in individual components of the selection media (dotdash lines) using as reference 2 M CL/TBS and TBS. DNA concentration in all cases was 5 µM and path length of the cuvette 1 mm, experiments were done in duplicate with negligible differences.

As has been previously found in other studies[15–17] and Chapter 5, the DNA of samples stored at RT was hydrolysed in physiological media. Interestingly, it was preserved in those samples containing the ionic liquid for up to 10 months with a very small decrease in positive peak intensity (Figure 6.8); however, the loss of the negative peak needs to be studied.

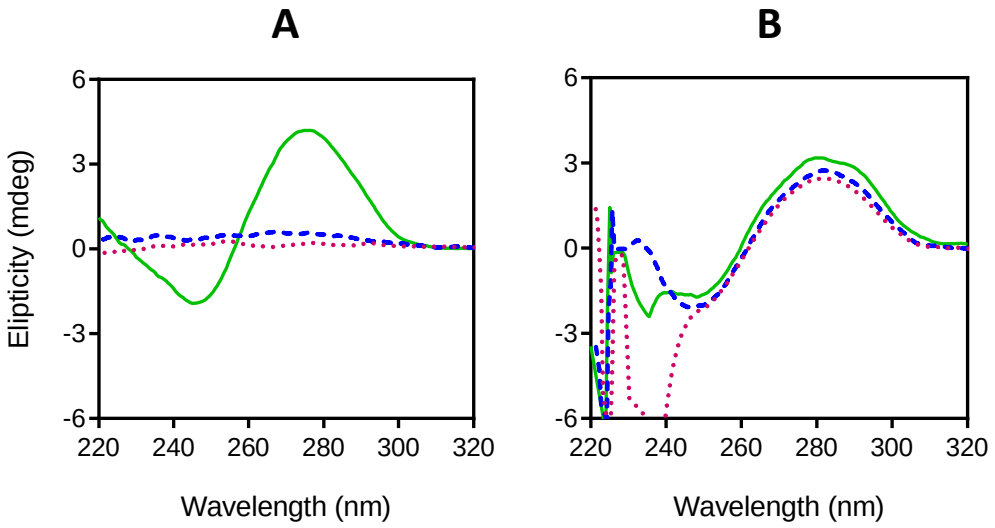

Figure 6.8. Spectra of the two sample of trun-CL5 solvated in TBS (**left**) and 2 M CL/TBS (**right**), after few hours (solid lines), 2 months (dashed lines) and 10 months (dotted lines). DNA concentration in all cases was 5 µM and path length of the cuvette 1 mm, experiments were done in duplicate with negligible differences.

6.3 Conclusions

The enrichment in the positive control SELEX was achieved after eight rounds of selection and the sequences found were in line with those reported by Huizenga and Szostak, validating the selection procedure. In presence of choline lactate, enrichment was observed after twelve rounds and while some sequences comprised the original binding motifs, four entirely different sequences were detected. Radioactive assays confirmed that in presence of choline lactate, two of these four sequences were able to recognize ATP beads with medium-specificity, not recognizing them in TBS media. Even more, the binding percentage of these new sequences (**CL3, CL5 and trun-CL5**) was higher than that of the classic ATP DNA-aptamer in 2 M CL/TBS media.

The results obtained suggest that a versatile functional molecule such as DNA can be used beyond physiological conditions. The selected new aptamers showed secondary structures that are rarely found in aqueous solution and were dependent of the ionic liquid presence but also the metallic salts. The finding of a functional sequence that can form unique interactions with its target, the DNA and non-aqueous media, proves the potential of ILs and DESs to select new DNA-aptamers or DNAzymes for novel nanotechnological uses. Additionally, due to their charged nature the IL controlled the activity of water preserving DNA from hydrolysis.

6.4 References

1. Nakano, S. I., Yamaguchi, D., Tateishi-Karimata, H., Miyoshi, D. & Sugimoto, N. Hydration changes upon DNA folding studied by osmotic stress experiments. *Biophys. J.* **102**, 2808–2817 (2012).

2. Zaks, A. & Klibanov, A. M. Enzyme-catalyzed processes in organic solvents. *Proc. Nat. Acad. Sci. USA* **82**, 3192 (1985).

3. Huizenga, D. E. & Szostak, J. W. A DNA Aptamer That Binds Adenosine and ATP. *Biochemistry* **34**, 656–665 (1995).

4. Lin, C. H. & Patel, D. J. Structural basis of DNA folding and recognition in an AMP-DNA aptamer complex: Distinct architectures but common recognition motifs for DNA and RNA aptamers complexed to AMP. *Chem. Biol.* **4**, 817–832 (1997).

5. Machado, I., Özalp, V. C., Rezabal, E. & Schäfer, T. DNA aptamers are functional molecular recognition sensors in protic ionic liquids. *Chem. Eur. J.* **20**, 11820–11825 (2014).

6. Chaou, T., Vialet, B. & Azéma, L. DNA aptamer selection in methanolic media: Adenine-aptamer as proof-of-concept. *Methods* **97**, 11–19 (2016).

7. Svigelj, R. *et al.* Selection of Anti-gluten DNA Aptamers in a Deep Eutectic Solvent. *Angew. Chemie - Int. Ed.* **57**, 12850–12854 (2018).

8. Zhao, H. DNA stability in ionic liquids and deep eutectic solvents. *J. Chem. Technol. Biotechnol.* **90**, 19–25 (2015).

9. Francisco, M., González, A. S. B., García de Dios, S. L., Weggemans, W. & Kroon, M. C. Comparison of a low transition temperature mixture (LTTM) formed by lactic acid and choline chloride with choline lactate ionic liquid and the choline chloride salt: physical properties and vapour–liquid equilibria of mixtures containing water and ethanol. *RSC Adv.* **3**, 23553 (2013).

10. Schafer, T. & Ozalp, V. C. DNA-aptamer gating membranes. *Chem. Commun.* **51**, 5471–5474 (2015).

11. Yadav, A., Kar, J. R., Verma, M., Naqvi, S. & Pandey, S. Densities of aqueous mixtures of (choline chloride??+??ethylene glycol) and (choline chloride??+??malonic acid) deep eutectic solvents in temperature range 283.15???363.15??K. *Thermochim. Acta* **600**, 95–101 (2015).

12. Fallahbaghery, A., Zou, W., Byrne, K., Howitt, C. A. & Colgrave, M. L. Comparison of Gluten Extraction Protocols Assessed by LC-MS/MS Analysis. *J. Agric. Food Chem.* **65**, 2857–2866 (2017).

13. Karsisiotis, A. I. *et al.* Topological characterization of nucleic acid G-quadruplexes by UV absorption and circular dichroism. *Angew. Chemie - Int. Ed.* **50**, 10645–10648 (2011).

14. Nakano, S., Ayusawa, T., Tanino, Y. & Sugimoto, N. Stabilization of DNA Loop Structures by Large Cations. (2019). doi:10.1021/acs.jpcb.9b06074

15. Vijayaraghavan, R., Izgorodin, A., Ganesh, V., Surianarayanan, M. & MacFarlane, D. R. Long-term structural and chemical stability of DNA in hydrated ionic liquids. *Angew. Chemie - Int. Ed.* **49**, 1631–1633 (2010).

16. Sharma M., Mondal D., Singh N., Trivedi N., B. J. and P. K. High concentration DNA solubility in bio ionic liquids with long lasting chemical and structural stability at room temperature. *RSC Adv.* **5**, 40546–40551 (2015).

17. Clark, K. D., Sorensen, M., Nacham, O. & Anderson, J. L. Preservation of DNA in nuclease-rich samples using magnetic ionic liquids. *RSC Adv.* **6**, 39846–39851 (2016).

6.5 Supplementary information

Figure S6.1. Enrichment studies of first SELEX done in aqueous media using (A) 0.1 mg/mL or (B) 1 mg/mL of salmon-sperm during the assays. Percentages of ^{32}P-DNA obtained in each step of the assay (**S**: Supernatant; **W1**: Washing 1; **W2**: Washing 2; **E**: Elution; **B**: Beads).

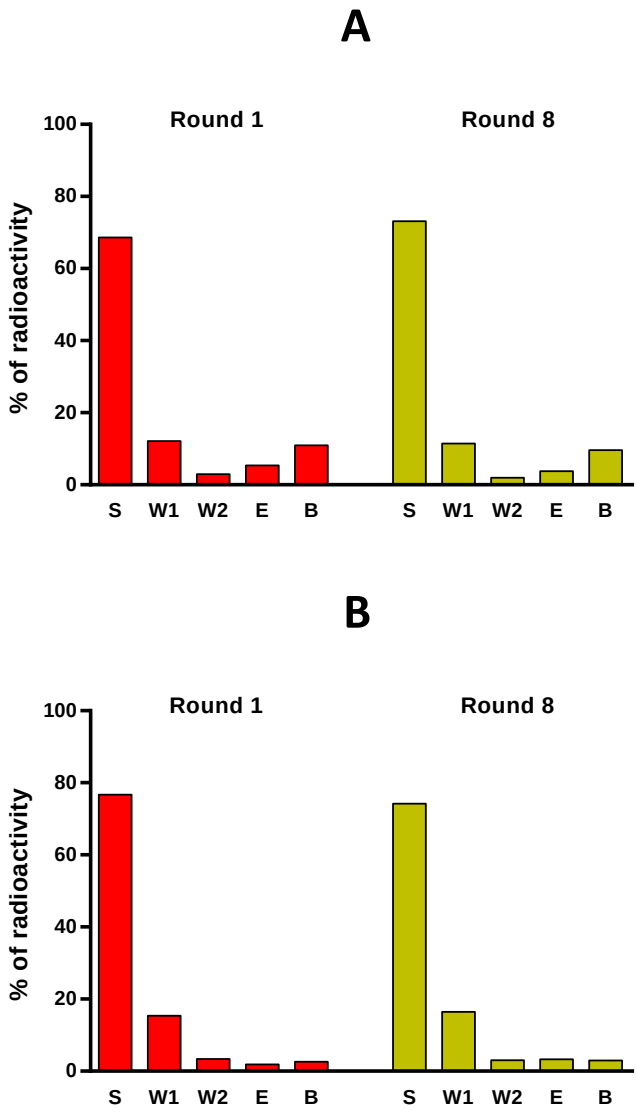

Figure S6.2. Alignments made by the bioinformatic software MUSCLE of the sequences obtained when using (A) TBS and (B)(C) 2 M CL/TBS. The asterisk below the sequences represent the only nucleotides, which are common for all the sequences in the groups.

A)

```
B01 ------------------CGGGGGAGAGC------------TTTTTTGGCGCGGCGGAGTTCCTAAGGATTAA------
B02 GCGGCTATG---------TGGAGGAGGTT------------TTCGCTATACCGGGGGAATATA----------------
B03 ---GATAAGCTTCTATACCGGTGGAGGAA-----------------TATAATGGGGGAGCCGA----------------
B04 --------GCGCCCATTATGGGGGAGGTA---------------CCATTACCGGAGGAATATTGTG-------------
B05 ACTTAGACAAGTATACAACGCGGGGGAAC---------------CTGTTCGTGGAGGA----------------------
B06 ---------------CATCGGGGGAGTTA-----------TAGTGTAATGGCGGAGAGGTTGACAGAAG----------
B07 -------------GTAGACGGGGGAGAAA----------TTTATCAAATTTCGGAGGAGTTACCTAC------------
B09 -----------------CCGGGGGAGGATATCCCCCAGATTCTGGGATTTCCGGAGGAGG-------------------
B10 ---------------ACGCGGGGGAGGGC-------------TAAGACGCCTGGAGGAGCTTTGCTAGATC--------
B11 -GGGATATAATGCACAACCGGGGGGAAGCA---------------------ATGGAGGAGGTTGCG--------------
B13 ----------TCAGTACCGGGGGGAGGT-----------------TAGGCGGAGGGAGGGACTAAGGATC-------
B16 ------------------CGGGGGAGAAC-----------------TAATCGGAGGAGGGGCATAAGTTTGAGGATAC
                       *  **                          ** *
```

B)

```
I22 --------------------CAGTCGGGGGAGAGG---------------TACGGAGGAGACGTATTTACACTAGAAGCA
I23 -----------CTGCAACCAAGTCGGAGGAGATTC-------------ATCGGGGGAGACCTGTGTC------------
I24 --------------ATGCAACAACCGGAGGAGCG---------------CGCGGGGGAGGGTATTGTCGAGT--------
I27 --------------TTACATCTTCGGGAGGAGTATTTTAG---------ACGGGAGGAGAAGATTT--------------
I28 GGACGTCACCGAAAGATCATGTGCCGGAGGAGG----------------GACGGGGGAG--------------------
I29 ----------CTCCCGTTGTGGCTCGGGGGAGAGGA-------------TTCGGAGGAGAGCCGAG--------------
I30 --------------------AGTCGGAGGAGGCTGTAGTAACCTACACACCGGGGGAGAATTA----------------
I31 --------------TCATCCATATTCAAGGTGACTCCAGC--------CCTCGGCGGTGTTGTGA---------------
I32 ----------------------GCGGGGGAGCCCAAGGT---------GGCGGAGGAG----CTCGCAAGGGGATCAA
I33 --------------------TTGCGGAGGAGAGTA-------------CTCGGGGGAG--CAATTCCACGTAAGTCGA
I36 ----------------------ACAGAAGAGCAGT-------------CGCGGGGGAGTAGCCTTTGCGGACGGAGGA
I37 -ATCTGCGACGAAGATACATGCCGCGGGGGAGAGA--------------CTCGGAGGA----------------------
                              * *                     ** **
```

C)

```
I21 ----------------------TACATCTATCCTTCTACTCTCACTTTTTAAGGGACCCCAAGTG-------------
I25 ----------------GGTGGAGTCA-------GTCGCATCAGTCACTTTAGGAAGTTAC--------------------
I26 GATGTAAGCATAGTGAATAGAAACCACGTTGAGGACGCGGCGC-----------------------------------
I38 ------------TGACTCCAAGCCAGGGTGTTGCCGTAGTCGGCGCGTGTGAAAT-----------------------
                           *
```

Figure S6.3. An example of the PAGE experiments done with radioactively labelled ssDNA to validate kinasation protocol.

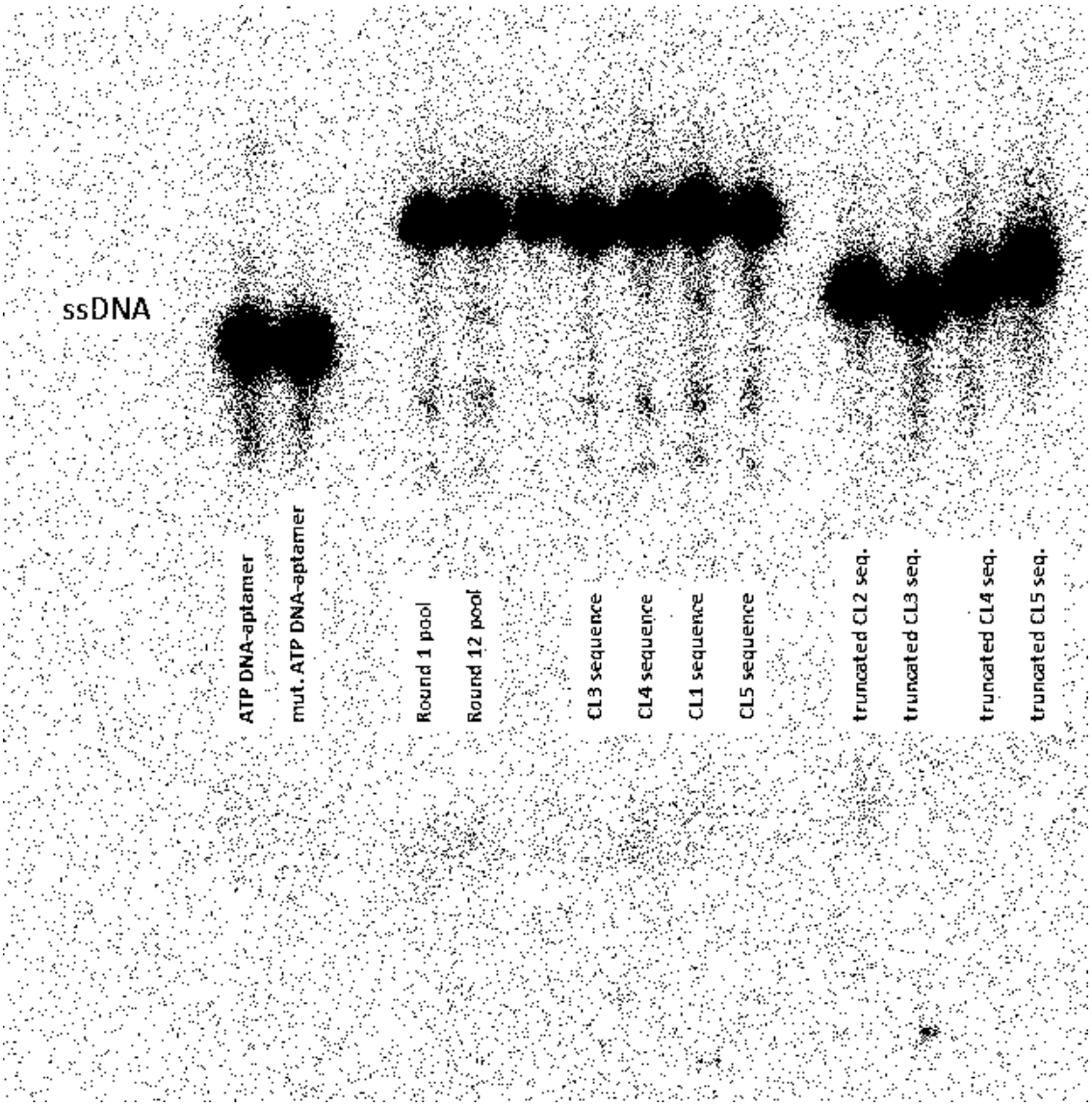

Table S6.1. Percentages obtained in each step of the binding assays of Figure 6.3.

		A		B	
		Mean %	SD	Mean %	SD
R1	*S*	80,0	3,7	85,8	0,9
	W1	5,5	2,1	5,6	0,7
	W2	1,8	0,9	1,2	0,1
	E	11,1	0,8	6,6	0,1
	B	1,6	0,3	0,8	0,0
R12'	*S*	54,7	7,0	61,2	5,2
	W1	5,1	0,2	3,2	1,4
	W2	3,5	0,6	1,1	0,2
	E	33,8	5,6	29,0	1,1
	B	2,8	0,9	5,6	2,5
CL1	*S*	51,5	5,5	31,3	3,2
	W1	5,6	0,4	1,8	0,1
	W2	5,2	0,3	1,0	0,1
	E	35,2	4,2	61,0	1,7
	B	2,5	0,5	4,9	1,4
CL2	*S*	78,2	2,0	88,5	0,7
	W1	4,2	0,1	4,2	0,5
	W2	1,3	0,1	0,9	0,1
	E	14,6	1,8	5,6	0,0
	B	1,7	0,3	0,9	0,2
Cl3	*S*	38,5	6,0	87,4	0,5
	W1	2,2	0,3	7,2	0,0
	W2	1,7	0,4	1,0	0,1
	E	54,6	5,4	3,6	0,5
	B	3,0	0,2	0,8	0,1
CL4	*S*	48,9	2,9	70,7	4,1
	W1	5,7	1,0	3,9	0,2
	W2	4,6	0,1	1,3	0,1
	E	37,5	1,8	22,0	2,8
	B	3,3	0,4	2,1	1,0
CL5	*S*	50,9	5,1	87,6	0,1
	W1	4,5	0,6	6,8	0,2
	W2	3,7	0,7	1,1	0,0
	E	37,6	3,5	4,0	0,1
	B	3,3	0,4	0,5	0,0

Table S6.2. Percentages obtained in each step of the binding assays of Figure 6.4.

		A			
		Mean %	SD		
mutated-ATPapt	S	71,3	5,0		
	W1	18,5	4,0		
	W2	4,7	0,5		
	E	4,9	0,4		
	B	0,5	0,1		
ATPapt	S	46,7	3,8		
	W1	15,7	0,6		
	W2	10,6	0,5		
	E	24,5	3,3		
	B	2,6	0,5		
trun-CL2	S	85,1	0,5		
	W1	5,3	0,5		
	W2	1,5	0,1		
	E	7,5	1,0		
	B	0,6	0,1		
trun-CL3	S	83,8	0,2		
	W1	5,9	0,1		
	W2	2,8	0,2		
	E	6,7	0,2		
	B	0,9	0,1		
trun-CL4	S	88,9	1,5		
	W1	6,5	1,5		
	W2	1,4	0,3		
	E	2,3	0,2	**B**	
	B	1,0	0,2	Mean %	SD
trun-CL5	S	43,9	0,4	86,5	1,1
	W1	4,9	0,5	6,4	0,6
	W2	4,0	0,2	1,5	0,1
	E	42,9	0,7	5,1	0,3
	B	4,4	0,5	0,5	0,1

Table S6.3. Percentages obtained in each step of the binding assays of Figure 6.5

		Target: γ-ATP		**Target: γ-GTP**	
		Mean %	SD	Mean %	SD
R1	*S*	83,4	0,1	84,4	1,7
	W1	4,5	0,1	4,8	0,2
	W2	1,3	0,1	1,4	0,1
	E	7,4	0,6	6,7	1,1
	B	3,4	0,7	2,7	0,9
R12'	*S*	76,0	2,4	88,7	1,7
	W1	4,7	1,4	4,2	1,0
	W2	3,5	0,3	1,1	0,3
	E	9,4	0,6	4,1	0,2
	B	6,5	1,3	1,9	0,6
CL1	*S*	68,5	3,3	90,2	0,2
	W1	7,6	1,2	4,4	0,1
	W2	4,8	0,3	0,9	0,1
	E	11,2	2,0	3,0	0,1
	B	7,9	0,1	1,6	0,1
CL2	*S*	83,9	3,3	81,5	0,9
	W1	2,6	0,1	3,2	0,2
	W2	1,0	0,2	1,2	0,1
	E	7,5	1,5	10,1	1,6
	B	5,1	1,5	4,0	0,5
CL3	*S*	89,5	1,0	90,7	1,2
	W1	3,8	0,1	3,1	0,3
	W2	1,0	0,3	0,8	0,2
	E	3,8	0,4	3,9	0,3
	B	2,0	0,1	1,5	0,5
CL4	*S*	83,9	1,2	87,3	1,6
	W1	5,4	0,5	4,4	0,3
	W2	2,5	0,0	1,2	0,2
	E	5,0	1,2	4,7	0,5
	B	3,1	0,6	2,5	0,6
CL5	*S*	71,1	6,9	88,2	0,7
	W1	8,9	2,9	2,4	0,7
	W2	5,0	1,8	0,8	0,0
	E	9,5	2,6	6,4	0,0
	B	5,4	0,4	2,1	0,1

Figure S6.4. CD spectra of trun-CL5 solvated different media (dashed and dotdash lines) and in 2 M CL/TBS (solid line) as reference.

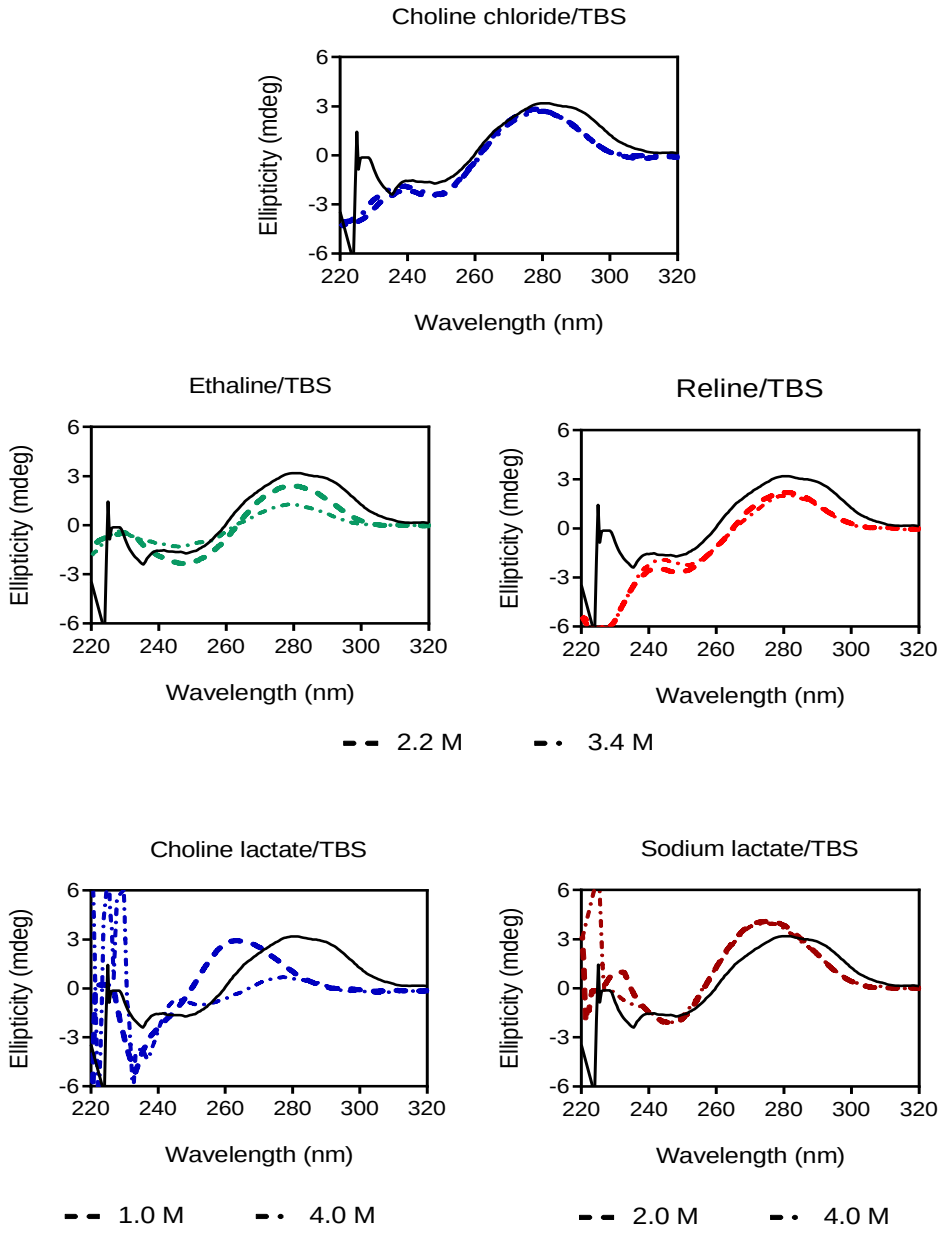

CHAPTER 7

Self-assembly and stimuli-responsiveness of DNA nanostructures

7.1 Introduction

DNA can be used to create stimuli-responsive nanostructures[1]. In order to achieve this, the DNA structures need a dynamic behaviour upon changes in the bulk phase or local stimuli. The bulk stimuli are usually related with changes in the pH, temperature, light or redox reactions[2]. On the other hand, the local stimuli are usually complementary DNA sequences or molecular targets. Functional nucleic acids such as DNA-aptamers are necessary to recognize the latter. These DNA-aptamers can interact non-covalently with the desired molecule and change their conformation or disengage from the nanostructure.

Among other uses, the accurate control of the recognition events can allow the opening or closing of porous materials[2–5]. The main challenges consist in achieving an appropriate sensitivity, specificity, reversible function and proper kinetics for the desired application[6]. Such stimuli-responsive designs can be used on nanoporous membranes, as they can act as modular building blocks combined with the mechanically resistant inorganic or polymeric support. Then, these designs can be applied in drug delivery, logic gates or sensing applications[7]. In this work, the focus will be put on the build-up and disassembly of a DNA nanostructure known as "supersandwich" that has sensing and gating applications and is based-on the traditional sandwich assay.

The traditional sandwich concept is used for peptide and nucleic acid based sensor assays due to their analytical sensitivity and specificity[8–10]: it consists of three different probes. Firstly, a capture probe is used to be immobilized onto the surface; secondly, there is a target probe which will be recognized by the capture probe, and thirdly there is a signal probe, able to

cause a response-signal in the system. Early, the signal probe was radioactively labeled[11] and then, other labels were proposed, such as fluorophores, redox molecules, enzymes or nanoparticles[12]. Moreover there also label-free techniques such as the quartz crystal microbalance (QCM)[13], the surface plasmon resonance (SPR)[14] or the microcantilever[15] that can provide simple and fast assay procedures. But, these traditional sandwich assays sometimes show an important limitation: each target binds to only one signal probe and there might not be enough receptors to obtain a reliable response.

To address this limitation, it was decided to build more receivers vertically, as the surface area is limited but the height can be significantly large. In the case of peptides, the creation of a vertical nanostructure is more complicated, but using the double helix structure of DNA and hybridization between complementary strands, it seems relatively straightforward. There are different supersandwich designs, but in essence, they are formed by a repetition of chains that act as a bridge and others that are capable of recognizing the target molecule (signal probes) (Figure 7.1). These kind of designs have enabled, in example, the detection of mercury by DNAzymes[16] or the recognition of a wide variety of targets using DNA-aptamers[329].

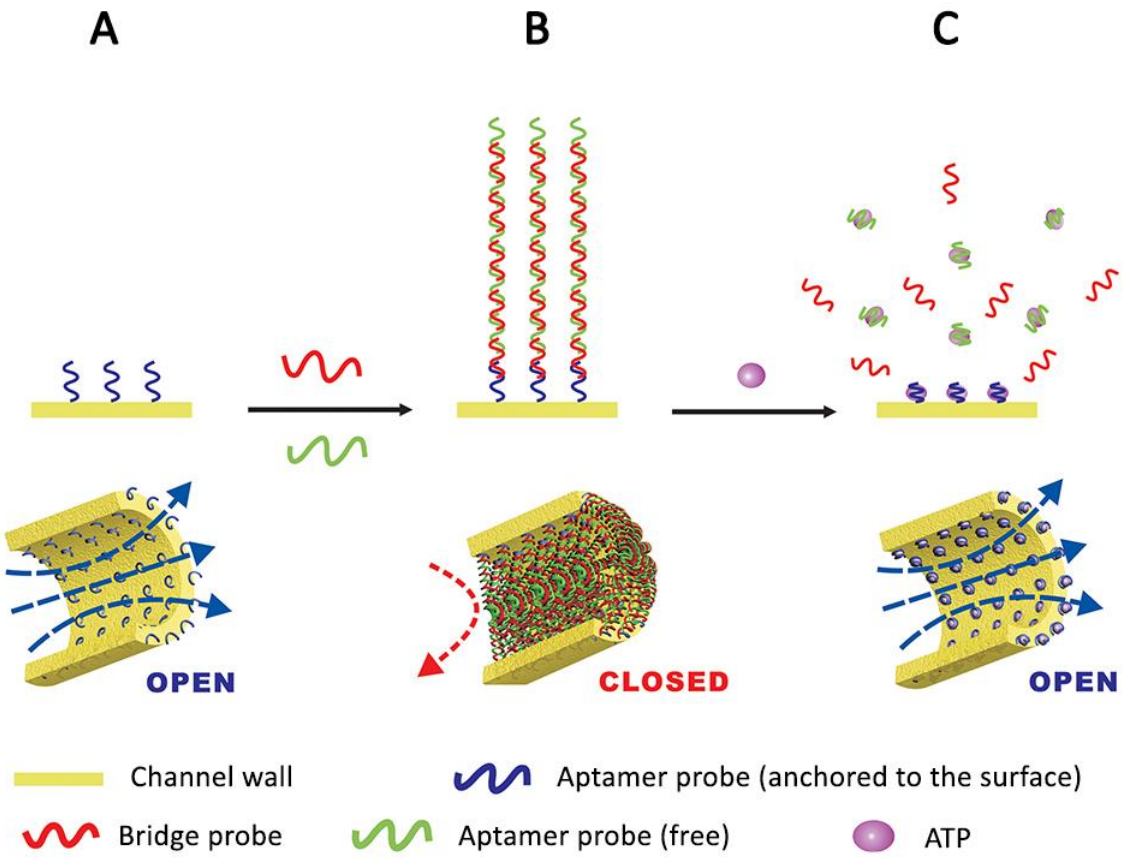

Figure 7.1. Scheme of the so-called ''DNA Supersandwich Structure''. Adapted with permission from ref. 17.

Apart from sensing using solid supports, these supersandwich nanostructures have been used in porous systems. In a design used in various studies[17–21], in absence of a molecular target, the structures self-assemble closing the pores of the inorganic support (Figure 7.1B) and upon exposure to the molecular target, the structures disassemble, opening the pores (Figure 7.1C). However, so far, the evidences have been acquired using voltammetry, which does not give information about the molecular events at the nanoscale.

In these supersandwich structures, the signal probe (also called aptamer probe) is forming a double helix with two bridge probes and this interaction is energetically more favorable than that of the molecular target (usually ATP or AMP). Therefore, although there does appear to be a response to the target molecule, it is not yet clear whether this is actually due to recognition of the molecule or due to changes produced by high concentrations of the molecule in the bulk phase.

Moreover, the supersandwich is supposed to have multiple bridge and aptamer probes, but there is no evidence of how long it really can be or the static stability of the nanostructure. In order to answer these questions and gain insights into the target recognition capacity of the DNA-aptamers when they are part of a nanostructure, in this study the supersandwich is monitored on-line by surface plasmon resonance (SPR) and quartz crystal microbalance with dissipation monitor (QCM-D). On the other hand, the use of non-physiological conditions is proposed as a strategy to not only prevent DNA degradation or solvent evaporation, but also increase the stimuli-responsiveness of the nanostructure.

7.2 Results and Discussion

7.2.1 Design of the layer-by-layer supersandwich build-up

In order to observe real-time kinetics of a DNA nanostructure, a supersandwich structure containing the ATP DNA-aptamer was built in SPR instrument. This supersandwich consists in a bridge probe (**BP**) and an aptamer probe (**AP 1**) able to recognize adenosine-based targets. The aptamer is equal to that studied in Chapter 5; the sequences are shown in Table 7.1.

Table 7.1. The DNA sequences used in this chapter.

Name	**Sequence 5' to 3'**
Capture probe 1 (**CP 1**)	CGG CAC CTG GGG GAG TAT TGC GGA GGA AGG TGC CG (5': Biotin-C6)
Capture probe 2 (**CP 2**)	TTT TTT TTT TTT TTT GCG GAG GAA GGT GCC G (5': Biotin-C6 or thioctic acid)
CP ATP DNA-aptamer (**CP ADA**)	ACC TGG GGG AGT ATT GCG GAG GAA GGT (5': Biotin-C6)
Bridge probe (**BP**)	TAC TCC CCC AGG TGC CGA CGG CAC CTT CCT CCG CA
Aptamer probe 1 (**AP 1**)	CGG CAC CTG GGG GAG TAT TGC GGA GGA AGG TGC CG
Aptamer probe 2 (**AP 2**)	AC CTG GGG GAG TAT TGC GGA GGA AGG T
Bridge probe mut 1 (**BP mut 1**)	TAC TCC CCC AGG TGC CGA CGG CAC CTT CCT CGG CA
Bridge probe mut 2 (**BP mut 2**)	TAC TCC CCT AGG TGC CGA CGG CAC CTT CCT CGG CA
Bridge probe mut 3 (**BP mut 3**)	TAC TCT CCT AGG TGC CGA CGG CAC CTT CCT CGG CA

The building process can be done using the one-step method (Figure 7.2A) or layer-by-layer (Figure 7.2B). The former method creates a highly polidisperse nanostructure as verified by gel-electrophoresis and GPC/SEC (Figure 7.3 and Figures S7.5 and S.7.6), therefore we tried with the latter hypothesizing that it would increase the control of the build-up process.

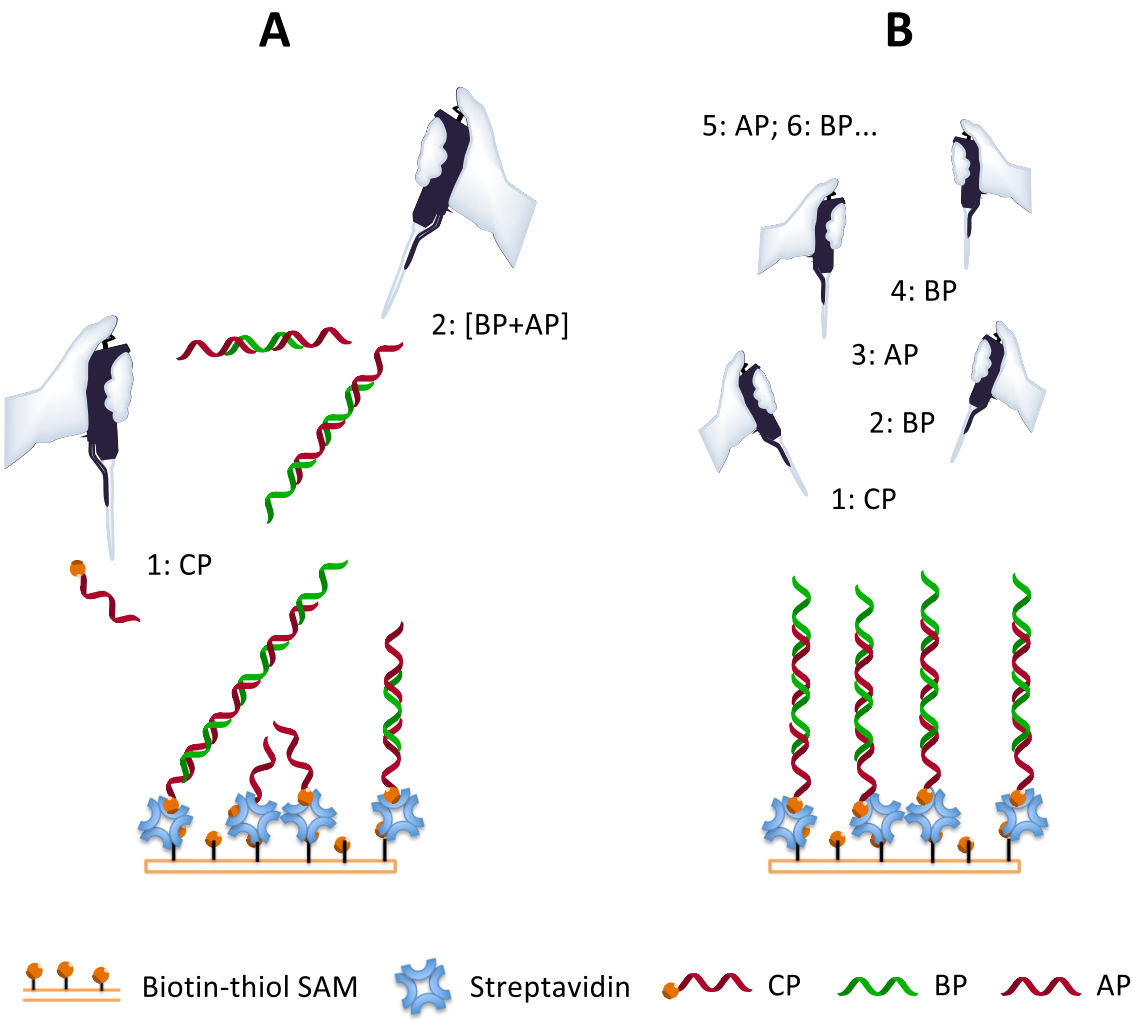

Figure 7.2. (A) One-step self-assembly build-up. (B) Layer-by-layer build-up.

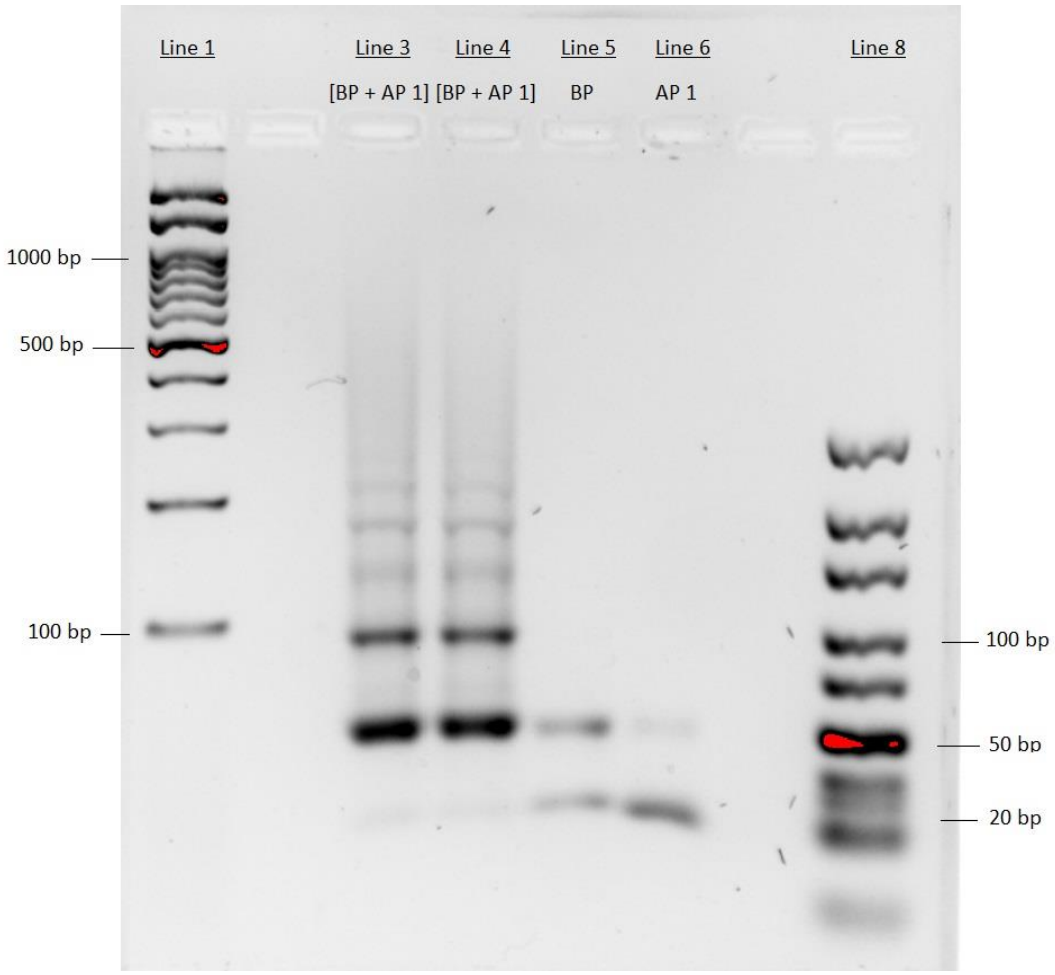

Figure 7.3. Three wt. percentage agarose gel electrophoresis. 90V 60 min. **Line 1**: 3000 bp ladder. **Lines 3 and 4**: 1 µM of **BP** and **AP 1** after being 24 hours mixing at RT. **Line 5**: 1 µM of **BP**. **Line 6:** 1 µM of **AP 1**. **Line 8**: 300 bp ladder.

In order to create the nanostructure in the sensorchip using the layer-by-layer method, firstly, it was necessary to immobilize covalently the first DNA layer (Figure 7.2B), this was named as capture probe 1 (**CP 1**; 11480 g/mol) and is equal to **AP 1** but modified with biotin that forms very strong interactions with streptavidin. After immobilizing **CP 1** (710 RU). The second layer, the bridge probe (**BP**; 10550 g/mol) was injected to the channel containing **CP 1**, obtaining a

maximum response of 600 RU (Figure 7.4A). Therefore, approximately the 85% of **CP 1** hybridized with the **BP**. Then, the third layer consisted on the aptamer probe 1 (**AP 1**; 10959 g/mol), that was injected to hybridize with the **BP**, but surprisingly there was no increase in the response (Figure 7.4B). While analyzing why this could happen, it was found that the upper half of the **BP** was able to hybridize with the bottom half of another **CP 1**.

This was undoubtedly a design flaw: by using the same supersandwich that was already published, we did not stop to think about possible unwanted structures. The problem arose from using the layer-by-layer method instead of the one-step method and showed the need to study in detail all possible interactions between chains when constructing the supersandwich. A modified capture probe was used in order to solve this issue and continue building-up the structure: the capture probe 2 (**CP 2**; 10013 g/mol) (Table 7.1).

The bottom half of **CP 2** has thymine nucleotides to avoid the possible hybridization with the upper part of **BP**. This **CP 2** was immobilized in the chip until 560 RU. The response after injecting **BP** was 560 RU (Figure 7.4A), obtaining in this case a 100% hybridization efficiency, probably because there was a lower capture probe density on the chip. Then, as expected, while injecting the **AP 1** there was a significant response (Figure 7.4B) and this confirmed that previously the bottom part of **CP 1** was interacting with the upper half of **BP** preventing the latter to hybridize with **AP 1**.

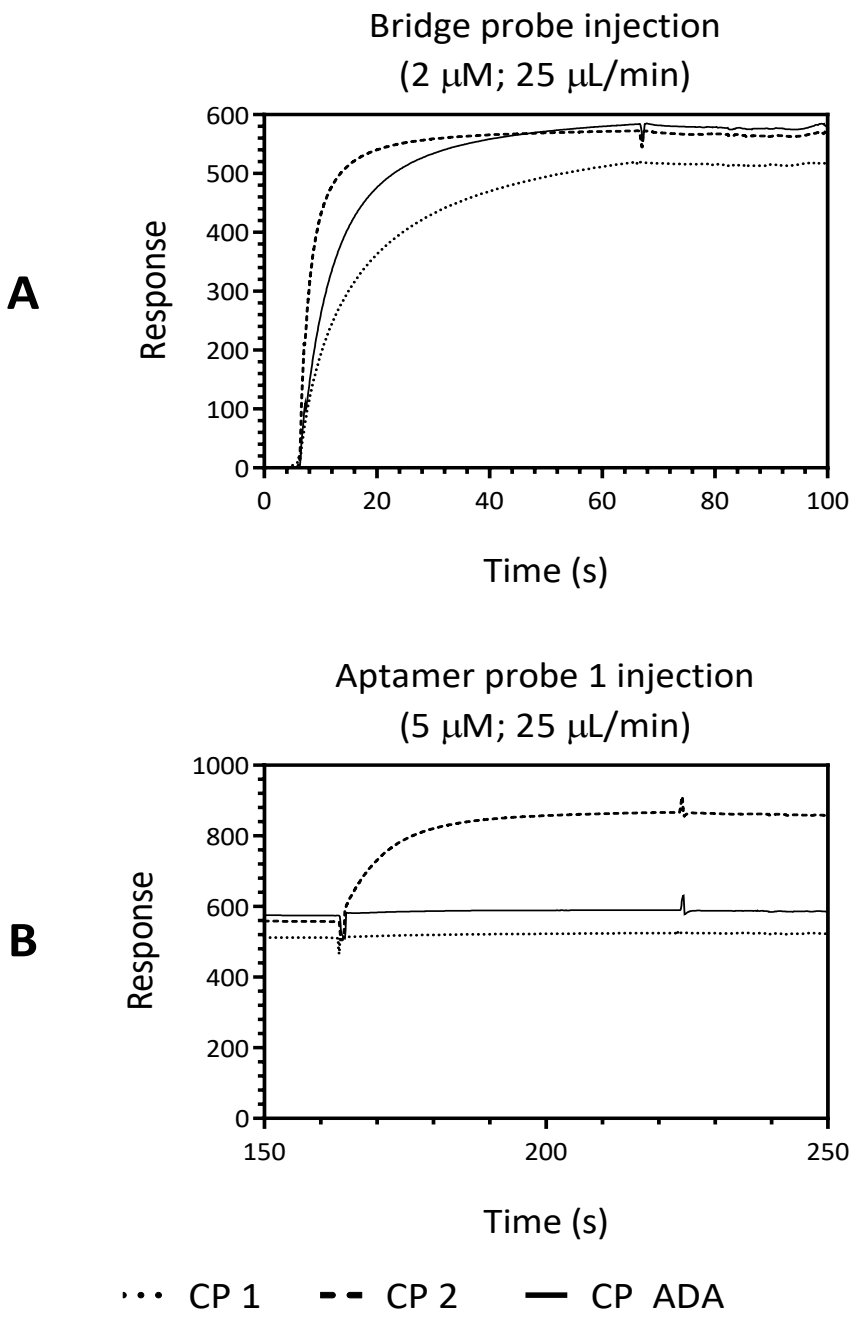

Figure 7.4. Response curves upon (A) injection of bridge probe to different capture probes or (B) injection of **AP 1** after the previous **BP** injections.

Respect to kinetics, there were clear differences in the K_{on} of bridge probe, depending on the capture probe used (Figure 7.4A). The hybridization kinetics between **CP 2** and **BP** were faster than those between **CP 1** and **BP**. The differences are caused because the **CP 1** (= **AP 1**), in absence of **BP**, forms a hairpin or interacts with other **CP 1** (observed in GE of Figure 7.3). This needs to be disrupted. In the other case, **CP 2**, it cannot acquire any stable hairpin conformation. This was verified using another capture probe named as ATP DNA-aptamer capture probe (**CP ADA**; 9006 g/mol), which instead of forming a hairpin of eight base pairs, forms it with four base pairs.

As could be expected, the K_{on} was faster than that found with **[CP 1 + BP]** but slower than that of **[CP2 + BP]** (Figure 7.4A). It was also possible to quantify the dissociation constant values between the capture probes and the bridge probe injecting the **BP** at different concentrations (Figure S7.1). The lowest K_d value was that obtained while injecting **BP** to **CP 2** (0.06 ± 0.02 μM). The second capture probe with highest affinity was **CP ADA** with a K_d of 0.13 ± 0.01 μM, and as could be expected due to the need of breaking the 8 base pair hairpin, **CP 1** had less affinity with a K_d of 0.25 ± 0.01 μM. On the other hand, both, **BP** and **AP 1** had a negligible K_{off} while being hybridized in 500 mM aqueous media denoting that the nanostructure could remain stable for long-periods (without considering hydrolysis) in absence of the target.

Even if it was possible to create the third layer of the supersandwich **[CP 2 + BP + AP 1]**, the response of the latter layer had a value of 290 RU what supposes that approximately only the 50% of **AP 1** hybridized to the **BP** (Figure 7.4B). This could be due to the hairpin of eight base pairs that **AP 1** forms, what limits its affinity towards **BP.** To verify this, the supersandwich was

built using the aptamer probe 2 (**AP 2**; 8775), equal to the **CP ADA**, with a hairpin of four base pairs. The strategy of reducing the stability of the aptamer probe succeeded and the hybridization efficiency of **[BP + AP 2]** was again close to 100%, in contrast with the lower efficiency obtained between **[BP + AP 1]** (Figure 7.5A and 7.5B).

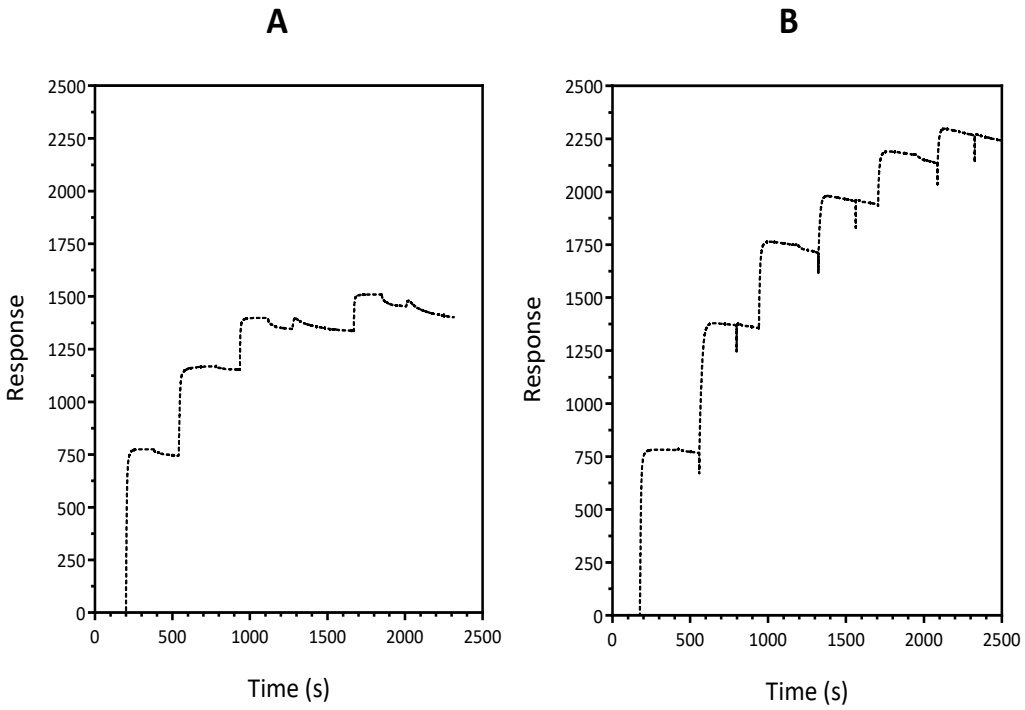

Figure 7.5. Response curves of supersandwich containing (A) **[CP 2 + (BP + AP 1)$_2$]** or (B) **[CP 2 + (BP + AP2)$_2$]**. The flow rate was of 25 µL/min and the concentration of bridge and aptamer probes, 2 and 5 µM, respectively.

With the system of **[CP 2 + BP + AP 2]**, the nanostructure would already have a length of 21 nm, assuming a rigid lineal double helical conformation. It was possible to build more layers maintaining an adequate structural stability, but it was not possible to maintain the 100%

hybridization efficiency in all of them (Table 7.2), what could mean that the steric and electrostatic effects limit the scalability of a well-defined supersandwich.

Before studying the disassemble of the supersandwich, the layer-by-layer design that consisted in **CP 2, BP** and **AP 2**, was also studied in a gold sensorchip in QCM-D, in order to elucidate if the construction was reproducible. The QCM-D technic is a very appropriate complementary technic that enables calculating the surface coverage and the viscoelastic properties of the supersandwich. The capture probe modified with thioctic acid caused a frequency change of 43 Hz, what supposes an approximate surface coverage of 765 ng/cm^2 (0.52 molecules/nm^2).

Previously, in SPR, it was observed that the modified layer-by-layer supersandwich was able to create multiple layers, but with a reduced hybridization efficiency after the second aptamer probe (five layers), probably due to steric and electrostatic effects (Figure 7.5B). While constructing the supersandwich on the gold sensorchip the first **BP** had a low hybridization efficiency, probably due to an excessive surface coverage. However, the reduction of hybridization efficiency after more layers than in SPR (Table 7.2 and Figure 7.6A). In any case, the approximate length of 25 nm (four layers) was the limit before losing the hybridization efficiency between probes. It can be observed that the efficiency decreased specially when **BP** was injected. Probably the **BP** did not bind to **AP 2** very efficiently because **BP** could form a dimer with another **BP** free in solution. The media was in all cases an aqueous buffer containing NaCl at 0.5 M.

Table 7.2. Different frequency and response values obtained with the supersandwich formed by [**CP 2 + BP + AP 2 + BP + AP 2 + BP**] and the hybridization efficiency (%).

	SPR			QCM-D		
	Resp. (RU)	Increase	Hybrid.	Freq. (Hz)	Increase	Hybrid. %
CP 2	0	780		-42	42	
BP	750	750	100 %	-66	24	60 %
AP 2	1375	625	100 %	-92	26	120 %
BP	1735	360	48 %	-124	32	100 %
AP 2	1965	230	76 %	-143	19	72 %
BP	2100	135	48 %	-159	16	70 %

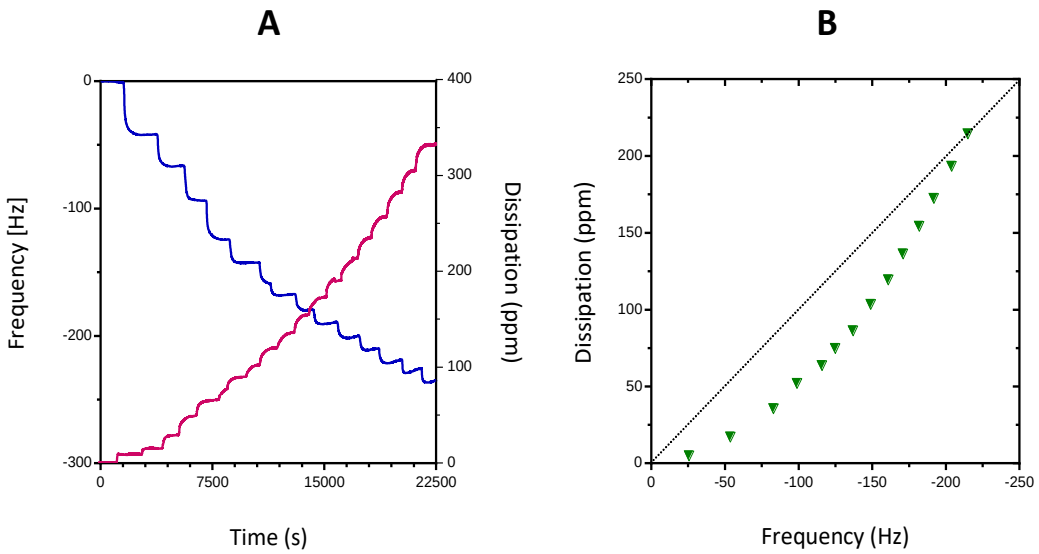

Figure 7.6. (A) Frequency and dissipation curves obtained in QCM-D upon immobilization of **CP 2** and consecutive injections of **BP** and **CP 2**. (B) Representation of the dissipation *versus* frequency values obtained in each layer of the supersandwich.

Regarding the viscoelastic properties of the built nanostructures, as can be seen in Figure 7.6B, the relationship between frequency and dissipation was linear in the first layer but then it seems that the structure acquired a more plastic behaviour in case of the gold sensorchip. However, this should be better studied with complementary technics.

7.2.2 Disassembly of the supersandwich by molecular target recognition

Apart from the build-up process of a nanostructure, its stimuli-responsiveness is of great importance. The capacity of the aptamer to recognize the adenosine-based molecules was firstly studied with binding assays between the capture probe and targets. For this purpose, the adenosine-based molecules were injected to channels containing the different capture probes, guanosine-based molecules were also used as negative probe (Figure S7.2). These experiments were similar to those of Chapter 5, but in this case the physiological media had 0.5 M of NaCl instead of 0.14 M.

The dissociation constants of **CP 1** (equal to **AP 1**) and **CP ADA** (equal to **AP 2**) towards ATP were 30 µM and towards AMP ≈ 75 µM (Table 7.3). **CP 2** was not able to recognize any target because the recognition site was partially replaced by thymine nucleotides. In case of adenosine target, it did not saturate the capture probes, probably because it bound non-specifically, therefore this target should be discarded for stimuli-responsiveness purposes. From these measurements, it can be concluded that in theory, it will be difficult for ATP or AMP to compete with the bridge probe, because the K_d of **AP 1** and **AP 2** towards **BP** ranged between 0.13 and 0.25 µM (Figure S7.1), more than 100 fold lower than the dissociation constant towards the molecular targets.

Table 7.3. Calculated dissociation constant and maximum RU values obtained upon addition of each target in aqueous buffered solution with 500 mM of NaCl.

Capture probe	**Dissociation constant** (μM) and **Max. Response** (RU)					
	ATP		**AMP**		**Adenosine**	
CP 1	30 μM	40 RU	70 μM	27 RU	-	28 RU
CP 2	-	-	-	8 RU	-	10 RU
CP ADA	30 μM	35 RU	75 μM	25 RU	-	22 RU

The latter was confirmed injecting the **BP** to the channel containing the capture probes already in presence of molecular targets (Figure S7.3). Their presence reduced the hybridization kinetics but did not prevented the **BP** to hybridize with the capture probes. On the other hand, using the contrary strategy, the targets were injected with **CP 1** already hybridized to **BP**. In theory, published studies stated that the hybridization between these two probes are disrupted in presence of 1 mM of ATP or AMP, opening the pores[17], but it was observed that the AMP did not affect the hybridized probes (Figure S7.4).

This inefficacy of the target to disrupt the duplex between the **CP 1** and **BP** was not surprising due to the strong interaction between the latter two. Therefore, the experiments were repeated but increasing the concentration of AMP until 4 mM (Figure S7.4), far above from the reported value. At the highest concentration, it was possible to disrupt the hybridization between **CP 1** and **BP**, being a specific response, because it did not happened with adenosine or GMP.

The latter was further verified with a supersandwich containing multiple layers. Nevertheless, observing that the steric impediments and electrostatic repulsions decreased the ability of aptamer probes to recognize ATP or AMP and disassemble the supersandwich: it was necessary to inject AMP at 30 mM in order to obtain a significant change in the K_{off} of a supersandwich with four layers (Figure 7.7).

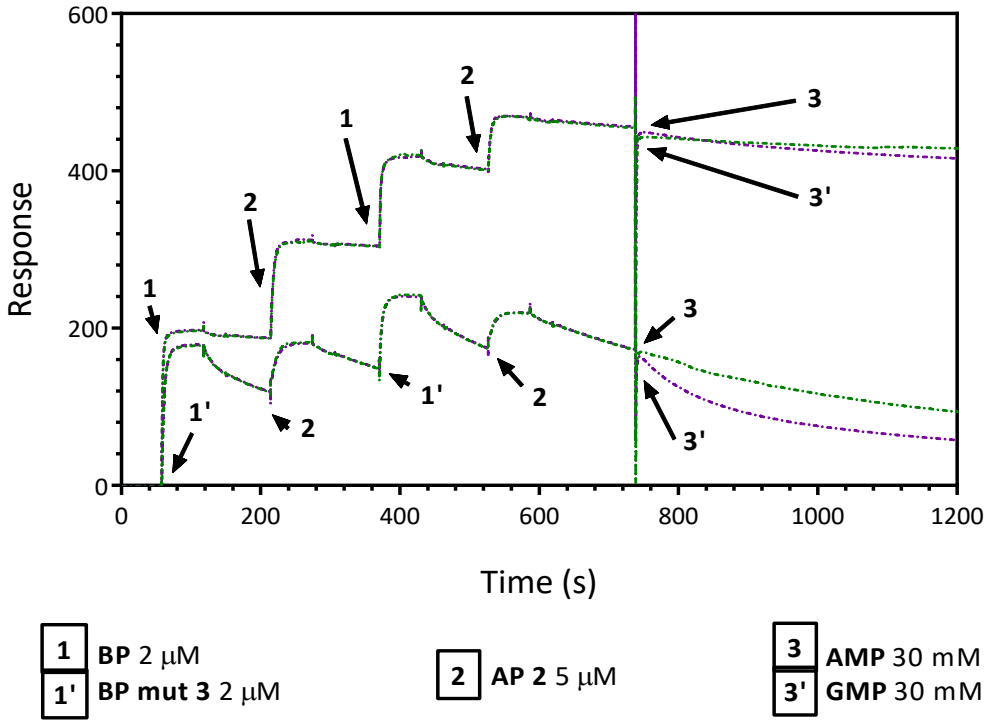

Figure 7.7. Response curves of the supersandwich build-up and the effect of target addition on channel containing **CP 2**. Flow rate was 25 μL/min. In this sensorchip the CP was immobilized until 200 RU, in order decrease the coverage density and electrostatic repulsions.

Then, the importance of reducing the gap of affinity towards probes and molecular targets was tested introducing three mismatches in each bridge probe of the supersandwich (**BP**

mut 3). As can be seen in Figure 7.7, this strategy accelerated the disassembly of the supersandwich in presence of 30 mM of AMP. However, it also reduced a lot the overall stability of the nanostructure. The previous findings are not in concordance with what is suggested in the literature. Where it is said that 1 mM of ATP or AMP should be enough to disassemble the supersandwich. Maybe, the different results might be caused by the different method used in the construction of the supersandwich (L-b-L *vs* one-step), therefore we did binding assay with the one-step supersandwich.

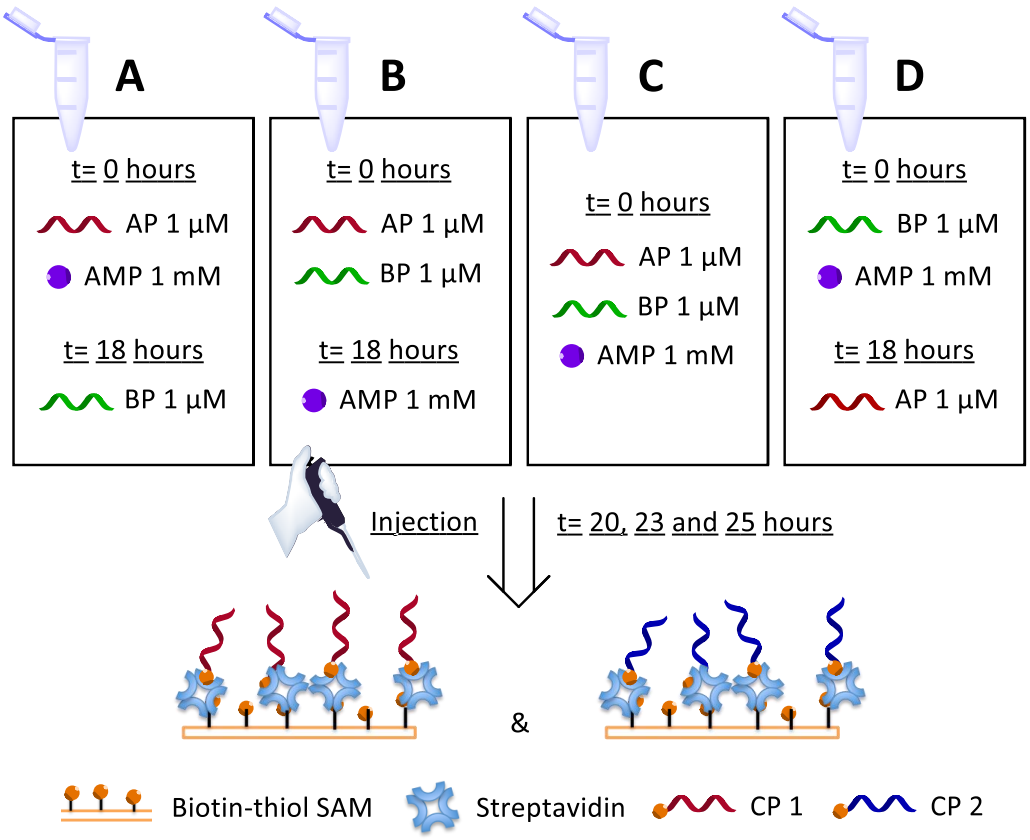

Figure 7.8. A strategy to evaluate the stimuli-responsiveness of the supersandwich.

Specifically, we adapted an already published strategy[17,22], but instead of using only gel-electrophoresis we included the use of SPR. In this experiment, four solutions were prepared and then injected to the sensorchip that had the capture probes immobilized. In solution A, **AP 1** (1 µM) and AMP (1 mM) were mixed for 25 hours (1 µM of BP was added in the last 7 hours). In solution B, **BP** and **AP 1** were mixed for 25 hours (AMP was added the last 7 hours). In solution C, both probes and AMP were mixed for 25 hours. In solution D, **BP** and AMP were in the solution for 25 hours (**AP 1** was added in the last 7 hours) (Figure 7.8).

Three possible results could be expected from these experiments, one, the AMP did not disturb the formation of the supersandwich, and while injecting the solutions to the channels containing the capture probes, all of them should give a similar response. Two, the AMP could have a dramatic effect on the formation of supersandwich, being all **AP 1** saturated by AMP, and while injecting the solutions only **BP** would be immobilized. Three, the AMP could have certain effect on the formation of the supersandwich, and different nanostructures would be obtained depending on the exposure time to the target.

The latter case was the one found, because as can be observed in Figure 7.9 there were significant differences in injections of solutions A, B, C and D while using both capture probes. It was of great importance the use of a nanoscale technic such as SPR to detect these events, because as can be observed in Figure S7.5, with gel-electrophoresis could not be appreciated any differences and in GPC/SEC (Figure S7.6) the mean molecular weight suffered minor changes.

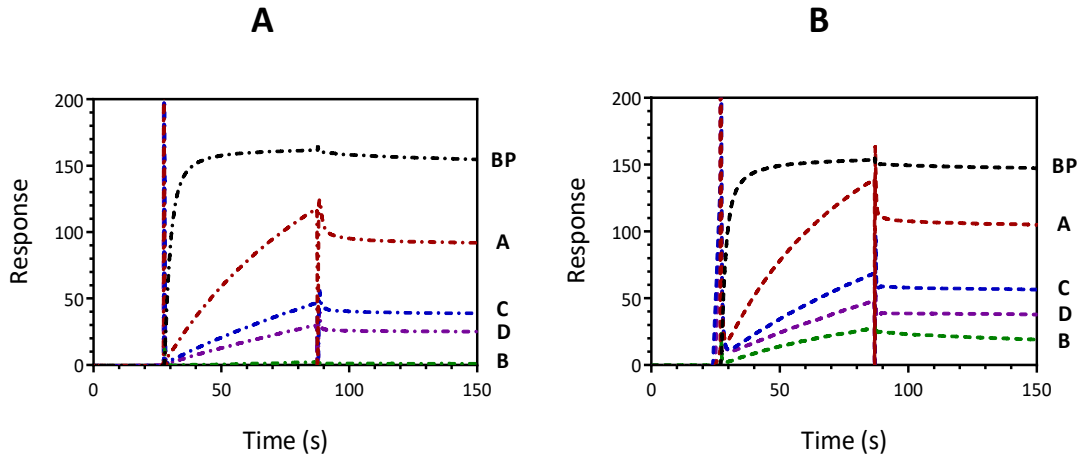

Figure 7.9. Injections of **BP** or solutions A, B, C or D after 25 hours channels with (A) **CP 1** and (B) **CP 2** immobilized. The flux rate was always 25 µL/min.

The solution A gave the highest response in both channels, followed by solution C, then solution D and finally solution B (Figure 7.9). When injection stopped, in some cases there was a huge instantaneous decrease in the response, this is due to the rapid K_{off} of AMP when it is released from the aptamer, what had been observed also in Chapter 5. The different response values obtained in each injection helped understanding which kind of nanostructure had formed in each solution.

In solution A there was more **BP** available to hybridize with the capture probes than in other solutions, because the **BP** was inserted in the solution in the last few hours. This means that the formation of the supersandwich in one-step self-assembly is a process that needs hours to be completed, this might be very important to take into account in designs with a reversible function. Moreover, two injections done after 20 and 23 hours revealed that the response obtained was significantly lower at the last injection (25 hours) than at the first one (20 hours), due to the continuous reduction of free **BP** that caused the formation of the supersandwich (Figure 7.10).

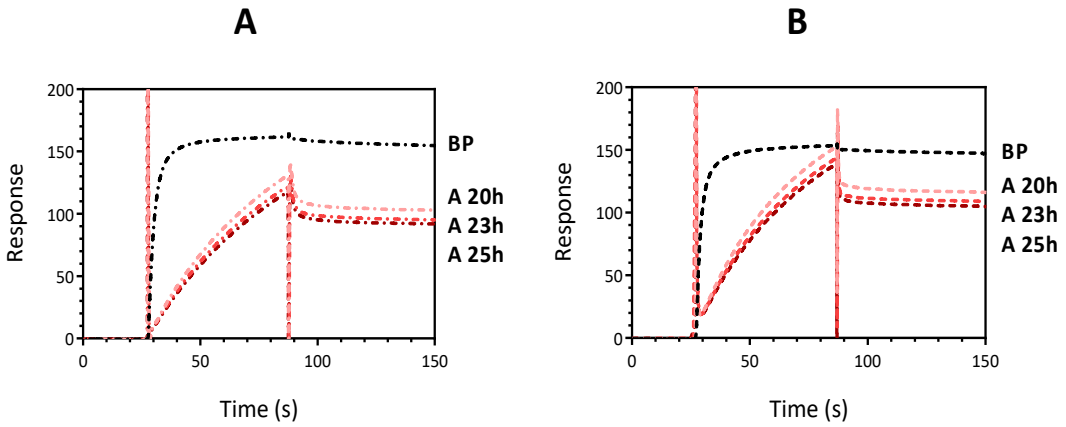

Figure 7.10. Injections of **BP** and solution A at different periods in channels with (A) **CP 1** and (B) **CP 2** immobilized. The flux rate was always 25 µL/min.

In solution B, there was a negligible response in channel of **CP 1**, and it gave the lowest response value in the channel of **CP 2**. This was the solution where **BP** and **AP 1** were mixed for the greatest period in absence of AMP, added in the last hours, therefore it can be supposed that the supersandwich had the hugest size. The **CP 1** that has a hairpin form did not hybridize

with this supersandwich because the major part of the **BP** would be hybridized, what reduces the affinity of the capture probe towards the **BP** by steric and electrostatic repulsion. In case of **CP 2,** it forms a random coil, and therefore, it is energetically favourable to hybridize with some **BP** of the supersandwich even if they have a lower affinity. Moreover, observing the injections after 20, 23 and 25 hours, it can be observed that AMP, in principle, had no capacity to disassembly the structure: there were no changes in response curves (Figure 7.11).

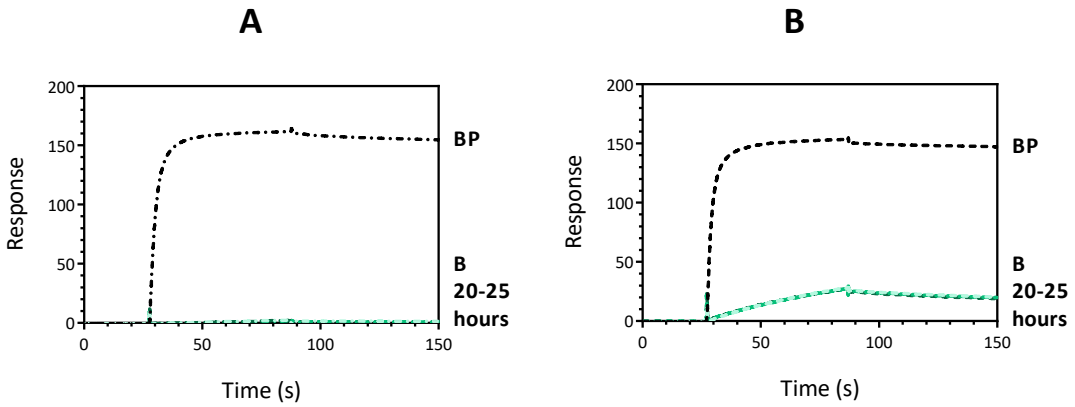

Figure 7.11. Injections of **BP** and solution B at different periods in channels with (A) **CP 1** and (B) **CP 2** immobilized. The flux rate was always 25 µL/min.

In case of solution C, both probes and AMP were mixed from the start, the kinetics were faster than in solution B but slower than in solution A. Following with the previous argumentation, in solution C there was more **BP** available than in solution B, because the AMP had been more time in the media and therefore, it prevented partially the formation of the nanostructure, but it did not prevent as well as in solution A, because in the latter, the **BP** was added in the last hours. In solution C there was no significant change in different injections, what means that the nanostructure was already at equilibrium after 20 hours and therefore 1 mM of

AMP was not able to disassembly it (also observed by GPC/SEC in Figure S7.6). This is contrary to what has been suggested in the literature[17,21–23] (Figure 7.12).

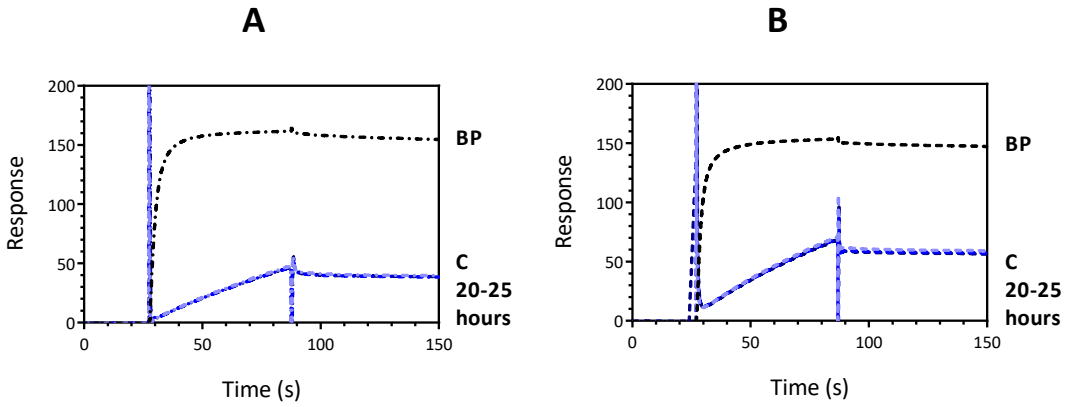

Figure 7.12. Injections of **BP** and solution C at different periods in channels with (A) **CP 1** and (B) **CP 2** immobilized. The flux rate was always 25 µL/min.

Finally, in solution D, where **BP** and AMP were in the solution for 25 hours and **AP 1** was added in the last 7 hours, the response values obtained were lower than in solution C but higher than solution B (Figure 7.13). The first question that raised was why solution A and solution D did not have the same response, if in both cases the **AP 1** and **BP** had been in contact for the same period. But it seems that in solution A there was more **BP** available than in solution D while injecting them. Therefore, in solution A, most part of the **AP 1** were already recognizing the AMP molecules when the **BP** was inserted in the solution, and probably this slower the process of recognizing the **BP**, even if it did not prevented it.

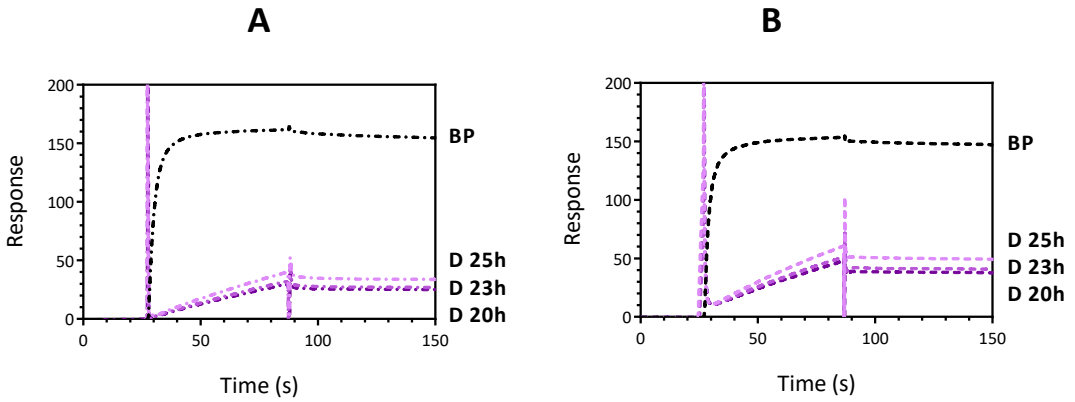

Figure 7.13. Injections of **BP** and solution D at different periods in channels with (A) **CP 1** and (B) **CP 2** immobilized. The flux rate was always 25 µL/min.

With obtained results, it can be observed that the molecular target was able to reduce the kinetics of hybridization between **BP** and **AP 1**, but the nanostructure was formed in all cases. Therefore, 1 mM of target was not able to compete with the hybridization between DNA strands and did not disassemble none of the supersandwichs created by one-step or L-b-L methods. It was detected that the main issue was the huge differences between affinities of aptamer probes towards **BP** and molecular targets. Following experiments consisted in introducing mismatched probes in the supersandwich, trying to reduce these differences without losing static stability.

7.2.3 Influence of mismatches in kinetics and stability of the supersandwich

It was observed that the supersandwich was able to disassemble upon ATP or AMP recognition, but it needed huge target concentrations due to the strong interactions that are formed between probes. One alternative to use lower concentrations of target is to change the

aptamer probe by another aptamer with higher affinity towards its target (with a K_d in the nanomolar range), but this would limit significantly the variety of aptamers that could be used in a supersandwich design. Therefore, reducing affinities between probes would be a better alternative. However, these affinities need to be high enough to maintain a static stability in the supersandwich preventing it to disassemble in absence of the molecular target. A systematic study was done using different bridge and aptamer probes containing mismatches (Table 7.1), in order to elucidate if an affordable trade-off between the static stability and the dynamic function could be achieved.

In case of mismatched bridges, all of them had one mismatch in the double helix formed with the upper part of capture and aptamer probes and they have a variable number of mismatches with the bottom part of capture and aptamer probes. In example, **BP mut 1** has no mismatches with the bottom part of **CP 1, BP mut 2** has one mismatch and **BP mut 3** two. As can be seen in Figure S7.7A, the more mismatches the slower was the K_{on}, due to a reduced affinity. On the other hand, the K_{off} was almost negligible due to the high number of base pairs formed showing that at least with two layers the nanostructure can maintain the static stability in aqueous buffer with NaCl at 0.5 M.

On the other hand, it is interesting to consider the kinetics of the different bridge probes, which are directly related with the affinity between probes. While injecting these mismatched bridge probes to the channel containing **CP ADA**, the kinetics with bridge probes were faster than those found with **CP 1**, due to the shorter hairpin (Figure S7.7C). The situation was quite different while using the **CP 2** (Figure S7.7B): instead of hybridizing with the lower part of

another **CP 2** which is formed by thymine nucleotides, the bridge probes formed unstable duplexes with other bridge probes. Thus, the responses almost duplicated the value found with the not mismatched bridge but then had a huge K_{off}.

The experiment was repeated twice and in one of these repetitions AMP was injected at second 920 at a concentration of 1 mM to each of the constructions. Previously, this target concentration did not affect the hybridization between probes. In Figure 7.14A can be observed that the molecular target was not able to disrupt the hybridization between **CP 1** and the different mismatched bridge probes and response curves were equal in absence or presence of AMP, excepting the construct with **BP mut 3**. In this case, the only change in response with AMP was to higher values, due to recognition of AMP by some free **CP 1**. In case of **CP 2**, as it is not able to recognize the target, there were no changes at all between the injection with and without AMP (not shown).

The situation changed while using **CP ADA** (Figure 7.14B); in this case, it was possible to cause a change in K_{off} with **BP mut 2** and **BP mut 3** when AMP was present in solution. However, it was not possible to achieve a negligible K_{off} in absence of the target in the latter two cases, showing the delicate balance between the static stability and the recognition capacity of the aptamer-based nanostructure.

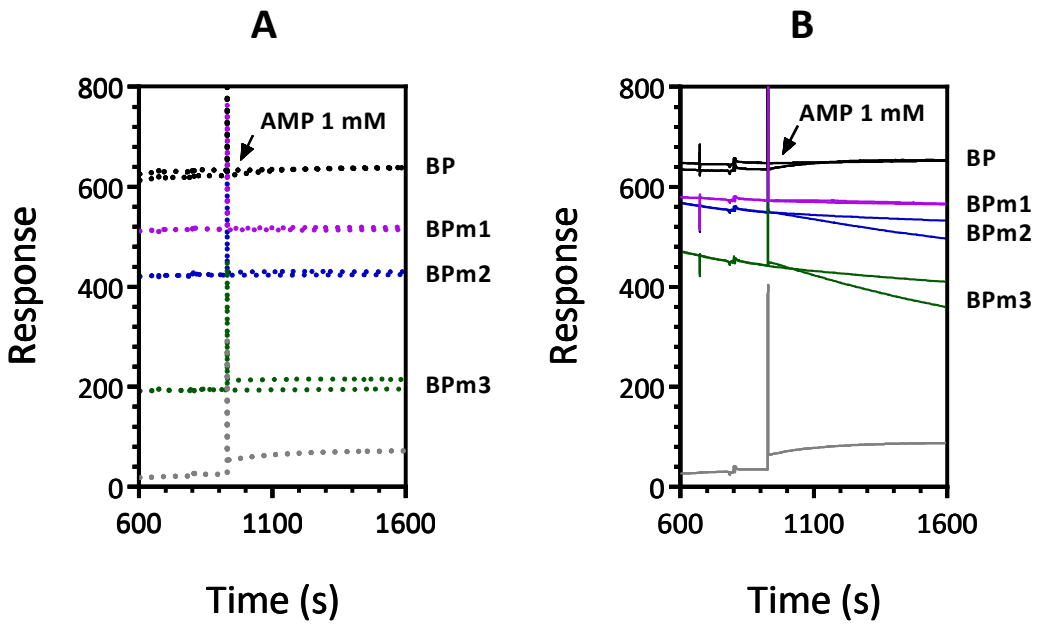

Figure 7.14. Response curves obtained upon addition of AMP at 1 mM to (A) **CP 1** or (B) **CP ADA** in presence of bridge probes. The flow rate was 25 µL/min.

7.2.4 Self-assembly and secondary structure in mixed solvents

In order to gain insight about its secondary and tertiary structures and the possible use of non-physiological media, the traditional supersandwich **[BP + AP 1]** was built-up by self-assembly in a variety of molecular solvents, ILs and DESs. These studies would help elucidating if the stabilities found in short oligonucleotides (Chapters 3-5) could be extrapolated to the nanostructure.

The formation of the nanostructures was characterized by circular dichroism and gel-electrophoresis. It was important to use at least 0.5 M of choline chloride in solutions containing molecular solvents to ensure the formation of the nanostructure which needs counterions to

maintain a certain rigidity. This was not necessary in ILs and DESs because they always had higher concentrations of choline cation. As a positive control, the same experiments were carried out with the aqueous buffer used in previous sections that contains 0.5 M NaCl.

It was previously observed by gel-electrophoresis (Figure 7.1) that **AP 1** can form intramolecular interactions due to its 8 complementary base-pairs whereas **BP** cannot and forms intermolecular interactions with other **BP** strands, a maximum of 20 base-pairs. This was verified with CD (Figure 7.15A). On the other hand, while mixing both probes, the formed supersandwich showed the B-form but, there was a significant shoulder at 280 nm probably because part of the **BP** was interacting with other **BP**. The supersandwich was then self-assembled at different concentrations of choline chloride (Figure 7.15B), as can be observed, it is able to form the nanostructure in all of them, further studies using gel-electrophoresis would show if there were differences in length.

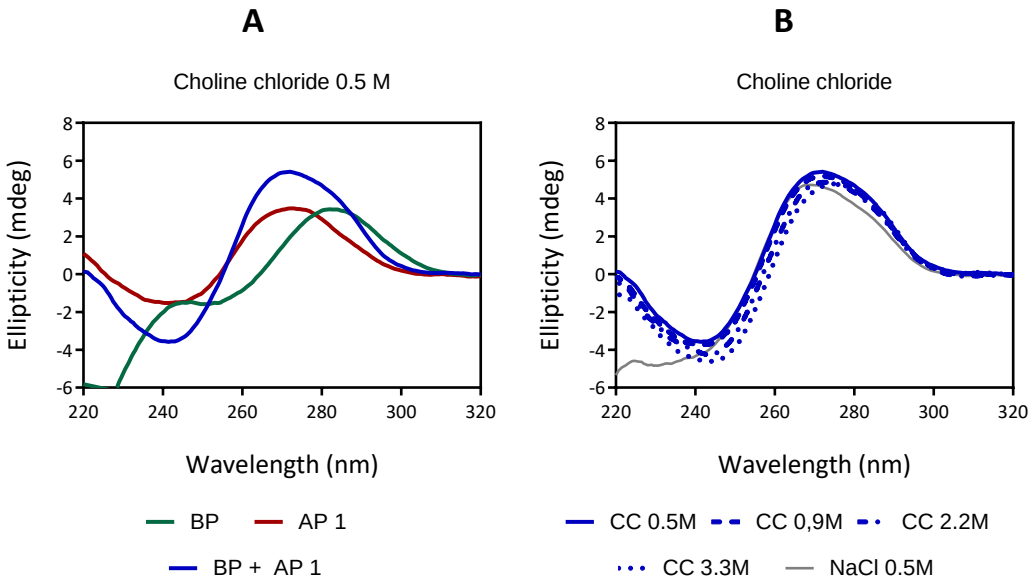

Figure 7.15. Circular dichroism measurements of (A) **BP, AP 1** and **[BP + AP 1]** in choline chloride 0.5 M or (B) **[BP + AP 1]** at different concentrations of choline chloride. All the oligonucleotides were at 5 μM and the temperature was 25 ^{o}C.

CD measurements continued using also molecular solvents, ILs and DESs (Figure 7.16). It can be observed that at their lowest concentration, the secondary structure of the supersandwich was similar to that in physiological media excepting reline and CDHP, equal results to those of Chapter 3 (Figure 3.7 and Figure S3.14).

It was possible to use DESs even up to 3.4 M (≥85 wt. %). At this concentration, the supersandwich was destabilized specially in ethaline and glyceline but less than the duplex formed between Oligo1 and Oligo2 showing that there was cooperativity between adjacent sequences of the nanostructure. On the other hand, the use of reline close to anhydrous conditions stabilized the duplex, probably because the denaturation effect of urea was prevented by choline, as seen with salmon-sperm DNA (Figure 3.15). In case of ionic liquids (Figure 7.16C), choline lactate did not affect the formation of the double helixes at 1 M, but at 2 and 4 M it was destabilized significantly. Choline dihydrogenphosphate destabilized more the duplexes at low concentrations due to its acidity; however, at 4 M the supersandwich was partially denatured.

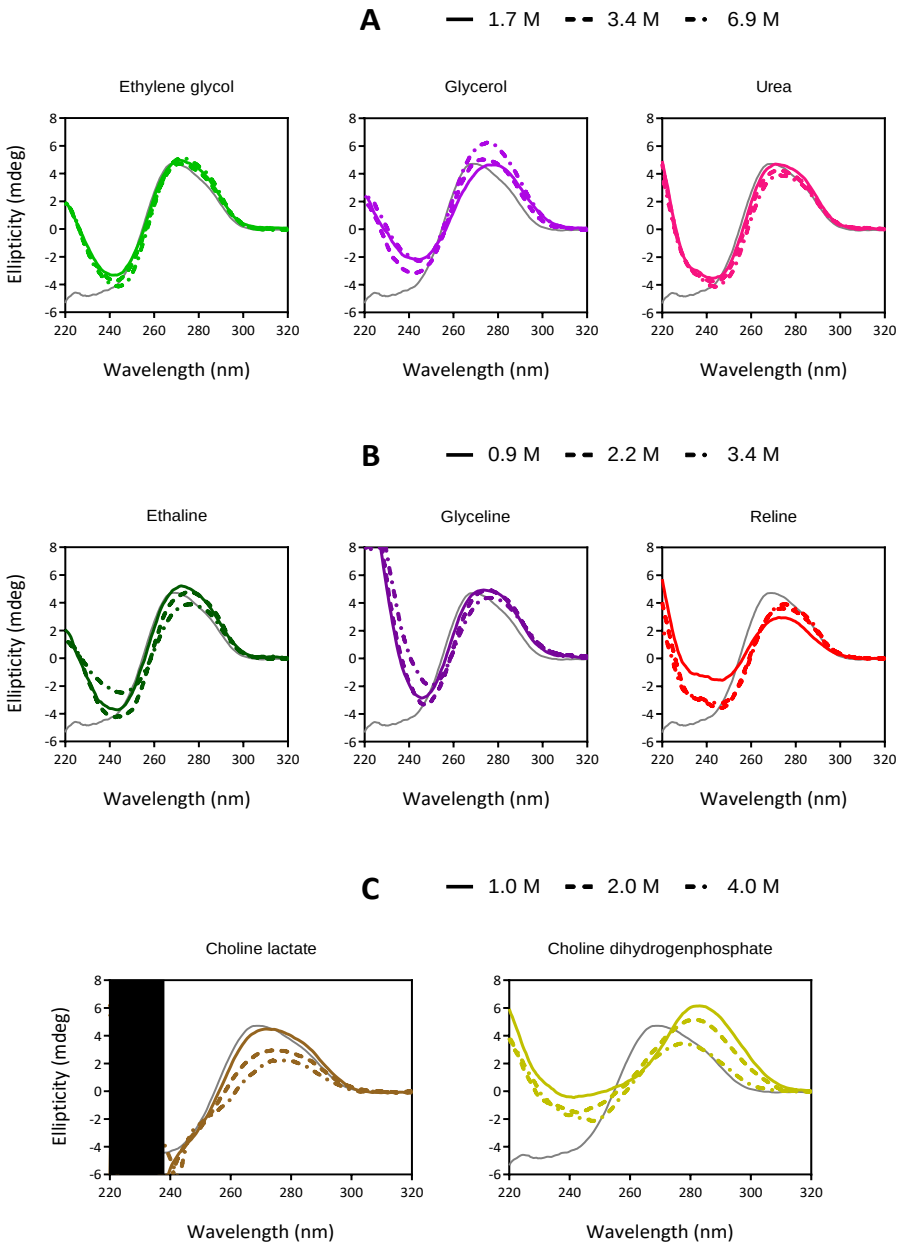

Figure 7.16. CD measurements of solutions containing **[BP + AP 1]** in (A) molecular solvents (B) deep eutectic solvents and (C) ionic liquids at different concentration in water. **[BP + AP 1]** in physiological media (NaCl 0.5 M) is always shown as reference (fine solid line). All the oligonucleotides were at 5 µM and the temperature was 25 ^{o}C.

A reduction in the thermal stability of the DNA double helixes should also lead to a shortening of the nanostructure, as multiple sequences will be less likely to hybridize at the same time. In order to corroborate this, the same samples were studied using gel-electrophoresis. In case of molecular solvents, samples containing ethylene glycol and urea did not show significant differences in the secondary structure but the length of the supersandwich shortens while increasing the concentration of EG and glycerol. On the other hand, the red shift found in the positive peak of CD using glycerol might be due to the partial denaturation of the sequences, as can be observed in the short segments that appear in lines 8-11 of the gel (Figure S7.8).

As could be expected after the studies done in Chapter 3, the supersandwich could be formed in choline chloride even at 3.4 M (45 wt. %). In case of DESs and ILs, at 0.9 M the supersandwich formed in all cases except in reline and CDHP (Figures S7.9 and S7.10). However, increasing the length of the supersandwich reduced in ethaline, glyceline and choline lactate whereas it increased significantly in reline and in CDHP but in a minor extent as observed in CD. These results show that the thermal stabilities of the oligonucleotides characterized in Chapter 3 were directly related with secondary structure and length of the supersandwich.

Previously, mismatches were used to reduce the thermal stability of duplexes and favour the stimuli-responsiveness of the supersandwich. Changing the media can be considered analogue to that strategy but with certain challenges and benefits. The main challenge will consist in maintain the affinity of the aptamer towards the target, because as observed in Chapter 5, the function of the aptamer can be reduced beyond the selection conditions. Therefore, it would be necessary to use aptamers selected in the desired non-aqueous media,

as those found in Chapter 6. On the other hand, the new environment prevents DNA from degradation and it can be used over a wider range of temperatures and pressures than water, or it can dissolve new molecules.

7.3 Conclusions

The nanostructure known as supersandwich has been studied, for which it has been constructed in one step and for the first time, using the layer-by-layer method. In addition to being studied by electrophoresis and GPC/SEC, the construction and disassembly of the nanostructure has been characterized for the first time online in SPR and QCM-D.

It has been necessary to redesign the nanostructure when building it layer-by-layer. This shows the need to take into account all possible interactions. The development of software could be of great help. On the other hand, the formation of dimers or secondary structures such as hairpins has been found to significantly reduce the efficiency of hybridization to the nanostructure. Nevertheless, it has been possible to achieve a nanostructure with 100 % hybridization efficiency. This nanostructure consists of 3 layers. It was possible to reach 4-5 layers (approx. 25 nm) and maintain a negligible K_{off}, albeit with reduced hybridisation efficiency. QCM-D has shown that as the nanostructure becomes longer, it behaves less rigid.

Regarding the ability of ATP or AMP to break down the nanostructure. The results obtained differ greatly from those reported in the literature. The target molecule was not able to undo the single-layer sandwich or the multilayer sandwich, at least at the published concentration (1 mM). In the case of the 1-layer sandwich, 4 mM the AMP was enough to undo it, but the sensitivity dropped dramatically when more layers were added. It was necessary to use 30 mM AMP to see a significant change compared to 30 mM GMP. To improve the sensitivity of the multilayer supersandwich, it has worked to reduce the affinity between oligonucleotides. However, introducing mismatches also significantly affects the stability of the nanostructure, so

it does not seem a useful strategy. Ideally, aptamers with a sensitivity towards the target molecule in the nanomolar range should be used.

On the other hand, the use of DNA nanostructures in non-physiological environments has also been considered, what permits the long-term use of these structures and the use of new targets as stimuli. Thermal stability has been found to be higher in the supersandwich than in individual duplexes of Chapter 3, demonstrating that there is cooperativity between the different layers of the nanostructure, similar to what was observed using the "long" salmon-sperm DNA. It has been shown for the first time that the nanostructure maintains the double helix shape even under very low hydration conditions. However, the length of the nanostructure has been significantly affected, as observed by gel electrophoresis.

7.4 References

1. Ariga, K. *et al.* Self-assembly as a key player for materials nanoarchitectonics. *Sci. Technol. Adv. Mater.* **20**, 51–95 (2019).
2. Kahn, J. S., Hu, Y. & Willner, I. Stimuli-Responsive DNA-Based Hydrogels: From Basic Principles to Applications. *Acc. Chem. Res.* **50**, 680–690 (2017).
3. Yu, Y., Jin, B., Li, Y. & Deng, Z. Stimuli-Responsive DNA Self-Assembly: From Principles to Applications. *Chem. - A Eur. J.* **25**, 9785–9798 (2019).
4. Liu, Z., Wang, W., Xie, R., Ju, X.-J. & Chu, L.-Y. Stimuli-responsive smart gating membranes. *Chem. Soc. Rev.* **45**, 460–475 (2016).
5. Lee, B. Y. *et al.* Bioinspired Dual Stimuli-Responsive Membranous System with Multiple On-Off Gates. *ACS Appl. Mater. Interfaces* **8**, 11758–11764 (2016).
6. Shiu, S. C. C. *et al.* The Three S's for Aptamer-Mediated Control of DNA Nanostructure Dynamics: Shape, Self-Complementarity, and Spatial Flexibility. *ChemBioChem* **19**, 1900–1906 (2018).
7. Ma, T., Janot, J. M. & Balme, S. Track-Etched Nanopore/Membrane: From Fundamental to Applications. *Small Methods* **2000366**, 1–36 (2020).
8. Ebrahimi, A., Ravan, H. & Khajouei, S. DNA nanotechnology and bioassay development. *TrAC - Trends Anal. Chem.* **114**, 126–142 (2019).
9. Sassolas, A., Leca-Bouvier, B. D. & Blum, L. J. DNA biosensors and microarrays. *Chem. Rev.* **108**, 109–139 (2008).
10. Palchetti, I., Laschi, S., Marrazza, G. & Mascini, M. Electrochemical imaging of localized

sandwich DNA hybridization using scanning electrochemical microscopy. *Anal. Chem.* **79**, 7206–7213 (2007).

11. Su, H., Kallury, K. M. R., Thompson, M. & Roach, A. Interfacial Nucleic Acid Hybridization Studied by Random Primer 32P Labeling and Liquid-Phase Acoustic Network Analysis. *Anal. Chem.* **66**, 769–777 (1994).
12. Xia, F., Zhang, X., Lou, X. & Yuan, Q. *Biosensors Based on Sandwich Assays*. *Biosensors Based on Sandwich Assays* (Springer Singapore, 2018). doi:10.1007/978-981-10-7835-4
13. Tang, W., Wang, D., Xu, Y., Li, N. & Liu, F. A self-assembled DNA nanostructure-amplified quartz crystal microbalance with dissipation biosensing platform for nucleic acids. *Chem. Commun.* **48**, 6678 (2012).
14. Mansouri, M. *et al.* SPR enhanced DNA biosensor for sensitive detection of donkey meat adulteration. *Food Chem.* **331**, 127163 (2020).
15. Hu, X. & Yuan, Q. Sandwich Assays Based on QCM, SPR, Microcantilever, and SERS Techniques for Nucleic Acid Detection. in *Biosensors Based on Sandwich Assays* 149–165 (Springer Singapore, 2018). doi:10.1007/978-981-10-7835-4_9
16. Yuan, T., Liu, Z., Hu, L., Zhang, L. & Xu, G. Label-free supersandwich electrochemiluminescence assay for detection of sub-nanomolar Hg2+. *Chem. Commun. (Camb).* **47**, 11951–11953 (2011).
17. Jiang, Y., Liu, N., Guo, W., Xia, F. & Jiang, L. Highly-Efficient Gating of Solid-State Nanochannels by DNA Supersandwich Structure Containing ATP Aptamers: A Nanofluidic IMPLICATION Logic Device. *J. Am. Chem. Soc.* **134**, 15395–15401 (2012).

18. Jia, Y. & Gu, H. Programming and preparing long single-stranded DNA with highly integrated sequence information for the self-assembly of DNA nanostructures. *Kexue Tongbao/Chinese Sci. Bull.* **64**, 1008–1017 (2019).

19. Jiang, X., Wang, L., Liu, S., Li, F. & Liu, J. Bioinspired artificial nanochannels: Construction and application. *Mater. Chem. Front.* (2020). doi:10.1039/d0qm00795a

20. Zhang, C. *et al.* The Recent Development of Hybridization Chain Reaction Strategies in Biosensors. *ACS Sensors* **5**, 2977–3000 (2020).

21. Yujuan, Q., Yue, Q., Mengfei, L. I. U., Nannan, L. I. U. & Xingxing, T. Nanopore-based DNA Supersandwich Structure for Detection of Streptavidin. 1–5 (2019). doi:10.1007/s40242-019-8378-0

22. Liu, N. *et al.* Two-way nanopore sensing of sequence-specific oligonucleotides and small-molecule targets in complex matrices using integrated DNA supersandwich structures. *Angew. Chemie - Int. Ed.* **52**, 2007–2011 (2013).

23. Xia, F. *et al.* An Electrochemical Supersandwich Assay for Sensitive and Selective DNA Detection in Complex Matrices. *J. Am. Chem. Soc.* **132**, 14346–14348 (2010).

7.5 Supplementary information

Figure S7.1. The injection of different concentrations of bridge probe (2, 5 and 10 μM) to channels containing (A) **CP 1,** (B) **CP 2** or (C) **CP ADA**. The flow rate was 25 μL/min in all cases.

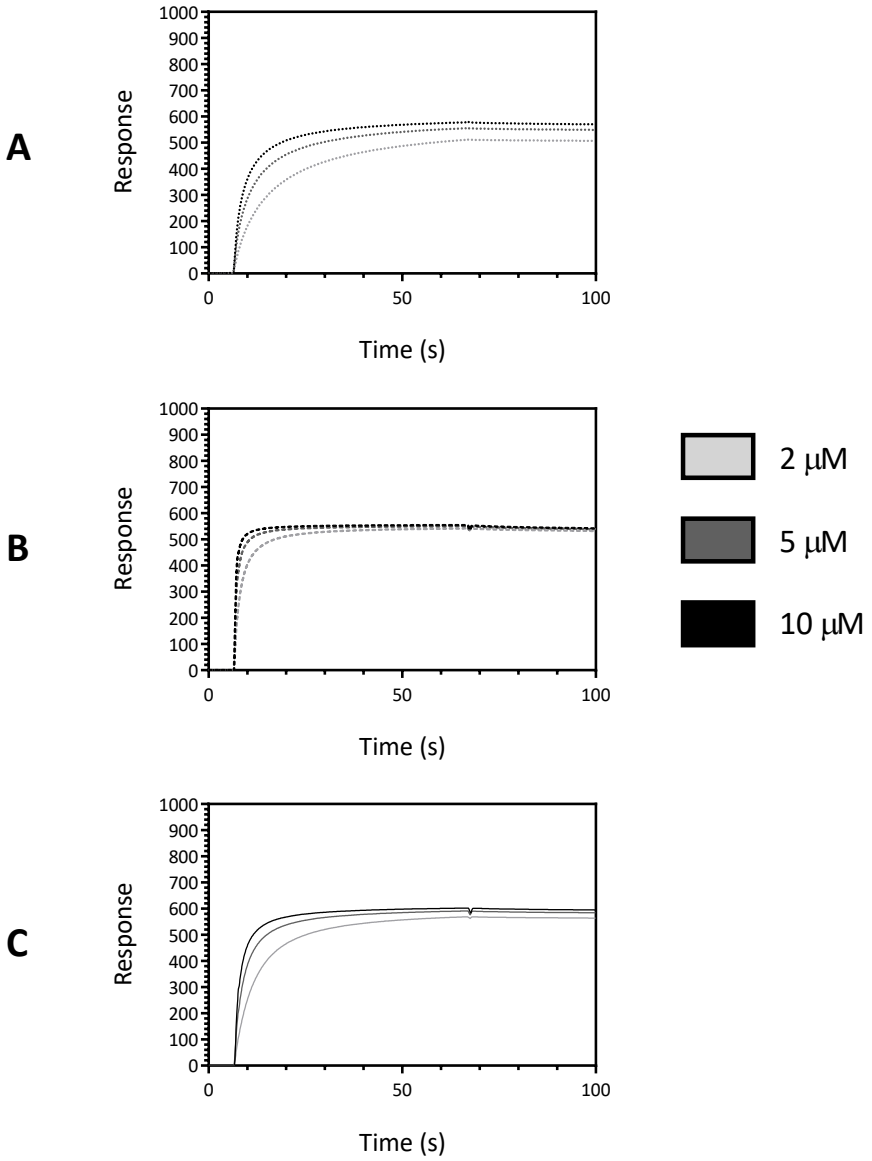

Figure S7.2. The injection of different concentrations of molecular targets to channels containing (A) **CP 1,** (B) **CP 2** or (C) **CP ADA**.

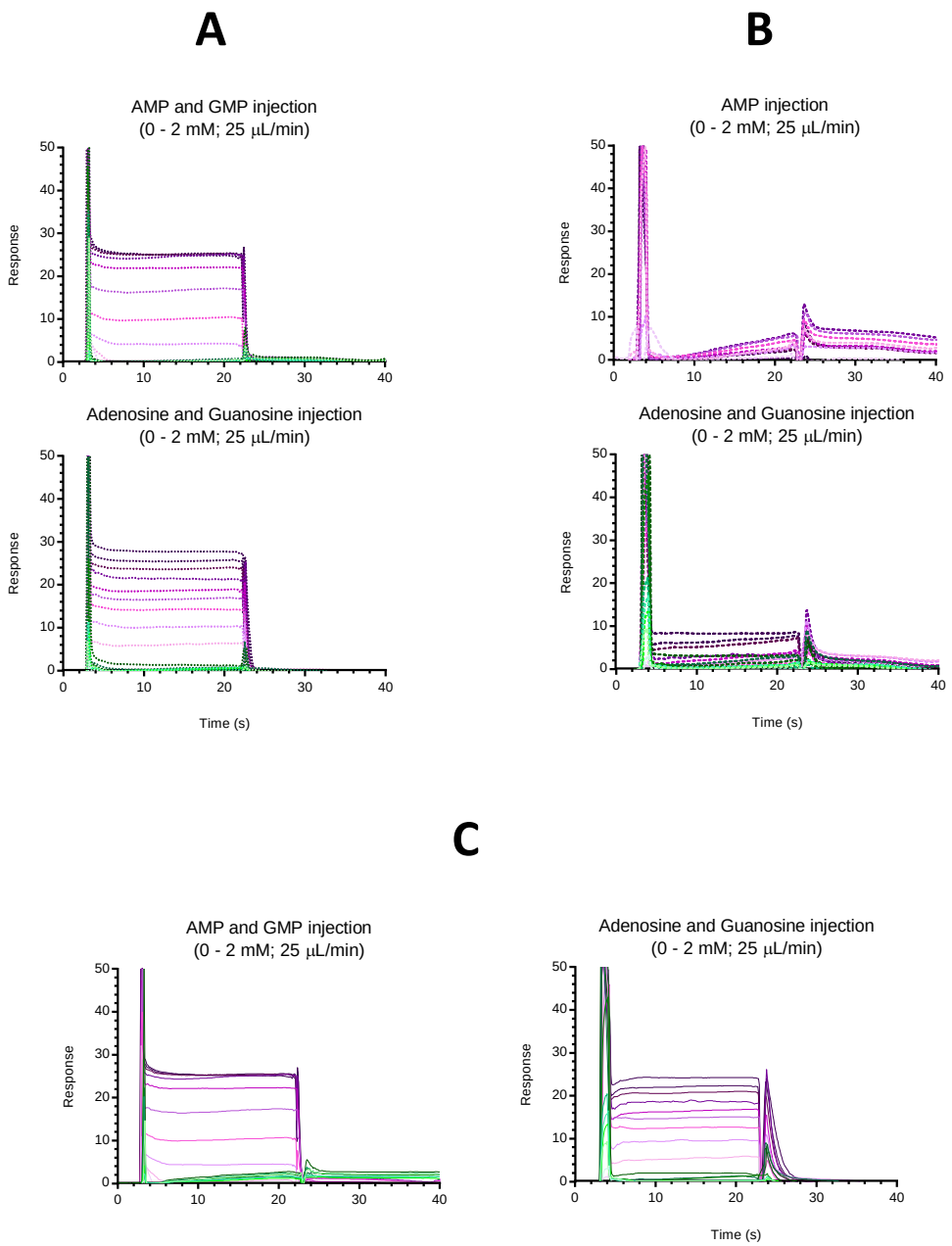

Figure S7.3. Two consecutive injection of molecular target and bridge probe to channels containing (A) **CP 1,** (B) **CP 2** or (C) **CP ADA**.

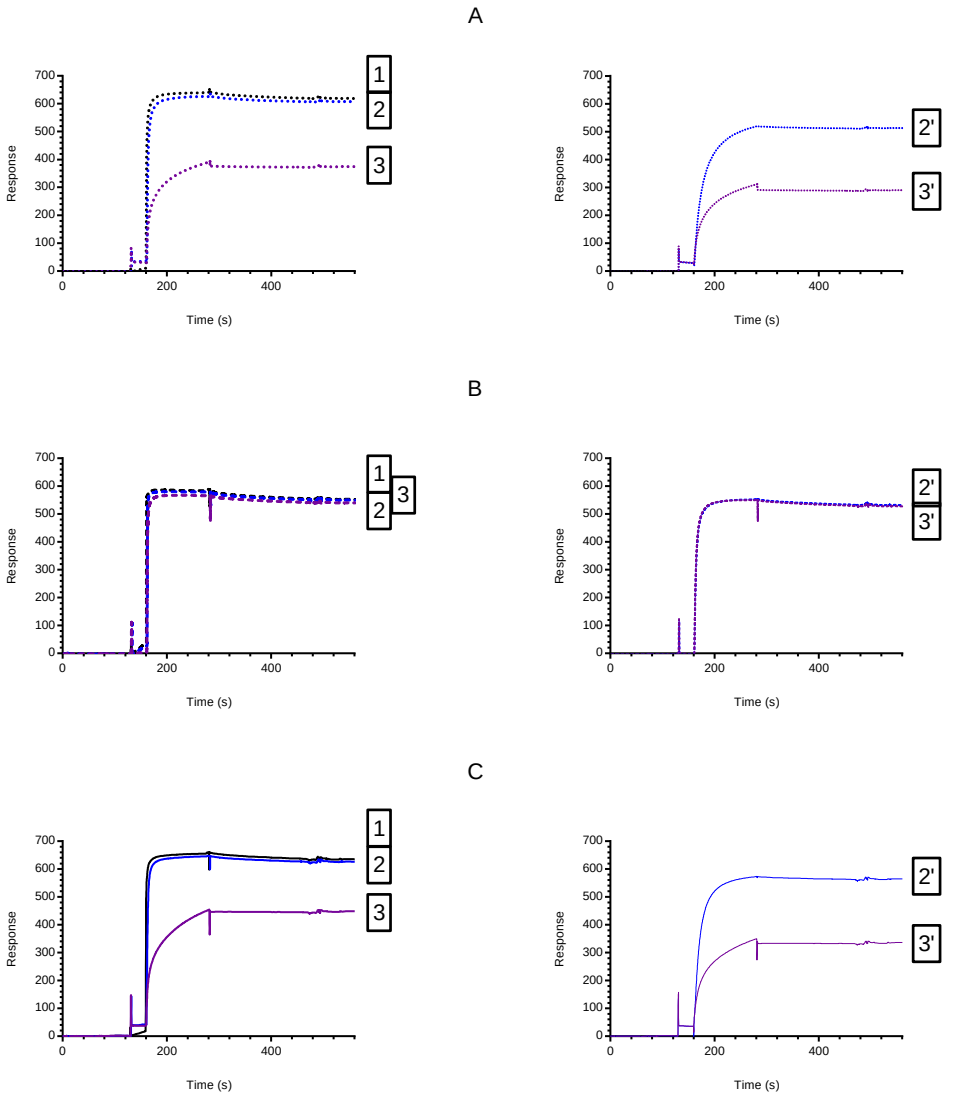

1 ATP 0 mM + [BP 10 μM]

2 ATP 1 mM + [BP 10 μM]

3 ATP 1 mM + [ATP 1 mM + BP 10 μM]

2' ATP 1 mM + [BP 2 μM]

3' ATP 1 mM + [ATP 1 mM + BP 2 μM]

Figure S7.4. The injection of **BP** at 2 μM and consecutive injection of different concentrations of (A) AMP, (B) Adenosine or (C) GMP to channel containing **CP 1**.

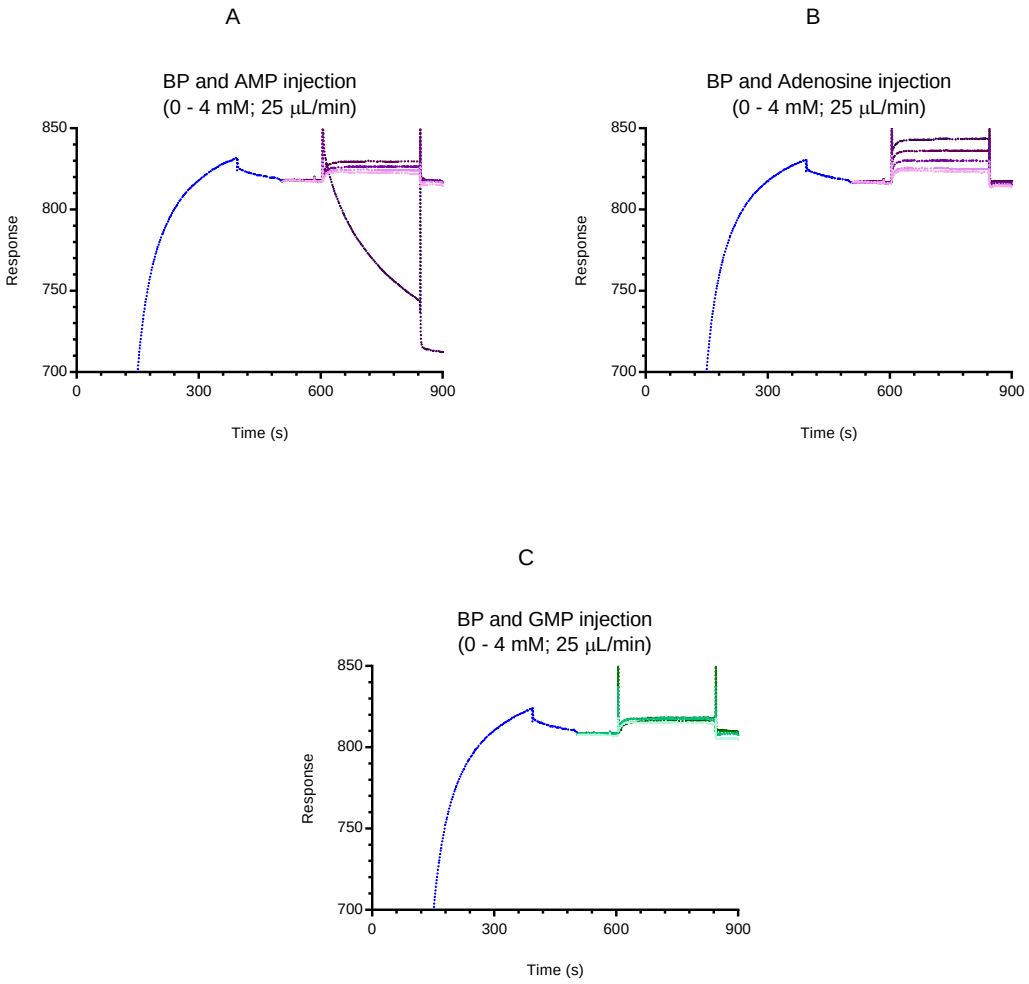

Figure S7.5. 3 wt. % agarose gel electrophoresis of solutions containing **[BP + AP 1]**. 90V 60 min. (A) **Line 1 and 1'**: 3000 bp ladder. **Line 3**: Solution A. **Line 4**: Solution B. **Line 5**: Solution C. **Line 6**: Solution D. **Line 8 and 8'**: 300 bp ladder. **Line 3'**: Solution A with GMP instead of AMP. **Line 4'**: Solution B with GMP instead of AMP. **Line 5'**: Solution C with GMP instead of AMP. **Line 6'**: Solution D with GMP instead of AMP. (B) **Line 1 and 5:** 0 mM NaOH. **Line 2 and 6:** 5 mM NaOH. **Line 3 and 7:** 20 mM NaOH. **Line 4 and 8:** 50 mM NaOH.

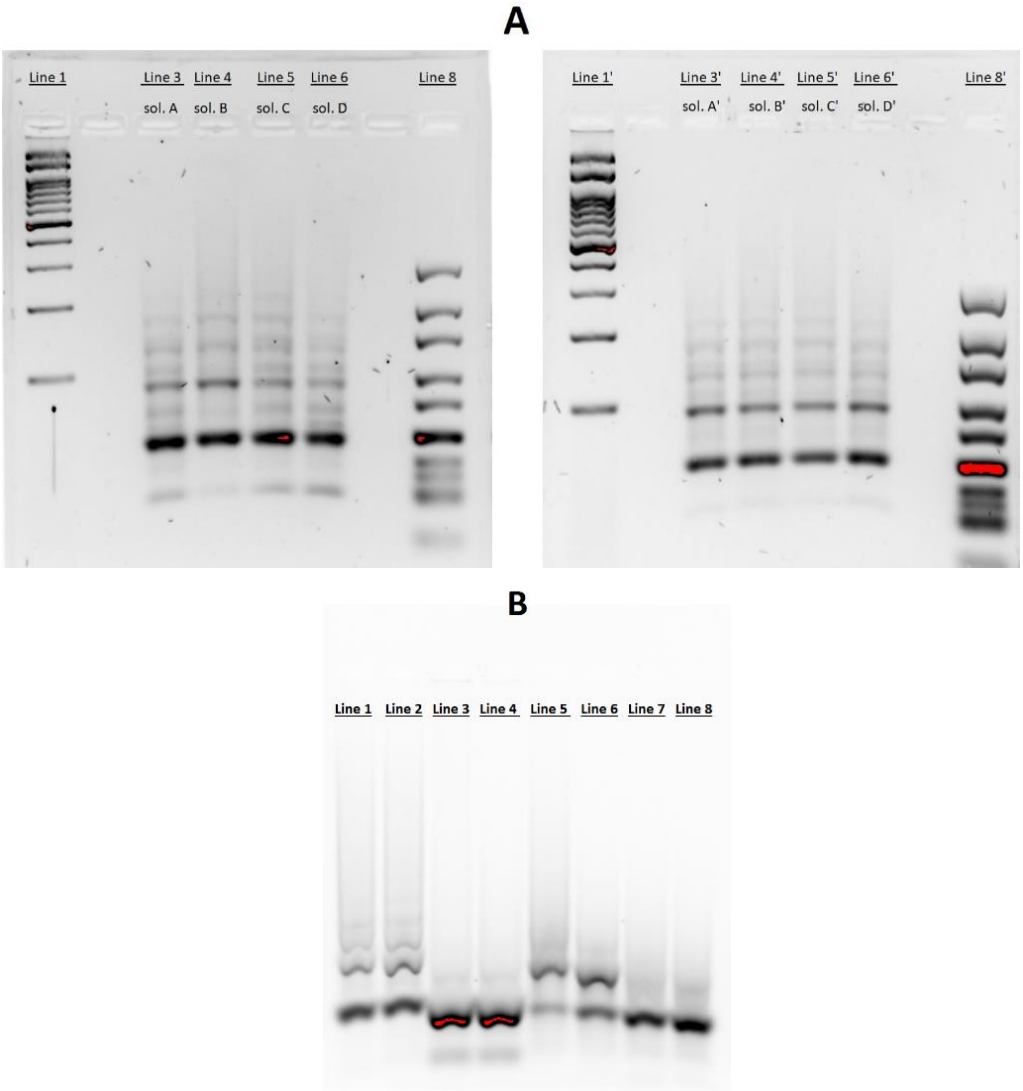

Figure S7.6. GPC/SEC results of solutions formed by **[BP + AP 1]**, **[BP + AP 1 + AMP]** or **[BP + AP 1 + GMP]** measured after 25 hours.

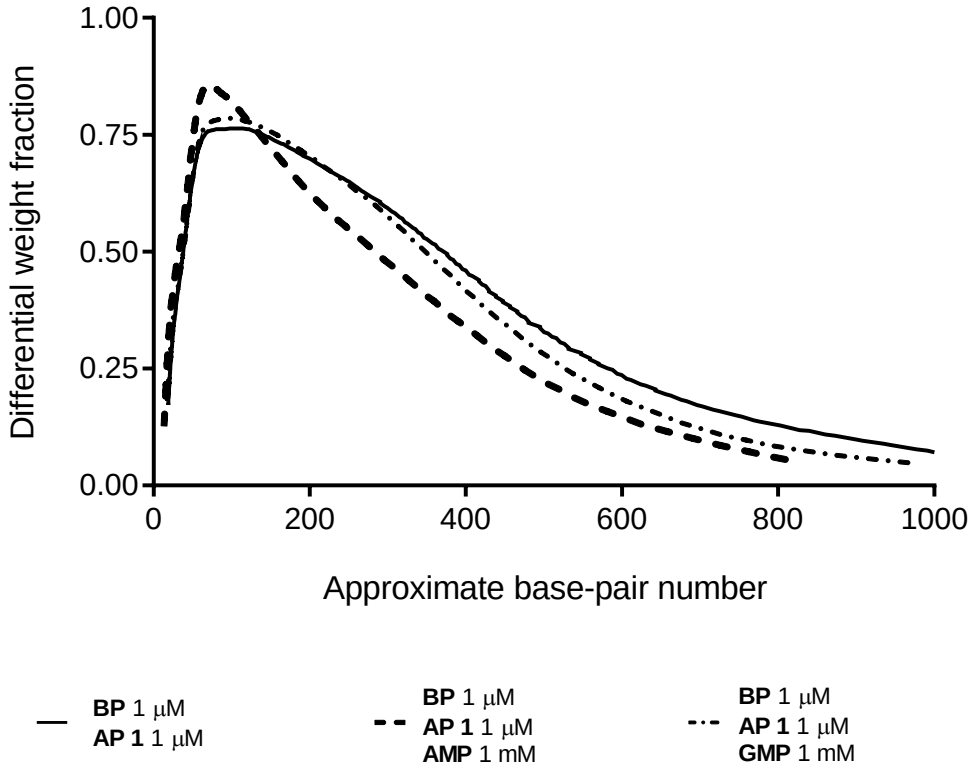

Figure S7.7. Response curves obtained upon injection of different bridge probes to (A) **CP 1**, (B) **CP 2** or (C) **CP ADA**. The flow rate was 25 µL/min.

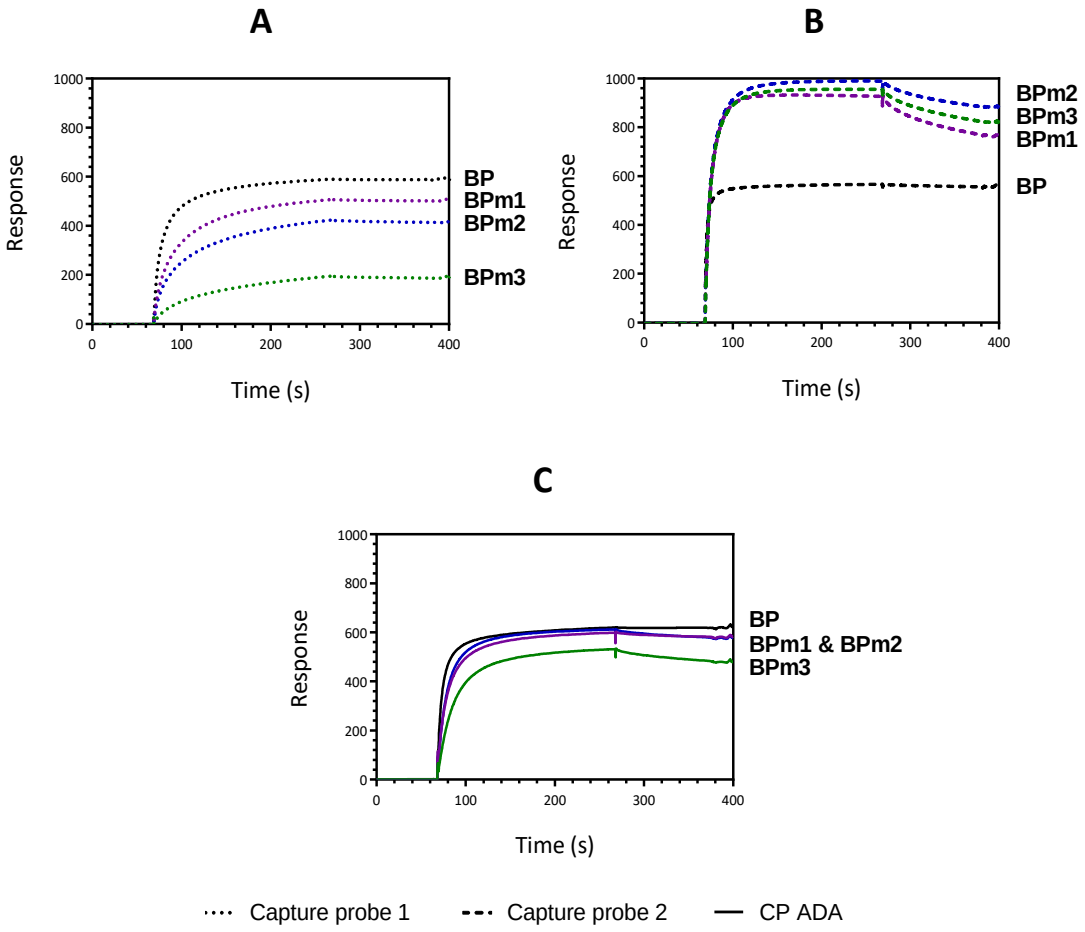

Figure S7.8. Raw images of agarose gels containing the mixture of **BP** and **AP 1** in molecular solvents. (A) One hour (B) one day and (C) one week after preparation.

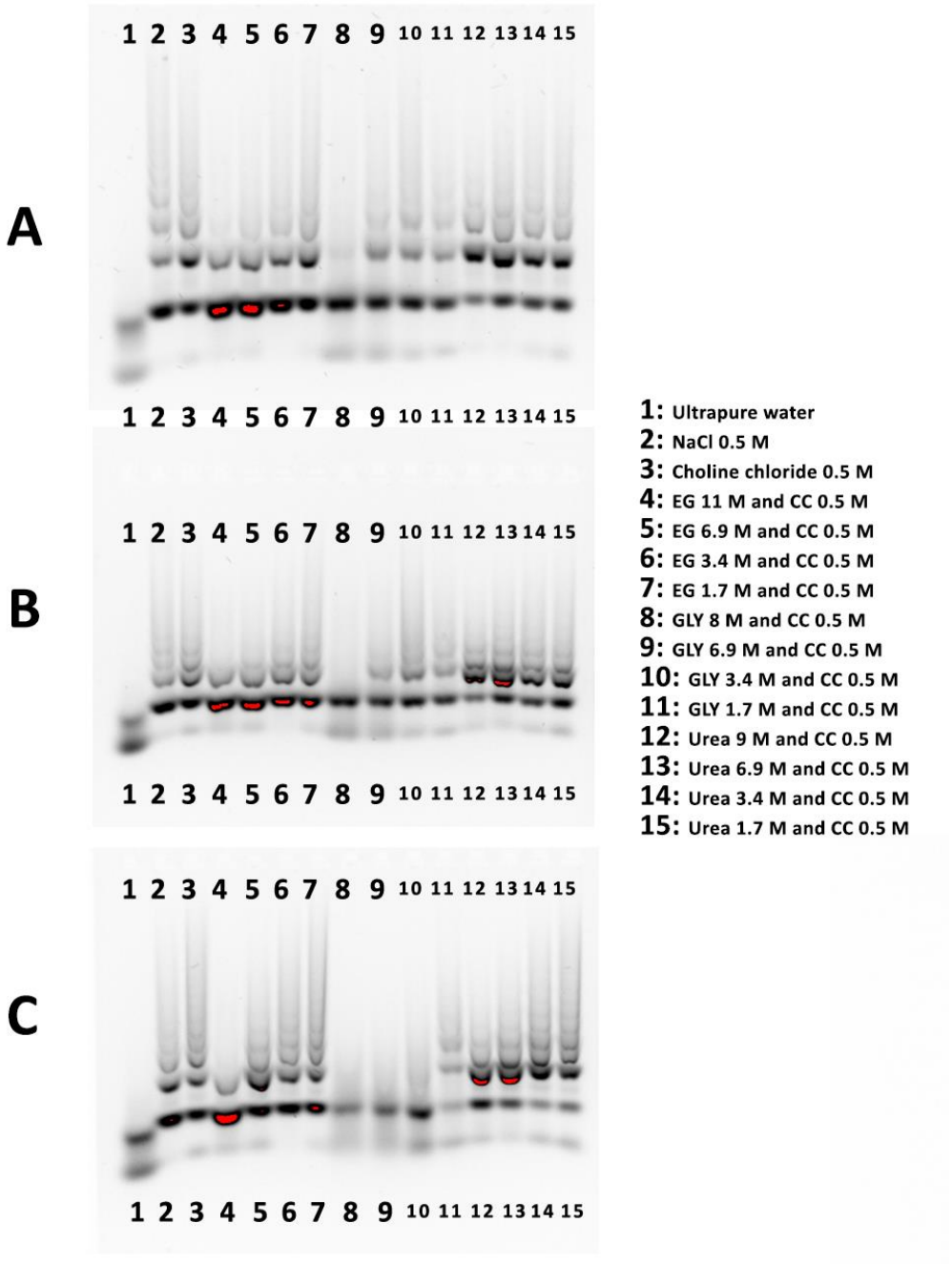

Figure S7.9. Raw images of agarose gels containing **BP**, **AP 1** or the mixture of **BP** and **AP 1** in HBA group and DESs at (A) 0.9 M (B) 2.2 M and (C) 3.4 M one week after preparation.

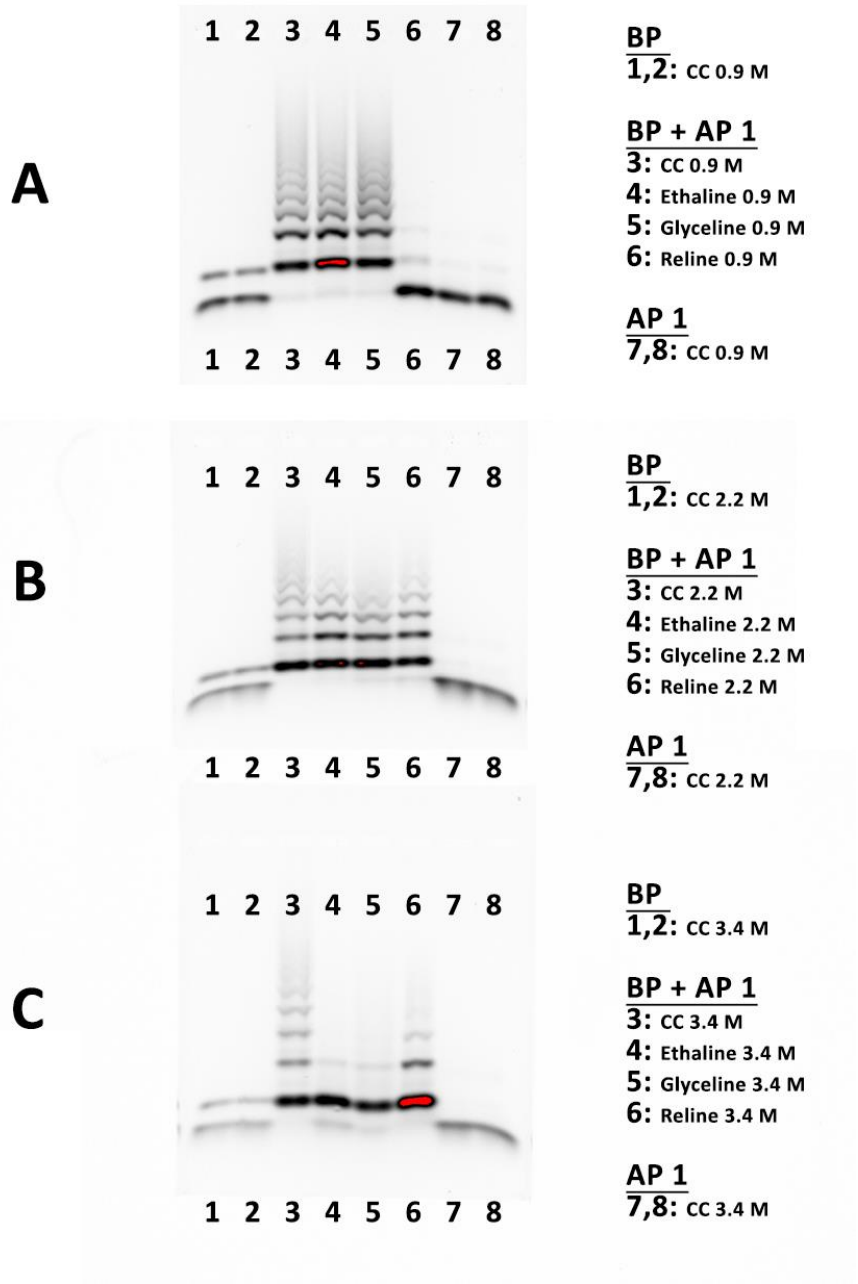

Figure S7.10. Raw images of agarose gels containing the mixture of **BP** and **AP 1** in ILs at (A) 1 M (B) 2 M and (C) 4 M one week after preparation.

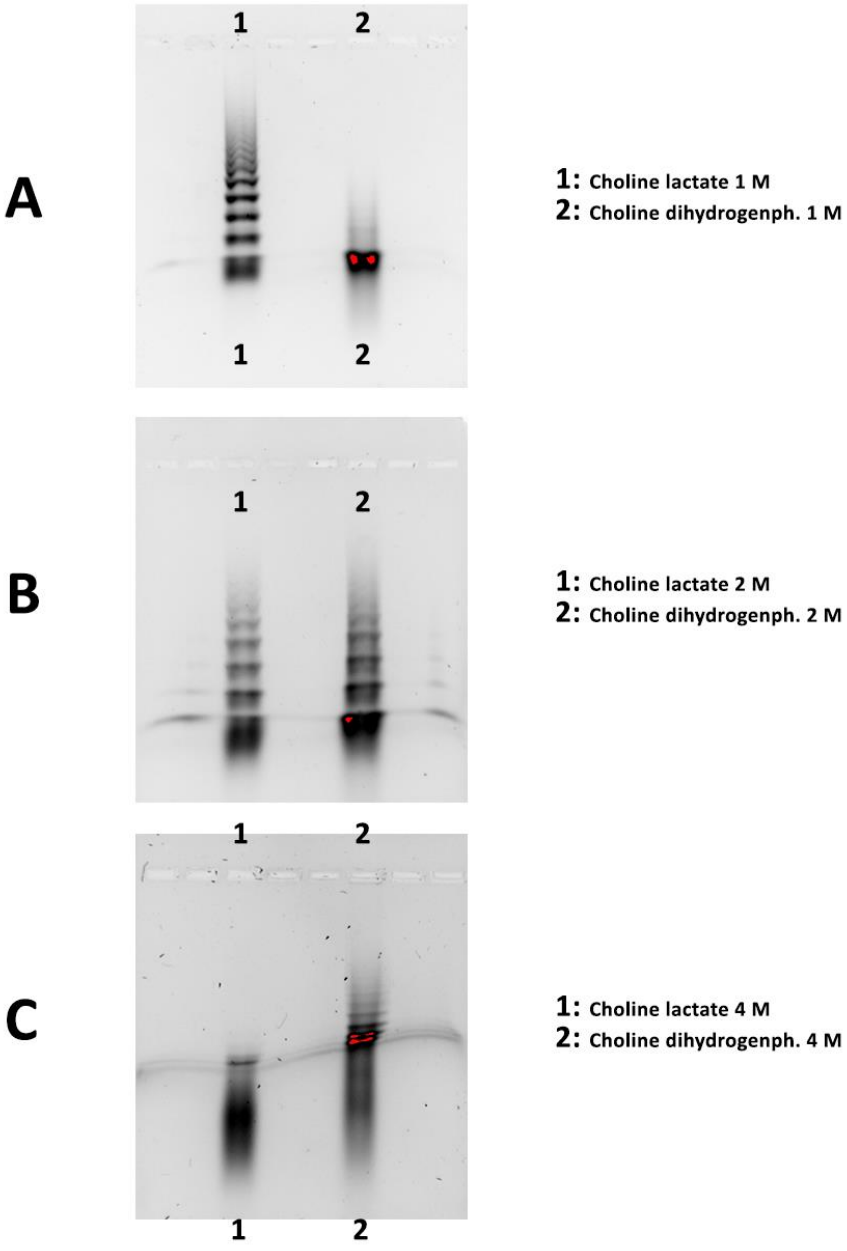

CHAPTER 8

DNA-based gating membranes and asymmetric catalysis

8.1 Introduction

This last chapter of the thesis departs slightly from the fundamental studies where the stability, kinetics and recognition capacity of DNA in non-conventional media have been studied. The first part of the chapter studies the strategy of anchoring DNA nanostructure on aluminum surfaces for further use with anodized aluminum oxide (AAO) membranes. It could permit to achieve applications with separation, detection and catalysis purposes.

The second part of the chapter consists in the design of a microfluidic diffusion cell and its manufacture in a local company, a need that arose due to different disadvantages found in classical diffusion cells and the lack of microfluidic alternatives commercially available. Once the final version of the microfluidic diffusion cell was fabricated, the DNA was supported on the AAO membrane to build the supersandwich of Chapter 7 and achieve a membrane with stimulus-response functions. Since this is the first time that a membrane modified with a DNA supersandwich has been studied in a microfluidic diffusion cell, the results have been compared with those obtained in a conventional diffusion cell.

In the third part of the chapter, the uses of DNA in the microfluidic device and in non-physiological media expands to an ongoing collaborative project that aims to create the first DNA-membrane reactor. In this chapter are included findings that suggest how a microfluidic reactor design could make DNA-mediated catalysis industrially applicable. The DNA-hybrid catalysis is normally achieved thanks to the coordination of DNA guanines with the metallic co-factors. The DNA double helix or G-quadruplex can transfer their chirality to the metal-catalyzed reaction generating products with an excess in one of the enantiomers[1].

Chapter 8

In the current ongoing work, the proof-of-concept studies consisted in the Diels-Alder cycloaddition, known as the first DNA-hybrid catalytic system discovered[2], but the DNA has been already used in a plethora of asymmetric reactions including Friedels-Craft alkylation, Michael addition and Henry reaction[3]. But for now, most studies have focused on understanding the reaction mechanism and not on designing a possible application on a larger scale or for longer periods of time. There are only two cases where a heterogeneous system using silica nanoparticles[4,5] or a cellulose column[6] were considered. These systems allow reuse of DNA for at least ten turn-overs, but there are still challenges to be addressed, such as avoiding DNA degradation or accelerating the reaction rate to achieve a competitive continuous reactor.

8.2 Results and Discussion

8.2.1 DNA nanostructures on anodized aluminum oxide

After studying the construction and disassemble of the supersandwich in Chapter 7, it was used to create DNA-modified membranes able to have the pores closed for long periods and response to local stimuli. An anodized aluminum oxide (AAO) membrane was chosen as support, in particular a commercial isoporous membrane that is sold with a theoretical average pore diameter of 20 or 100 nm. However, the mean pore diameter of the former membrane was experimentally calculated to be of 35 ± 10 nm using SEM (Section 2.8.1). A picture of the membrane surface is shown in Figure 8.1A. On the other hand, the procedure to immobilize the DNA in AAO surfaces was adapted from a published protocol as explained in Section 2.8.2.

In order to confirm that DNA was immobilized, a three-layer supersandwich based on an amino modified **CP 2**, **BP** and **AP 3** functionalized with the fluorophore Atto 488 (Table S8.1) was built-up on the 35 nm mean pore-size membrane. The DNA immobilization protocol was validated while obtaining high fluorescence values using confocal microscopy (Section 2.8.1). The limitations of the technic prevented confirming if DNA was also inside the pores, but it was assumed that this happened because DNA was immobilized in both faces of the membrane emitting similar fluorescence intensities (Figure 8.1B). The width of the membrane was measured with the reflection of the laser using ImageJ Software, obtaining an average width of 55 µm (Figure 8.1C), a value close to 60 µM, measured with the micrometer.

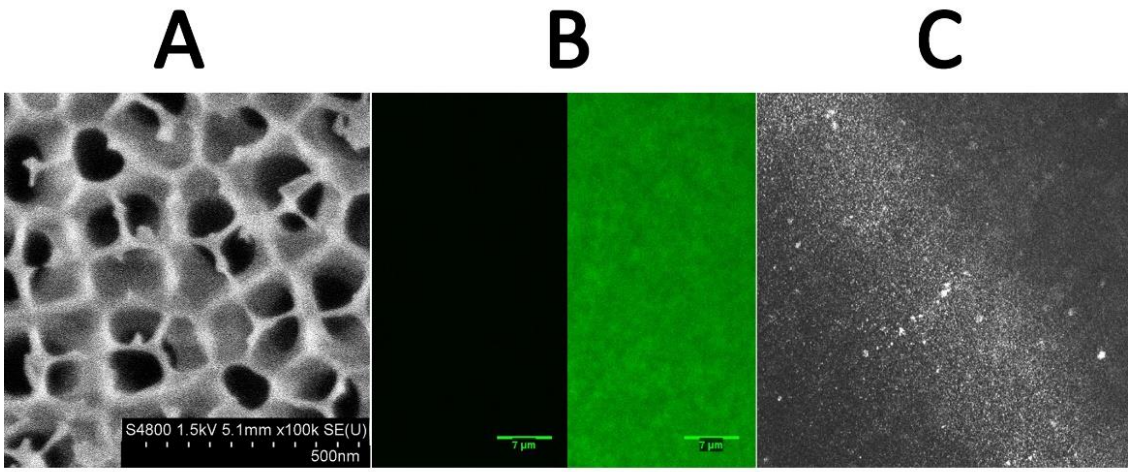

Figure 8.1. (A) The SEM picture obtained of membrane surface. (B) Fluorescence studies of the membrane without or with DNA immobilized and (C) a picture of the membrane obtained with the reflection of the laser in confocal microscopy.

Once the procedure to immobilize the DNA on the membrane was validated and prior studying the usefulness of stimuli-responsive membranes, the surface coverage that DNA would have on the membrane was estimated using QCM-D, as did previously with the gold-sensorchip (Figure 7.4), but in this case using an aluminum oxide sensorchip (Section 2.8.2). Supposing that the surface was completely silanized and functionalized with gluteraldehyde and the capture probe (**CP 2**) was also distributed homogeneously, the frequency value obtained equals to a DNA coverage of 605 ng/cm^2 (0.42 molecules/nm^2) (Figure S8.1), slightly below the density of 0.52 molecules/nm^2 obtained with the gold-sensorchip.

With QCM-D measurements, it was concluded that it was possible to build-up the supersandwich in the AAO membrane but with less surface coverage density than that of the supersandwich built in gold surface. This could reduce the efficiency of a sensing or gating

system but it can benefit the mass transport due to less steric limitations, thus improving the responsiveness of the system. Then, the supersandwich was built on the AAO membrane with an average pore diameter of 35 nm, because 100 nm would be probably too large to be closed by the nanostructures and it was seen in previous chapter that above five layers the stability of the supersandwich decreases significantly. The closure and opening of the pores was verified by permeation studies using the commercial Side-Bi-Side diffusion cell and the erioglaucine disodium salt dye as described in Section 2.8.3. In Figure 8.2 can be observed that pores of the membrane were efficiently closed using five layers of the L-b-L supersandwich or the one-step build-up. However, the slow permeation of the dye made necessary several days to achieve the same concentration of dye in both chambers (when absorbance fraction equals 1). This encouraged the design of a microfluidic system that would improve the rate of matter transfer.

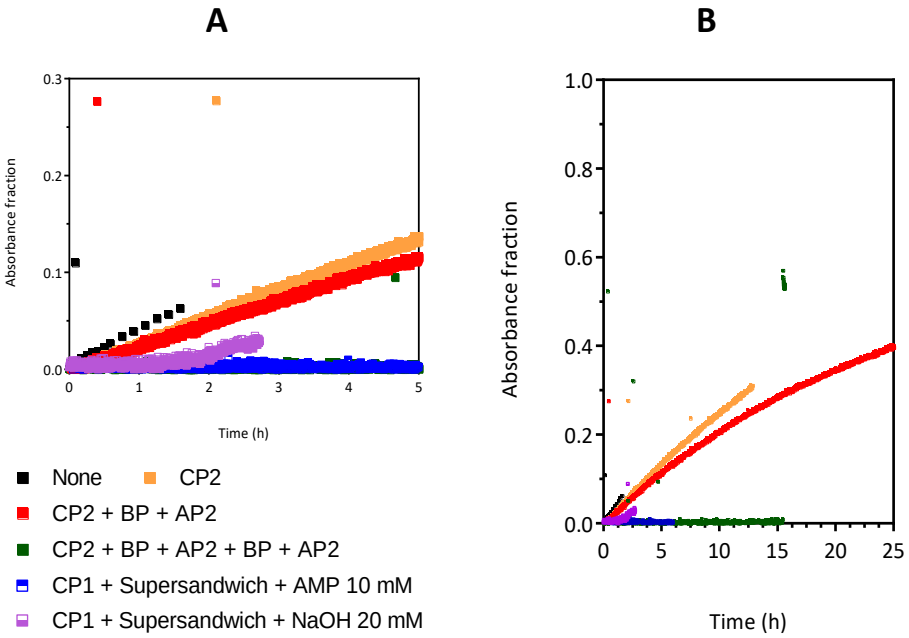

Figure 8.2. The absorbance fraction of the dye (one unit is the half of the initial absorbance of the dye in the donor chamber) *versus* the (A) first five hours and (B) the whole measurement period. The solvent was always physiological media containing 0.5 M NaCl. The initial dye concentration in the donor chamber was 0.1 mM.

8.2.2 A custom-made microfluidic diffusion cell

The channel of the microfluidic diffusion cell (Figure 8.3) was inspired by that of the flow modules of the QCM-D. The flow passes through the top or bottom without coming into contact up to the area where the membrane is placed. The flow then separates again into two channels identical to the previous ones. The total volume of each channel within the cell is about 100 µL.

The main challenges for the cell was, first, to achieve a connection to the tube system without any leakage or breakage from frequent use. Secondly, to create a membrane placement system that avoids breakage of the fragile alumina and was adaptable to other membrane types and sizes, it was achieved by means of two black Viton® gaskets. Thirdly, a complete closure of the cell, to be able to submerge it and prevent the escape of volatile solvents, for this, the central area was raised on one side and lowered on the other, so that they can fit together. The machining was carried out at Poliprecis S.L. (Asteasu, Spain), using polyether ether ketone (PEEK)[7].

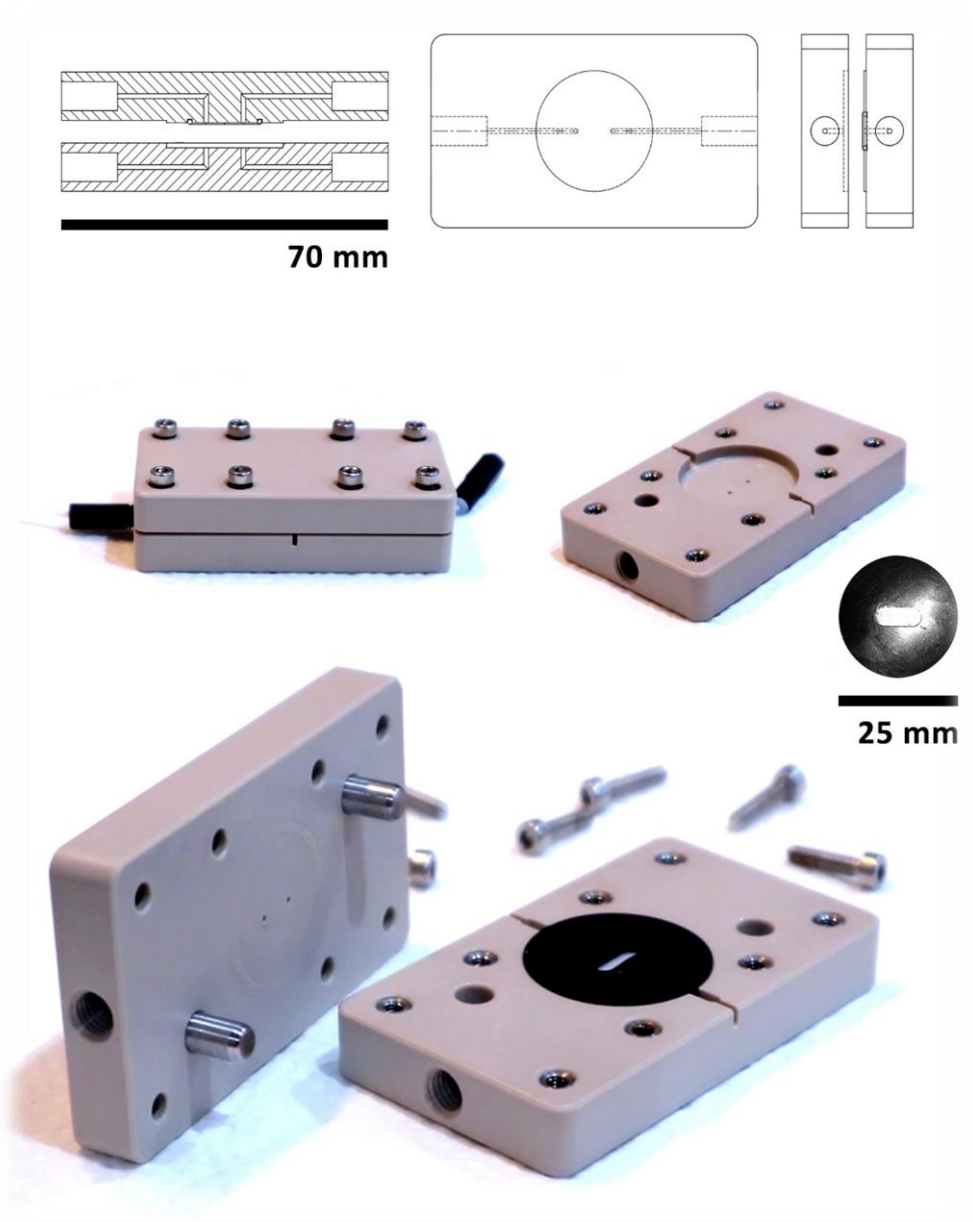

Figure 8.3. The custom-made PEEK microfluidic diffusion cell.

The benefits of using the microfluidic system were soon observed. It was possible to use a broad range of flow rates with minor changes in the diffusion coefficient and close to the

reported values[8], which means that diffusion is not controlled in a great manner by the thickness of the boundary layer. In example, in pure water, the dye had a diffusion coefficient of 1.1E-10, 1.1E-10 and 1.0E-10 m^2/s using a flow rate of 0.05, 0.25 and 0.5 mL/min, respectively (Figure 8.4A). The value was calculated using the procedure shown in Section 2.8.4, considering an initial volume of 0.9 and 0.8 mL in the donor and acceptor channels, respectively. 0.1 mM initial concentration, a 0.143 cm^2 diffusion area and a membrane thickness of 0,006 cm. It was necessary to work below 1 mL/min in order to avoid membrane fracture.

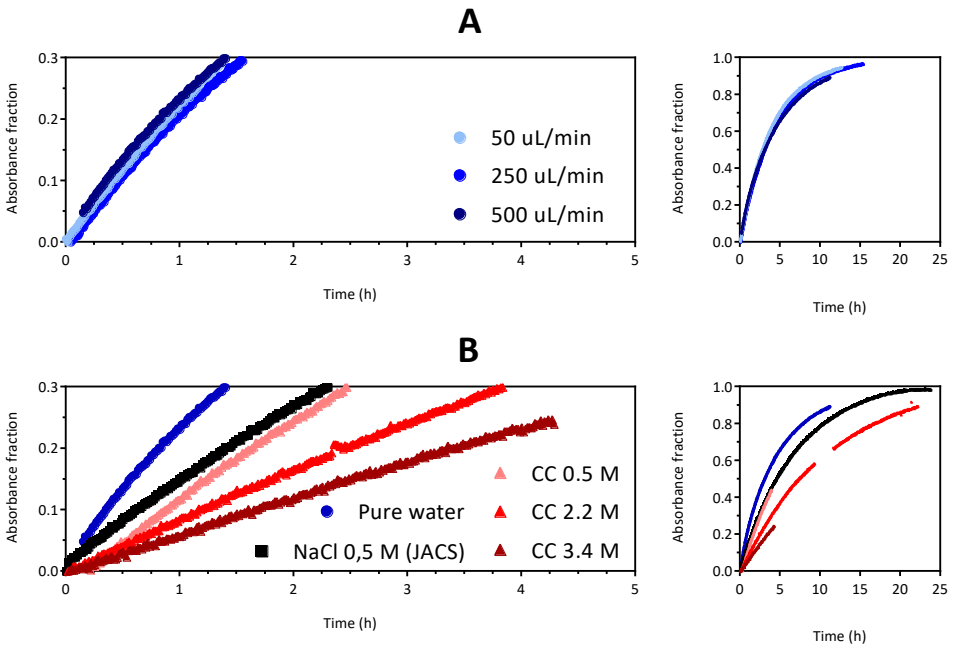

Figure 8.4. The absorbance fraction of the dye *versus* the first five hours or the whole period using (A) pure water or (B) different media at 500 µL/min. The initial dye concentration in the donor channel was 0.1 mM and membrane had no modifications.

On the other hand, in 0.5 M NaCl media, the equal dye concentration in both channels was achieved in 20 hours, significantly less than the 5-6 days needed in the Side-Bi-Side cell

(Figure 8.4B). With the DNA-modified membranes used in the Side-Bi-Side cell, it was found something surprising, not described in the literature. The dye permeated the membrane with virtually the same diffusion coefficient regardless of the supersandwich layers (Figure 8.5). It was confirmed that this was not due to DNA degradation or detachment from the membrane by performing the same measurements on the Side-Bi-Side cell, in which the dye did not permeate with a supersandwich of more than five layers.

It was therefore concluded that the small pressures that can be generated in microfluidic systems allow the supersandwich to move like algae in the sea. This movement could allow the dye to diffuse independently of the length of the nanostructure, as the nanostructure is not anchored at both ends, which could prevent this peculiar circumstance. Future studies are needed to understand how microfluidic systems affect the behaviour of DNA nanostructures.

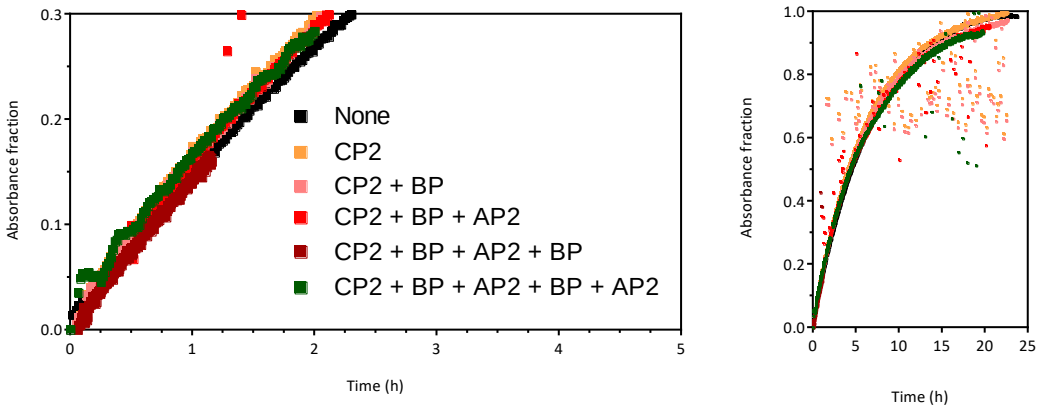

Figure 8.5. The absorbance fraction of the dye *versus* the first five hours or the whole period using different DNA-modified membranes. The solvent was physiological media containing 0.5 M NaCl. The flux rate was always of 100 µL/min. The initial dye concentration in the donor channel was 0.1 mM.

8.2.3 DNA-based asymmetric catalysis

The last section of the thesis is the initial part of a collaborative project that is being carried out together with Fernando P. Cossio's group. This consists in the creation of a versatile DNA-reactor. The project will combine the knowledge generated in this thesis about DNA conformation, stability and conservation, and on the other hand, the experience of Fernando P. Cossio's group on the use of DNA in catalysis. In this section is presented a preliminary study that aims to detect the main challenges that can appear while doing DNA-catalysis in a large-scale. A proof-of-concept reaction was used to detect these challenges and propose the preliminary design of a DNA-reactor.

The proof-of-concept reaction consisted in the Diels-Alder reaction (Figure 8.6A), the first asymmetric DNA-mediated reaction that was proposed[2]. First, the reaction protocol was done in homogeneous conditions as described in the literature (Section 2.8.5), using the ligands **1a-d** (Figure 8.6B) and obtaining the already reported enantiomeric excess values for the ligands **1a** and **1b**. The ligands **1c** and **1d** are employed by the group of Fernando Cossio in different catalytic reactions and have been used for the first time in this DNA-mediated reaction. It was observed that DNA can also transfer its chirality to these ligands and as could be expected, the reaction loses the asymmetry in absence of DNA in all cases (Table 8.1 and Figure S2).

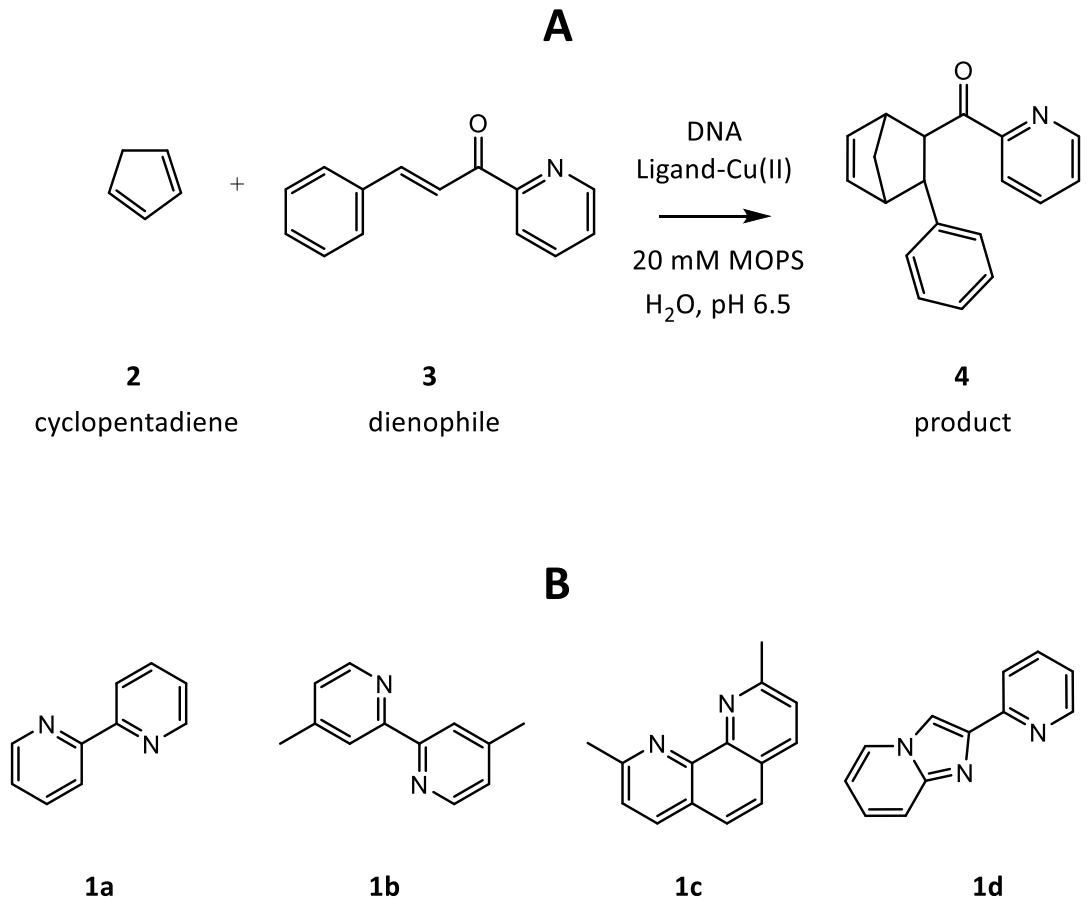

Figure 8.6. (A) Schematic representation of the asymmetric Diels-Alder reaction of cyclopentadiene (**2**) with aza-chalcone (**3**). (B) The different ligands studied (**1a-d**).

Table 8.1. Enantiomeric excess found in different reactions*.

Ligand	Enantiomeric excess in the endo product
DNA	
No ligand	-21.0 ± 9.5
1a	99.0 ± 0.1
1b	99.6 ± 0.6
1c	-54.5 ± 2.2
1d	87.6 ± 2.0

No DNA	
No ligand	-1.1 ± 6.4
1b	-7.4 ± 8.8
1c	-5.1 ± 2.0
1d	-10.2 ± 3.3

The temperature was always between 4 and 6 °C, the volume of the solution was 1 mL and the reaction was done under maximum stirring for 5 days in a vial. The solvent consisted on an aqueous buffer (MOPS 20 mM, H_2O, pH 6.5). The DNA, if used, was the "long" s-sDNA at a concentration of 1.33 mg/mL and the ligands and metal were at a concentration of 0.39 and 0.3 mM, respectively. The concentration of the reactants **2 and **3** was 15 and 1 mM, respectively. The SD is calculated from two independent reactions.*

Using the published protocol, it was soon observed a challenge that needed to be faced: the extraction of the products with diethyl ether or dichloromethane by decantation caused an undesired removal of DNA from the aqueous solvent (Figure 8.7A). This entails a high economic cost and therefore this type of extraction would be unfeasible on a large scale. It was possible to reduce considerably the loose of DNA by stirring only the organic phase (Figure 8.7B) but this strategy needed few days to complete the extraction. The most efficient way to extract the product without losing DNA was the use of a filter (Figure 8.7C). Integrating an AAO membrane with a mean pore diameter of 35 nm in the microfluidic device presented in the previous chapter. The extraction of the product (1 mM in 2 mL) ended in a considerable time (18 hours), but this was due the small permeation area of 0.25 cm^2.

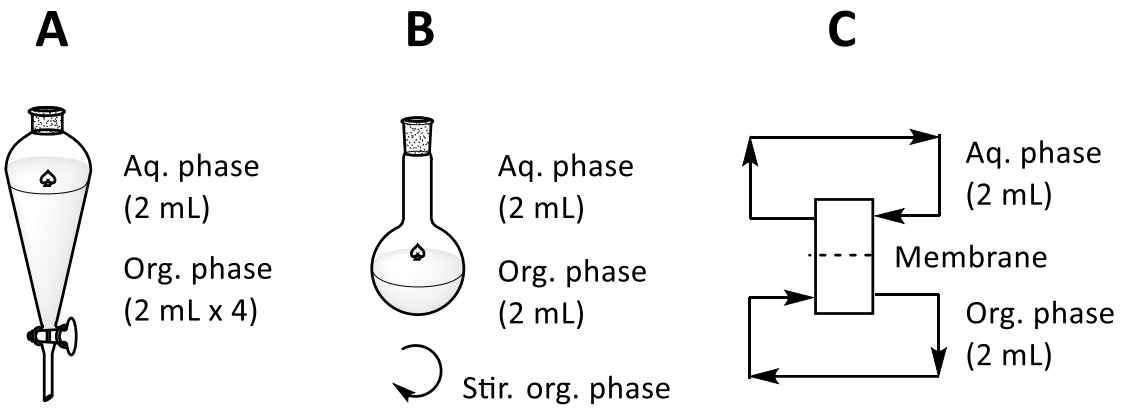

Figure 8.7. The different extraction strategies used.

During the DNA permeation studies done at RT, it was found that the salmon-sperm DNA started degrading significantly after 10 days, this was detected by UV-Vis and gel-electrophoresis (data not shown), and it can be observed also in permeation curves (Figure S8.3). This fact is not considered in any article about DNA-catalysis, probably because the reaction is done at 6 °C and in few days, but it is of upmost important if the catalysis wants to be done at higher temperatures and for several cycles. In order to prevent the DNA hydrolysis, the salmon-sperm DNA, ligand **1a,** metal and dienophile were solvated in mixed solvents based-on ethylene glycol. The use of EG and reline DES was due to the greater solubility of the dienophile (**3**) in these media compared to that in physiological media (Figure S8.4).

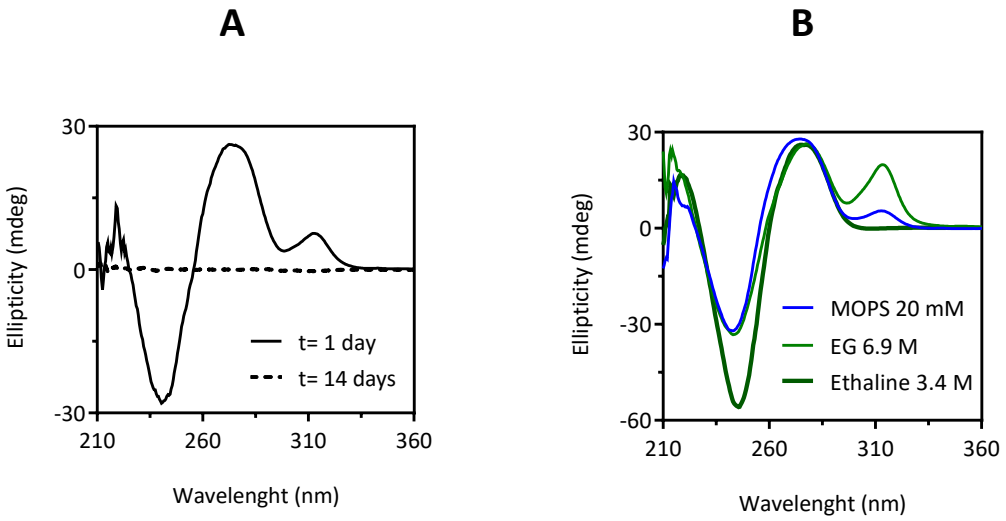

Figure 8.8. Circular dichroism spectra of different samples containing "long" salmon-sperm DNA (1.33 mg/mL), the ligand **1a** (0.39 mM) and metal (0.3 mM) in (A) physiological media (MOPS) after one day or two weeks at RT. (B) After one day in physiological media, ethylene glycol (6.9 M) or ethaline (3.4 M).

Contrary to MOPS buffer, where salmon-sperm DNA was degraded after two weeks at RT (Figure 8.8A), it was found that mixed solvents prevented this, in concordance with the results of Chapter 5. Unfortunately, the presence of choline salts reduced the affinity of the ligands towards DNA, and as can be observed in CD spectra, it might affect to the asymmetry of the reaction. On the other hand, in ethylene glycol, it seems that the ligand binds to DNA with higher affinity what could have great implications (Figure 8.8B). The next steps of the project will be first to refine the microfluidic system to create a continuous reactor and then to address the option of including non-physiological media to avoid DNA degradation, increase the solubility of the reactants and also to expand the repertoire of possible reactions.

8.3 Conclusions

First, the protocol for immobilizing DNA on aluminium oxide was validated by confocal microscopy. Then, using QCM-D, the DNA density on the surface was found to be somewhat lower than on gold, but still an acceptable value (0.42 molecules/nm^2). In addition, excessive surface saturation can be counterproductive, as discussed in the previous chapter. Next, the supersandwich was built on an AAO membrane with an average pore size of 35 nanometers. Permeation experiments were carried out using this membrane in a Side-Bi-Side permeation cell. It was found that the supersandwich was able to recognize 10 mM AMP specifically and disassemble, but unfortunately the permeation is very slow and it would take too much time to perform systematic studies.

The latter motivated us to build a microfluidic permeation cell, the material used was PEEK. Once designed and manufactured, the membrane with the supersandwich was inserted into this cell. The permeation of the dye was much faster, allowing complete measurements to be made in hours rather than days/weeks. Unfortunately, although this is a very interesting fact, it has been observed that, as the supersandwich is only anchored at one end, due to the pressure produced in the microfluidic system, the nanostructure has not closed the pore against the EGDS dye. We imagine that the pressure has made it possible for the supersandwich to move like a bank of "algae". We yet need to study a design anchored at both ends to verify this event.

Finally, the DNA-mediated catalysis was studied in order to further use at a larger scale or with new reactions. The first reaction published a decade and a half ago has been successfully replicated, and new ligands have been included. In the process, the following main challenges

have been identified: DNA degradation and its extraction to the organic phase. To address the first challenge, and also to improve the solubility of the reagents, the use of non-physiological media has been proposed. However, this must be done with caution, as it has been shown by circular dichroism, that in the presence of other cations, the ligand does not bind efficiently to the DNA. On the other hand, to avoid DNA extraction, the use of a membrane is proposed and by integrating this into the microfluidic system it would be possible to create a continuous reactor. This project is ongoing and we will continue to study the design.

8.4 References

1. Duchemin, N., Heath-Apostolopoulos, I., Smietana, M. & Arseniyadis, S. A decade of DNA-hybrid catalysis: From innovation to comprehension. *Org. Biomol. Chem.* **15**, 7072–7087 (2017).
2. Roelfes, G. & Feringa, B. L. DNA-based asymmetric catalysis. *Angew. Chemie - Int. Ed.* **44**, 3230–3232 (2005).
3. Dijk, E. W., Boersma, A. J., Feringa, B. L. & Roelfes, G. On the role of DNA in DNA-based catalytic enantioselective conjugate addition reactions. *Org. Biomol. Chem.* **8**, 3868–3873 (2010).
4. Sakashita, S., Park, S. & Sugiyama, H. Copper-containing DNA–Silica Mineral Complexes for the Asymmetric Diels–Alder Reaction. *Chem. Lett.* **46**, 1165–1168 (2017).
5. Park, S., Ikehata, K. & Sugiyama, H. Solid-supported DNA for asymmetric synthesis: a stepping-stone toward practical applications. *Biomater. Sci.* **1**, 1034 (2013).
6. Benedetti, E. *et al.* DNA-cellulose: an economical, fully recyclable and highly effective chiral biomaterial for asymmetric catalysis. *Chem. Commun.* **51**, 6076–6079 (2015).
7. Zalaznik, M., Kalin, M. & Novak, S. Influence of the processing temperature on the tribological and mechanical properties of poly-ether-ether-ketone (PEEK) polymer. *Tribol. Int.* **94**, 92–97 (2016).
8. Syms, R. Rapid evaporation-driven chemical pre-concentration and separation on paper. *Biomicrofluidics* **11**, 044116 (2017).

8.5 Supplementary information

Table S8.1. Used DNA sequences.

Name	**Sequence 5' to 3'**
Capture probe 1 (**CP 1**)	CGG CAC CTG GGG GAG TAT TGC GGA GGA AGG TGC CG (5': Thioctic acid or amino)
Capture probe 2 (**CP 2**)	TTT TTT TTT TTT TTT GCG GAG GAA GGT GCC G (5': Thioctic acid or amino)
Bridge probe (**BP**)	TAC TCC CCC AGG TGC CGA CGG CAC CTT CCT CCG CA
Aptamer probe 1 (**AP 1**)	CGG CAC CTG GGG GAG TAT TGC GGA GGA AGG TGC CG
Aptamer probe 2 (**AP 2**)	AC CTG GGG GAG TAT TGC GGA GGA AGG T
Aptamer probe 3 (**AP 3**)	CGG CAC CTG GGG GAG TA (5': Atto 488)

Figure S8.1. (A and C) Frequency and dissipation curves obtained in QCM-D upon immobilization of **CP 2** and consecutive injections of **BP** and **CP 2**. (B and D) Representation of the dissipation *versus* frequency values obtained in each layer of the supersandwich. The A and B data correspond to gold sensorchip and C and D data to aluminum oxide sensorchip.

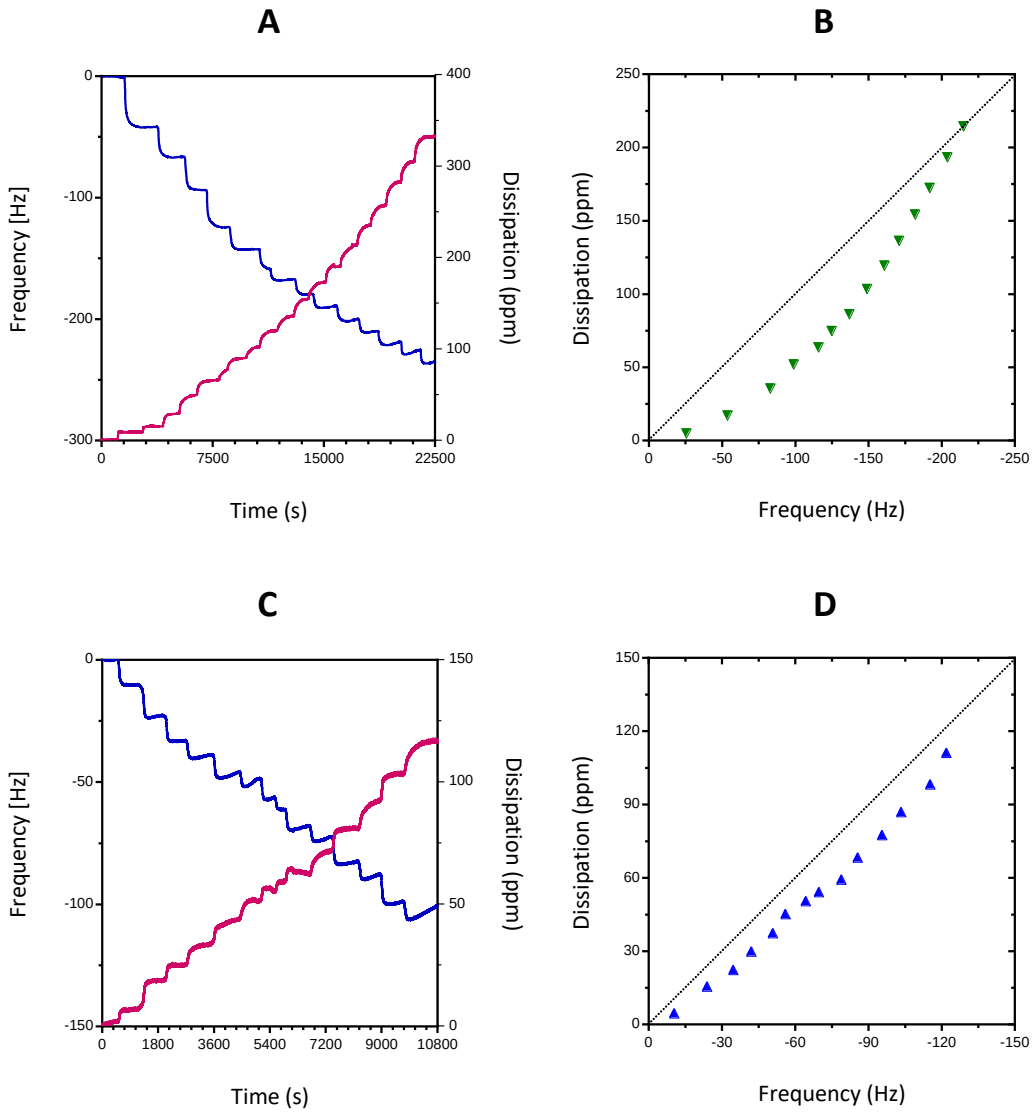

Figure S8.2. Circular dichroism spectra of different samples containing the metal (0.3 mM). In some cases the "long" salmon-sperm DNA (1.33 mg/mL) and/or the ligand (0.39 mM). In (A) there is no ligand, in (B) the ligand is **1b,** in (C) the ligand is **1c** and in (D) the ligand is **1d.**

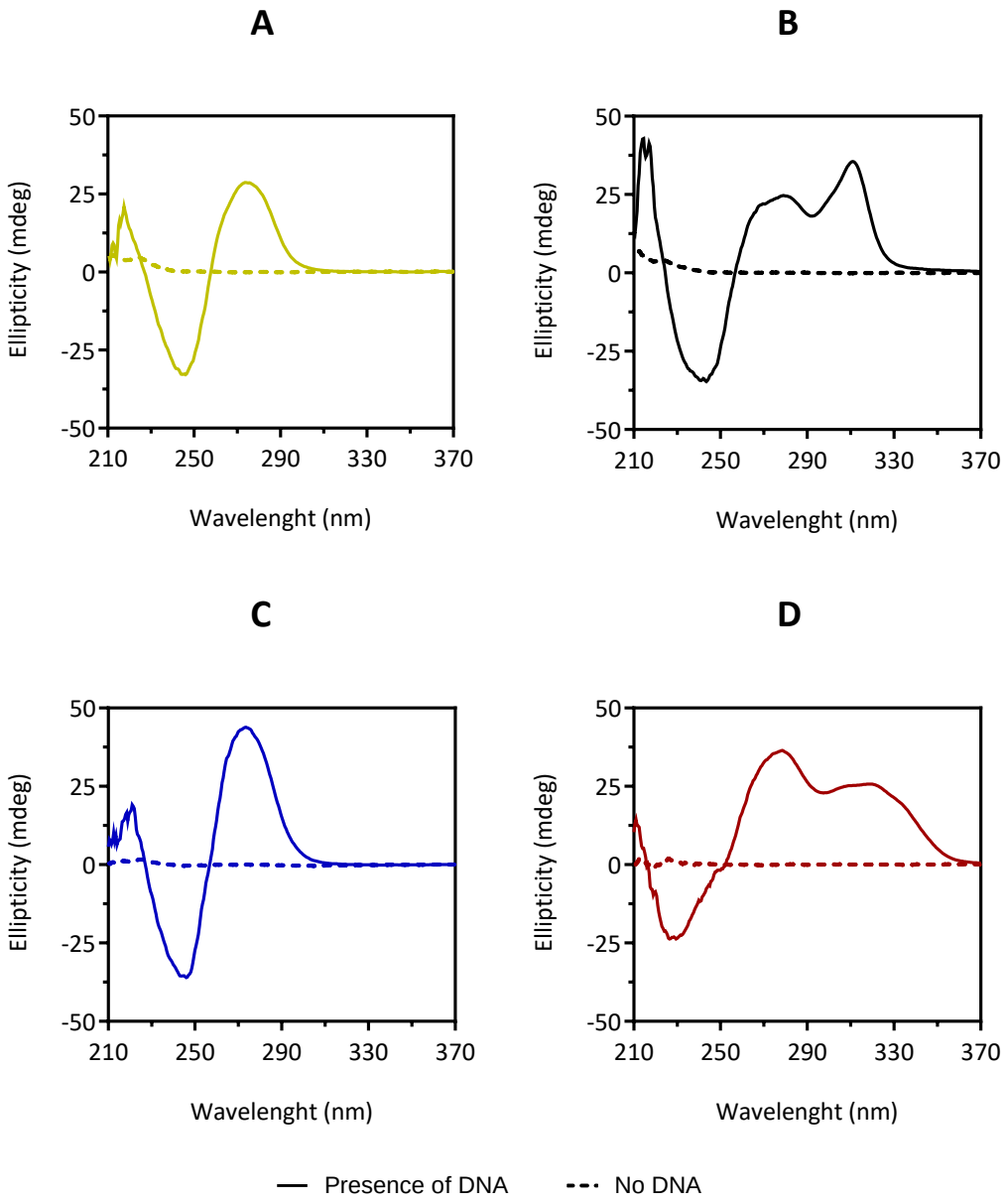

Figure S8.3. (A) DNA concentration in the donor chamber when performing a permeation experiment of both salmon-sperm DNA (s-sDNA) samples in the Side-Bi-Side cell with pure water in both chambers and using the alumina membrane with mean pore diameter of 35 nm. (B) Agarose gels after gel-electrophoresis of both s-sDNA before starting the permeation experiments.

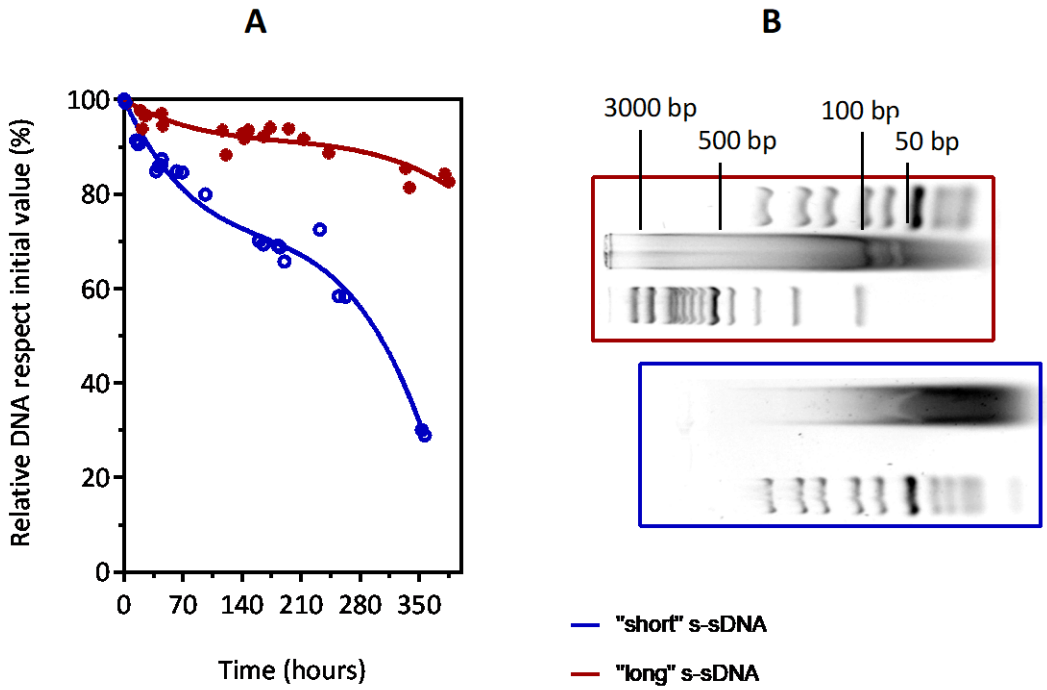

Figure S8.4. Absorbance measurements done during the preliminary solubility test. 2 mM of dienophile (**3**) were added to 2 mL of each media and stirred at 60 ºC overnight. Then, the solutions were cooled and filtered. The obtained liquid was measured by UV-Vis.

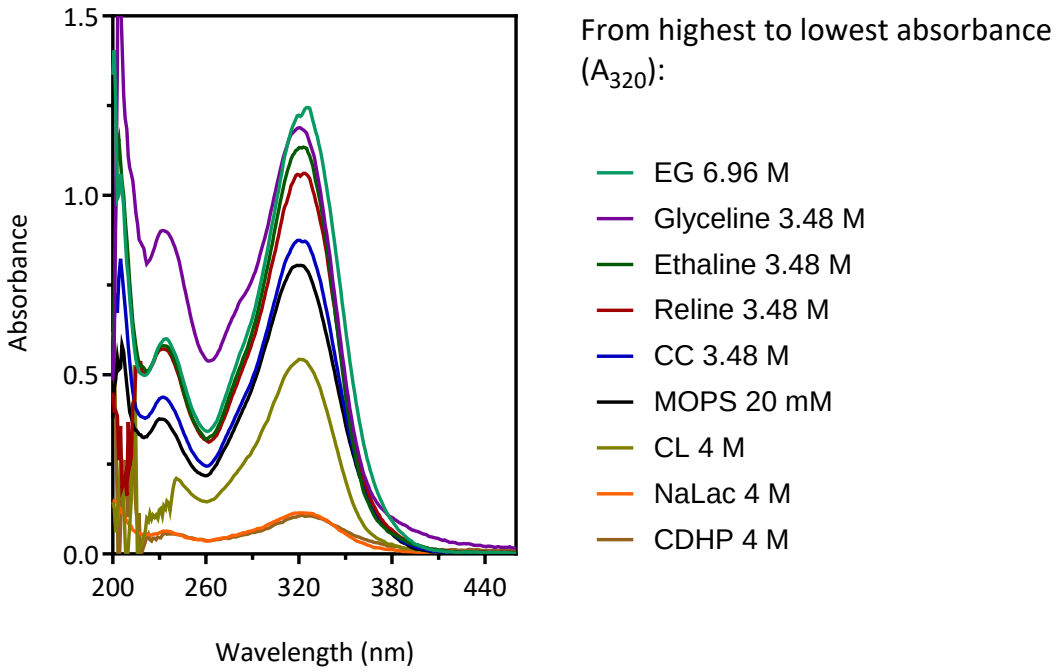

CHAPTER 9

General Conclusions

The main objective of this thesis was to develop knowledge about the intramolecular interactions of DNA and those formed between DNA and its environment. This has been achieved by studying the DNA in a variety of mixed solvents and creating different DNA nanostructures. Below, are shown some general conclusions obtained from the experimental work.

- The thermal stability of the short duplexes decreases following a polynomial trend while changing the water content. This allows the melting temperature to be adjusted adding specific amounts of water.
- On the other hand, at an equal concentration, the DESs destabilized more the dsDNA than molecular solvents, probably due to the reduction of water. Interestingly, reline DES was an exception. Using molecular dynamics simulations, it has been possible to see that in the presence of choline, urea interacts less with DNA, especially in the major groove.
- Thanks to the cooperativity in the double helix, the “long” salmon-sperm DNA maintained its B-form almost in anhydrous reline.
- It has been observed that choline cation has different peculiarities: it displaces the metallic cations from DNA, favors the formation of local secondary structures in DNA and destabilizes more the GC-rich duplexes than AT-rich ones. These experimental observations could be verified also with computational methods.
- Regarding the conformational stability of dsDNA, new secondary structures appeared in GC-rich duplexes, but other duplexes maintained, in general, the B-form structure or denatured forming a random coiled ssDNA.

- In a relative fast and cost-effective manner, the computational calculations allowed the detection of several key points that explain the experimental results.
- By analyzing the ATP DNA-aptamer by circular dichroism, it has been possible to observe how its double helix and its recognition pocket are altered in a plethora of mixed solvents. The results are in agreement with the conformational and thermal stabilities of the duplexes.
- Interestingly, it was found that the ATP DNA-aptamer suffered significant changes in its secondary structure during the storage period, it is argued that these structures are not observed in physiological media because the aptamer follows a different pathway.
- As observed using circular dichroism, 0.9 M choline chloride is sufficient to prevent DNA degradation at RT for at least several years. Even in the absence of salts, the mere fact of using solvents other than water has already reduced hydrolysis. The increase in the ellipticity of the negative peak after several months needs to be better studied as it could be due to DNA aggregation.
- Circular dichroism as not useful for monitoring aptamer binding to the target, so SPR and fluorescence techniques were instead. This is the first time that SPR has been used to study aptamer recognition in non-physiological solvents. It was possible to calculate the different K_d at low concentrations of mixed solvents, but unfortunately the refractive index has severely limited the range of mixed solvents that can be used.
- It has been observed that the capacity of the aptamer to recognize its target varies greatly with temperature, needing a temperature lower than 0 degrees for example, while using

DESs above 2 M. Although this is a handicap in several cases, it also presents new opportunities for the use of functional DNA, as ethaline DES, for example, can be liquid until -80 °C.

- Selecting *de novo* the ATP DNA-aptamer in non-conventional media, it was possible to obtain aptamer sequences specially adapted to the new solvent. Two of these sequences were able to recognize ATP beads with solvent-specificity, not recognizing them in physiological media.
- The selected new aptamers showed G-quadruplex structures that are rarely found in aqueous solutions and were dependent of the ionic liquid presence but also the metallic salts. Additionally, due to the charged nature of the IL, it was possible to control the activity of water preserving DNA from hydrolysis.
- The nanostructure known as supersandwich has been constructure for the first time using the layer-by-layer method, apart from using the already published one-step method. It has been necessary to redesign the nanostructure when building it layer-by-layer. This shows the need to take into account all possible interactions. The development of software could be of great help.
- The formation of dimers or secondary structures such as hairpins has been found to significantly reduce the efficiency of hybridization to the layer-by-layer nanostructure. Nevertheless, it has been possible to achieve a nanostructure with 100 % hybridization efficiency. This nanostructure consists of 3 layers. It was possible to reach 4-5 layers (approx. 25 nm) and maintain a negligible K_{off}, albeit with reduced hybridization efficiency.

- Regarding the ability of ATP or AMP to break down the nanostructure. The results obtained differ greatly from those reported in the literature. The target molecule was not able to undo the single-layer sandwich or the multilayer sandwich, at least at the published concentration (1 mM).
- In the case of the 1-layer supersandwich, 4 mM of AMP was enough to undo it, but the sensitivity dropped dramatically when more layers were added. It was necessary to use 30 mM AMP to see a significant change compared to GMP.
- To improve the sensitivity of the multilayer supersandwich, it has worked to reduce the affinity between oligonucleotides. However, introducing mismatches also significantly affects the stability of the nanostructure, so it does not seem a useful strategy. Ideally, aptamers with a sensitivity towards the target molecule in the nanomolar range should be used.
- The use of DNA nanostructures in non-physiological environments has also been considered, what permits the long-term use of these structures and the use of new targets as stimuli. Thermal stability has been found to be higher in the supersandwich than in individual duplexes, demonstrating that there is cooperativity between the different layers of the nanostructure.
- It has been shown for the first time that the nanostructure maintains the double helix shape even under very low hydration conditions. However, the length of the nanostructure has been significantly affected, as observed by gel electrophoresis.

- The supersandwich has been successfully immobilized on alumina surface, for further use in membranes. The permeation experiments were carried out using an isoporous membrane in a Side-Bi-Side permeation cell and the stimuli-responsiveness of the DNA-functionalized membrane was successfully tested.
- Interestingly, in the microfluidic permeation cell, it has been observed that, as the supersandwich is only anchored at one end, due to the pressure produced in the microfluidic system, the nanostructure has not closed the pore against the dye.
- The first asymmetric Diels-Alder reaction mediated by DNA has been successfully replicated, and new ligands have been included. In the process, the following main challenges have been identified: DNA degradation and its extraction to the organic phase.
- To address the DNA degradation, and also to improve the solubility of the reagents, the use of non-physiological media has been proposed. However, this must be done with caution, as it has been shown by circular dichroism, that in the presence of choline, the ligand does not bind efficiently to the DNA.
- In order to avoid DNA extraction, the use of a membrane is proposed and using the microfluidic device it would be possible to create a continuous reactor. This project is ongoing and we will continue studying the design.